

Doctor Dissertation

**Characteristics of the mechanical motions and
electric performance on the Triboelectric
generator and Piezoelectric generator
- Preliminary stage for ocean energy harvester**

(摩擦及び圧電効果による発電体の機械的運動特性と起電力特性
- 海洋エネルギーハーベスターに関わる基礎的検討 -)

September 2022

Graduate School of Engineering
Faculty of Engineering
Hiroshima University

Ede Mehta Wardhana

Abstract

High innovation in the field of the internet of things (IoT) and Microelectromechanical systems (MEMS) have led to the dire need for a new sustainable power source. The current power source for the IoT and MEMS mainly depends on the batteries, supercapacitors, and micro-fuel oil cells have the main disadvantages since it only has a finite amount of energy. There is a need for developing generator that can scavenge energy for longer, especially if the device's main location is in a difficult and hazardous place (such as the ocean). In order to solve those problems, This study proposed, developed, and improved energy harvester devices using the triboelectric generator (TEG) and piezoelectric generator (PEG). This study served as the first stage for developing the actual ocean energy harvester, focusing on the fundamental characteristics of the mechanical motions and the device's electric performance. Four main phases were studied and elucidated in separate chapters. The investigation is started by measuring the output voltage of the single TEG periodically under its output voltage time histories with strong responses found without electrical noise. The output voltage has good results, and the characteristics of the working mechanism of the TEG were clarified in the separation, contact, and compression modes. In the next phase, we developed the theoretical model of the vertical contact-separation modes with a dielectric elastomer. Using the theoretical model, the resulting average, maximum, and minimum output agreed well with the experimental data. This similarity means that the model could be used as a basic design tool for predicting the FC-TEG before practical usage. To improve the TEG's electrical output, we expanded and created a multi-layer TEG setup for the vertical vibration tests. Characteristics of the multi-TEGs under the contact and compression modes were clarified. In addition, the relationship between key parameters such as vibration frequency, vibration amplitude, initial distance, and compression force was investigated. We found that the vibration frequency and amplitude have a direct correlation and positive relationship to multi-TEG outputs. However, the initial distance and compression force only have a small role in increasing the voltage results. This means that the separation velocity plays a major role compared with separation distance. Since natural energy fields (such as ocean waves or wind) have several spectrums for energy harvesting, a study on hybrid energy harvesters has been conducted using the combination of multi-TEG with PEG devices for scavenging more energies. We found that all key parameters are similar to previous studies. Furthermore, we also found that each PEG and TEG could compensate for the deficiencies of each device under different distance spectra.

Acknowledgements

Bismillahirrahmanirrahim, Alhamdulillah. All thanks are to the presence of *Allah Subhanahu wa ta'ala*, for of his grace and all-doing, I could finish my doctorate study.

The works of the alternative generators, especially those that use the triboelectric and piezoelectric principles, have been improving over the past few years. However, this phenomenon had not yet reached Indonesia when I started interested in this topic. Combined with the vision of current Indonesia's president to improve the maritime and ocean field, I have great motivation to help the government solve some problems in that area by utilizing this study. So, it is a blessing for me to not only learn about this topic here in Japan and continue it for the well-being of the people in my home country. It also allows me to meet so many experts, share our understanding, and widen my horizons which were collected and presented in this study. As the world keeps evolving and moving towards society 5.0, I believe that the works of this dissertation study will greatly help that progress. The study that I would never be able to finish without the help of many great human beings I met.

First, I would like to express my sincere and best gratitude to my supervisor, *Prof. Hidemi Mutsuda*, who has been helping me in academics and settling down for Japan life at Hiroshima University. With his inspiration, guidance, and great enthusiasm, he provided valuable advice, ideas, and suggestions for my research. His immeasurable kindness has helped me in every aspect of my life. It is my honor to be his student, and I will be forever grateful for meeting, knowing and learning from Him. I also wish to express my gratitude to *Assoc. Prof. Yoshikazu Tanaka* and *Assoc.Prof. Takuji Nakashima*, who also greatly helped me complete my research and as my advisor for the genuine support, valuable advice, sincere comments, and encouragement which helped me a lot to finish this study and improve it beyond what I thought was possible. I also would like to thank *Prof. Hidetsugu Iwashita* for his thoughtful comments on improving this dissertation content and making it more appealing to the general public.

I want to thank my Doctors (*Dr.Rie Sasaki-Sensei M.D.*, *Dr.Kubo-Sensei*, *Mrs.Sachiyo Nose-San*, and *Dr.Okamoto-Sensei*) and *all Nurses of Higashihiroshima memorial hospital*, who were always eager to help me and care for my wellbeing. I will be forever grateful for everything they have done for me. I would like to acknowledge and say my thanks as well to *Ast. Prof. Taiga Kanehira* who helped me so much during my study and helped me adjust to life in Japan.

This work will never be able to start without the help, support and collaboration with *Sumitomo Electric Industries, Ltd and MUNEKATA Co., LTD* for providing the materials in this study. This study was also supported in part by *Grants-in-Aid for Scientific Research, KAKENHI (17H03494, 19K22931) and KAKENHI (19K229310A)*. I would like to thank all individuals for the invaluable support.

Next, I would like to specifically thank my fellow compatriot (Dimas Angga F.M, Zulhaj Aliansyah, Firly R. Baskoro, Ibadurrahman, Ndaru C.S, Ufafa Anggarini, Gilang, Faruq, Nanda-Ulil, Ali, Lukman Hakim and Qingyu Wang-San) for always helping and supporting me so we can graduate together. For the juniors and friends that I will leave behind (Nadia, Ayo, Hanif, Eka, Dimas B, Du-San, Yan-San, Oliver, Stella A, Niimi, Jacqueline, Tingjia, Ueda-San and Uchida-San, Thin Thin HTUT, Fujita-San and fellow Graduate school support officers, Fikry P. Lugina, Rino, Suhendri, Herry, Putro Pradana, Diana, Sucharita, Seo, Hasebe, Wasada, Namatame, Nakashima, Nobuki, Hasegawa, Mizunaru, and Kizaki) thank you so much for accompanying me during my life here in Japan. I want to be grateful to the seniors as well (Mr. Takumi Ozawa, Mr. Taichi Yamada, and Mr. Takeshi Kubota for always accompanying me and helping me complete this study, Mr. Takuya Yamazaki for becoming my first and best friend here in Japan, Dr. Shade, Dr. Puji, Dr. Iis, Dr. Aruni, Dr. Nakamura-Sensei, Adina Staicov.Ph.D. and my fellow writing colleague: Thu, Van, Yoshie, Duc, and Mohammad), Okamoto, Takashi, Kato, Suehiro, and Juang for accompanied me with very good suggestions and shared their story with me. For living a great Japanese life, I would like to thank Mitsuyo-Okaa San, Syifa, John King, Cyril, Jade, my fellow eigomura friends, and all my friends and colleague in PPIH, KMIH and in ITS (specifically Dr. Dhimas Widhi H, Dr. Adi Kurniawan, Dr. Septia H.S and Mr. Yoyok). Because of all of you, I have a warm and caring new family.

Finally, I dedicate this dissertation to the most special people in my life. I want to thank my parents (Meitha Soetardjo and Wisnu Wardhana) and my uncle (Benny) for their unlimited support and care. My sisters (Diar M W and Frea M W), both of their husbands (Rio and Habib), and my handsome + beautiful niece and nephew (Zeyndio, Zyana, and my future nephew in a few months) for become my motivational fuel while I am away from home. I want to mention the Late Dr. Ary, Mrs. Dien, Mr. Darno, Mrs. Donna, Mrs. Yonna, and all the Soetardjo family for always accepting and supporting me while I am away from Indonesia.

I hope the works of this study can be useful in the future.

Contents

| | |
|---|------------|
| Abstract | i |
| Acknowledgements | iii |
| 1 Introduction | 1 |
| 1.1 Background | 1 |
| 1.1.1 Internet of things and its power source | 1 |
| 1.1.2 Energy Harvesting | 2 |
| 1.1.3 Previous research of Piezoelectric generator and triboelectric generator | 6 |
| 1.2 Ocean Space situation, Marine Domain Awareness and the necessity of the Ocean energy harvesters | 19 |
| 1.3 Gaps, Aims, and Objectives | 24 |
| 1.4 Structure of the Dissertation | 27 |
| Bibliography | 28 |
| 2 Energy Harvesting based on triboelectric materials using a single dielectric elastomer | 35 |
| 2.1 Background | 35 |

| | | |
|----------|---|-----------|
| 2.2 | Device overview + fabrication of TEG | 36 |
| 2.2.1 | Device overview | 38 |
| 2.2.2 | Fabrication of single TEG based on dielectric elastomer | 38 |
| 2.2.3 | Taping Mechanism/fixation method | 40 |
| 2.3 | Vertical contact-separation-compression Experiment Setup and Condition | 43 |
| 2.4 | FC-TEG only experiments results | 46 |
| 2.4.1 | Output voltage results based on a various taping mechanism | 46 |
| 2.4.2 | Output voltage characteristics in the separation – contact – compression modes | 49 |
| 2.4.3 | Effect of separation velocity on the output voltage | 59 |
| 2.4.4 | Effect of the compression load on the output voltage | 64 |
| 2.5 | Summary | 67 |
| | Bibliography | 68 |
| 3 | Theoretical section of a single dielectric elastomer energy harvesting | 71 |
| 3.1 | Background | 71 |
| 3.2 | Theoretical and Numerical Section | 72 |
| 3.3 | Estimation of the output voltage based on the theoretical model | 76 |
| 3.4 | Summary | 91 |
| | Bibliography | 92 |
| 4 | Multi-layered triboelectric generator | 95 |
| 4.1 | Background | 95 |

| | | |
|----------|---|------------|
| 4.2 | Device overview + fabrication of multi-TEG | 96 |
| 4.3 | Multi-TEG experiments results | 100 |
| 4.3.1 | Effect of the multi-layered structure | 100 |
| 4.3.2 | Effect of the Frequency and Amplitude on the Multi-layered TEG output voltage | 103 |
| 4.3.3 | Relationship of initial distance with vibration amplitude and vibration frequency | 105 |
| 4.3.4 | Single Layer Vs. Multi-Layered TEG in Contact and Compression Modes | 108 |
| 4.3.5 | Comparison of compression force and acceleration amplitude to Multi- layered TEG output voltage | 114 |
| 4.4 | Summary | 119 |
| | Bibliography | 123 |
| 5 | TEG-PEG hybrid device | 125 |
| 5.1 | Background | 125 |
| 5.2 | Device Overview + Fabrication of TEG-PEG | 127 |
| 5.2.1 | Device Overview of TEG-PEG case 1 and case 2 | 135 |
| 5.3 | TEG-PEG hybrid device experimental results | 140 |
| 5.3.1 | Characteristics of output voltage generated from TEG-PEG in the pre- liminary vibration test | 140 |
| 5.3.2 | Relationship between vibrated amplitude to the PEG and TEG output voltage | 148 |
| 5.3.3 | Relationship between initial distance to the PEG and TEG electrical output under various frequencies | 152 |

| | | |
|----------|---|------------|
| 5.3.4 | Relationship between initial distance to the PEG and TEG output voltage under various amplitudes | 154 |
| 5.3.5 | TEG-PEG Hybrid Mutual Complementary | 159 |
| 5.3.6 | TEG-PEG Power Density Comparison | 162 |
| 5.4 | Summary | 168 |
| | Bibliography | 169 |
| 6 | Conclusions and Future Works | 173 |
| 6.1 | Conclusions | 173 |
| 6.2 | Future Works | 175 |

List of Tables

- 4.1 Table 1: TEG roughness surface data 100
- 4.2 Multi-TEG vertical vibration tests. 100

- 5.1 PEG Dimensions 129

List of Figures

| | | |
|------|--|----|
| 1.1 | Shiojiri environmental data and the IoT sensor network [Narvaez Rojas et al., 2021] | 3 |
| 1.2 | Estimated of the device usage for each person [Safaei et al., 2018] | 3 |
| 1.3 | Power sources for IoT [Raj and Steingart, 2018] | 3 |
| 1.4 | Electronics component and its power requirements [Zi and Wang, 2017] | 5 |
| 1.5 | Four power generation methods in vibration power generation | 5 |
| 1.6 | Three major applications of the nanogenerators [Wang, 2017a] | 6 |
| 1.7 | Several Wind energy PEGs. | 8 |
| 1.8 | TEG's wind energy harvester | 9 |
| 1.9 | Nanogenerators based on human movement. (a) PEG based on jaw movement [Delnavaz and Voix, 2014]; (b) TEG on the wearable devices [Zou et al., 2020, Li et al., 2017, Rodrigues et al., 2019]; and (c) in-vivo energy harvesting for biomedical applications [Dagdeviren et al., 2014, Lin et al., 2014, Mannsfeld et al., 2010, Zhu et al., 2014b] | 10 |
| 1.10 | Applications of the machine vibration energy harvesting. | 12 |
| 1.11 | Energy density in each period of the ocean movements [Kinsman, 1984]. Source: Source : Renewable Energy Technologies for Sustainability | 13 |
| 1.12 | Resource zone of the Ocean kinetic energy [Zhao et al., 2021] | 13 |

| | | |
|------|--|----|
| 1.13 | Several applications of the ocean generators with the rolling ball concept. | 15 |
| 1.14 | Several applications of the ocean generators on the wave and current interaction zone. | 17 |
| 1.15 | Generators with PEG and TEG on the deep ocean | 18 |
| 1.16 | Application of MDA in Japan | 21 |
| 1.17 | Ocean monitoring devices. Potential for future ocean energy harvesters | 22 |
| 1.18 | State-of-art ocean sensors and ocean sensors system. Collected and reviewed in the work of [Zhao et al., 2021] | 23 |
| 2.1 | Working mechanism of the TEG with the electrode and dielectric elastomer | 37 |
| 2.2 | Four working modes of TEG [Wang, 2014] | 37 |
| 2.3 | Surface roughness (average of 200 nm) of the FC-TEG | 39 |
| 2.4 | Concept and Prototype of Single TEG | 40 |
| 2.5 | Taping mechanism and the Prototype of Single TEG. | 42 |
| 2.6 | Experimental Setup and Measurement System | 44 |
| 2.7 | Separation distance and instantaneous capture of the separation mode of the Single TEG | 44 |
| 2.8 | The mechanism of vertical contact-separation-compress state | 45 |
| 2.9 | FC- TEG on the separation, contact, and compression mode | 45 |
| 2.10 | Voltage and stroke for all taping mechanism on 10 Hz | 47 |
| 2.11 | Voltage and stroke for all taping mechanism on 20 Hz | 47 |
| 2.12 | Voltage and stroke for all taping mechanism on 30 Hz | 48 |
| 2.13 | Comparison of best taping mechanism on various contact areas | 48 |

| | | |
|------|--|----|
| 2.14 | Three working modes and time histories of the FC-TEG | 50 |
| 2.15 | Time history of FC-TEG in the Separation mode ($A_v = 0.3$ mm, $f_v = 10$ Hz) | 52 |
| 2.16 | Time history of FC-TEG in the Contact mode ($A_v = 0.5$ mm, $f_v = 10$ Hz) | 52 |
| 2.17 | Time history of FC-TEG in the Compress mode ($A_v = 0.9$ mm, $f_v = 10$ Hz) | 52 |
| 2.18 | Effect of initial separation distance and separation velocity on the output voltage | 54 |
| 2.19 | The $V - \delta'$ diagram in separation mode | 56 |
| 2.20 | The $V - \delta'$ diagram in contact mode | 57 |
| 2.21 | The $V - \delta'$ diagram in compress mode | 58 |
| 2.22 | Comparisons of the $V - \delta'$ diagrams from all cases | 59 |
| 2.23 | Time histories of output voltage and separation velocity: (a) separation mode ($A_v = 0.3$ mm), (b) separation mode ($A_v = 0.4$ mm), (c) contact mode ($A_v = 0.5$ mm), (d) compression mode ($A_v = 0.6$ mm), and (e) compression mode ($A_v = 0.9$ mm) | 61 |
| 2.24 | Relationship between max./min. output voltages and separation frequency | 62 |
| 2.25 | Relationship between max./min. output voltages and separation velocities | 63 |
| 2.26 | Relationships between the output voltages and the compression load of the FC-TEG | 65 |
| 2.27 | Relationships between the output voltages and the vertical strain rates of the FC-TEG | 66 |
| 3.1 | Theoretical model of power generation of the FC-TEG in three different modes | 73 |
| 3.2 | Comparisons of the time histories of output voltage, separation stroke, and separation velocity in separation mode ($A_v = 0.3$ mm). | 78 |

| | | |
|------|--|----|
| 3.3 | Comparisons of the time histories of output voltage, separation stroke, and separation velocity in separation mode ($A_v = 0.4\text{mm}$). | 79 |
| 3.4 | Comparisons of the time histories of output voltage, separation stroke, and separation velocity in separation mode ($A_v = 0.5\text{mm}$). | 80 |
| 3.5 | Comparisons of the time histories of output voltage, separation stroke, and separation velocity in contact mode ($A_v = 0.6\text{mm}$). | 81 |
| 3.6 | Comparisons of the time histories of output voltage, separation stroke, and separation velocity in compress mode ($A_v = 0.8\text{mm}$). | 82 |
| 3.7 | Comparisons of the experimental and theoretical averaged output voltages at a vibration frequency of 10 Hz | 83 |
| 3.8 | Comparisons of the experimental and theoretical averaged output voltages at a vibration frequency of 20 Hz | 84 |
| 3.9 | Comparisons of the experimental and theoretical averaged output voltages at a vibration frequency of 30 Hz | 85 |
| 3.10 | Comparisons of the experimental and theoretical averaged output power density at a vibration frequency of 10 Hz | 86 |
| 3.11 | Comparisons of the experimental and theoretical averaged output power density at a vibration frequency of 20 Hz | 87 |
| 3.12 | Comparisons of the experimental and theoretical averaged output power density at a vibration frequency of 30 Hz | 88 |
| 3.13 | Estimations of the maximum output voltage versus separation frequency and separation velocity. | 89 |
| 3.14 | Estimations of the maximum output power density versus separation frequency and separation velocity. | 90 |

| | | |
|------|---|-----|
| 4.1 | Multi-layer TEG device. | 99 |
| 4.2 | Vertical vibration setup | 101 |
| 4.3 | Comparison of the single layer and multi-layered TEG output voltage | 102 |
| 4.4 | Relationship between vibration amplitude and multi-layered TEG electrical output on selected initial distance condition. | 104 |
| 4.5 | Relationship between vibration amplitude and initial distance on various frequencies. | 106 |
| 4.6 | Relationship between vibration frequency and initial distance on various amplitude. | 107 |
| 4.7 | TEG output voltage and its separation stroke on frequency 20 Hz, $A_v = 6.0$ mm and $\delta_c = 3.0$ mm – contact mode | 109 |
| 4.8 | TEG output voltage and its separation stroke on frequency 20 Hz, $A_v = 6.0$ mm and $\delta_c = 2.5$ mm – compress mode | 109 |
| 4.9 | Comparison of the single-layer TEG and multi-layered TEG output voltages (contact mode) | 110 |
| 4.10 | Comparison of the single-layer TEG and multi-layered TEG output voltages (compress mode) | 111 |
| 4.11 | Comparison of the single-layer TEG and multi-layered TEG power density (contact mode) | 112 |
| 4.12 | Comparison of the single-layer TEG and multi-layered TEG power density (compress mode) | 113 |
| 4.13 | Example of the TEG output voltage in contact mode ($f_v = 20$ Hz, $A_v = 4.0$ mm, $\delta_c = 20$ mm. | 116 |
| 4.14 | Example of the TEG output voltage in compress mode ($f_v = 20$ Hz, $A_v = 4.0$ mm, $\delta_c = 7$ mm. | 117 |

| | |
|--|-----|
| 4.15 Relationship between compression force and acceleration amplitude with TEG output voltage. | 118 |
| 4.16 Power density of the multi-layer TEG device in this experiment | 120 |
| 4.17 State-of-art ocean sensors and ocean sensors system that could be powered with the Multi-layer TEG [Zhao et al., 2021] | 121 |
| 5.1 PEG device | 128 |
| 5.2 TEG-PEG device | 129 |
| 5.3 Concept of the TEG-PEG device as ocean energy harvester network | 130 |
| 5.4 Indonesia's regional map of annual and seasonal wave properties. Middle figures is showing the mean period in Indonesia's ocean [Kench and Mann, 2017] | 132 |
| 5.5 Applications of the additional part for improving TEG output - Gear and flywheel. | 133 |
| 5.6 Applications of the additional part for improving TEG output - Spring | 134 |
| 5.7 Vibration experiment setup case 1 | 136 |
| 5.8 Vibration experiment setup case 2 | 139 |
| 5.9 Example of the TEG-PEG output voltage on study case 1 | 142 |
| 5.10 Relationship of compression force with PEG max voltage | 143 |
| 5.11 Relationship of PEG free end amplitude with the PEG output voltage | 143 |
| 5.12 Relationship of compression force with TEG max voltage | 144 |
| 5.13 Relationship of PEG free end amplitude with the TEG output voltage | 144 |
| 5.14 Example of the TEG-PEG output voltage on study case 2 | 145 |
| 5.15 TEG-PEG output voltage on study case 1 | 146 |
| 5.16 TEG-PEG output voltage on study case 2 | 147 |

5.17 Relationship between the output voltage and vibration amplitude 150

5.18 Relationship between the electrical output per area and vibration amplitude . . 151

5.19 Relationship between the initial distance and electrical output on frequency 5 Hz 153

5.20 Relationship between the initial distance and electrical output on frequency 10 Hz 153

5.21 Relationship between the initial distance and electrical output on frequency 20 Hz 153

5.22 Relationship between the initial distance and electrical output on frequency 30 Hz 154

5.23 Relationship between the electrical output and the initial distance (δ_c) on PEG. 156

5.24 Relationship between the electrical output and the initial distance (δ_c) on TEG. 158

5.25 Relationship between the electrical output and the initial distance (δ_c) on the
vibration frequency ($f_v= 30$ Hz). 161

5.26 Multi-layer TEG power density on the Hybrid Harvester. 164

5.27 Flexible PEG power density on the Hybrid Harvester. 166

5.28 State-of-art ocean sensors and ocean sensors system that could be powered with
the Hybrid Harvester [Zhao et al., 2021] 167

6.1 Details of the Future work of the TEG-PEG ocean energy harvester 177

Chapter 1

Introduction

1.1 Background

1.1.1 Internet of things and its power source

The Internet of Things (IoT) is a term to describe the rapid evolution of information and communications (ICT) to improve society. In addition, the development of ICT also created a new Microelectromechanical system (MEMS) (also referred to as micromachines or microsystem technology) based on the silicon revolution. Typically, the MEMS devices are sized at the nanoscales level between 1 and 100 micrometers in size (i.e., 0.001 to 0.1 mm) with total devices size range from 20 micrometers to a millimeter (i.e., 0.02 to 1.0 mm). The main points of the IoT and MEMS are utilizing a billion/trillion, micro/nano scale size, and interconnected electronics as sensors/actuators in a decentralized place. The distribution of the sensors/actuators created a distributed intelligence and provided multiple information to help the decision-making process. The development of the IoT and MEMS signals a new age of society named society 5.0, which is the new concept for a digital society in the future. The usage of the IoT was also developed, and one of the examples made by the Shiojiri-Japan city council could be seen in Fig.1.1 [Narvaez Rojas et al., 2021].

Many daily devices commonly used in daily lives are moving towards the IoT concept. One

of the main proof is smartphones, computers, and wearable devices as sensors to measure our health and environmental condition. Researchers believe that the number of devices will increase exponentially around 2020 – 2025, as shown in Fig.1.2 [Safaei et al., 2018]. Due to the rapid increase of the items, stable, efficient, and dependable power sources are heavily needed for the IoT networks devices.

Abhi Raj and Dan steingart have reviewed currently available power sources to power the IoT devices. Based on their findings, three types of power sources, namely: storage type, distribution, and harvesting, are commonly used, as shown in Fig.1.3 [Raj and Steingart, 2018]. Since it has high output; batteries, supercapacitors, and micro-fuel cells are the most commonly used items. However, there are major drawbacks since it has only a finite amount of energy available. The battery, in particular, constantly needs to be changed/charged once it is run out, which makes it not suitable for the long-term power source of the billions of IoT electronics in the very near future. In addition, there are concerns about the maintenance cost and difficult accessibilities if the IoT electronics are in a hazardous location or difficult places (such as the ocean or inside the human body), and potential environmental issues for the battery. To accommodate this issue, this research proposed “energy harvesting” as one of the alternative solutions for the power source.

1.1.2 Energy Harvesting

The energy harvesting method (or scavenging) collects tiny amounts of dissipating energy to be converted into electrical energy [Akinaga et al., 2018, D., 2005, Krikke, 2005]. The main benefit of this type of energy harvesting is the longevity of electrical energy. Energy harvesting has gained much popularity due to the recent reduction in power consumption for the sensors and actuators, which is typically only needed around 10 μ W as illustrated in Fig.1.4. Therefore, this type of energy harvesting could charge the device independently, without constant monitoring and supervision, and without maintenance.

Energy converters such as solar panels, ocean wave energy, or wind power plants are considered conventional energy harvesting. As a conventional energy harvesting technology, they typically

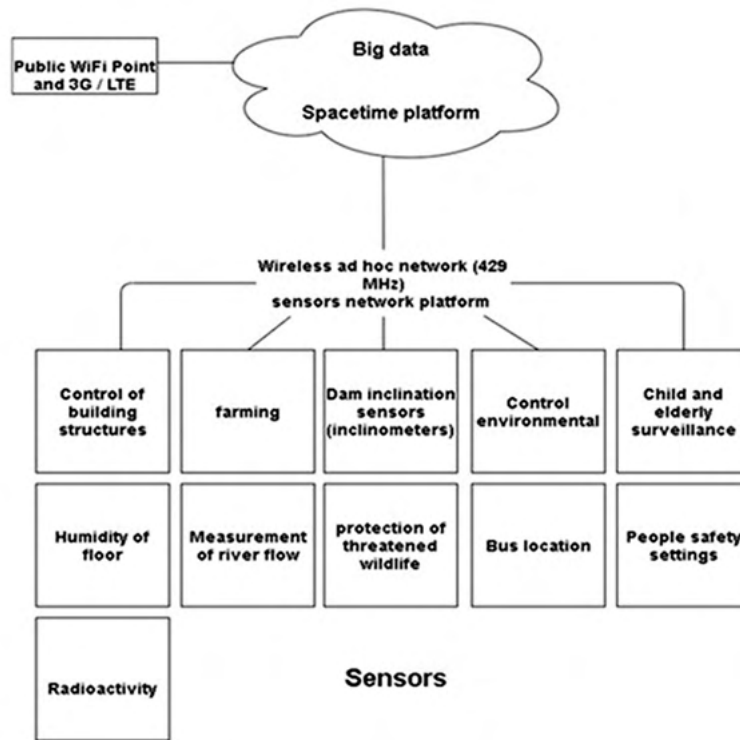


Figure 1.1: Shiojiri environmental data and the IoT sensor network [Narvaez Rojas et al., 2021]

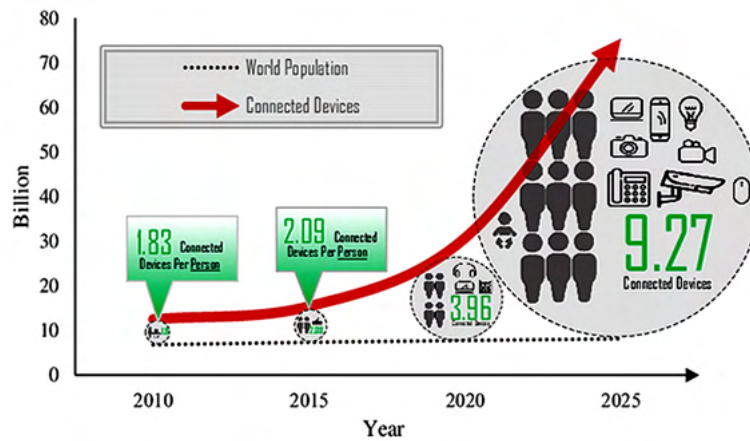


Figure 1.2: Estimated of the device usage for each person [Safaei et al., 2018]

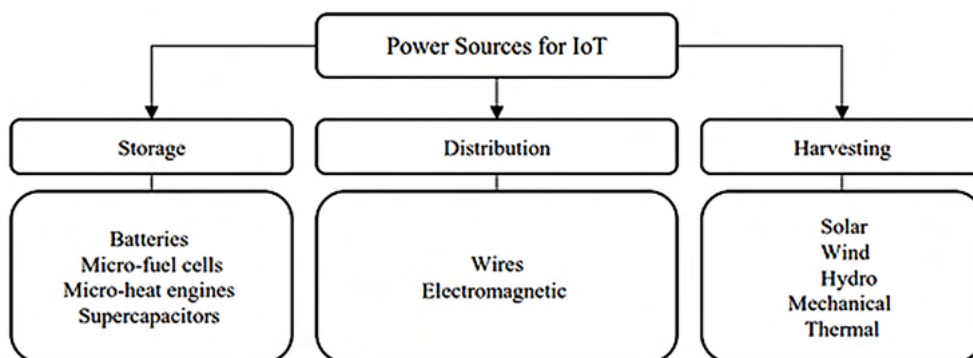


Figure 1.3: Power sources for IoT [Raj and Steingart, 2018]

have a large-capacity power generation facility that connects to a grid power source as a farm of their respective natural energies. However, due to the need for grid power sources, it is difficult to apply this type of technology for the small wireless sensor network in the IoT and MEMS, especially if they have a long physical distance from the power supply. To accommodate these problems, a new type of energy harvesting is actively proposed based on the mechanical source on a small scale (i.e., nanogenerators, micro generator or any device that uses the ***displacement current*** From *Maxwell-Heaviside equations* as the main force to convert mechanical energy into electric power/signal).

One of the most promising concepts of these generators is utilizing vibrational energy harvesting based on the mechanical vibration around our environment. Four methods are commonly used to generate electrical power: Inverse magnetostriction, Electromagnetic induction, Piezoelectric effect, and Electrostatic Induction, shown in Fig.1.5. The inverse magnetostriction typically harvests the vibrational energy using the rare-earth iron alloy Terfenol-D and the Fe-Ga alloy Galfenol to produce the electrical energy [Palumbo et al., 2019]. Electromagnetic induction typically combines the electric current and magnetism by changing the magnetic flux penetrating the coil due to the relative movement of the coil and magnet. The electromagnetic induction is very durable; however, it is often inefficient both at low frequencies and small sizes, making it not ideal for IoT devices. Therefore, two remaining methods are commonly used and developed as a power source for the sensors/actuators.

The piezoelectric devices use the piezoelectric effect that deformed due to the mechanical movement, causing electric charges within the crystal disrupted. The resulting positive and negative charges are then collected by the metal plates usually placed on top and bottom piezoelectric material and used as voltage to create electric current to generate electricity. The piezoelectric effect also works in reverse; when the electrical energy is applied to the piezo material, the crystals expand and contract to release the mechanical energy. The piezoelectric generator (PEG) or also called as piezoelectric nanogenerator (PENG) or piezoelectric harvester (PEH) is very suitable for many applications since it can produce high output voltage and easily integrate with small electronics. However, the production cost due to the quality of materials used is one of its drawbacks.

On the other hand, developing a power generation device using electrostatic induction is also mainly used. The electrostatic device can reversibly convert mechanical and electrical energy in the same way as piezoelectric materials. In addition, unlike existing power generating materials (electrets and piezoelectric elements), it does not require voltage application or polarization processing, so the impact on production costs is negligible. Since this harvesting device also uses the triboelectric effect, it is commonly called a Triboelectric generator (TEG) or triboelectric nanogenerator (TENG) or as triboelectric harvester (TEH). The TEG typically offers high-output voltages and is easy to scale + adjustable (making it a low-cost system). One of the PEG and TEG application requirements is the constant movement sources. Therefore, various natural sources formerly used by conventional energy harvesting technology can also be applied to PEG and TEG. This includes the usage based on the wind, human motion, machinery, and ocean field. Several findings from various researchers based on the field as mentioned above are explained in the following sub-section.

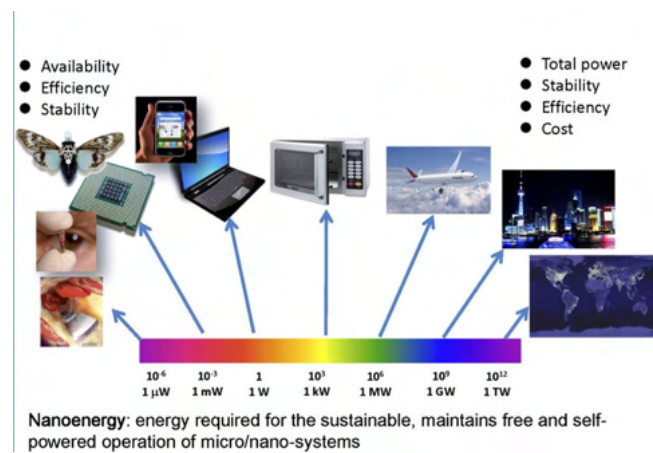


Figure 1.4: Electronics component and its power requirements [Zi and Wang, 2017]

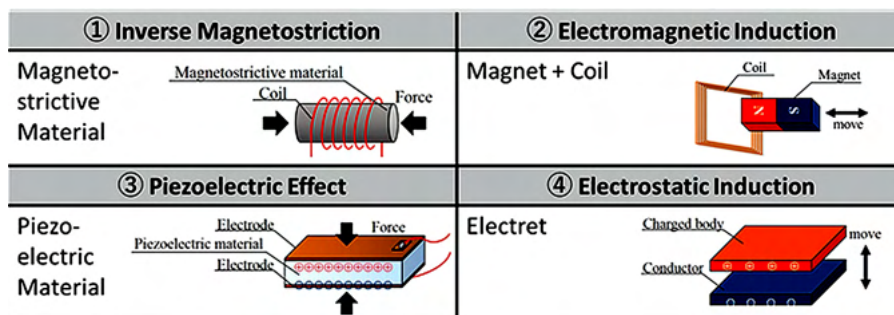


Figure 1.5: Four power generation methods in vibration power generation

1.1.3 Previous research of Piezoelectric generator and triboelectric generator

Wang proposes a summary of the nanogenerators' three major application fields as a micro-/nano-energy source, blue energy, and self-powered systems that could be seen in Fig.1.6 [Wang, 2017b]. The applications of TEG and PEG are based on the mechanical energy available around our environment [Haroun et al., 2021]. Examples of such mechanical motions could be wind currents [Gong et al., 2019, Han et al., 2020], human motion, and ocean waves. This indicates that both TEG and PEG are very versatile, and many concepts and ideas could be applied to maximize the energy harvesting process. Current and ongoing concepts + ideas developed by various researchers are presented in the next mini-subsections as an example:

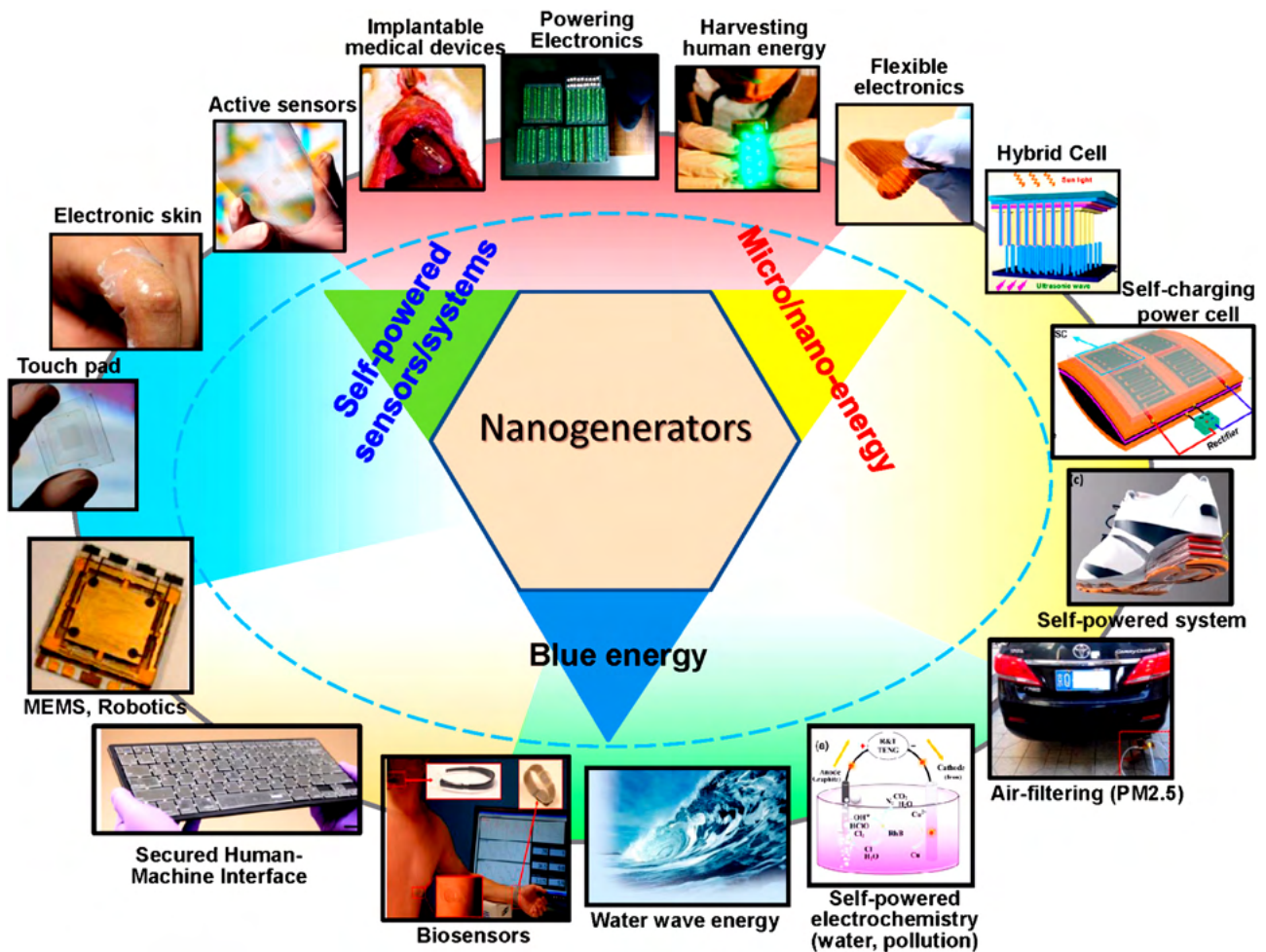


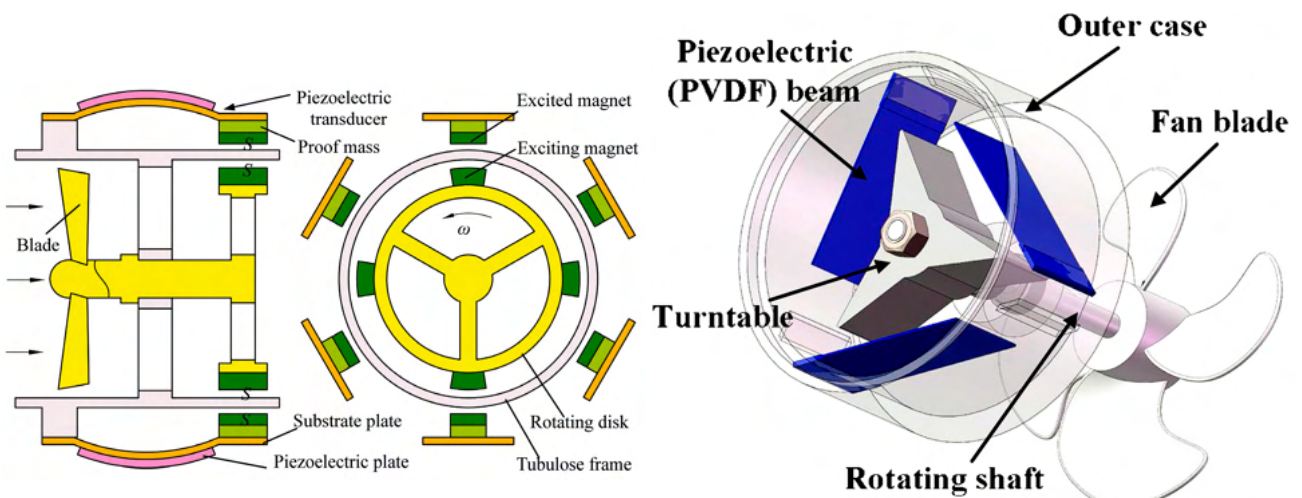
Figure 1.6: Three major applications of the nanogenerators [Wang, 2017a]

Wind Energy

Wind energy mainly consists of two types of energy harvesting: the rotational and vibration energy harvester. The proposed ideas of the rotational harvester for PEG mainly use the rotating blade with either the PEG beam layer attached to the body [Kan et al., 2016, Zhang et al., 2017], bluff bodies [Liu et al., 2019, Wang et al., 2020], or “flag” shape [Orrego et al., 2017]; with the figures shown in Fig.1.7. On the other hand, the example of vibrational wind harvesters are a wind tunnel or flow-induced concept. A wind-rolling type of trapping wind + moving the sphere; and the flow-induced vibration type TEG are shown in Fig.1.8 to illustrate the wind utilization for the TEG device [Yong et al., 2016, Zeng et al., 2020].

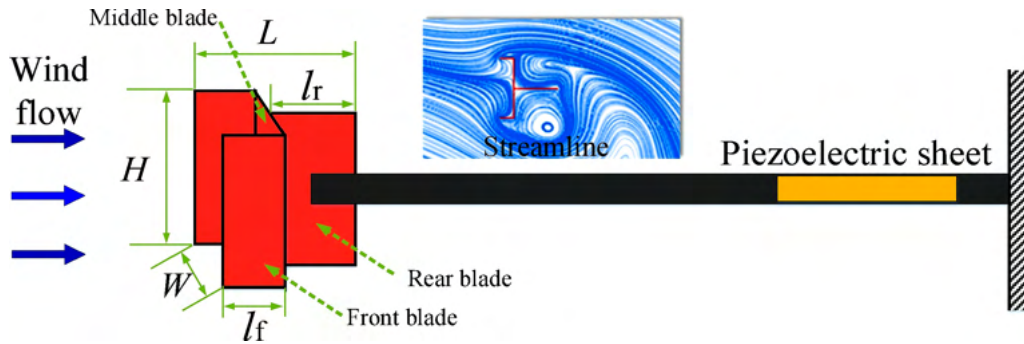
Human movement

Energy harvesting based on human movement mainly has benefits with its main purpose to provide information on human health. Since the device is placed very closely with the human body; the data could transfer instantly to monitor, or power up the device to improve human lives. In terms of device placement, two types are mainly being researched: the harvesting via body parts movement and in-vivo systems. The example of the body parts movement is shown in Fig.1.9a and Fig.1.9b, which uses the jaw movement and walking+running movement on wearable devices [Delnavaz and Voix, 2014, Niu et al., 2015, Zou et al., 2020]. The concept of the in-vivo systems as implantable medical devices with TEGs as its power source is shown in Fig.1.9c [Dagdeviren et al., 2014, Lin et al., 2014, Mannsfeld et al., 2010, Zhou et al., 2014]. recent progress regarding the study of biomedical applications with PEG and TEG could be seen in Zheng et al works [Zheng et al., 2017].



(a) Piezo-windmill [Kan et al., 2016]

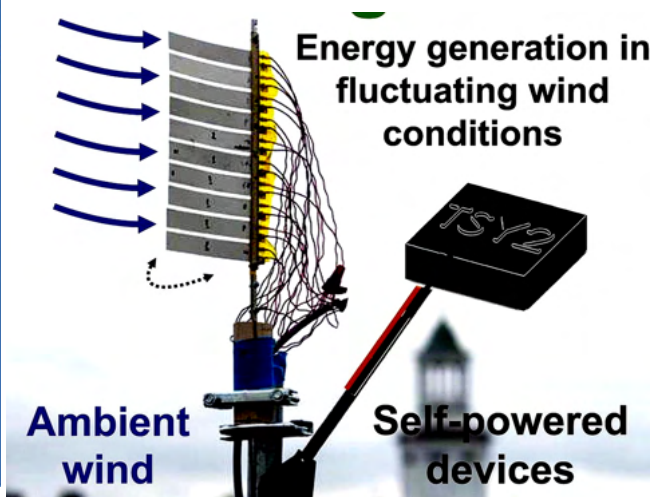
(b) PVDF beam in a rotational piezoelectric energy harvester [Zhang et al., 2017]



(c) fork-shaped bluff body [Liu et al., 2019]

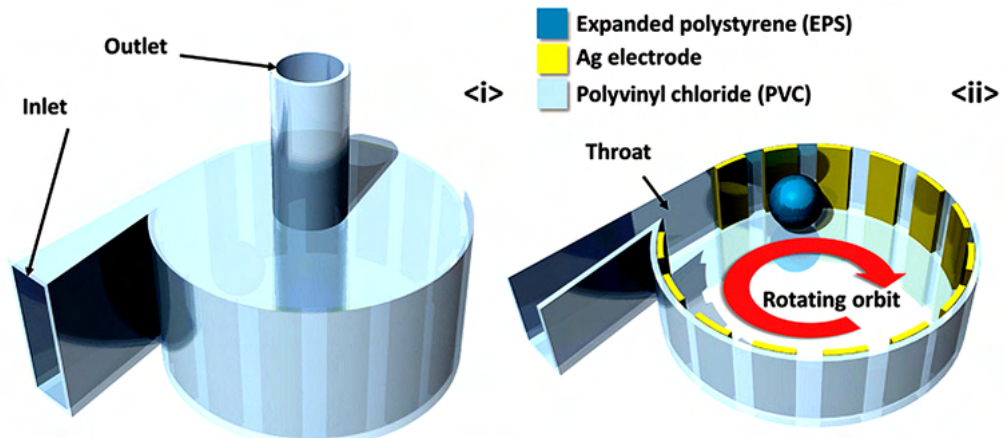
| | | Proposed bluff bodies | | | | Conventional bluff bodies |
|------------|-----------|-----------------------|------------|------------|----------|---------------------------|
| Direction | Shape | $\eta=0.3$ | $\eta=0.5$ | $\eta=0.7$ | $\eta=1$ | |
| Vertical | Spindle | | | | | Cuboid |
| | Butterfly | | | | | |
| Horizontal | Spindle | | | | | |
| | Butterfly | | | | | |

(d) Various bluff body shapes including Spindle-like and butterfly-like cross-sections [Wang et al., 2020]

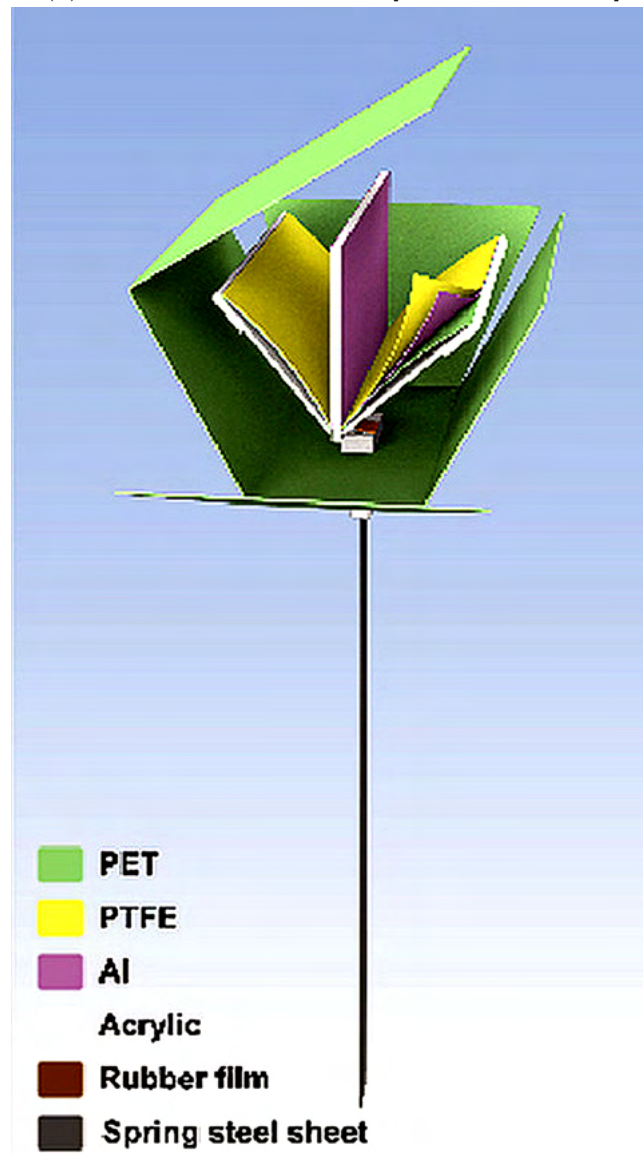


(e) Piezoelectric flag. [Orrego et al., 2017]

Figure 1.7: Several Wind energy PEGs.



(a) wind-rolling type TEG [Yong et al., 2016]



(b) flow-induced vibration type TEG [Zeng et al., 2020]

Figure 1.8: TEG's wind energy harvester

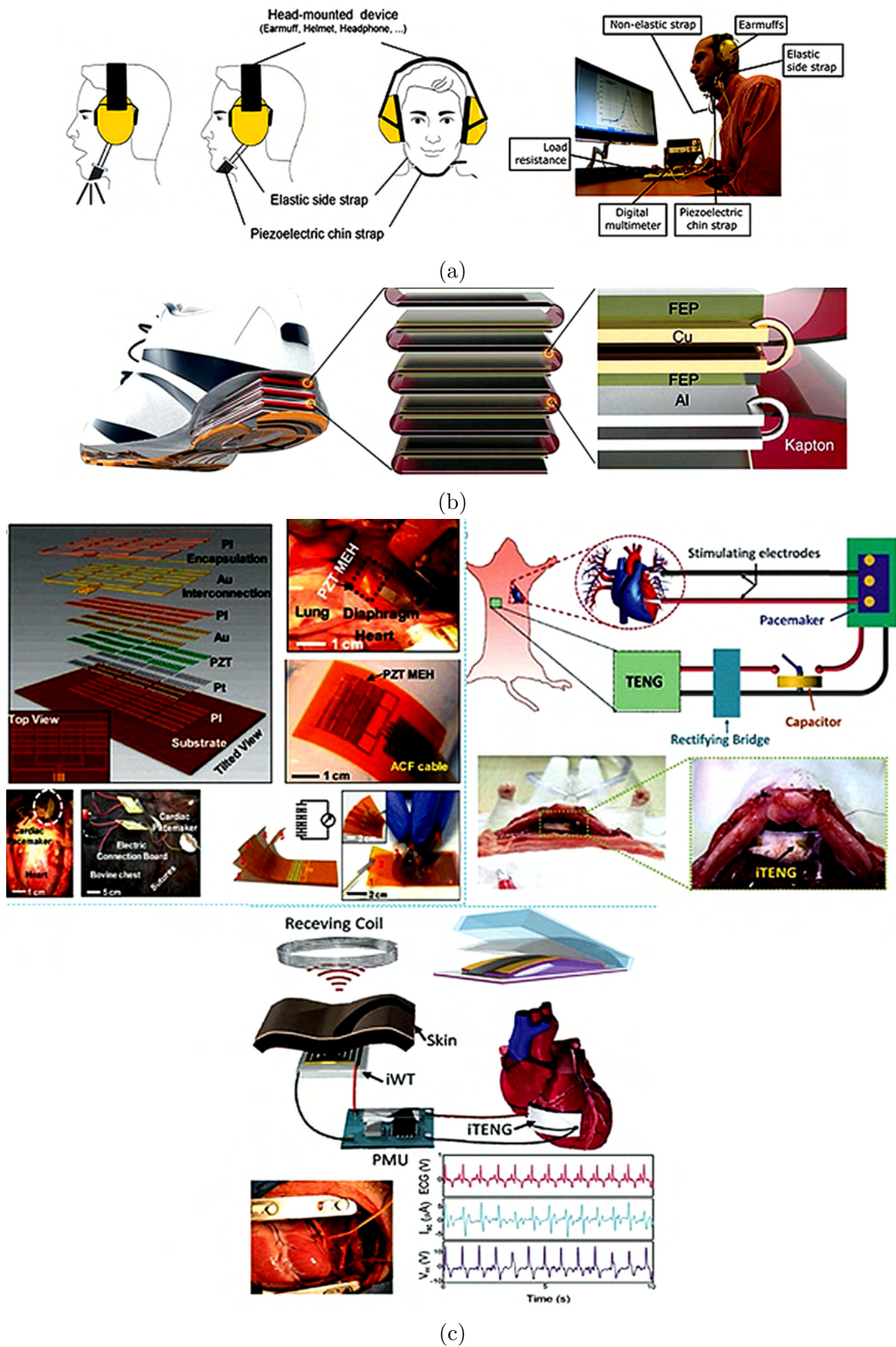


Figure 1.9: Nanogenerators based on human movement. (a) PEG based on jaw movement [Delnavaz and Voix, 2014]; (b) TEG on the wearable devices [Zou et al., 2020, Li et al., 2017, Rodrigues et al., 2019]; and (c) in-vivo energy harvesting for biomedical applications [Dagdeviren et al., 2014, Lin et al., 2014, Mannsfeld et al., 2010, Zhu et al., 2014b]

Machine vibration

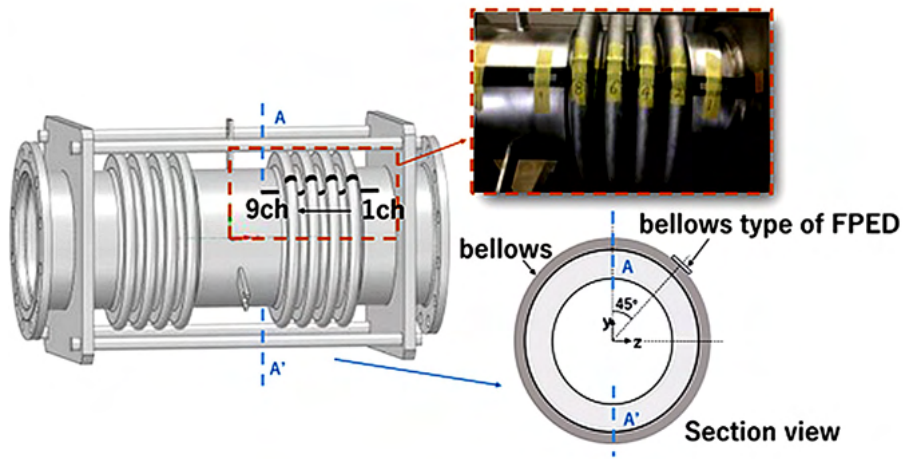
The machinery engine generates a fair to disturbing amount of vibration. Due to the vibration that could cause disruption, some dampers are commonly installed. This excess vibration could then be used as the primary vibration source for the generators. The generators are then used to power up microsensors to monitor the engine's health or the supporting system (such as the pipeline or the piping system). The example of the machine vibrations energy harvesting with PEG is shown by Xinru Du et al. with the usage of a bellows-type of a flexible piezoelectric device (FPED) to monitor the pipeline device's structural health [Du et al., 2020]. For TEG, the honeycomb structure and the bouncing-ball triboelectric nanogenerator extracted the vibration energy as self-powered engine condition monitoring [Xiao et al., 2019, Du et al., 2021]. The illustration of both PEG and TEG based on the machine vibration can be seen in Fig.1.10.

Ocean energy

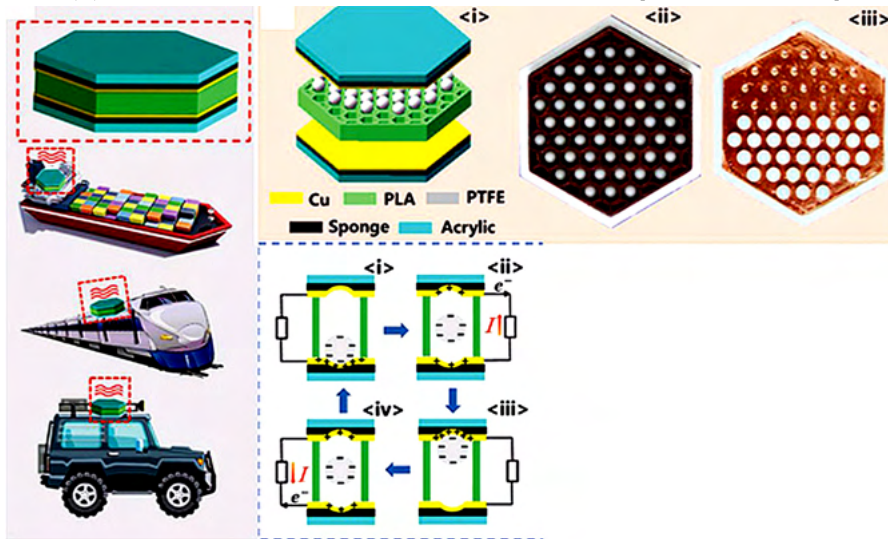
Ocean energy is the sector where it could provide a high energy source for the generators. The reason for this is due to the space availability and the energy density inside the ocean itself. Ocean energy contains various energy distributions. The illustration of these energy wave scales is commonly pioneered by Kinsman, as shown in Fig.1.11 with the wave period and its power spectrum [Kinsman, 1984]. The waves caused by the wind and gravity (namely, the tidal energy and wave energy) have the largest energy scale that could be applied for the generators. Additionally, the ocean in the other period also showed a small energy density. This small energy density is specifically suitable for TEG that could harvest low mechanical energy.

Zhao et al argue that there is three resource zone in the ocean kinetic energy with the ocean wave energy resource zone, wave and current interaction zone, and the marine current energy resource zone shown in Fig.1.12. Consequently, ocean energy harvesters could be developed based on the usage of those three ocean positions.

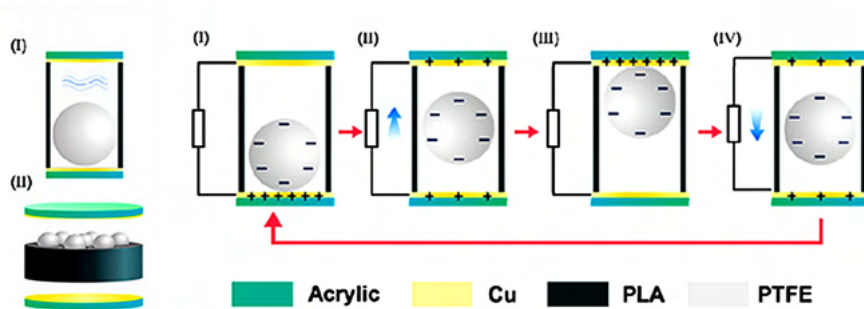
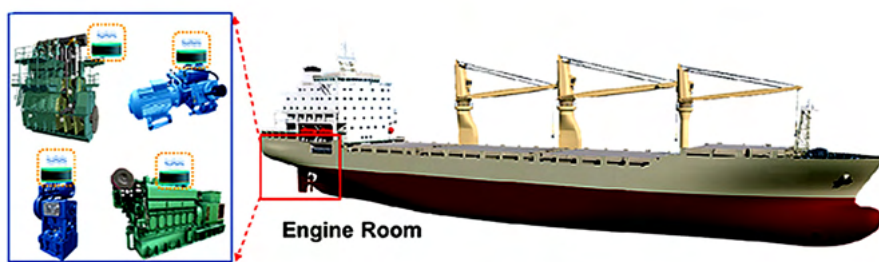
One of the generator applications on the ocean surface (wave energy resource zone) is using the



(a) Bellows-type flexible piezoelectric device [Du et al., 2020]



(b) Honeycomb structure for self-powered engine monitoring [Xiao et al., 2019]



(c) Bouncing ball for the ship equipment vibration monitoring [Du et al., 2021]

Figure 1.10: Applications of the machine vibration energy harvesting.

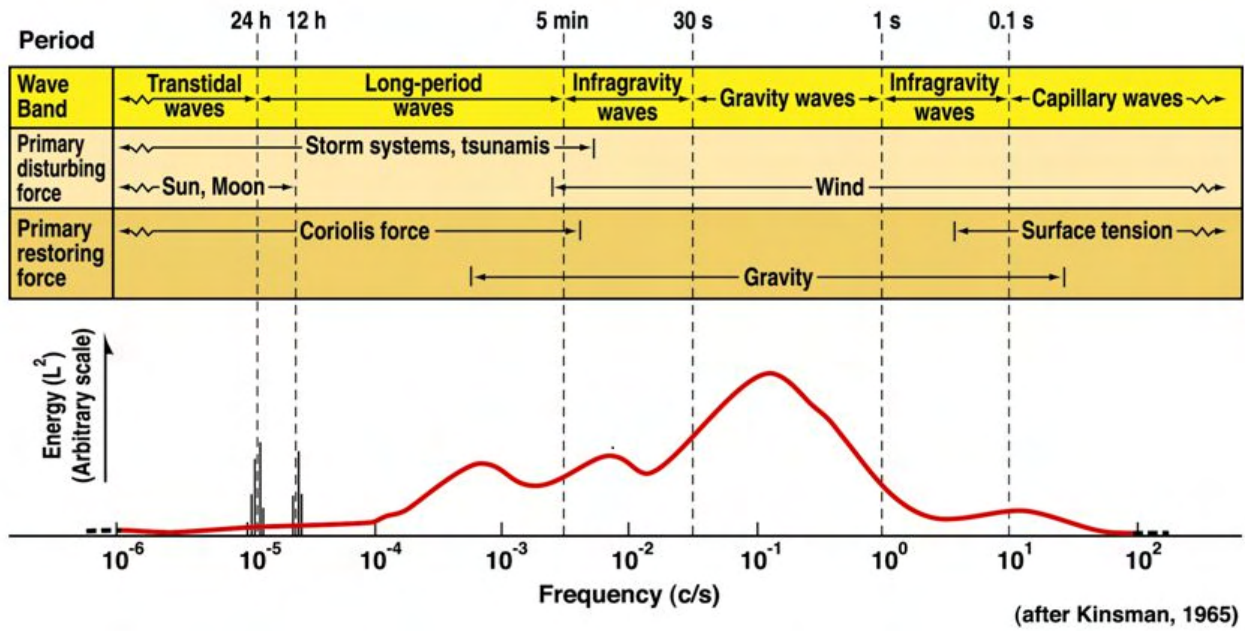


Figure 1.11: Energy density in each period of the ocean movements [Kinsman, 1984]. Source: Source : Renewable Energy Technologies for Sustainability

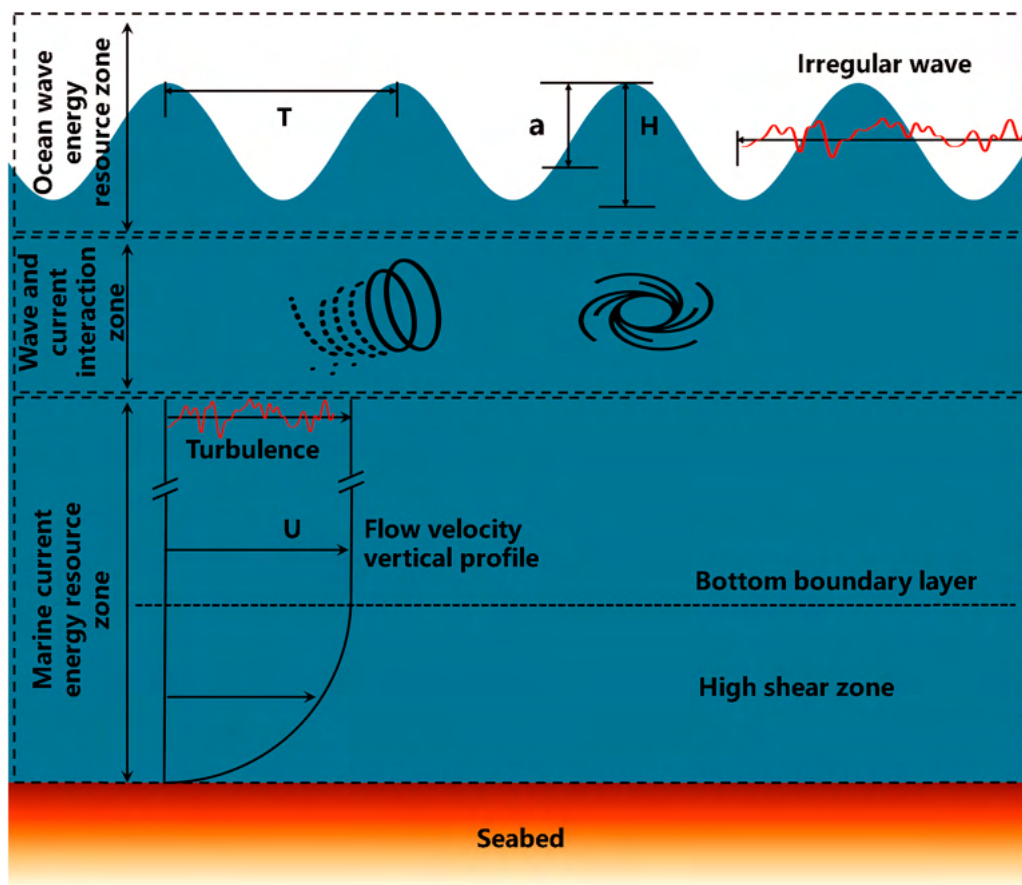
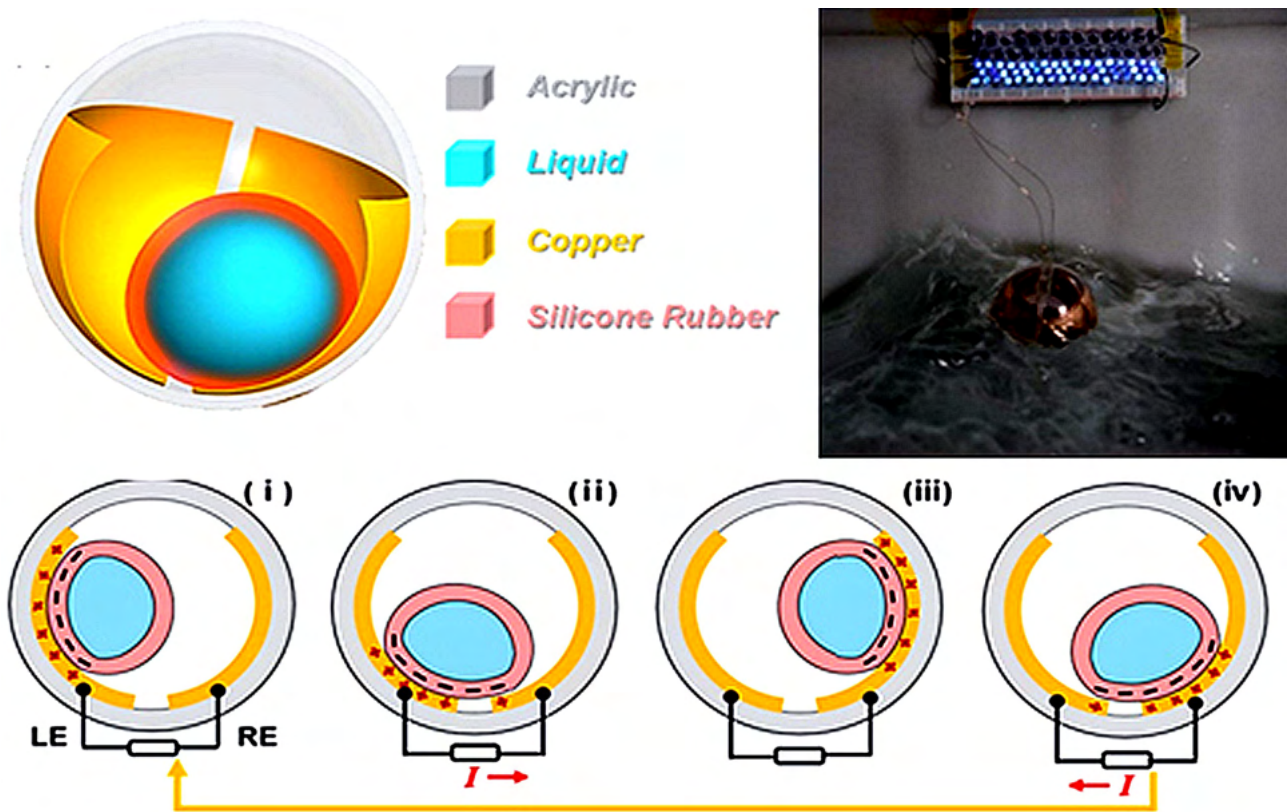


Figure 1.12: Resource zone of the Ocean kinetic energy [Zhao et al., 2021]

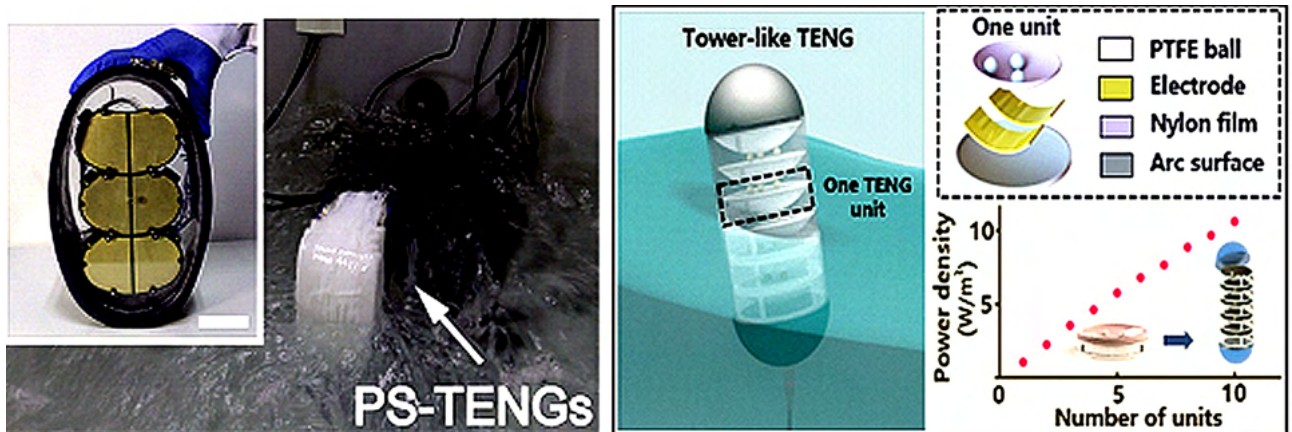
ball inside a sphere-shaped structure to roll and transfer the electrical energy [Wang et al., 2015, Yuan et al., 2021]. This idea was then improved in 2 ways by stacking the TEG in a pendulum system [Zhong et al., 2019] or distributing the TEGs on a vast ocean space and connecting them to an ocean energy harvesters networks [Xu et al., 2018]. The illustration of This spherical TEG network can be seen in Fig.1.13.

On the wave and current interaction zone, there is a mix between the ocean wave in the surface and current. Due to this mixing, it is predicted that the ocean energy density in this zone is much higher than on the ocean surface. Based on that prediction, many PEG devices could be deployed to harvest the energy. An example of this concept is proposed by Mutsuda et al. using the FPED in an EFHAS – elastic floating unit with hanging structures [Mutsuda et al., 2013]. By placing the FPED on both zones (the ocean surface and the area below the ocean surface). For TEG in this zone, the liquid-solid contact-based TEG has mainly been used [Zhu et al., 2014a, Li et al., 2018, Xu et al., 2019a]. In this design, the structure (either square-shaped or its improvement) is placed in front of the wave to absorb the contact. Once the water comes up inside the model, the water will transfer from one layer to another to transfer the electron and generate electrical output. The illustration of PEG and TEG used on the wave, and current interaction zone is shown in Fig.1.14.

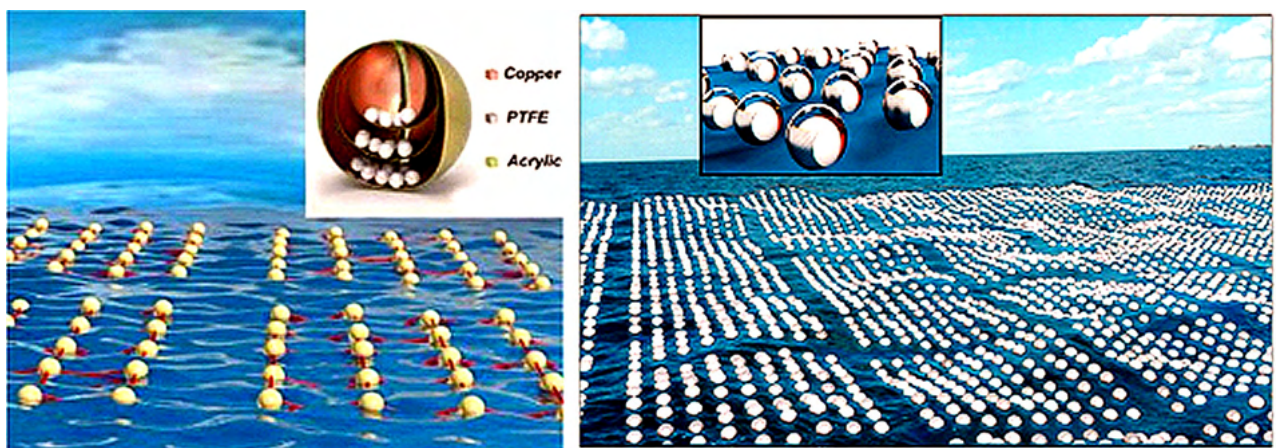
Marine current energy resource zone is where several underwater vehicles (AUV) or observation ROV system devices are located. Due to this zone being located deeply in the ocean, the deployment of ocean harvesters tends to be very difficult. Some underwater PEG and TEG technology are developed in this zone with a submerged body in mind. For PEG, the energy harvesting eel concept made with the piezoelectric polymers behind a bluff body is mainly considered as the main concept in this zone [Taylor et al., 2001], with the experimental investigation under a controlled environment has been studied in 2020 to investigate its electrical output [Latif et al., 2020]. This concept gave a similar idea for TEG with Yan wang et al proposed and investigated the flag-like triboelectric generator to harvest the flow-induced vibration on the extremely low-velocity ocean current [Wang et al., 2021]. The concept and placement for the PEG and TEG in the deep ocean can be seen in Fig.1.15.



(a) Ball inside a sphere-shaped structure [Cheng et al., 2019]

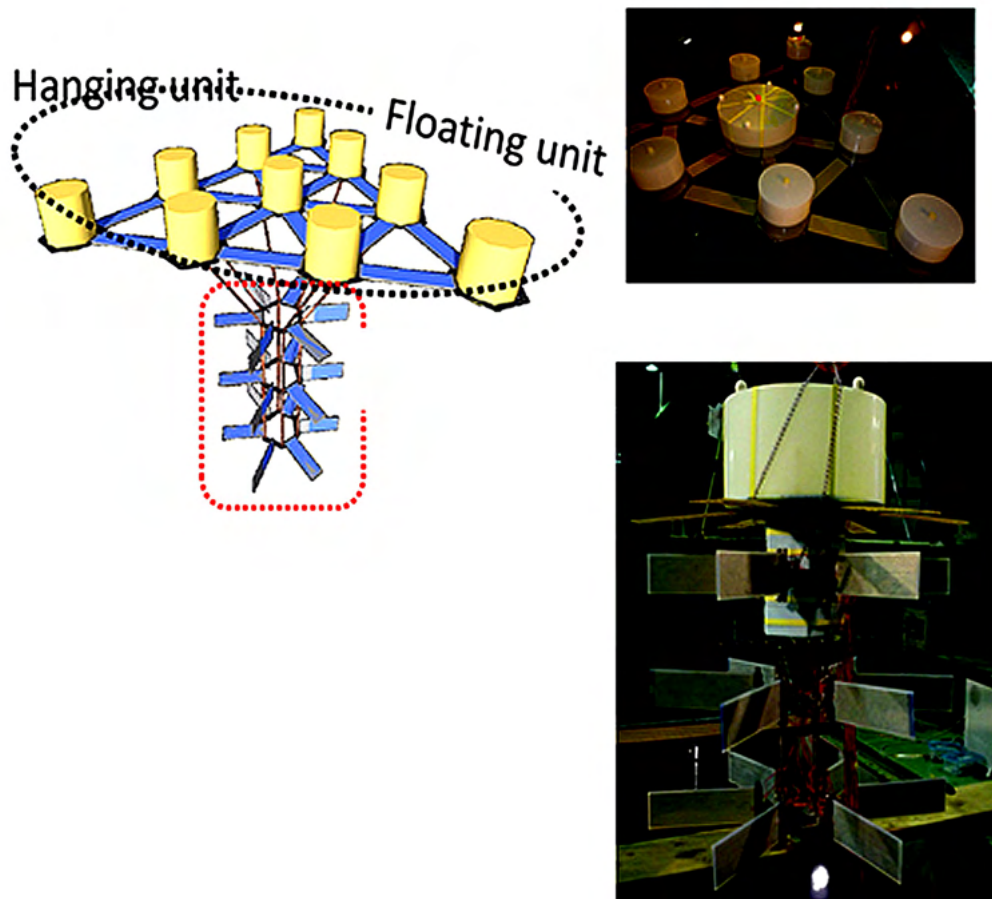


(b) Stacked ocean harvesters using TEG [Zhong et al., 2019]

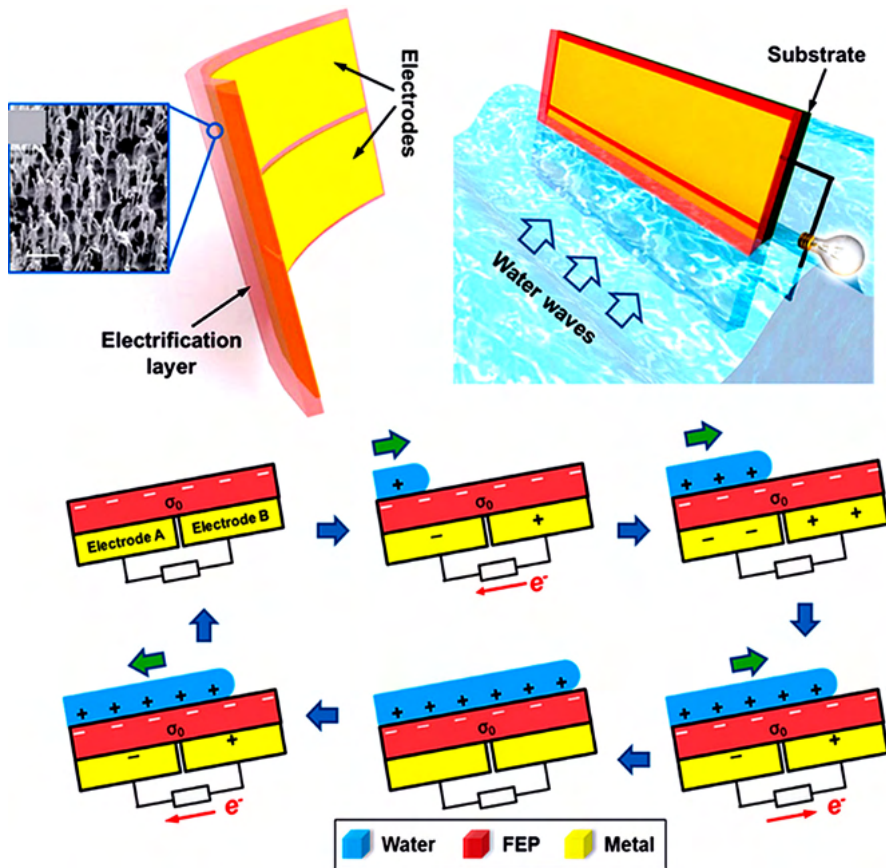


(c) Networks of the spherical ball based TEG for large-scale blue energy harvesting [Wang, 2017a]

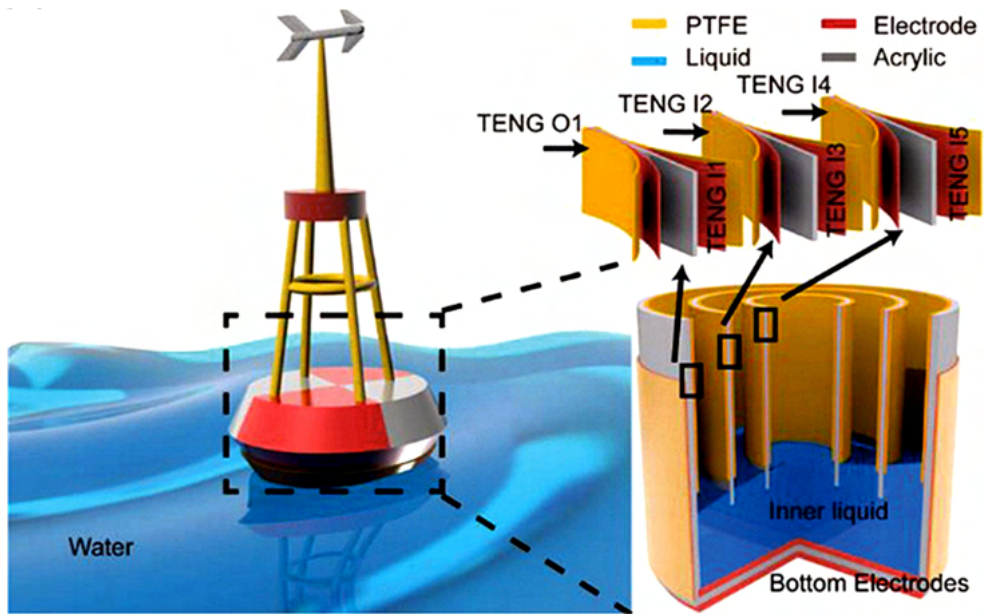
Figure 1.13: Several applications of the ocean generators with the rolling ball concept.



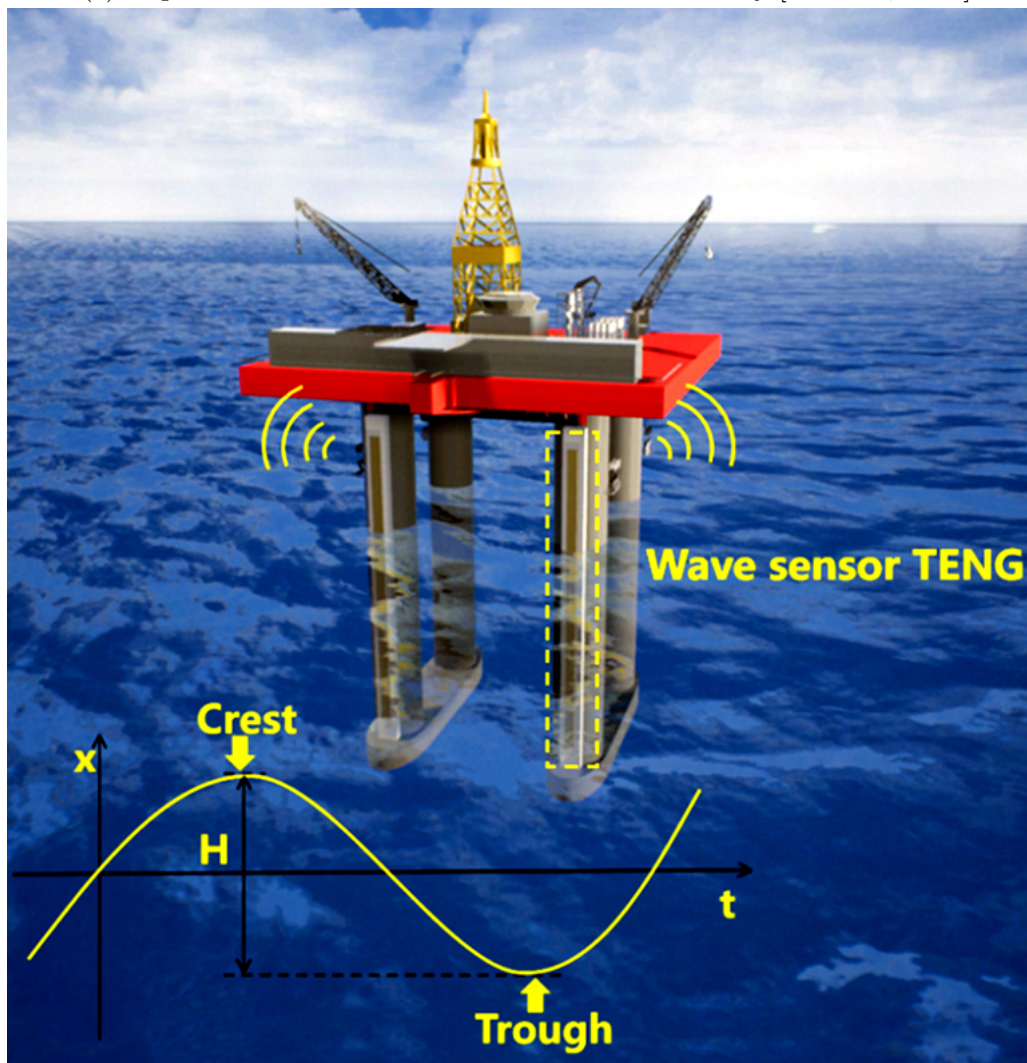
(a) FPED on the EFHAS structure [Mutsuda et al., 2012, Mutsuda et al., 2013],



(b) Liquid-solid TEG on a thin film surface [Zhu et al., 2014b]

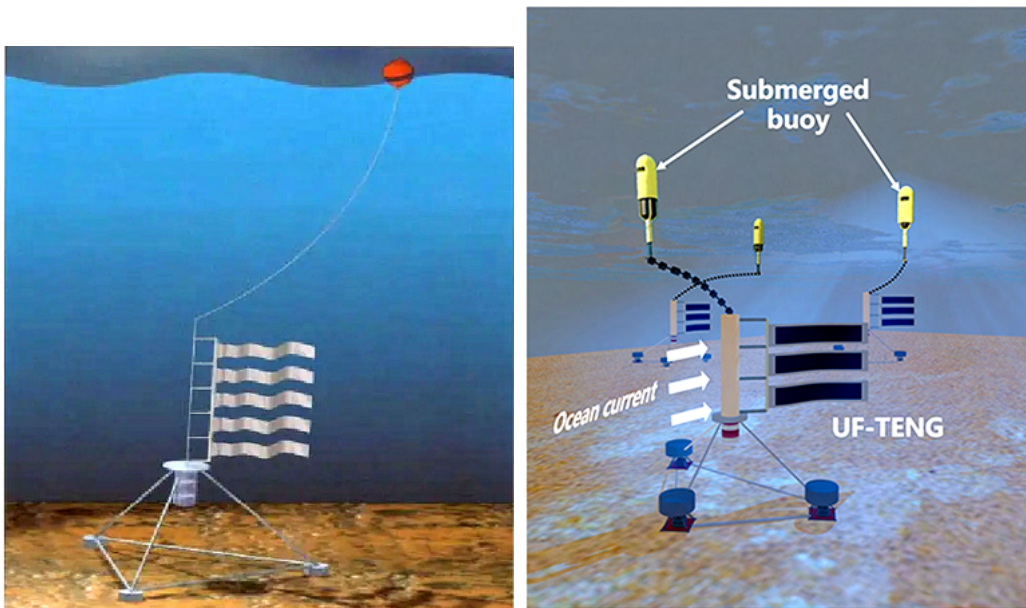


(c) Liquid-solid TEG contact electrification on a buoy [Li et al., 2018]



(d) Liquid-solid TEG for wave sensor [Xu et al., 2019b]

Figure 1.14: Several applications of the ocean generators on the wave and current interaction zone.



(a) Piezoelectric eel [Taylor et al., 2001] (b) Underwater flag-like triboelectric generator [Wang et al., 2021]

Figure 1.15: Generators with PEG and TEG on the deep ocean

1.2 Ocean Space situation, Marine Domain Awareness and the necessity of the Ocean energy harvesters

Based on the subsections mentioned earlier, it is clear that developing an alternative power source to power the IoT and MEMS is essential. More importantly, due to the recent trends of the IoT and society 5.0, many sensors and transducers that were previously difficult to use in specific locations can now be utilized. One of that examples is the ocean space.

Countries such as Indonesia, Japan, Philippines, and United Kingdom are mainly covered by seas and islands with huge potential in their ocean. Based on their land and ocean geography, Indonesia and Japan are included in the top 10 of the highest Exclusive economic zone (EEZ). Due to the EEZ, the island country is able to :

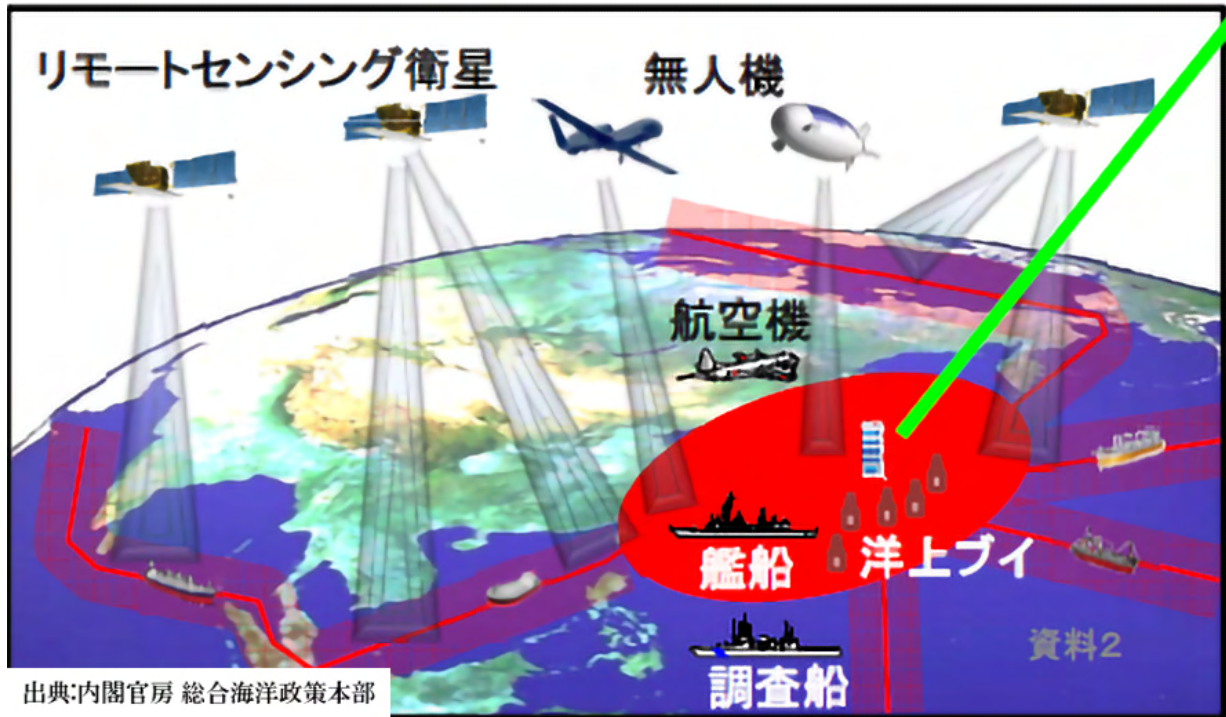
- Explore and exploit the resources in their exclusive zone.
- Conserving and managing the natural resources, whether a living or nonliving creature overlying the seabed and the subsoil.
- Able to build, install, establish and use their developed artificial islands and build the ocean structure for business or other public benefits.
- Conduct the marine scientific research and improve the scientific knowledge.

However, since the EEZ is unlike the territorial sea, other countries have much higher freedom to cross. For example, their vessel can enjoy navigation and overflight for transportation, and it is allowed for other countries to install and lay off their submarine cables and pipelines on it. To prevent future disputes and use the EEZ more efficiently, the technology of IoT and MEMS is one of the proposed solutions. The usage of the technology can help the country and the world organization to obtain three main information related to the EEZ:

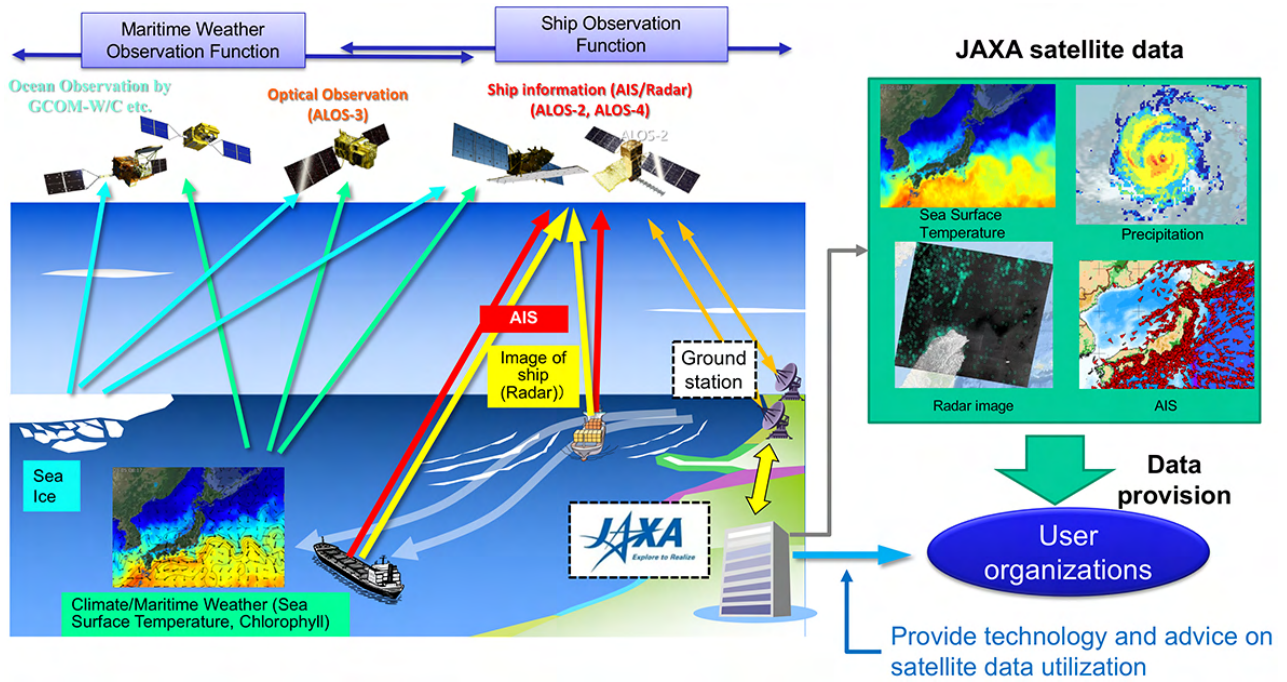
- Gathering the information on the Ocean Cadastre, which provides a spatial indication of the boundary of rights and interests in the ocean zone.

- Gathering the natural science information. The technology in the future needs to be able to collect the data in fewer intervals and constantly update automatically.
- Gathering the natural science information related to vessel activity, which changes daily. Pioneered by the Automatic Identification System (AIS), future technology could improve the results of AIS by using artificial satellite and artificial intelligence (AI) combined to collect and process the data simultaneously.

Maritime Domain Awareness (MDA) is one of the solutions proposed and agreed upon by the world's nations to help bridge the issue and help standardize obtaining the three main information. The MDA concept is to collect various information on ocean security and marine environment conservation and to grasp the information on the ocean. This information is needed to respond to various ocean man-made and natural threats (including natural disasters, high ocean waves during monsoon season, or typhoons). Additionally, we can also collect more information on the ocean, such as: measuring the salinity of the ocean, the wind speed and direction detector, weather detection, wave period/height/wavelength recorder, early disaster sensors and warning system, and sea temperature to preserve and track the natural habitat in the ocean using ocean devices and sensor. The sensors such as wave logger, wave gauge, Tidal and wave recorder, up to the ocean sensor system such as Low-cost sensor buoy and ocean environmental monitoring buoy could be installed with the ocean energy harvester device. The illustration of the MDA in Japan can be seen in Fig.1.16, while the ocean monitoring appliances is shown in Fig.1.17 to demonstrate the scope and devices required. As illustrated in the figures, the target information in the ocean is wide-area and large. That large space can only be covered by installing many buoys, transducers, and sensors in a small size but in a huge number and spread alongside the sea lane. That huge number created a necessity for small-scale and distributed independent power supplies to power those devices. The estimated energy required for various ocean sensors' electrical needs have been researched, collected, and reviewed by the works of Tiancong Zhao et al. [Zhao et al., 2021] and can be seen in Fig. 1.18.

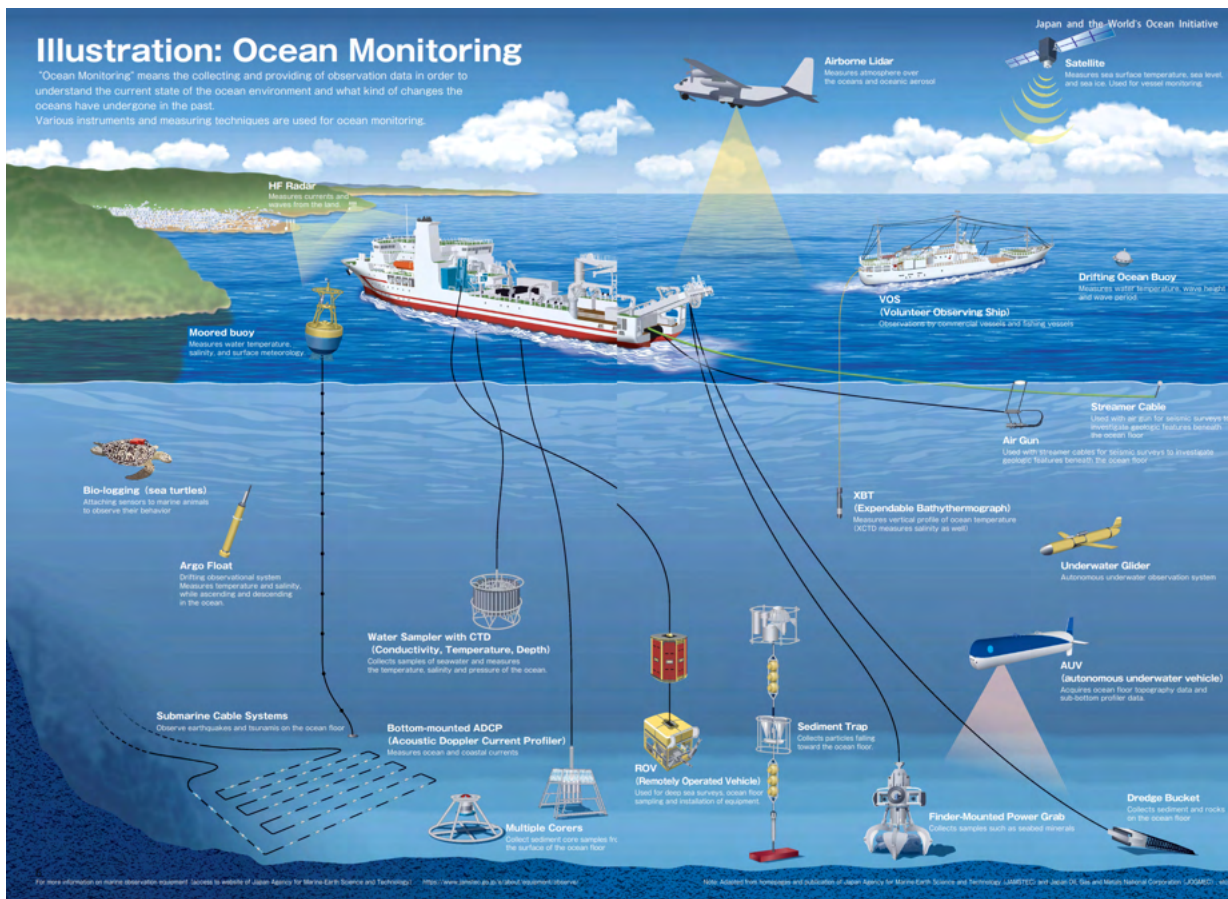


(a) Concept of MDA in Japan. Source: Cabinet Secretariat General Ocean Policy Headquarters

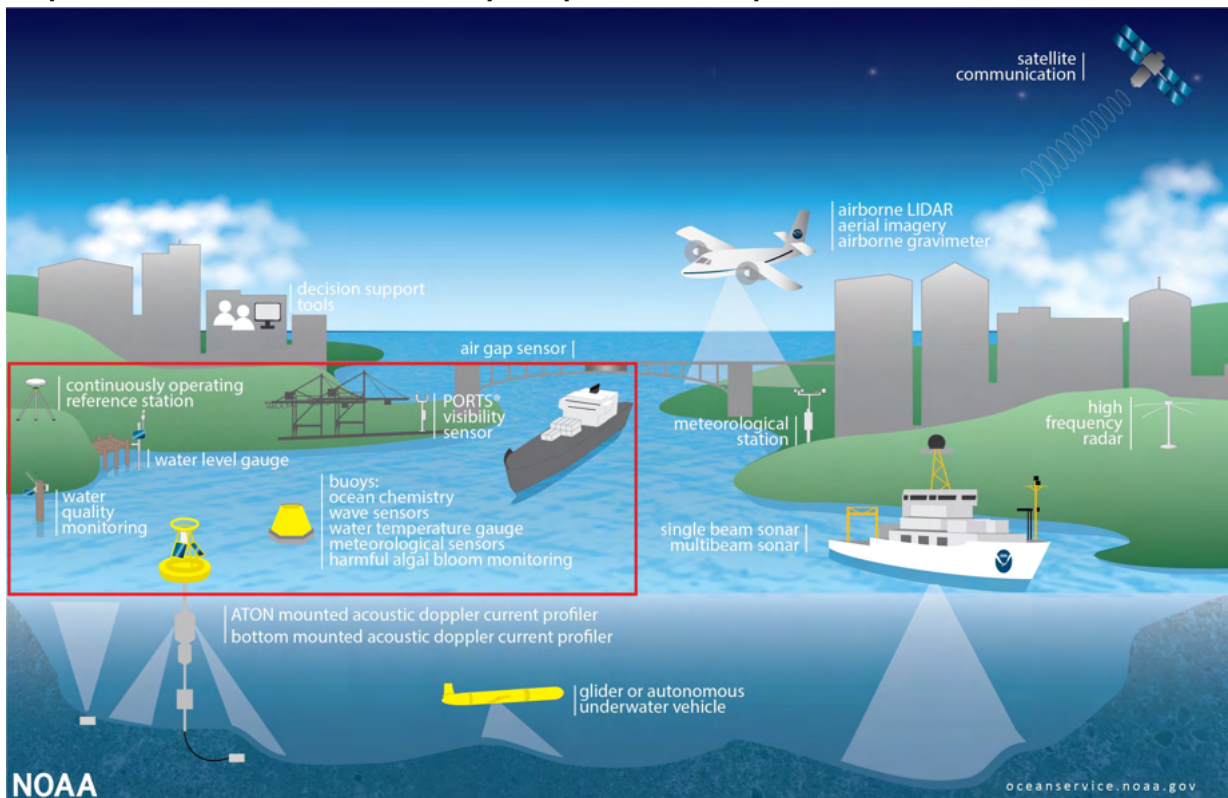


(b) Jaxa satellite for collecting data on ships and oceans. Source : Jaxa satellite

Figure 1.16: Application of MDA in Japan



(a) Ocean monitoring. Adapted from homepages and publication of Japan Agency for Marine-Earth Science and Technology and Japan Oil, Gas and Metals National Corporation. Published on [Sasakawa Peace Foundation, 2019] and [Tsumoda, 2019]



(b) Application of ocean monitoring, the potential device that could be powered by TEG and PEG is marked with the red box. Source : Source : National Oceanic and Atmospheric Administration - United States of America Department of Commerce

Figure 1.17: Ocean monitoring devices. Potential for future ocean energy harvesters

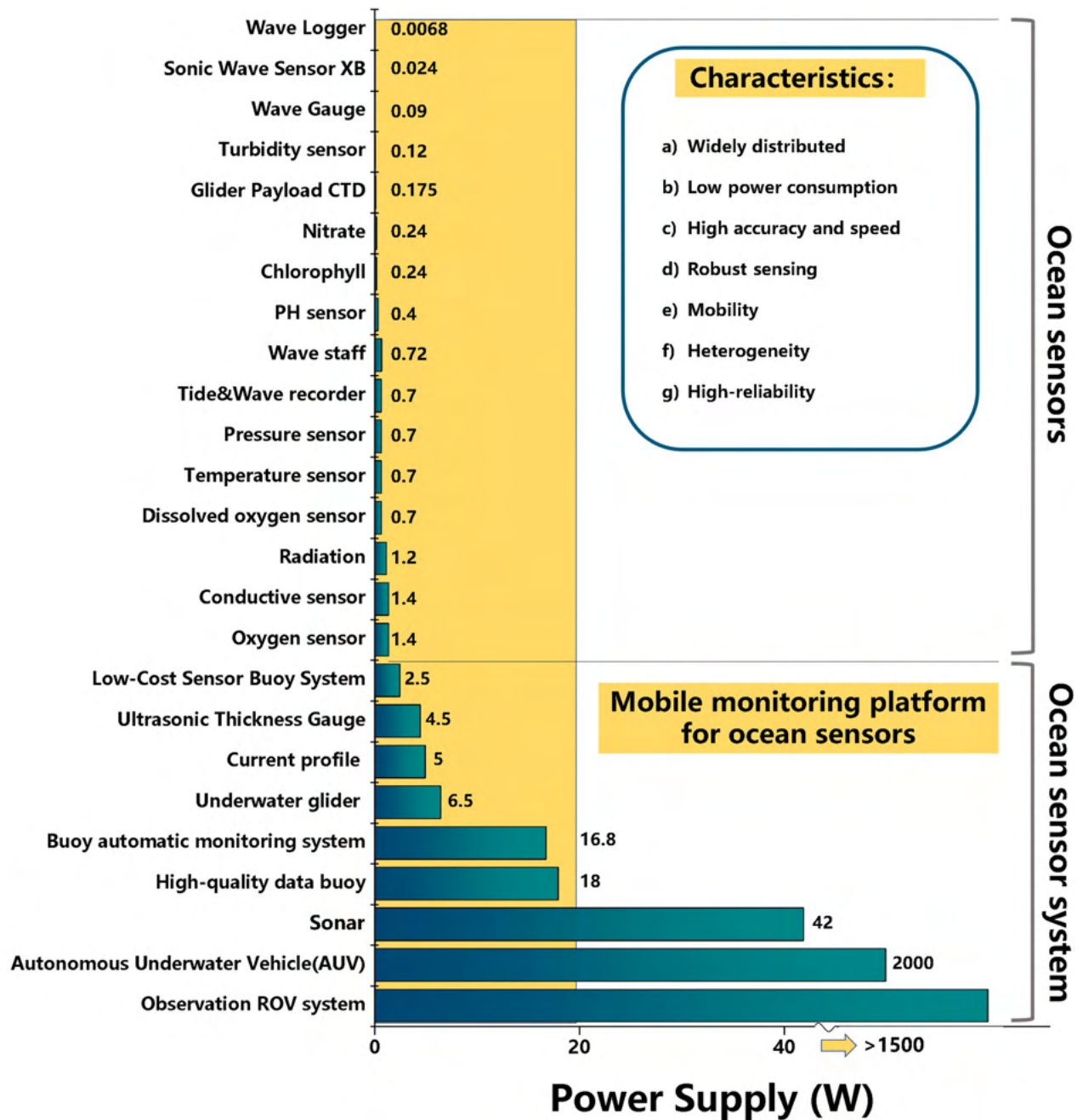


Figure 1.18: State-of-art ocean sensors and ocean sensors system. Collected and reviewed in the work of [Zhao et al., 2021]

One of the proposed solutions from the scientific and engineering community is developing and utilizing the ocean energy harvesters (see again in the previous subsection). Ocean energy harvesting collects and scavenges the ambient energy in the wave motion, tidal current, or temperature difference under the sea to produce electricity. In the previous decades, the main generator for ocean energy harvesting was built based on the electromagnetic principle. Thus, it resulted in a huge structure and platform ocean energy converter (OEC). The size of the OEC

is not suitable for the IoT and MEMS devices; (typically small size but has a large number). For that reason, many current and prospective future ocean energy harvester is moving toward the use of Triboelectric Generator (TEG) and Piezoelectric Generator (PEG). Both TEG and PEG generally produce high voltage, have multiple diverse modes, and have a diverse choice of environment-friendly materials. The benefits combined with the low electricity needed to power the small sensors have created a wide opportunity for developing TEG and PEG for the ocean energy harvesters.

1.3 Gaps, Aims, and Objectives

There are multiple benefits to applying the TEG and PEG as an ocean energy harvester. The main contribution is powering the millions of sensors and small MEMS as a replacement for the electromagnetic generator. By switching the current electromagnetic generator for the ocean sensors and devices to the TEG or PEG device, similar electrical voltage and power could be achieved with fewer materials. That could lead to more power source longevity (which led to less maintenance and replacement) and lower cost than a big electromagnetic generator.

However, the previous trend of TEG and PEG also has several drawbacks. In order to create an effective generator, previous TEG and PEG devices require materials that have been synthesized by different complex chemicals and physical processes. Due to that specific synthesization, it needs certain tools to create. As a result, the previous TEG and PEG become more complicated to make, more expensive, and time-consuming to produce. Thus, finding an easy method to fabricate highly efficient TEGs and PEGs from readily available materials, simple and low-cost for production, is one of the main points for developing the energy harvester.

To solve those issues, we propose and developing a flexible and compressible triboelectric generator and flexible piezoelectric device as hybrid energy harvesters. Both PEG and TEG devices are made based on our research group's development of triboelectric and piezoelectric materials. The triboelectric generator is made with a dielectric elastomer and developed into a flexible and compressible triboelectric generator (FC-TEG). The piezoelectric generator is made using

our previously developed Flexible piezoelectric device (FPED).

The benefit of using the flexible and compressible types of TEG and PEG as energy harvesters are:

- Can be utilized in various locations that provide consistent vibrational motions (e.g., railroad, ocean, machine vibrations, wind space, etc.).
- For PEG: the flexible type can withstand more force without breaking the cover of the piezo materials. Therefore, more electrical output can be generated.
- For PEG: Since the output voltage generated from piezoelectric material is proportional to the strain rate of an energy harvester, the deformation and frequency of an energy harvester are very important to consider. On the other hand, ambient kinetic energies in the ocean field have various magnitudes as external forces can be widely varied in real-world scenarios. Therefore, our PEG, which is highly flexible and adaptable, could harvest energy from various extent of the forces, frequencies, and periods. Besides that, the PEG can also be customized and optimized to match the forcing magnitude and electrical demand.
- For TEG, due to the thinness and the compressibility of the elastomer, more dielectric elastomers could be made and stacked upon each other.
- Due to the stack-ability of the generators, more piezoelectric and triboelectric materials can be installed in one device. Creating more robust and durable generators.
- Easier to scale based on the electrical needs and less space for operating the device.

However, since there is no information regarding the electrical performance characteristics, a fundamental study to focus on the output and mechanical characteristics is necessary before the actual application in the real-world situation (e.g., The ocean space). In addition, we also need to focus on and identify the main variables for the TEG and PEG device efficient output. The fundamental study is important not only to our research group or similar type of TEG and

PEG future application but also to the research of energy harvesters in general. This is because there is a huge lack of information regarding the relationship between the mechanical variable and electrical output since previous similar studies mainly focus on the device's design, shape, or model but not on the "energy harvesting" process.

This study offers the first stage of our ocean energy harvesters. The main purpose of this first stage of the study is to elucidate the fundamental characteristics of the TEG and PEG electrical performance. Besides that, examination and finding the main variables that could affect the electrical output are also our goals in this study. Hence, the energy harvesting device was investigated using the triboelectric generator and the piezoelectric generator. Vertical vibration tests were then conducted to elucidate the working mechanism and clarify each variable effect on the device's electrical output. Then, the synergy between PEG and TEG devices is also studied to find whether they could be combined into hybrid energy harvesting devices and scavenge more energy.

Within this aim, the specific objectives of this study to be reached are focused on the followings:

- To explain characteristics of the TEG based on the vertical contact-separation-compression vibrations.
- To clarify the effect of the vibration amplitude, acceleration amplitude, frequency, and the initial distance (i.e., the separation velocity and separation distance) to the TEG electrical output.
- To design and develop a multi-layered TEG for maximum electrical output.
- To investigate whether the TEG device could be combined with the PEG device to create a hybrid TEG-PEG device and check their complementary abilities.

Afterward, the results of this first stage study will be used as a base for future development of the hybrid ocean energy harvester using flexible and compressible TEG-PEG. The estimated stages for continuing the development of this ocean energy harvester until the application in real ocean space is briefly mentioned as:

1. Fundamental characteristics of the TEG and PEG generators. Elucidating the mechanical characteristics and electrical performance
2. Laboratory stage.
3. Component validation in relevant environment and controlled space (such as Towing Tank).
4. Prototype in the ocean : Deployment in the small port (e.g., fishing port).
5. Ocean Energy Harvester

Further details of the next stage of this study will be explained in more detail in the Final Chapter subsection [6.2 Future works](#).

1.4 Structure of the Dissertation

The dissertation is structured as follows. Chapter [1](#) introduces and explains this study's background, which provides previous research concerning this study. Hereafter, the author clarifies the study's objectives and closes this chapter with the dissertation structure. The energy harvesting based on the triboelectric effect principle needs to be explained in more detail to elucidate our findings. Moreover, the electrical output from our original TEG device needs to be described as well.

As a result, Chapter [2](#) explains the result of the FC-TEG on the vertical vibration tests. The FC-TEG experimented with three modes that mainly occurred on the TEG device: separation mode, contact mode, and compression mode. The output on each mode is then clarified, and each factor is then looked at in more detail to illustrate the effect of those factors on generating electrical output.

Chapter [3](#) improves the previous chapter by developing a theoretical and numerical model based on the FC-TEG vertical vibration tests. The numerical model mainly focuses on estimating the FC-TEG output voltage alongside the separation stroke and separation velocity. Comparing

the results of the experimental and theoretical modelling tool can help future studies and create a reasonable estimation when the FC-TEG are utilized under various conditions.

Chapter 4 follows the previous two chapters by creating multi-layered triboelectric generators based on the folding type of TEG. The simple folding type using an origami technique is chosen due to its simplicity and illustrates our finding in the triboelectric effect. This finding includes the effect of the multi-layers for the TEG device and what factors could directly affect the electrical results. Afterwards, the comparison of the compression mode and the contact mode for the multi-layer TEG is studied to verify the best mode for our TEG

In Chapter 5, our PEG based on the FPED is combined with the multi-layer TEG to create a hybrid TEG-PEG device. The combination of PEG and TEG aims to extract more energy in a broad energy spectrum of vibrational energy. The relationship of vibration amplitude, initial distance, frequency, and amplitude with TEG-PEG output voltage is then studied. In addition, the TEG-PEG hybrid mutual complementary are also examined to verify both devices' suitability as ocean generators.

Finally, the final chapter (Chapter 6) has the conclusions from all results and findings in the previous chapters. These conclusions summarise these dissertation thesis findings, including required future works for improving this research in the next steps before the generators are utilized as ocean energy harvesters devices.

Bibliography

- [Akinaga et al., 2018] Akinaga, H., Fujita, H., Mizuguchi, M., and Mori, T. (2018). Focus on advanced materials for energy harvesting: prospects and approaches of energy harvesting technologies. *Science and Technology of Advanced Materials*, 19(1):543–544.
- [Cheng et al., 2019] Cheng, P., Guo, H., Wen, Z., Zhang, C., Yin, X., Li, X., Liu, D., Song, W., Sun, X., Wang, J., and Wang, Z. L. (2019). Largely enhanced triboelectric nanogenerator

- for efficient harvesting of water wave energy by soft contacted structure. *Nano Energy*, 57(November 2018):432–439.
- [D., 2005] D., K. A. (2005). Harvesting Energy by Improving the Economy of Human Walking. *Science*, 309(5741):1686–1687.
- [Dagdeviren et al., 2014] Dagdeviren, C., Yang, B. D., Su, Y., Tran, P. L., Joe, P., Anderson, E., Xia, J., Doraiswamy, V., Dehdashti, B., Feng, X., Lu, B., Poston, R., Khalpey, Z., Ghaffari, R., Huang, Y., Slepian, M. J., and Rogers, J. A. (2014). Conformal piezoelectric energy harvesting and storage from motions of the heart, lung, and diaphragm. *Proceedings of the National Academy of Sciences*, 111(5):1927 LP – 1932.
- [Delnavaz and Voix, 2014] Delnavaz, A. and Voix, J. (2014). Flexible piezoelectric energy harvesting from jaw movements. *Smart Materials and Structures*, 23(10).
- [Du et al., 2021] Du, T., Zuo, X., Dong, F., Li, S., Mtui, A. E., Zou, Y., Zhang, P., Zhao, J., Zhang, Y., Sun, P., and Xu, M. (2021). A Self-Powered and Highly Accurate Vibration Sensor Based on Bouncing-Ball Triboelectric Nanogenerator for Intelligent Ship Machinery Monitoring.
- [Du et al., 2020] Du, X., Mutsuda, H., Yamada, T., Nakashima, T., Doi, Y., Du, A. X., Mutsuda, H., Yamada, T., Nakashima, T., and Doi, Y. (2020). A Bellows Type of Flexible Piezo-Electric Energy Harvester for Structural Health Monitoring of Pipelines. *The 30th International Ocean and Polar Engineering Conference*, pages ISOPE–I–20–2152.
- [Gong et al., 2019] Gong, Y., Yang, Z., Shan, X., Sun, Y., Xie, T., and Zi, Y. (2019). Capturing flow energy from ocean and wind. *Energies*, 12(11):1–23.
- [Han et al., 2020] Han, K., Luo, J., Feng, Y., Lai, Q., Bai, Y., Tang, W., and Wang, Z. L. (2020). Wind-Driven Radial-Engine-Shaped Triboelectric Nanogenerators for Self-Powered Absorption and Degradation of NOX. *ACS nano*, 14(3):2751–2759.
- [Haroun et al., 2021] Haroun, A., Le, X., Gao, S., Dong, B., He, T., Zhang, Z., Wen, F., Xu, S., and Lee, C. (2021). Progress in micro/nano sensors and nanoenergy for future AIoT-based smart home applications. *Nano Express*, 2(2):022005.

- [Kan et al., 2016] Kan, J., Fan, C., Wang, S., Zhang, Z., Wen, J., and Huang, L. (2016). Study on a piezo-windmill for energy harvesting. *Renewable Energy*, 97:210–217.
- [Kinsman, 1984] Kinsman, B. (1984). *Wind Waves: Their Generation and Propagation on the Ocean Surface*. Dover Books on Chemistry and Earth Sciences. Dover Publications.
- [Krikke, 2005] Krikke, J. (2005). Sunrise for energy harvesting products. *IEEE Pervasive Computing*, 4(1):4–5.
- [Latif et al., 2020] Latif, U., Ali, E., Uddin, E., Ali, Z., Sajid, M., Shah, S. R., and Younis, M. Y. (2020). Experimental investigation of energy harvesting eel in the wake of bluff body under ocean waves. *Proceedings of the Institution of Mechanical Engineers, Part M: Journal of Engineering for the Maritime Environment*, 235(1):81–92.
- [Li et al., 2017] Li, S., Wang, J., Peng, W., Lin, L., Zi, Y., Wang, S., Zhang, G., and Wang, Z. L. (2017). Sustainable Energy Source for Wearable Electronics Based on Multilayer Elastomeric Triboelectric Nanogenerators. *Advanced Energy Materials*, 7(13):1602832.
- [Li et al., 2018] Li, X., Tao, J., Wang, X., Zhu, J., Pan, C., and Wang, Z. L. (2018). Networks of High Performance Triboelectric Nanogenerators Based on Liquid–Solid Interface Contact Electrification for Harvesting Low-Frequency Blue Energy. *Advanced Energy Materials*, 8(21):1800705.
- [Lin et al., 2014] Lin, Z.-H., Cheng, G., Wu, W., Pradel, K. C., and Wang, Z. L. (2014). Dual-Mode Triboelectric Nanogenerator for Harvesting Water Energy and as a Self-Powered Ethanol Nanosensor. *ACS Nano*, 8(6):6440–6448.
- [Liu et al., 2019] Liu, F.-R., Zhang, W.-M., Peng, Z.-K., and Meng, G. (2019). Fork-shaped bluff body for enhancing the performance of galloping-based wind energy harvester. *Energy*, 183:92–105.
- [Mannsfeld et al., 2010] Mannsfeld, S. C. B., Tee, B. C.-K., Stoltenberg, R. M., Chen, C. V. H.-H., Barman, S., Muir, B. V. O., Sokolov, A. N., Reese, C., and Bao, Z. (2010). Highly sensitive flexible pressure sensors with microstructured rubber dielectric layers. *Nature Materials*, 9(10):859–864.

- [Mutsuda et al., 2013] Mutsuda, H., Watanabe, R., Azuma, S., Tanaka, Y., and Doi, Y. (2013). Ocean power generator using flexible piezoelectric device. In *Proceedings of the International Conference on Offshore Mechanics and Arctic Engineering - OMAE*, volume 8. American Society of Mechanical Engineers Digital Collection.
- [Mutsuda et al., 2012] Mutsuda, H., Watanabe, R., Hirata, M., Doi, Y., and Tanaka, Y. (2012). Elastic floating unit with piezoelectric device for harvesting ocean wave energy. In *Proceedings of the International Conference on Offshore Mechanics and Arctic Engineering - OMAE*, volume 7, pages 233–240. American Society of Mechanical Engineers Digital Collection.
- [Narvaez Rojas et al., 2021] Narvaez Rojas, C., Alomia Peñafiel, G. A., Loaiza Buitrago, D. F., and Tavera Romero, C. A. (2021). Society 5.0: A Japanese concept for a superintelligent society. *Sustainability (Switzerland)*, 13(12).
- [Niu et al., 2015] Niu, S., Wang, X., Yi, F., Zhou, Y. S., and Wang, Z. L. (2015). A universal self-charging system driven by random biomechanical energy for sustainable operation of mobile electronics. *Nature Communications*, 6(1):8975.
- [Orrego et al., 2017] Orrego, S., Shoele, K., Ruas, A., Doran, K., Caggiano, B., Mittal, R., and Kang, S. H. (2017). Harvesting ambient wind energy with an inverted piezoelectric flag. *Applied Energy*, 194:212–222.
- [Palumbo et al., 2019] Palumbo, S., Rasilo, P., and Zucca, M. (2019). Experimental investigation on a Fe-Ga close yoke vibrational harvester by matching magnetic and mechanical biases. *Journal of Magnetism and Magnetic Materials*, 469:354–363.
- [Raj and Steingart, 2018] Raj, A. and Steingart, D. (2018). Review—Power Sources for the Internet of Things. *Journal of The Electrochemical Society*, 165(8):B3130—B3136.
- [Rodrigues et al., 2019] Rodrigues, C., Gomes, A., Ghosh, A., Pereira, A., and Ventura, J. (2019). Power-generating footwear based on a triboelectric-electromagnetic-piezoelectric hybrid nanogenerator. *Nano Energy*, 62(May):660–666.

- [Safaei et al., 2018] Safaei, B., Monazzah, A. M. H., Bafroei, M. B., and Ejlali, A. (2018). Reliability side-effects in Internet of Things application layer protocols. *2017 2nd International Conference on System Reliability and Safety, ICSRS 2017*, 2018-Janua(December):207–212.
- [Sasakawa Peace Foundation, 2019] Sasakawa Peace Foundation (2019). White Paper on the Oceans and Ocean Policy in Japan. Technical report.
- [Taylor et al., 2001] Taylor, G. W., Burns, J. R., Kammann, S. A., Powers, W. B., and Welsh, T. R. (2001). The Energy Harvesting Eel: a small subsurface ocean/river power generator. *IEEE Journal of Oceanic Engineering*, 26(4):539–547.
- [Tsunoda, 2019] Tsunoda, T. (2019). New Developments in Japan ’ s Marine Information Management.
- [Wang et al., 2020] Wang, J., Zhang, C., Gu, S., Yang, K., Li, H., Lai, Y., and Yurchenko, D. (2020). Enhancement of low-speed piezoelectric wind energy harvesting by bluff body shapes: Spindle-like and butterfly-like cross-sections. *Aerospace Science and Technology*, 103:105898.
- [Wang et al., 2015] Wang, X., Niu, S., Yin, Y., Yi, F., You, Z., and Wang, Z. L. (2015). Triboelectric Nanogenerator Based on Fully Enclosed Rolling Spherical Structure for Harvesting Low-Frequency Water Wave Energy. *Advanced Energy Materials*, 5(24):1501467.
- [Wang et al., 2021] Wang, Y., Liu, X., Chen, T., Wang, H., Zhu, C., Yu, H., Song, L., Pan, X., Mi, J., Lee, C., and Xu, M. (2021). An underwater flag-like triboelectric nanogenerator for harvesting ocean current energy under extremely low velocity condition. *Nano Energy*, 90:106503.
- [Wang, 2017a] Wang, Z. L. (2017a). Catch wave power in floating nets.
- [Wang, 2017b] Wang, Z. L. (2017b). On Maxwell’s displacement current for energy and sensors: the origin of nanogenerators. *Materials Today*, 20(2):74–82.
- [Xiao et al., 2019] Xiao, X., Zhang, X., Wang, S., Ouyang, H., Chen, P., Song, L., Yuan, H., Ji, Y., Wang, P., Li, Z., Xu, M., and Wang, Z. L. (2019). Honeycomb Structure Inspired Tri-

- boelectric Nanogenerator for Highly Effective Vibration Energy Harvesting and Self-Powered Engine Condition Monitoring. *Advanced Energy Materials*, 9(40):1902460.
- [Xu et al., 2018] Xu, L., Jiang, T., Lin, P., Shao, J. J., He, C., Zhong, W., Chen, X. Y., and Wang, Z. L. (2018). Coupled Triboelectric Nanogenerator Networks for Efficient Water Wave Energy Harvesting. *ACS Nano*, 12(2):1849–1858.
- [Xu et al., 2019a] Xu, M., Wang, S., Zhang, S. L., Ding, W., Kien, P. T., Wang, C., Li, Z., Pan, X., and Wang, Z. L. (2019a). A highly-sensitive wave sensor based on liquid-solid interfacing triboelectric nanogenerator for smart marine equipment. *Nano Energy*, 57:574–580.
- [Xu et al., 2019b] Xu, M., Zhao, T., Wang, C., Zhang, S. L., Li, Z., Pan, X., and Wang, Z. L. (2019b). High Power Density Tower-like Triboelectric Nanogenerator for Harvesting Arbitrary Directional Water Wave Energy. *ACS Nano*, 13(2):1932–1939.
- [Yong et al., 2016] Yong, H., Chung, J., Choi, D., Jung, D., Cho, M., and Lee, S. (2016). Highly reliable wind-rolling triboelectric nanogenerator operating in a wide wind speed range. *Scientific Reports*, 6(1):33977.
- [Yuan et al., 2021] Yuan, Z., Wang, C., Xi, J., Han, X., Li, J., Han, S.-T., Gao, W., and Pan, C. (2021). Spherical Triboelectric Nanogenerator with Dense Point Contacts for Harvesting Multidirectional Water Wave and Vibration Energy. *ACS Energy Letters*, 6(8):2809–2816.
- [Zeng et al., 2020] Zeng, Q., Wu, Y., Tang, Q., Liu, W., Wu, J., Zhang, Y., Yin, G., Yang, H., Yuan, S., Tan, D., Hu, C., and Wang, X. (2020). A high-efficient breeze energy harvester utilizing a full-packaged triboelectric nanogenerator based on flow-induced vibration. *Nano Energy*, 70:104524.
- [Zhang et al., 2017] Zhang, J., Fang, Z., Shu, C., Zhang, J., Zhang, Q., and Li, C. (2017). A rotational piezoelectric energy harvester for efficient wind energy harvesting. *Sensors and Actuators A: Physical*, 262:123–129.
- [Zhao et al., 2021] Zhao, T., Xu, M., Xiao, X., Ma, Y., Li, Z., and Wang, Z. L. (2021). Recent progress in blue energy harvesting for powering distributed sensors in ocean. *Nano Energy*, page 106199.

- [Zheng et al., 2017] Zheng, Q., Shi, B., Li, Z., and Wang, Z. L. (2017). Recent Progress on Piezoelectric and Triboelectric Energy Harvesters in Biomedical Systems. *Advanced Science*, 4(7):1–23.
- [Zhong et al., 2019] Zhong, W., Xu, L., Wang, H., Li, D., and Wang, Z. L. (2019). Stacked pendulum-structured triboelectric nanogenerators for effectively harvesting low-frequency water wave energy. *Nano Energy*, 66(September):104108.
- [Zhou et al., 2014] Zhou, Y. S., Zhu, G., Niu, S., Liu, Y., Bai, P., Jing, Q., and Wang, Z. L. (2014). Nanometer resolution self-powered static and dynamic motion sensor based on micro-grated triboelectrification. *Advanced Materials*, 26(11):1719–1724.
- [Zhu et al., 2014a] Zhu, G., Su, Y., Bai, P., Chen, J., Jing, Q., Yang, W., and Wang, Z. L. (2014a). Harvesting Water Wave Energy by Asymmetric Screening of Electrostatic Charges on a Nanostructured Hydrophobic Thin-Film Surface. *ACS Nano*, 8(6):6031–6037.
- [Zhu et al., 2014b] Zhu, G., Yang, W. Q., Zhang, T., Jing, Q., Chen, J., Zhou, Y. S., Bai, P., and Wang, Z. L. (2014b). Self-powered, ultrasensitive, flexible tactile sensors based on contact electrification. *Nano Letters*, 14(6):3208–3213.
- [Zi and Wang, 2017] Zi, Y. and Wang, Z. L. (2017). Nanogenerators: An emerging technology towards nanoenergy. *APL Materials*, 5(7):74103.
- [Zou et al., 2020] Zou, Y., Libanori, A., Xu, J., Nashalian, A., and Chen, J. (2020). Triboelectric Nanogenerator Enabled Smart Shoes for Wearable Electricity Generation. *Research*, 2020:7158953.

Chapter 2

Energy Harvesting based on triboelectric materials using a single dielectric elastomer

2.1 Background

The dielectric elastomer is one kind of a substance with high permittivity to generate electricity via polarization [Muscle et al., 2008, Chiba et al., 2011, CHIBA and WAKI, 2014]. Due to this high permittivity, the electric polarization could be obtained by applying the external movement as the mechanical energy. This phenomenon is a reversible process, which means when the electric field is applied to the substance, the strain is generated, and the device could convert the electrical energy into mechanical motion (i.e., stretching, moving, etc.) as the actuator. Details of this concept can be seen in Fig.2.1. In addition, unlike the electrets and piezoelectric elements, the elastomer does not require polarization processing. This independence makes the production costs of the elastomer relatively lower compared with other elements.

One of the applications of this elastomer is using it as the triboelectric generator (TEG). TEG is a device that converts the mechanical to generate electricity via triboelectric effect and the

electrostatic induction at the same time. Proposed by Prof. Zhong Lin Wang's group in the year 2012 at Georgia Institute of Technology [Wang, 2013] for driving small electronic devices. Fig.2.2 presents the typical power generation mechanism of the FC-TEG. The four fundamental modes of the TEG were first introduced in [Wang, 2014], namely, vertical contact-separation mode, in-plane sliding mode, single-electrode mode, and free-standing triboelectric-layer mode. Nowadays, many researchers have iterated the device to improve its application.

Han et al. 2019 has been observing the effects of the environmental atmosphere on the TEG performance in the contact-separation mode [Han et al., 2019]. Jurado, Pu, and White 2017 describe ocean wave impact compressed air bubbles on the dielectric metal contact separation mode triboelectric generator (DMCS-TEG) electrical output [Jurado et al., 2017]. While Patnam et al. 2020 developed a Ca-doped BZT/PDMS composite in a film-based generator to harvest mechanical energy via the synergetic effects [Patnam et al., 2020].

Among the previous research works, the relationship between the contact-separation-compression process due to the external loads and the electric performance of triboelectric generators is generally unclear. Especially, the explanation of the effects of separation-distance and separation-velocity on the TEG output voltage is still obscure. Additionally, elucidating key parameters for the TEG output voltage in more detail is needed for developing a suitable sustainable energy harvester before practical use.

2.2 Device overview + fabrication of TEG

In this chapter, a flexible and compressible triboelectric generator (FC-TEG) is proposed, developed, and tested via the mechanical vertical test. A vertical contact-separation-compression test is preliminarily conducted to examine the output voltage generated by the FC-TEG, the working mechanism of power generation of the FC-TEG, and the effects of various key parameters, such as separation distance and separation velocity in the contact/separation/compression modes.

Among many experiments that we tested are the output voltage results on various taping

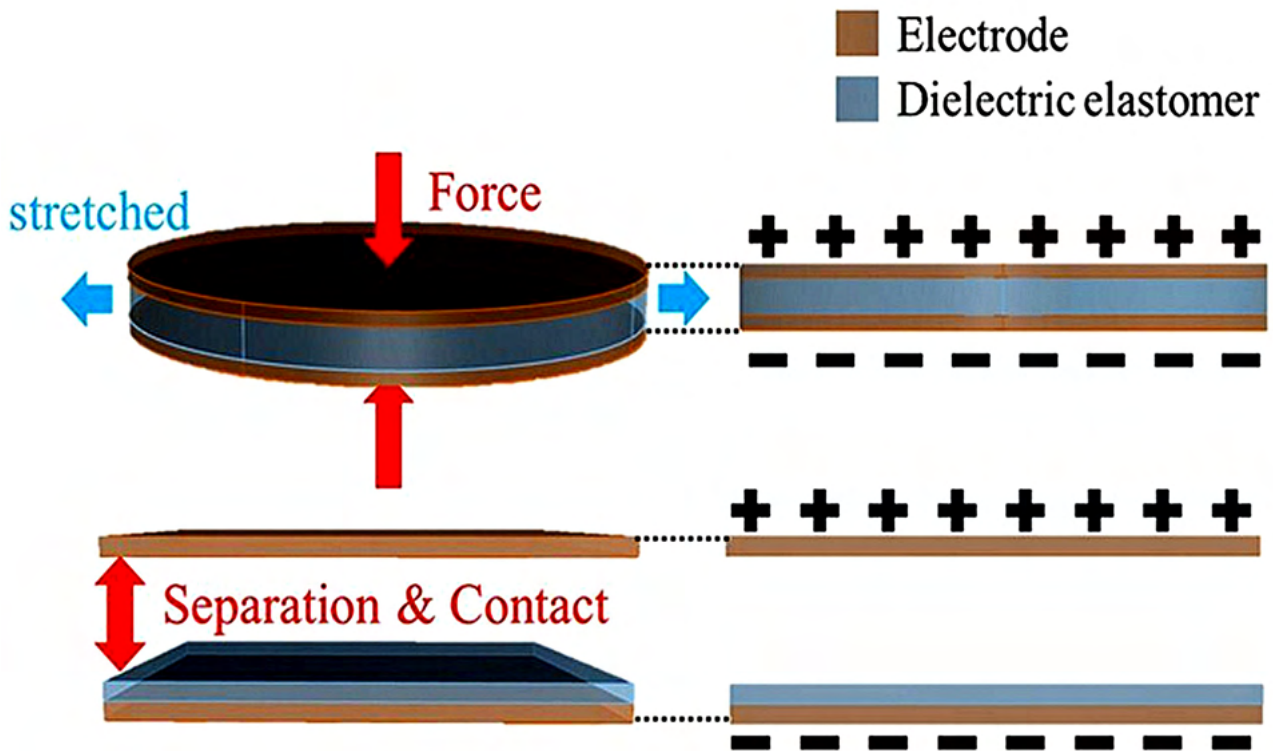


Figure 2.1: Working mechanism of the TEG with the electrode and dielectric elastomer

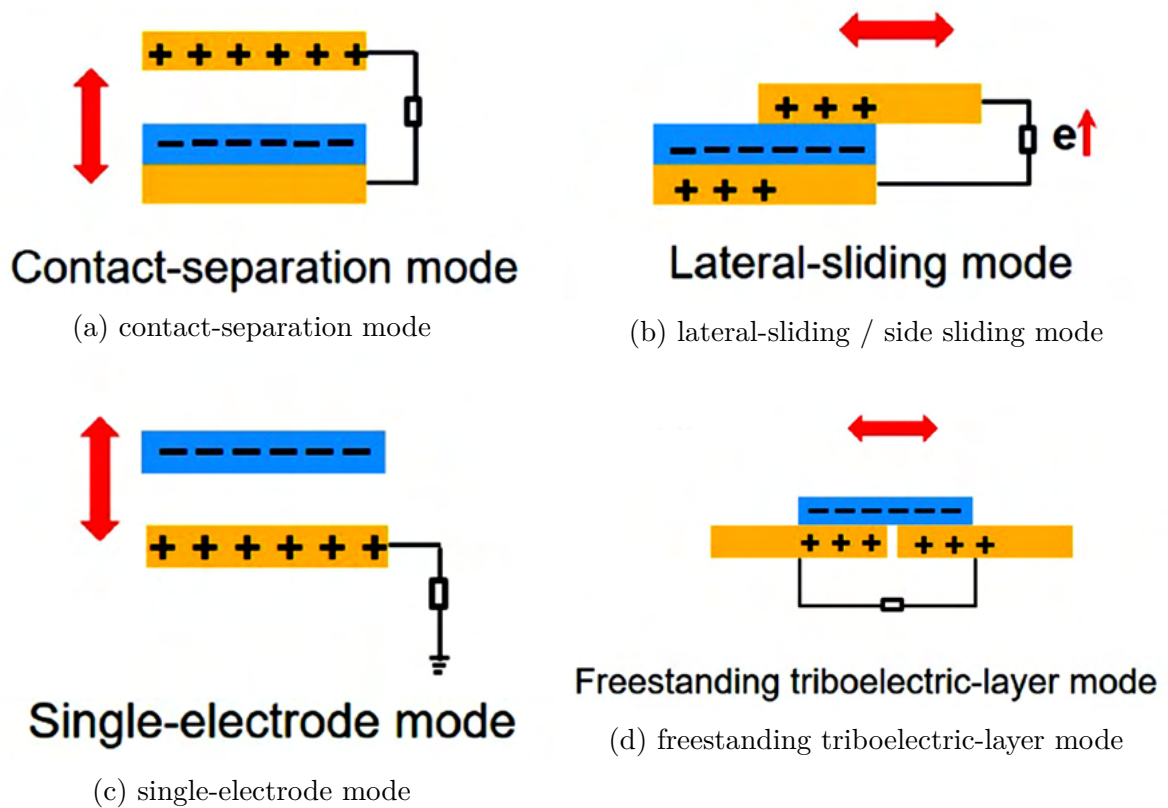


Figure 2.2: Four working modes of TEG [Wang, 2014]

mechanisms, output voltage characteristics in the separation-contact-compression modes, the effect of the separation distance for FC-TEG output voltage, and the effect of the separation velocity for FC-TEG output voltage.

2.2.1 Device overview

The FC-TEG is a simple, low-cost, easy-to-fabricate generator using a flexible polymer to harvest random and ambient energy in our living environment. The FC-TEG is made based on the combination of the copper tape (as the electrode) and the dielectric elastomer. The FC-TEG has an area of around 9 cm² tested in the vertical test. Since the device is relatively small, with the proper mechanism and protection, it could be applied in various fields such as the ocean, wind, wearable or implantable devices, etc., as the energy harvesters. modes.

2.2.2 Fabrication of single TEG based on dielectric elastomer

The typical structure of a polymer-based FC-TEG is displayed in Fig.2.3. A dielectric elastomer sheet (10-mm thickness) with an average roughness of 200 nm is used in the experiment. The roughness of the dielectric elastomer was accurately captured by the non-contacted/three-dimensional surface roughness and contour measuring instrument (TOKYO SEOMITSU, Opt Scope, R model).

The FC-TEG is constructed both from this elastomer and the copper films (1-mm thickness) as electrodes on both the bottom side with bonding and on the top side without adhesive to maintain an interlayer between the dielectric elastomer sheet and the top electrode, which is called the separation distance. The bonding to make the device could contact-separate with each other is done by using a layer of masking tape. The conductors are connected to both electrodes. The dimensions of the FC-TEG are as follows: length is= 30 mm, width = 30 mm, and thickness = 12 mm. The concept and prototype of the FC-TEG are presented in Fig.2.4.

The FC-TEG developed herein is of the vertical contact-separation type with a dielectric elastomer. Contact-separation-compression generates electrical charges between the dielectric elas-

tomers and the electrode, creating a triboelectric potential layer. The separation distance between the dielectric elastomer and the electrode is changed by a periodic vertical approach, contact-compression, and leaving states. A change in capacitance generates a current flow in an external load, and free electrons are accelerated across the electrodes to minimize the total energy in the circuit. Periodic separation and contact-compression between the dielectric elastomer and the electrode drive the induced electrons to flow forward and backward between the two electrodes on the top and bottom sides. Therefore, the electricity generation process depends on the separation distance between the contact-separation-compression states of the dielectric elastomer and the electrode, the separation velocity in terms of separation amplitude, and the separation period.

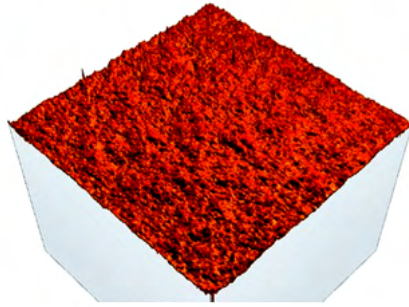
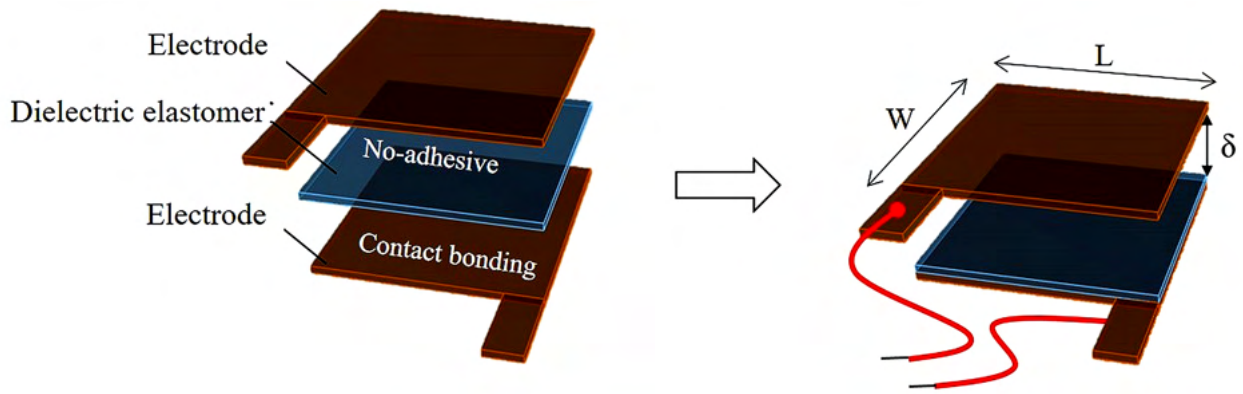
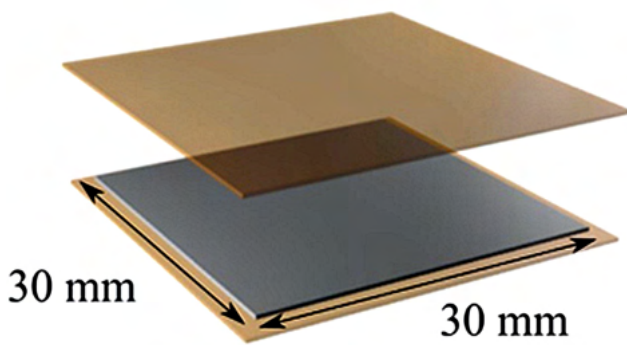


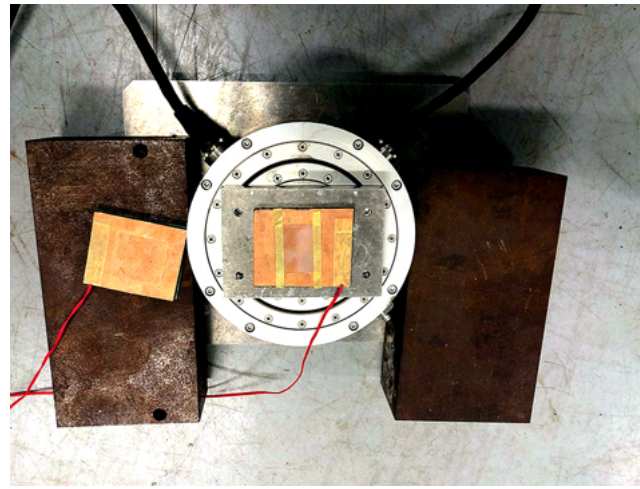
Figure 2.3: Surface roughness (average of 200 nm) of the FC-TEG



(a) Bonding of the single TEG



(b) size of the copper tape



(c) Photo of the Single TEG

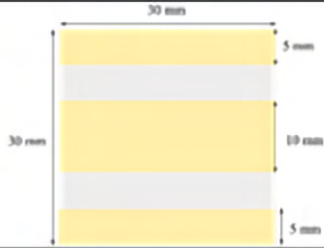



Figure 2.4: Concept and Prototype of Single TEG

2.2.3 Taping Mechanism/fixation method

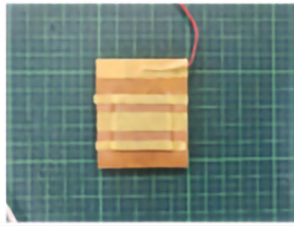
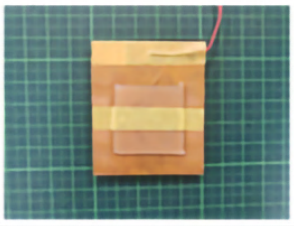
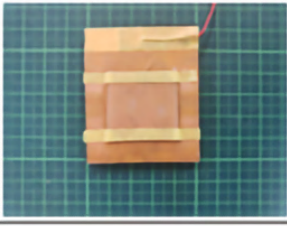
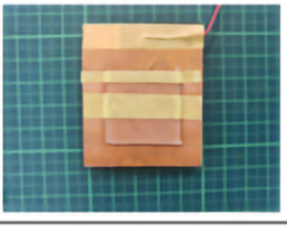
To identify the most suitable settings, we tried various settings that eventually resulted in the four types of the taping mechanism. Fig.2.5a shows the schematics of the taping mechanism in the preliminary experiments. The yellow color illustrates the tape, while the gray color illustrates the elastomer. There are four fixation methods to bond the elastomer and the copper films named as type 1 – type 4. Since the fixation method is different, the surface area of the elastomer can be different or has the same area but has a different taping position.

The surface area means the area of the elastomer that will be directly contact-separate with the copper films as part of the tribological process to generate electricity. In type 1, three

tapes are used, and the surface area of the elastomer is 300 mm². Type 2 has the same surface area as type 3 with 400 mm²; however, the fixation method is different. Type 2 only uses one larger tape in the middle, while type 3 uses two smaller tapes at the top and bottom end of the elastomer. Lastly, type 4 uses a combination of one large tape in the middle and one small tape at the top end with a surface area of around 450 mm². The difference of this surface area via the variations of fixation method illustrates whether in this mm² scale, the surface area could provide a more efficient electrical output. Fig.2.5b shows the actual prototype of the FC-TEG taping mechanism in the preliminary experiment, with the elastomer itself, is bonded using yellow tape to the copper films (the orange color beneath the elastomer). After the bonding is finished, the FC-TEG is placed on top of the vibration generator for the vertical contact-separation-compression experiments.

| Device Type | Type 1 | Type 2 |
|---------------------------------|---|---|
| Schematics |  |  |
| Contact Area (mm ²) | 300 | 600 |
| Device Type | Type 3 | Type 4 |
| Schematics |  |  |
| Contact Area (mm ²) | 600 | 450 |

(a) Taping mechanism of FC-TEG

| Device Type | Type 1 | Type 2 |
|---------------------------------|---|---|
| Device Image |  |  |
| Contact Area (mm ²) | 300 | 600 |
| Device Type | Type 3 | Type 4 |
| Device Image |  |  |
| Contact Area (mm ²) | 600 | 450 |

(b) Prototype of Single FC-TEG

Figure 2.5: Taping mechanism and the Prototype of Single TEG.

2.3 Vertical contact-separation-compression Experiment Setup and Condition

The vertical contact-separation-compression experiments were conducted to investigate single FC-TEG output voltage characteristics. Additionally, key parameters such as separation distance and the separation velocity in all three modes (separation, contact, compression modes) are also observed.

The setup of the experiments is shown in Fig.2.6. At the beginning of the experiment, the FC-TEG is placed on the upper side of the vibration generator (EMIC, 513 Series Standard Model). The generator is controlled via a multifunction generator (NF 30 MHz Multifunction Generator, WF1973) and power amplifier (EMIC, Power Amplifier 374-A) to move the generator under several amplitudes and frequencies. To capture the height and movement data of the FC-TEG, a laser displacement sensor (KEYENCE, CMOS Multi-Function Analog Laser Sensor, IL 300) was placed on the upper side of the vibration generator. Additionally, one high-speed video camera (NOBBY TECH, Phantom, 1,000 2,000 frames per second) with high resolution (approximately 0.01 mm/pixel) was also placed on one side of the FC-TEG to capture the separation-contact-compression states of the FC-TEG. The reference markers can be traced to measure the separation distance of (δ) between the dielectric elastomer and the top electrode. The output voltage of the single FC-TEG was recorded using a multi-input data logger (KEYENCE, Multi-input data logger, NR-500 Series) with a sampling frequency of 1,000 Hz. The internal resistance was set at $1M\Omega$, and a laptop computer converted the analog data into digital. Two parameters, namely the separation distance and separation velocity, were then controlled using the equipment mentioned above.

The separation distance (δ) and the instantaneous capture of the separation mode of the FC-TEG are presented in Fig.2.7. A dynamometer was fixed with jigs on the top side to measure the contact-compression forces acting on the FC-TEG. The initial separation distance (δ_c) was set to 0.5, 1.0, 2.0, and 3.0 mm. To investigate output voltage under the three modes of separation, contact, and compression, the separation amplitude A_v was set to 0.2, 0.3, and 0.4

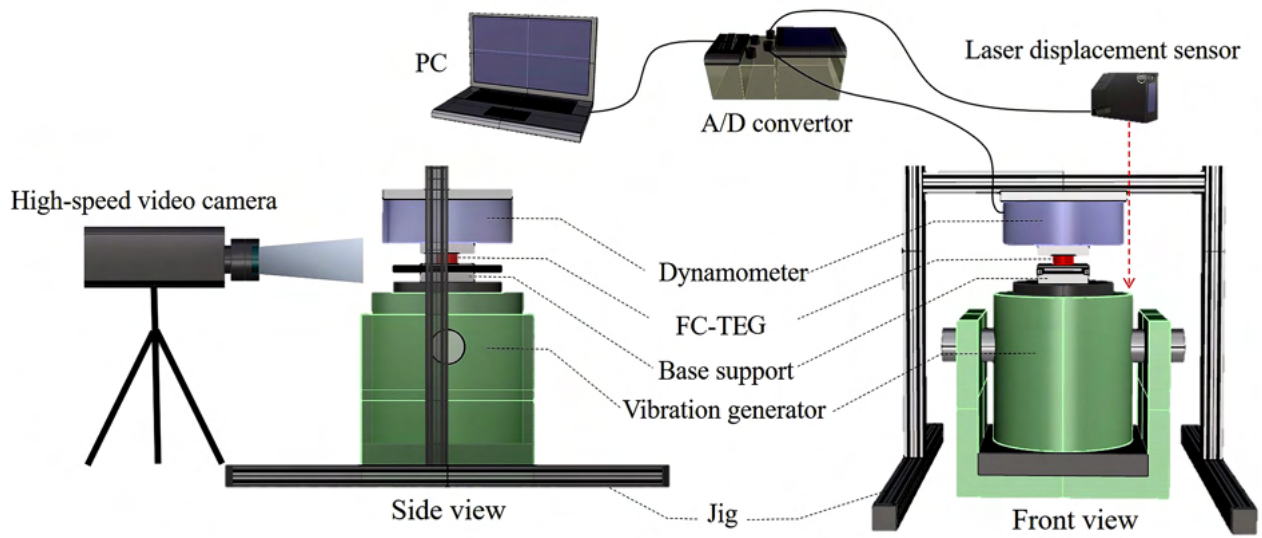


Figure 2.6: Experimental Setup and Measurement System

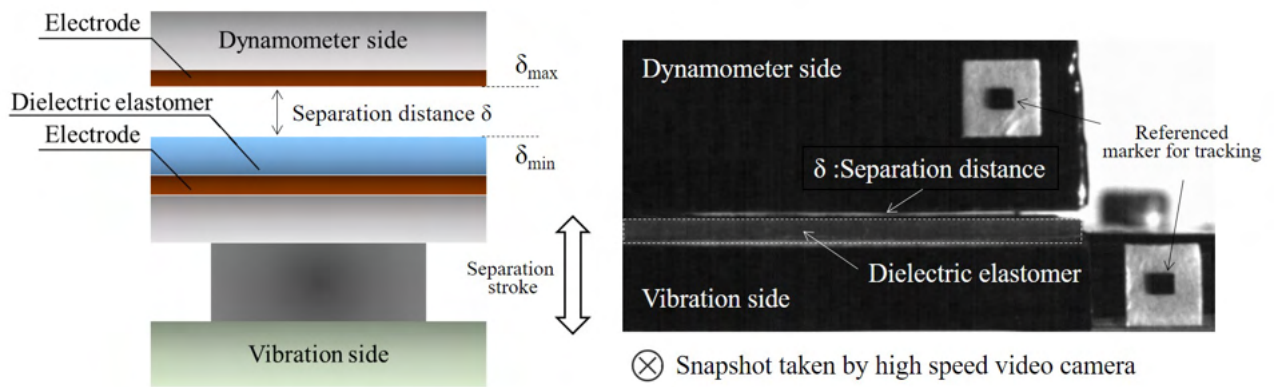


Figure 2.7: Separation distance and instantaneous capture of the separation mode of the Single TEG

mm for the separation mode; 0.5 mm for the contact mode; and 0.6, 0.7, 0.8, and 0.9 mm for the compression mode. To control the separation velocity, the vibration frequency (f_v) was set to 1, 2, 4, 6, 8, 10, 15, 20, 25, and 30 Hz. The mechanism of the vertical contact-separation-compression state is illustrated in Fig.2.8, while the illustration for all working modes and Fig.2.9.

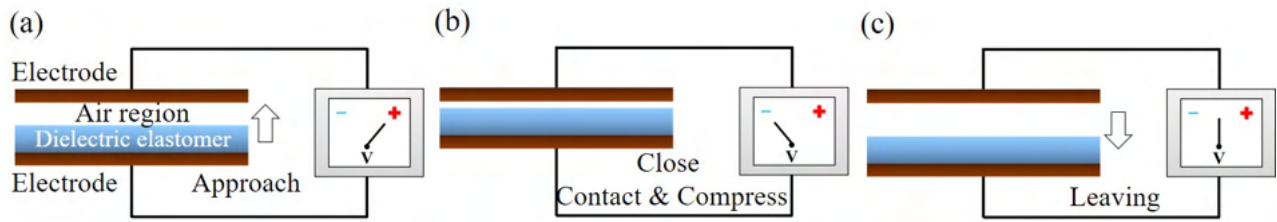


Figure 2.8: The mechanism of vertical contact-separation-compression state

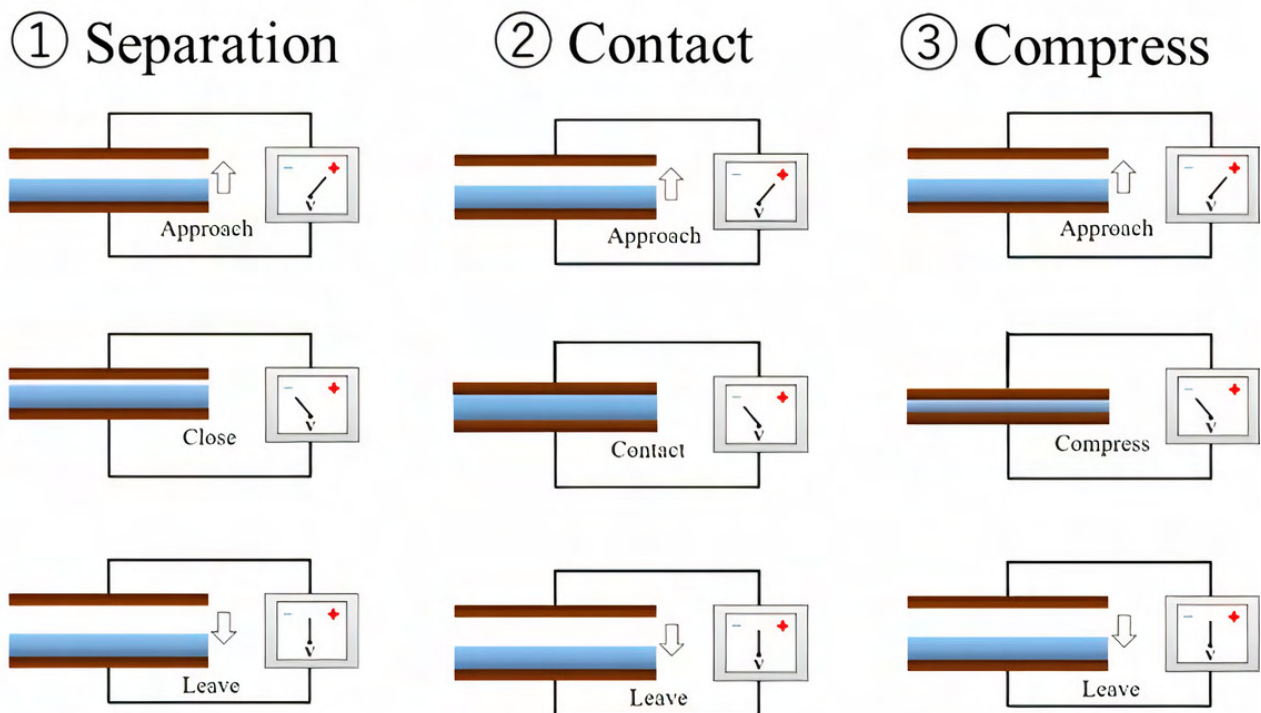


Figure 2.9: FC- TEG on the separation, contact, and compression mode

2.4 FC-TEG only experiments results

2.4.1 Output voltage results based on a various taping mechanism

The taping mechanisms results are shown in Fig.2.10 for the experiments at 10 Hz, Fig.2.11 for the experiments at 20 Hz, and Fig.2.12 for the experiments at 30 Hz. The dots represent a type of taping mechanism in the figure, with each color illustrating each type. All four-taping mechanisms of the elastomer were also tested on different frequencies. The voltage value in the figures was selected based on the time history result of the vertical experiment test. Based on those time-history results, we chose the highest output value once the electrical output voltage has been stable.

We can see that all results between several frequencies are similar to each other. In general, type 2 provides the highest voltage in all cases. Interestingly, type 2 does not have the highest surface area value but can generate the largest output voltage for the FC-TEG. The 2nd largest voltage is achieved by type 4, which has a similar setup as type 2 but with the addition of 1 small tape at the top of the elastomer. Surprisingly, type 3 that has the same surface area as type 2 (highest taping mechanism result), has much a lower output voltage value. Finally, type 1 has the smallest surface area is also shown in the figures.

Based on all the results, the maximum output voltage value on each surface area of the elastomer is shown in Fig.2.13. The surface area provides a minor relationship to the voltage result. The results of type 2 and type 3 demonstrated that the voltage difference is relatively high even though they have the same surface area. Therefore, we conclude that the output value could be changed depending on the contact point between elastomer and the copper films. Additionally, we found that the electricity tends to be larger when the endpoint of the elastomer is not fixed.

Based on the results, we hypothesized that with the higher frequencies, the output voltage results tend to be higher as well. It will be interesting to identify the highest frequency applied on the FC-TEG that could generate the most efficient result. In addition, because the results

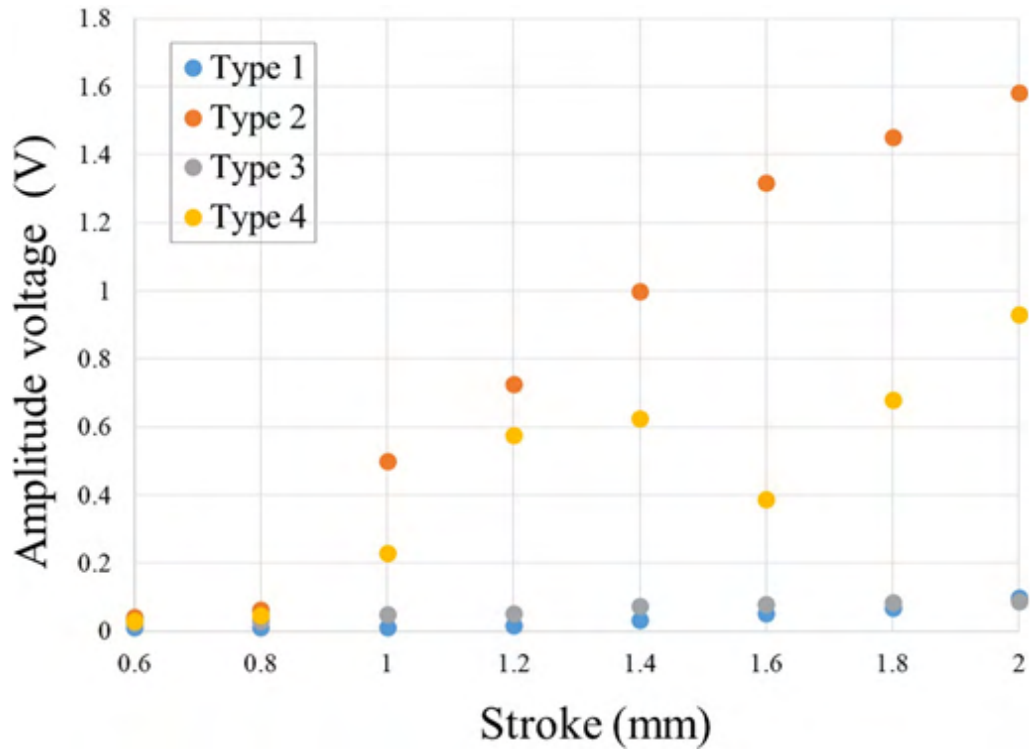


Figure 2.10: Voltage and stroke for all tapping mechanism on 10 Hz

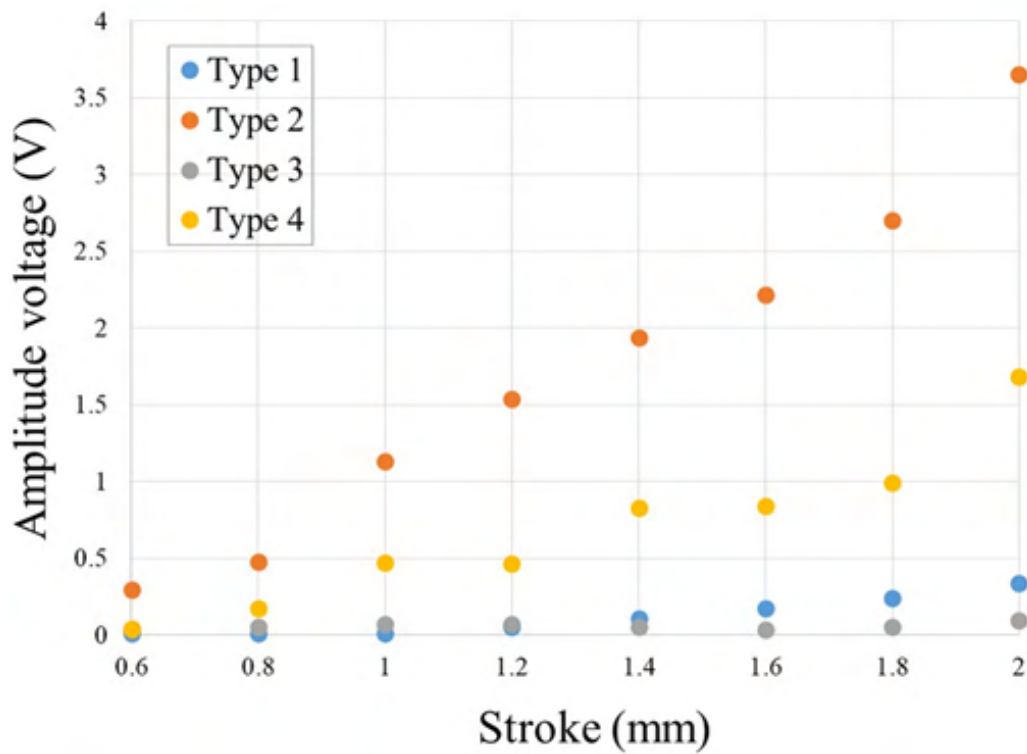


Figure 2.11: Voltage and stroke for all tapping mechanism on 20 Hz

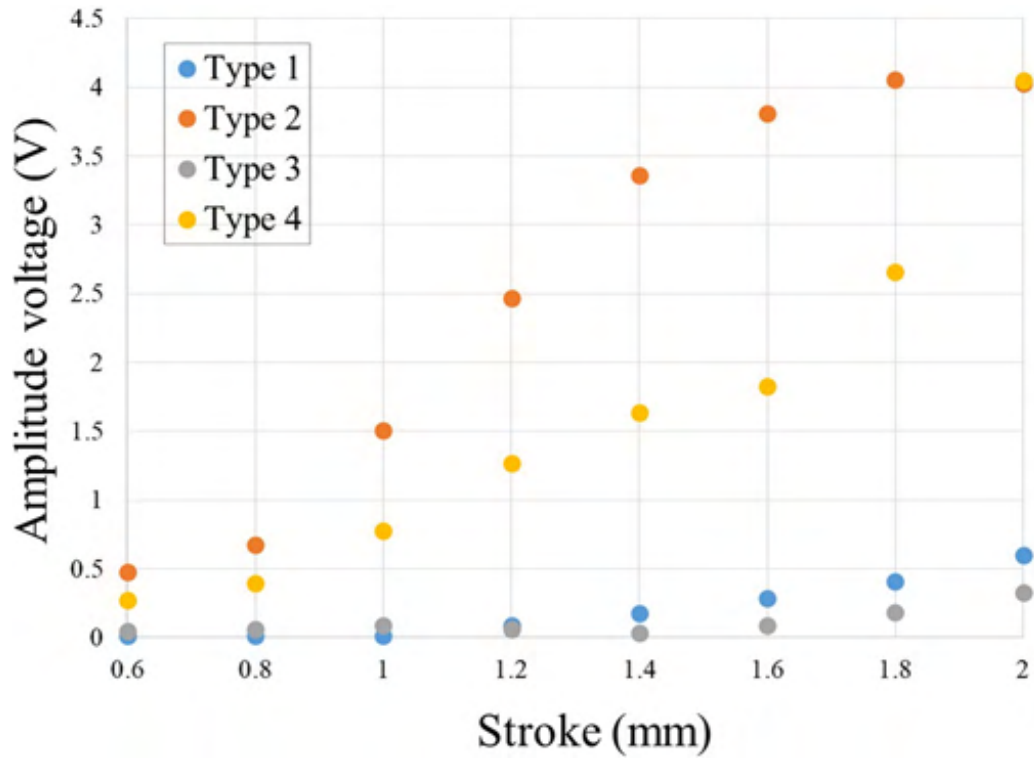


Figure 2.12: Voltage and stroke for all tapping mechanism on 30 Hz

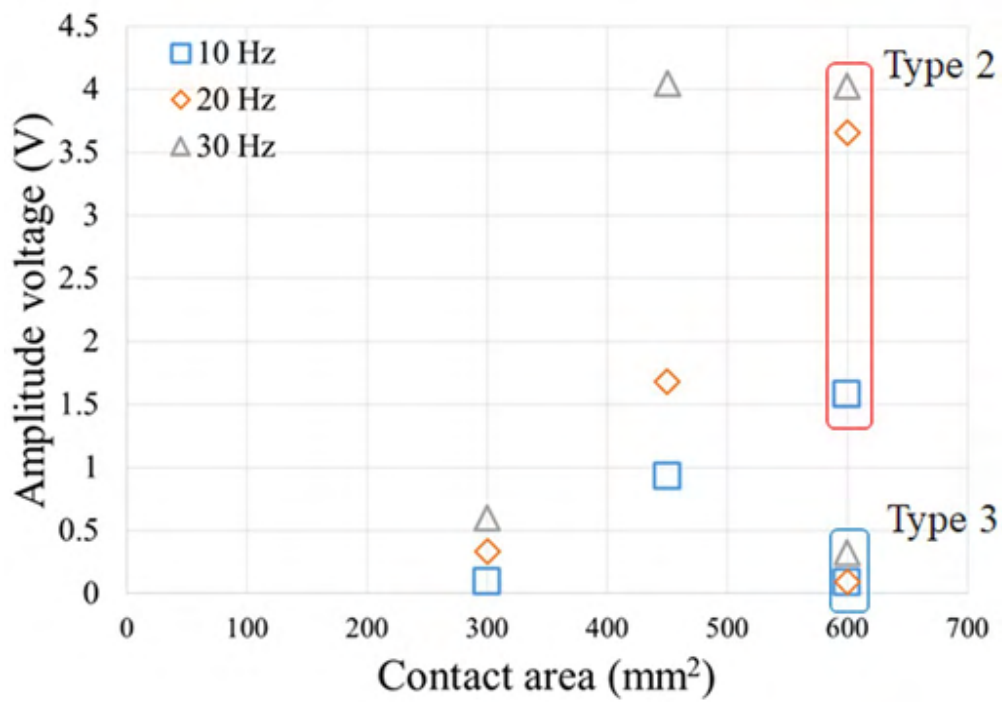


Figure 2.13: Comparison of best tapping mechanism on various contact areas

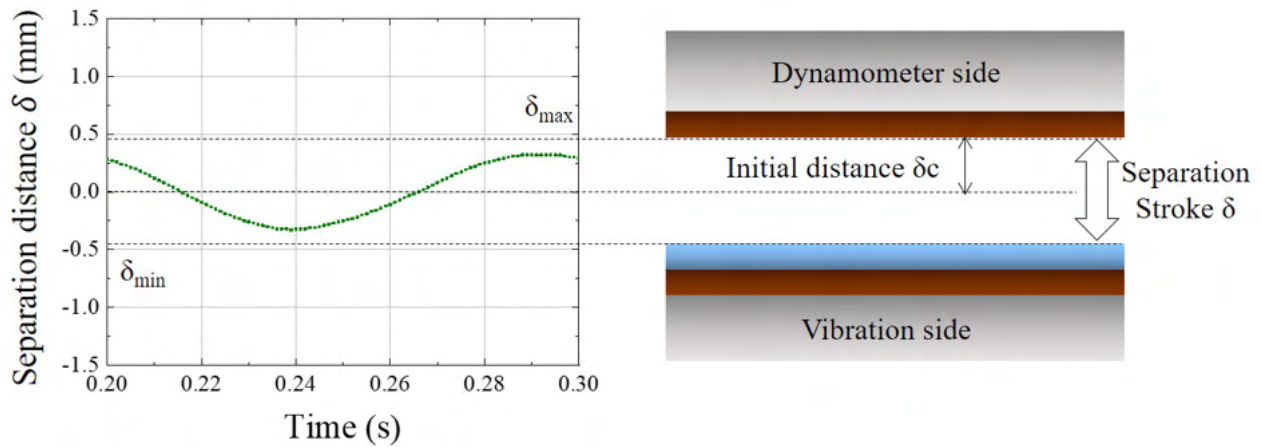
show that type 2 has the most efficient output, we decided to focus and use this setup on all following subsections and the rest of our study.

2.4.2 Output voltage characteristics in the separation – contact – compression modes

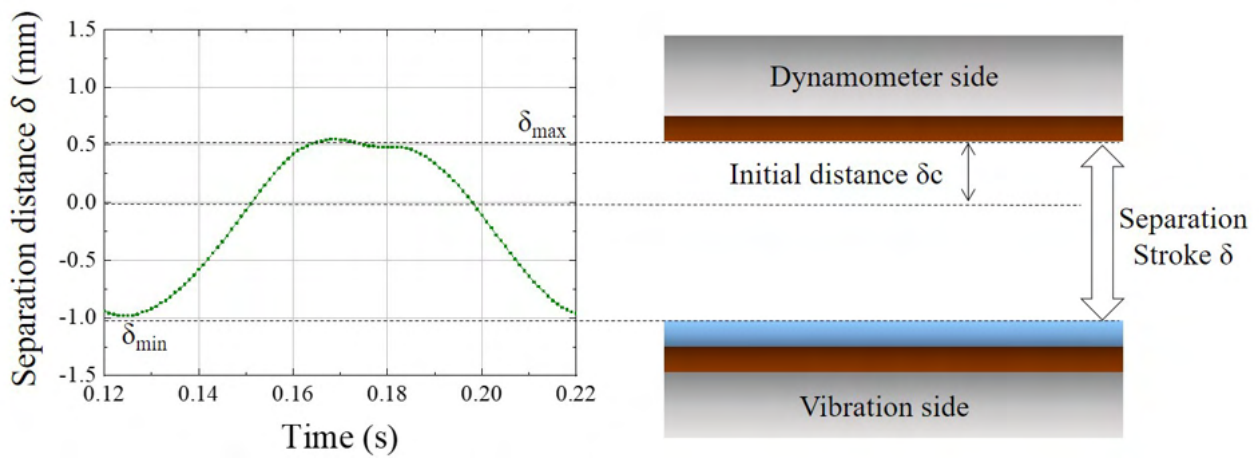
This section explains the output voltage characteristics based on the FC-TEG's fundamental working modes. Before presenting the output voltage result, the elastomer's time history and its separation distance need to be explained. The working mode and the time histories of the FC-TEG are presented in Fig.2.14. δ_c is the initial distance varied in the experiments (0.5, 1.0, 2.0, and 3.0 mm). In comparison, the δ_{max} and δ_{min} are the separation stroke in the elastomer that is changed based on the set of the amplitude A_v .

The time history based on the separation mode can be seen in Fig.2.14a, while the contact/compress mode is displayed in Fig.2.14b. In the separation mode, a condition with $A_v = 0.4$ mm and an initial distance $\delta_c = 0.5$ mm was chosen as an example; the dielectric elastomer did not come into contact with the top electrode. Even though this may be the case, a triboelectric potential layer was still created between them. In contrast, for the compression mode case with the $A_v = 0.9$ mm and $\delta_c = 0.5$ mm, the dielectric elastomer came into contact with the top electrode. Since the amplitude A_v is higher than its δ_c the elastomer was compressed. This state can be seen in Fig.2.14b during $t = 0.16 \sim 0.19$ s with the green line showing no separation distance. In the contact mode, the initial separation distance δ_c was equal to the separation amplitude A_v , and the compression load on the dielectric elastomer was nearly equal to zero.

The FC-TEG output voltage sample results alongside the separation stroke and the load stress are shown in Fig.2.15 – Fig.2.17. The sample results are the FC-TEG vibration test results that are chosen to represent the characteristics of FC-TEG output on three different modes. The separation mode ($A_v = 0.3$ mm) is presented on Fig.2.15, contact mode ($A_v = 0.5$ mm) is presented on Fig.2.16, while Fig.2.17 displayed the compression mode ($A_v = 0.9$ mm), with



(a) Separation mode ($A_v = 0.4\text{mm}$, $f_v = 10\text{Hz}$)



(b) Contact/compress mode ($A_v = 0.9\text{mm}$, $f_v = 10\text{Hz}$)

Figure 2.14: Three working modes and time histories of the FC-TEG

the tested vibration frequency (f_v) of 10 Hz. For this sampling, the initial distance was set at 0.5 mm. We periodically measured the output voltages and ensured that the FC-TEG were observed without electrical noise.

We can see clearly that Fig.2.15 presents the separation mode since the value of the stress was very minimal (almost non-existent); the value of the separation stroke ($A_v = 0.3$ mm) is shown in Fig.2.15b. Since the separation stroke was lower than the initial distance ($\delta_c = 0.5$ mm), the dielectric elastomer is not in contact with the top electrode. However, it can be seen in Fig.2.15a that the output voltage can still be generated even though the value itself is quite small.

In the contact mode shown in Fig.2.16, the output voltage sharpened relatively and almost doubled the result of the separation mode. However, the stress load was nearly zero since the separation stroke ($A_v = 0.5$ mm) equals the initial distance ($\delta_c = 0.5$ mm). Therefore, we conclude that the elastomer is only touching the top elastomer (not compressing or pressing the elastomer), which creates a better electrical response than the separation mode.

On the other hand, the output voltage of the compression mode in Fig.2.17 showed a different pattern compared with previous modes. In this mode, the output result becomes spiky with disturbances alongside its time history. Additionally, the amplitudes showed higher values than the amplitudes in the two previous figures because the elastomer was stressed repeatedly. Due to this repeated stress, the air region as part of the triboelectric layer is disappeared once the separation stroke ($A_v = 0.9$ mm) is higher than the initial distance ($\delta_c = 0.5$ mm). The maximum value of stress load was generated once the elastomer was contacted with the top electrode. This contact resulted in a restriction of the separation stroke; thus, the contact stress in the initial time is developed into compress stress for the elastomer.

Based on the result of the experiment, the effect of initial separation distance δ_c for the FC-TEG output voltage needs to be observed. A comparison of FC-TEG output voltage under several initial distances δ_c versus separation velocity controlled via vibration frequency (f_v) is shown in Fig.2.18. Based on the figures, the output voltage increases once the δ_c decrease. The maximum output voltage was also obtained in the lowest setting of $\delta_c = 0.5$ mm. This

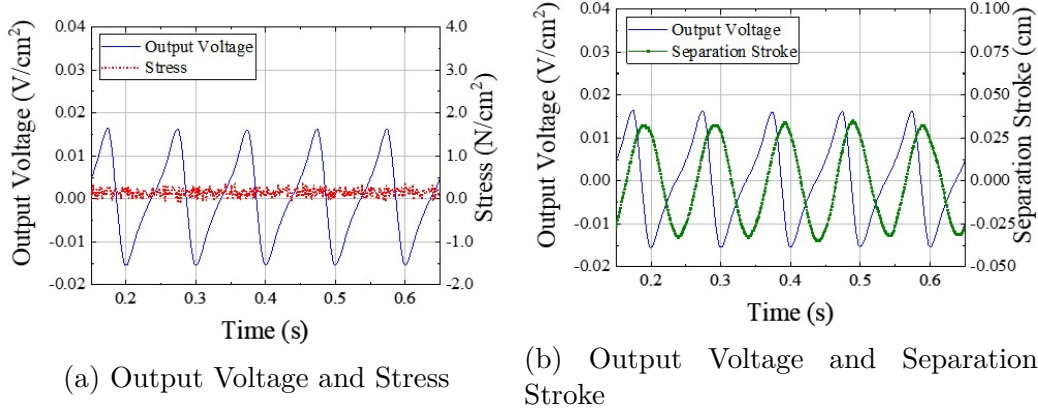


Figure 2.15: Time history of FC-TEG in the Separation mode ($A_v = 0.3$ mm, $f_v = 10$ Hz)

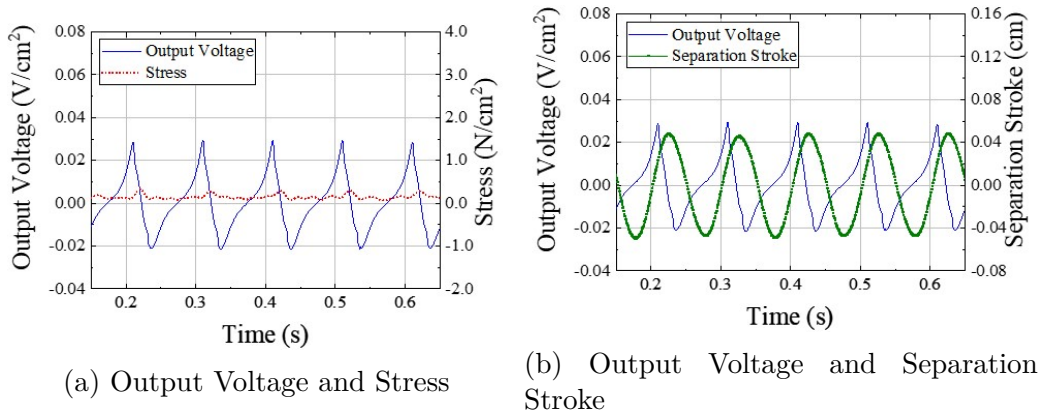


Figure 2.16: Time history of FC-TEG in the Contact mode ($A_v = 0.5$ mm, $f_v = 10$ Hz)

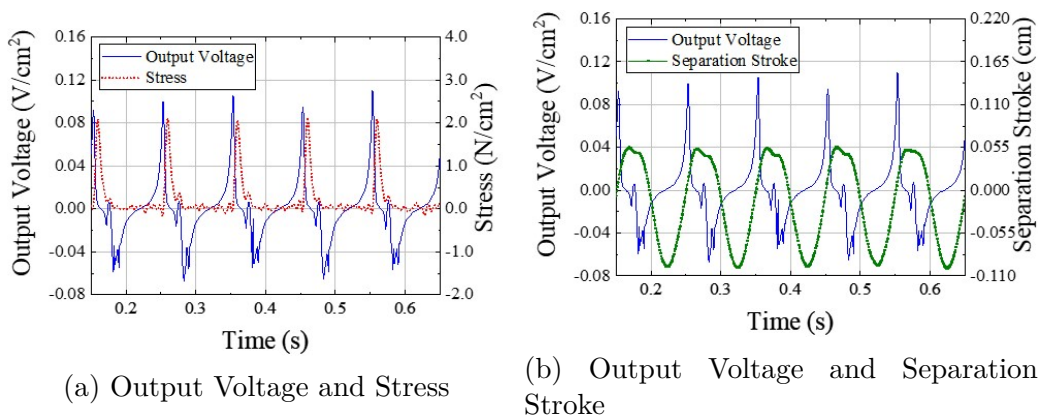
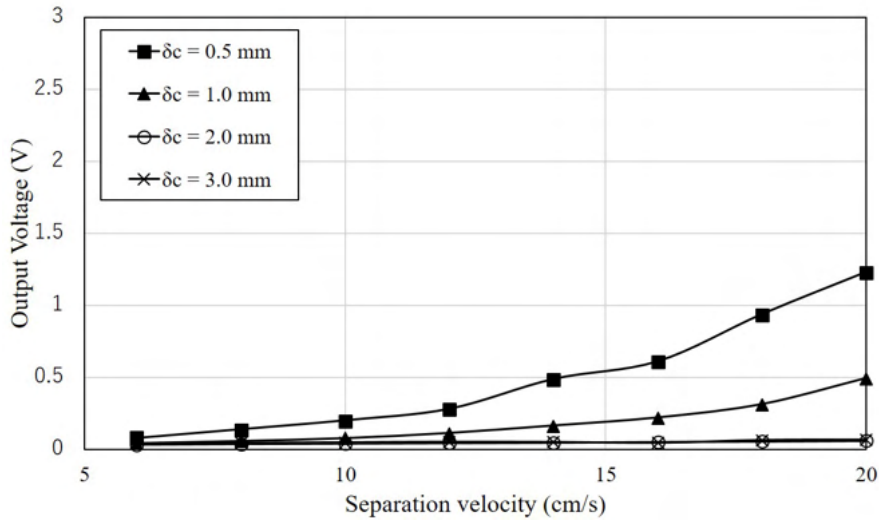


Figure 2.17: Time history of FC-TEG in the Compress mode ($A_v = 0.9$ mm, $f_v = 10$ Hz)

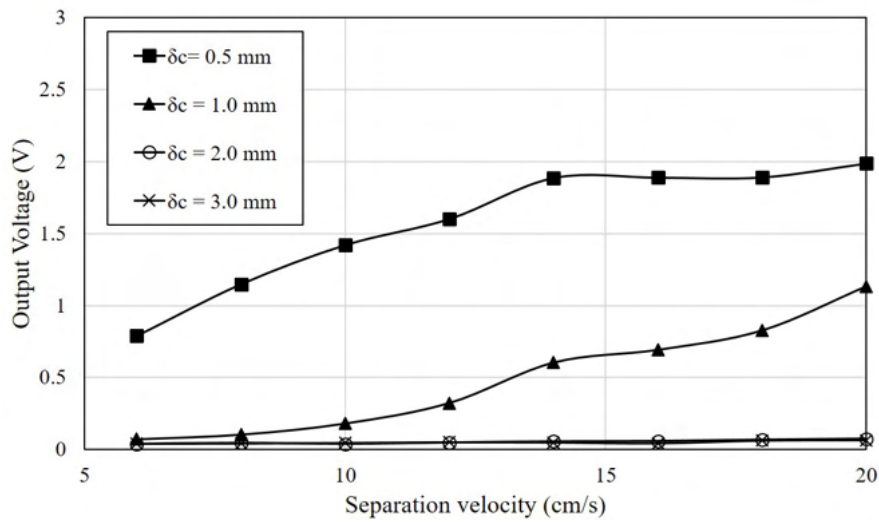
indicates that the lowest δ_c tend to provide better output; however, further research found was later found that this tendency to be slightly inaccurate on much further research. The initial separation distance δ_c needs to be appropriately selected to create the triboelectric potential layer. By creating the optimum layer, high electric performance could be achieved. The figures also showed that the output voltage value increases when the separation velocity also increases; this was especially apparent when the δ_c was smaller. The effect of the separation velocity on the FC-TEG output voltage will be explained on “2.4.3” Effect of separation velocity on the output voltage”.

Since the explanation of the FC-TEG’s power generation mechanism is limited due to the usage of the sampling, Fig.2.19 – Fig.2.22 display the working mechanism of the FC-TEG in more detail. This figure is also named the $V - \delta'$ diagram in order to give more explanation for the relationship between the separation-contact-compress status and the voltage produced by the FC-TEG.

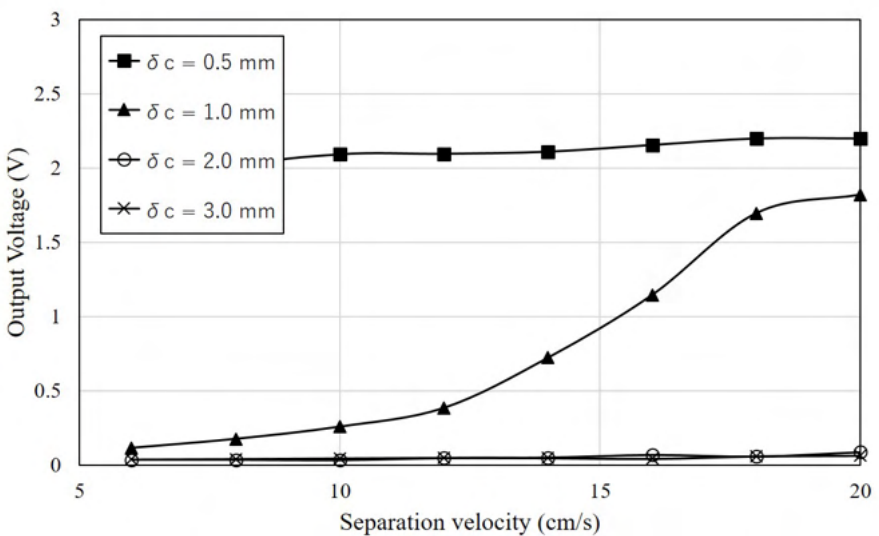
Firstly, the separation mode of the FC-TEG working mechanism is shown in Fig.2.19. This figure shows 50 cycles of FC-TEG operation on a periodic vertical vibration. The separation distance δ' is a distance captured via the high-speed video camera that is normalized via the neutral position based on the $\delta_c = 0.5\text{mm}$. The value of the positive voltage seemingly increases with decreasing δ' once the elastomer surface is approaching the top electrode surface via the movement of the vibration generator. Once the elastomer is very close to the top electrode, the δ' is minimized, but since this is the separation, both materials are not contacting each other, and the positive output voltage is reversed here. Afterward, the output voltage decreases to zero, signaling that the dielectric elastomer is withdrawing from the maximum of the δ' . Then, the negative triboelectric charges on the elastomer to drive the free-electron inside a current flow through back the external circuits. With this vertical movement, the FC-TEG acts as a producer of the electron that causes the electrons to move forward and backward between two electrodes on the top and lower side (top and bottom copper films). Based on the triboelectric cycle, these electrons are extracted from the surface of the dielectric elastomer to both electrodes.



(a) Vibrated frequency of 10 Hz



(b) Vibrated frequency of 20 Hz



(c) Vibrated frequency of 30 Hz

Figure 2.18: Effect of initial separation distance and separation velocity on the output voltage

Secondly, the $V - \delta'$ diagram of the contact mode is presented in Fig.2.20. In the figure, it can be seen that the tendency of the $V - \delta'$ diagram is similar to the separation mode that was mentioned before. However, the magnitude of the output voltage and the δ' in the diagram is much greater, with the minimum δ' equal to the amplitude ($A_v = 0.5$ mm). This equality indicates that the elastomer is contacting the top elastomer when the output voltage is nearly equal to zero. But no stress load was present in this state and only slightly touched on both the elastomer and the top electrode surface. The highest output voltage occurs slightly before the contact between two materials. This tendency is also apparent in the separation mode before (see Fig.2.19).

Lastly, Fig.2.21 shows the $V - \delta'$ diagram of the compression mode. Unlike two previous modes, the output voltage increases rapidly once the δ' decreases. However, the maximum output voltage is also attained before contact on the “approaching state,” even in the absence of the compression in the elastomer.

Once the dielectric elastomer is contacted and compressed at $\delta' = 0.5$ mm, the triboelectric potential layers in the air region disappear. Next, the output voltage suddenly drops from a positive value to a minimum when the distance $\delta' \leq 0.25$ mm.

The comparison of all $V - \delta'$ diagrams for all modes is presented in Fig.2.22 to clarify the characteristics of the working mechanism of the FC-TEG. This figure shows that the magnitude shown in $V - \delta'$ diagram increases gradually when the separation stroke (A_v) increases under the same frequency ($f_v = 10$ Hz). The minimum output voltage is generated at the maximum $\delta' = 0.5$ mm. This means that in this distance, the elastomer has already touched with the top electrode both in contact and compression modes. This also means that the minimum output voltage for the compression mode is generally limited by the thickness of the elastomer, which is equal to 12 mm in this study.

In contrast, the maximum output voltage in all cases was occurred right before the contact or compression of the elastomer, even in the compression mode. This indicates that the electrical voltage of the FC-TEG tends to be significantly dependent on the separation velocity rather than the separation distance δ' . As previously displayed on the time histories (Fig.2.15 –

Fig.2.17), the phase observed in the time history slightly differs between the output voltage and the separation stroke. That difference is the time variation of the thickness of the triboelectric potential later. This is what is called the separation velocity. The separation velocity indicates that this parameter could be the key-points for achieving high electrical performance from the FC-TEG that will be explained in the following sub-section.

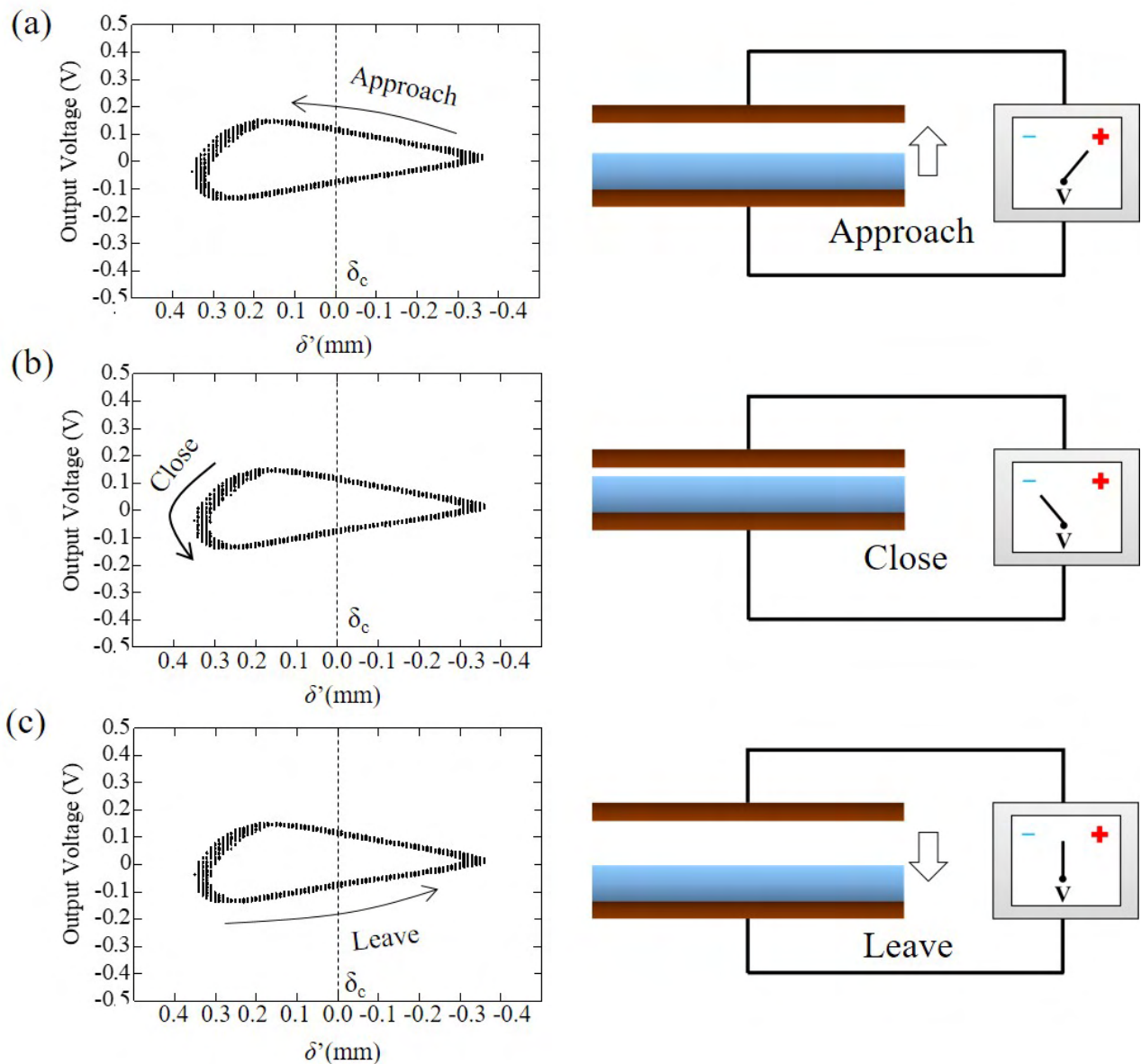


Figure 2.19: The $V - \delta'$ diagram in separation mode

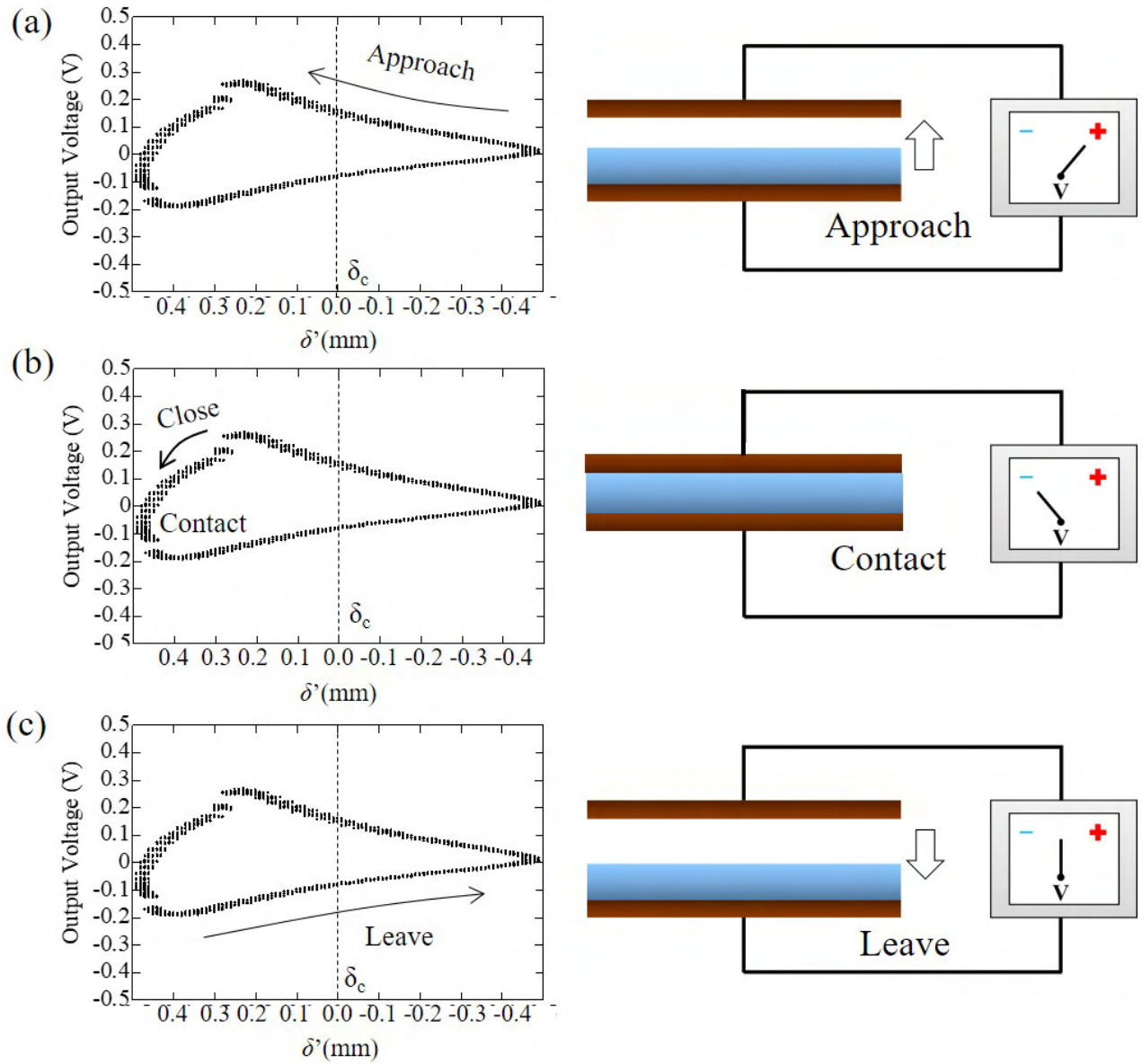


Figure 2.20: The $V - \delta'$ diagram in contact mode

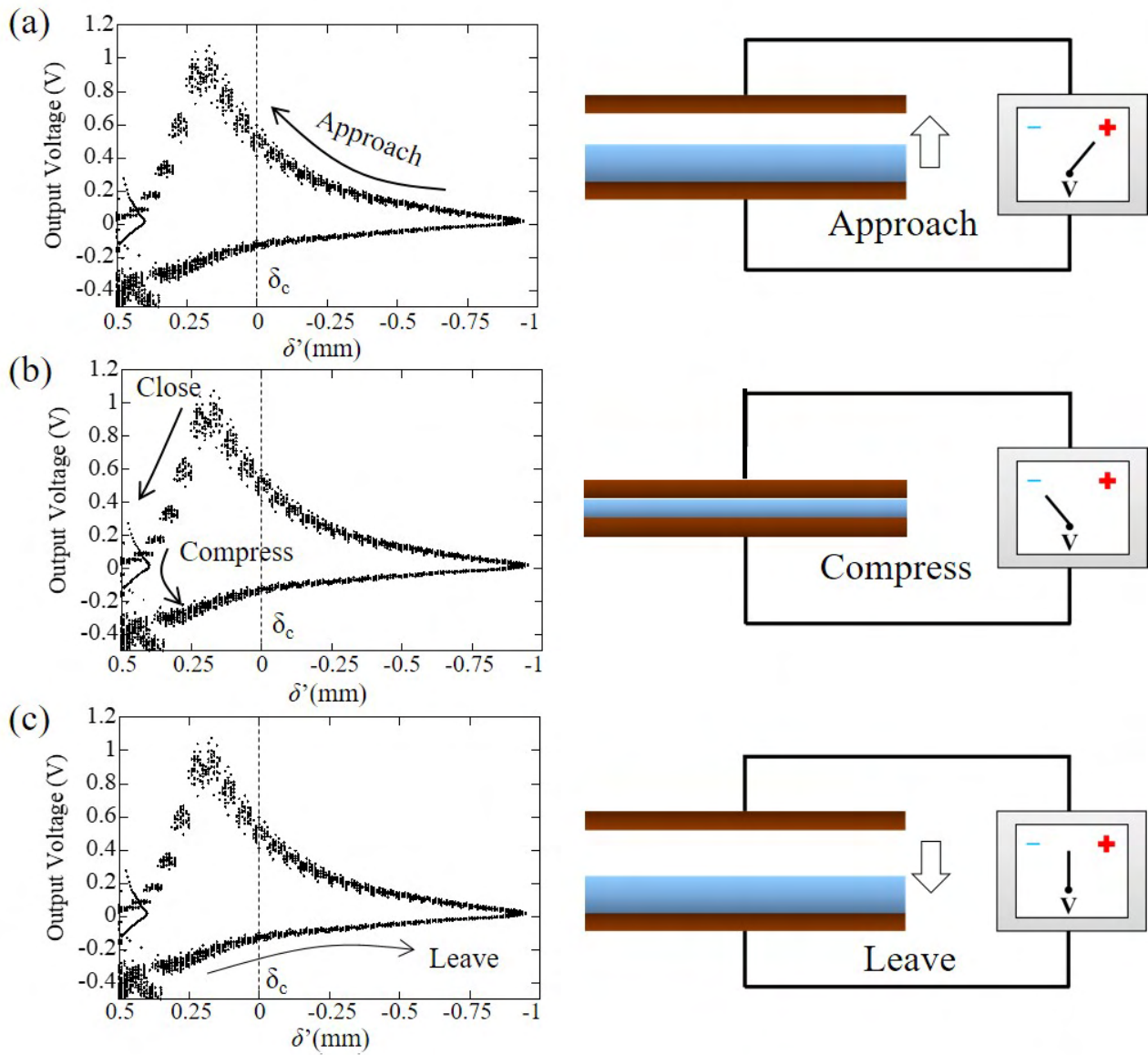


Figure 2.21: The $V - \delta'$ diagram in compress mode

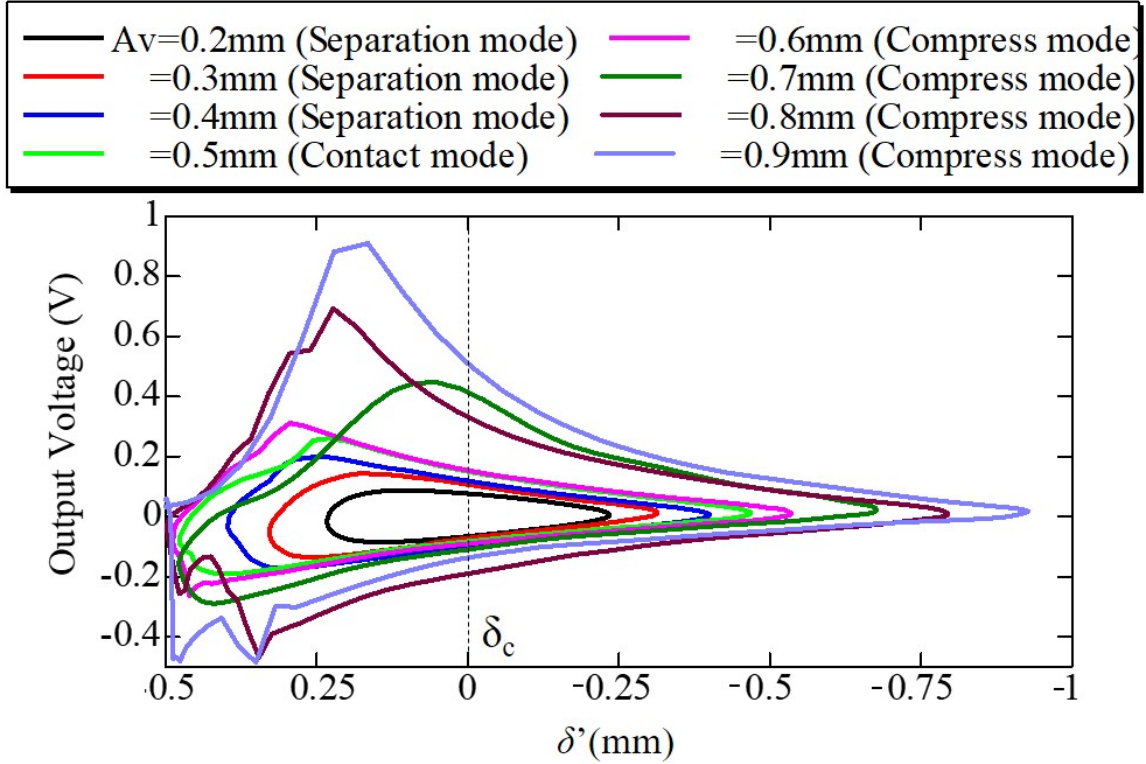


Figure 2.22: Comparisons of the $V - \delta'$ diagrams from all cases

2.4.3 Effect of separation velocity on the output voltage

This section investigates the effects of the separation velocity on FC-TEG on its output voltage. The illustration of the time variations of the output voltage generation and the separation velocity can be seen in Fig.2.23. All five images were chosen to represent all modes of the FC-TEG (separation, contact, and compress mode).

Firstly, it could be seen on the separation mode (Fig.2.23a and Fig.2.23b) that the phase between separation velocity and the output voltage almost coincides. This informs us that output voltage is generated alongside the separation velocity during the vibration tests. In the contact mode (Fig.2.23c), the maximum and minimum values of the output voltages are generated when the value of separation velocity is also maximized and minimized. Thus, the contact mode has a similar tendency to the separation mode. In the compression mode (Fig.2.23d and Fig.2.23e), the tendency is similar but has a small difference. The minimum output voltage occurs during the contact and compression process of the dielectric elastomer

and the copper films. In contrast, when the separation velocity is close to zero, the output voltages also decline and approximately have zero value. Based on these tendencies, it can be indicated that the maximum output voltage peak increases when the separation velocity is also increased (positive correlation).

Fig.2.24 shows the relationship between the maximum/minimum voltages value and the frequency, while Fig.2.25 shows the relationship between maximum / minimum voltage value and the separation velocity. The solid marks are for the separation-contact modes in the figures, while open marks are for the compression mode. Both figures illustrate the direct relationship between the frequency with FC-TEG output voltage and separation velocity with the output voltage.

As seen in both figures, the value of the maximum/minimum output voltages increases with both the frequency and the separation velocity. Since the separation and contact modes have similar tendencies, the maximum and minimum voltages values are almost equal. However, in the compression mode, the maximum velocity increases rapidly. This rapid increase is due to the maximum output voltage that can be superimposed via the contact and separation effects alongside the compression effect.

Therefore, it can be concluded that by increasing the separation velocity, the amount of output voltage could be increased as well.

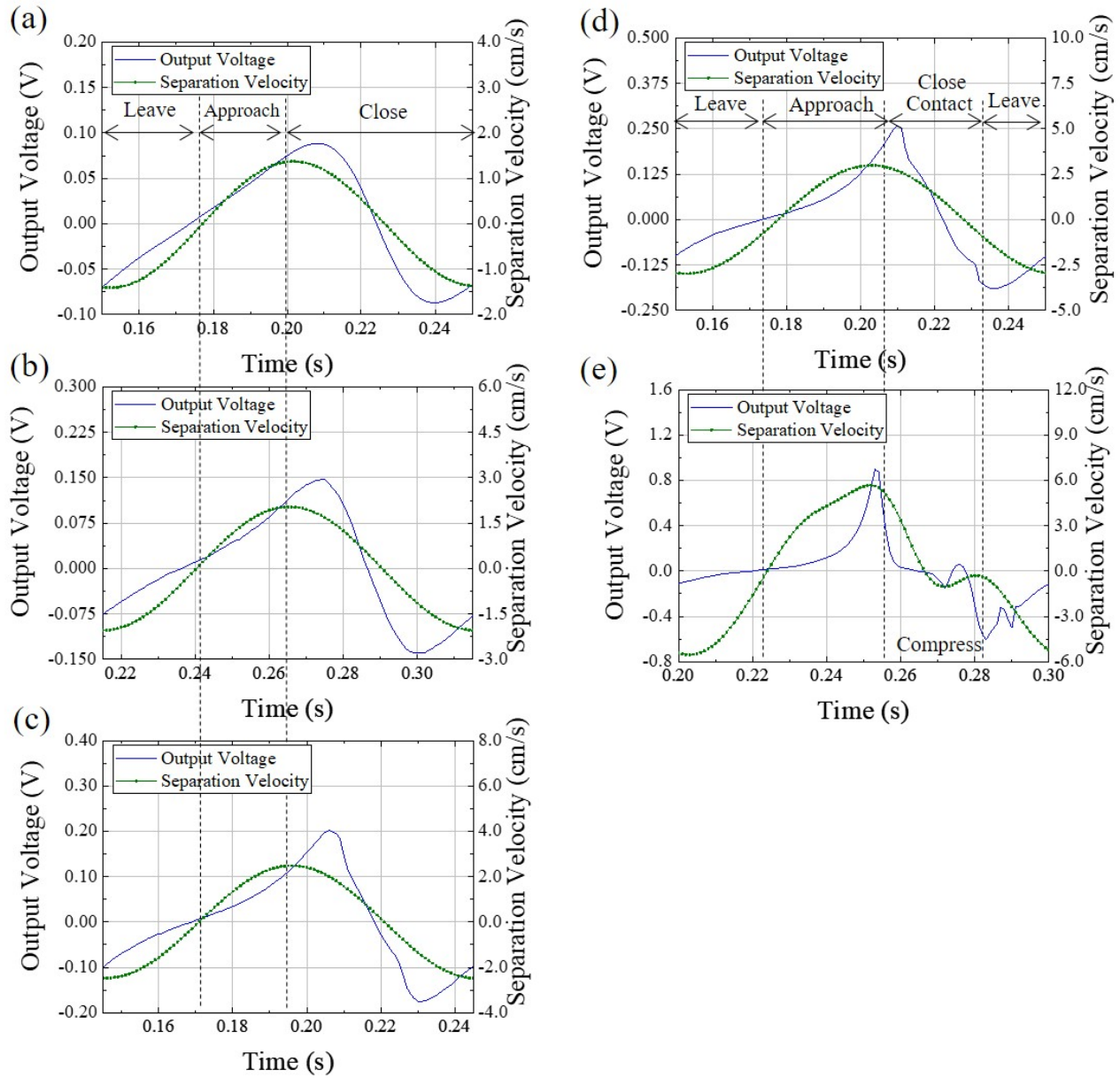
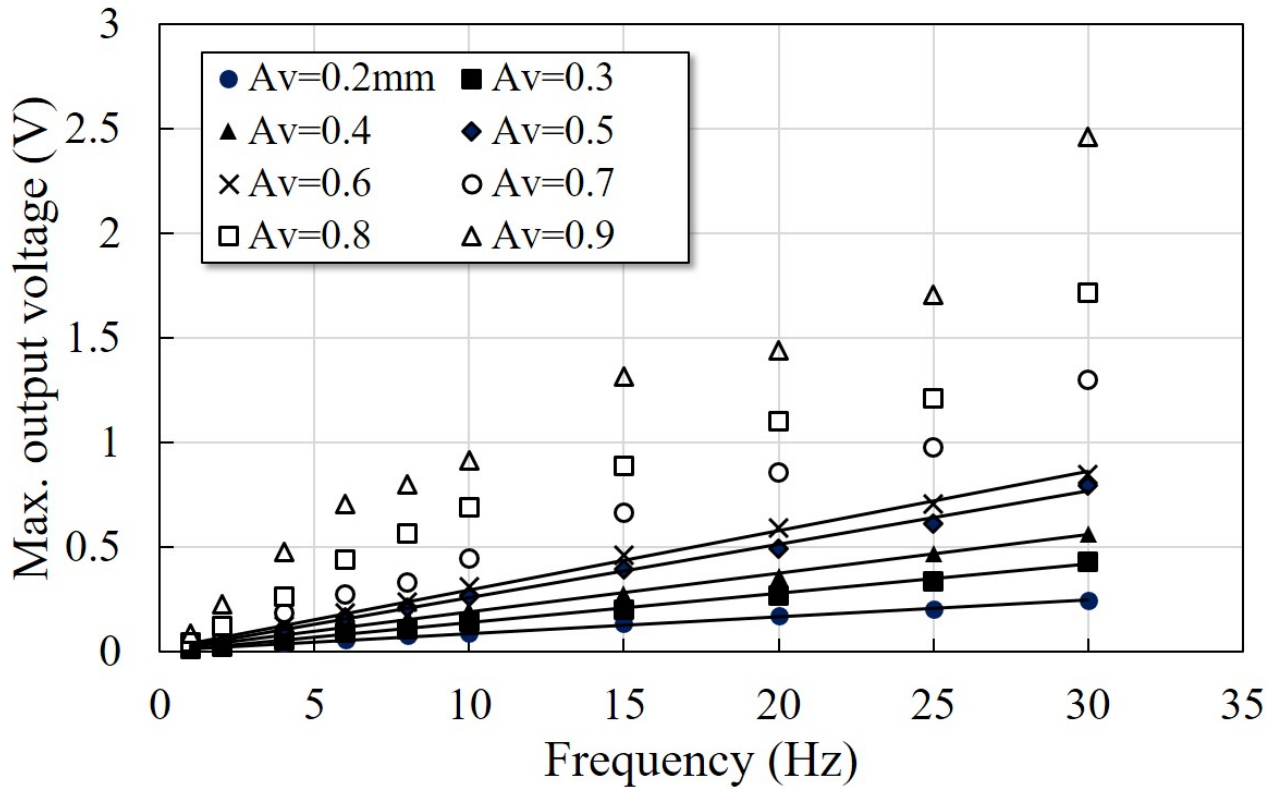
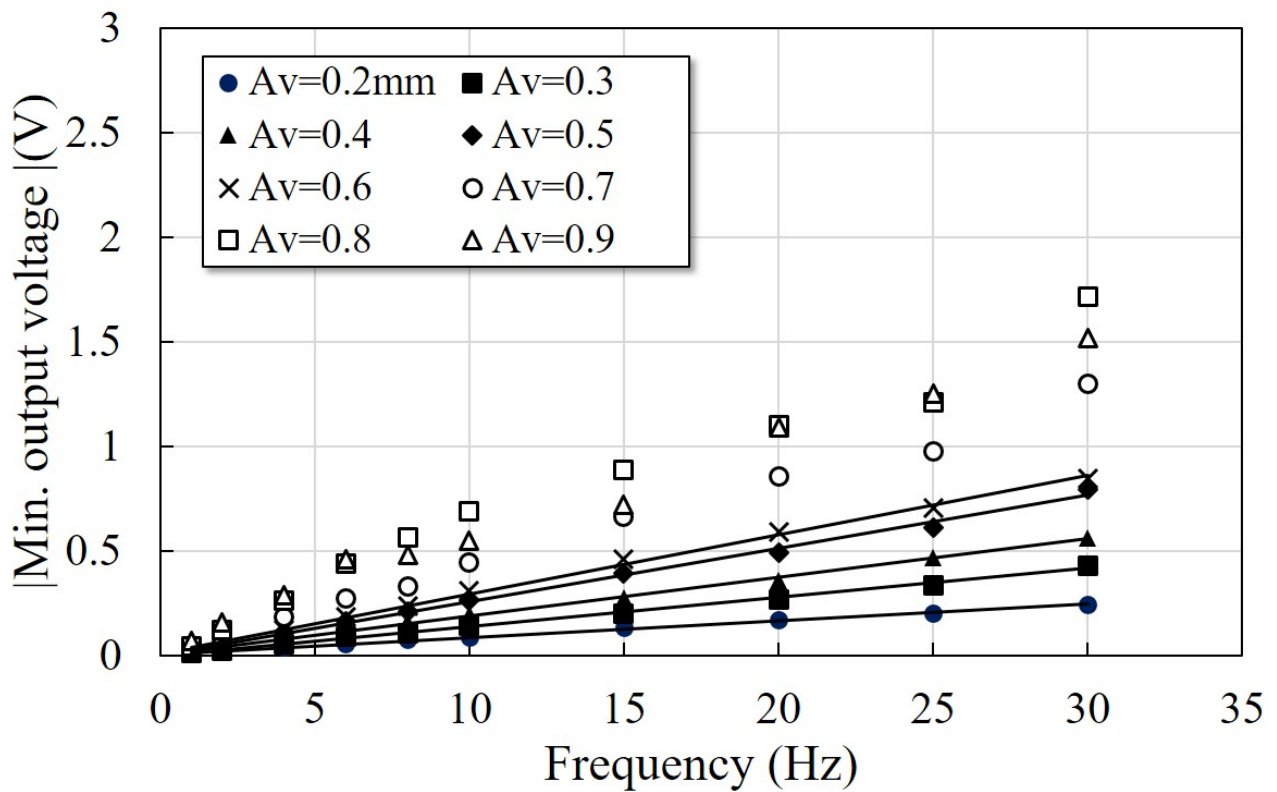


Figure 2.23: Time histories of output voltage and separation velocity: (a) separation mode ($A_v = 0.3$ mm), (b) separation mode ($A_v = 0.4$ mm), (c) contact mode ($A_v = 0.5$ mm), (d) compression mode ($A_v = 0.6$ mm), and (e) compression mode ($A_v = 0.9$ mm)

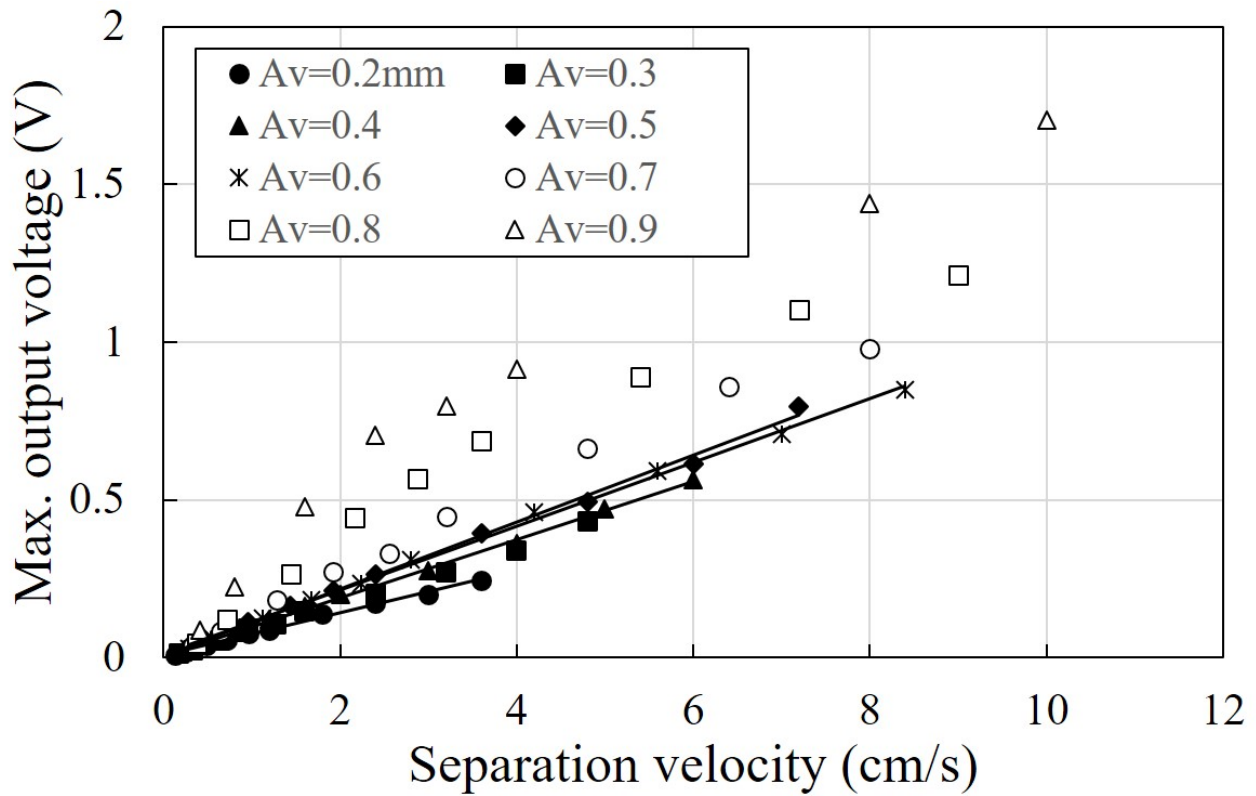


(a) Maximum output voltage

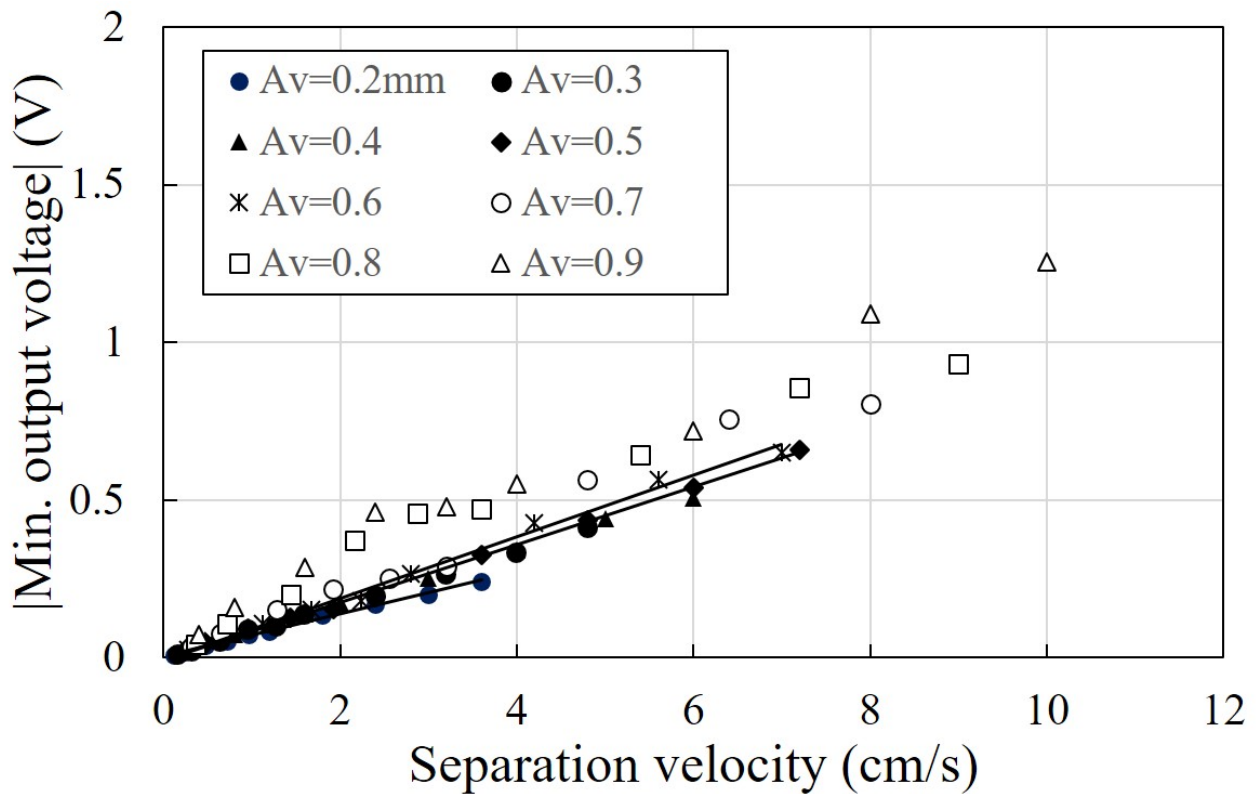


(b) Minimum output voltage

Figure 2.24: Relationship between max./min. output voltages and separation frequency



(a) Maximum output voltage



(b) Minimum output voltage

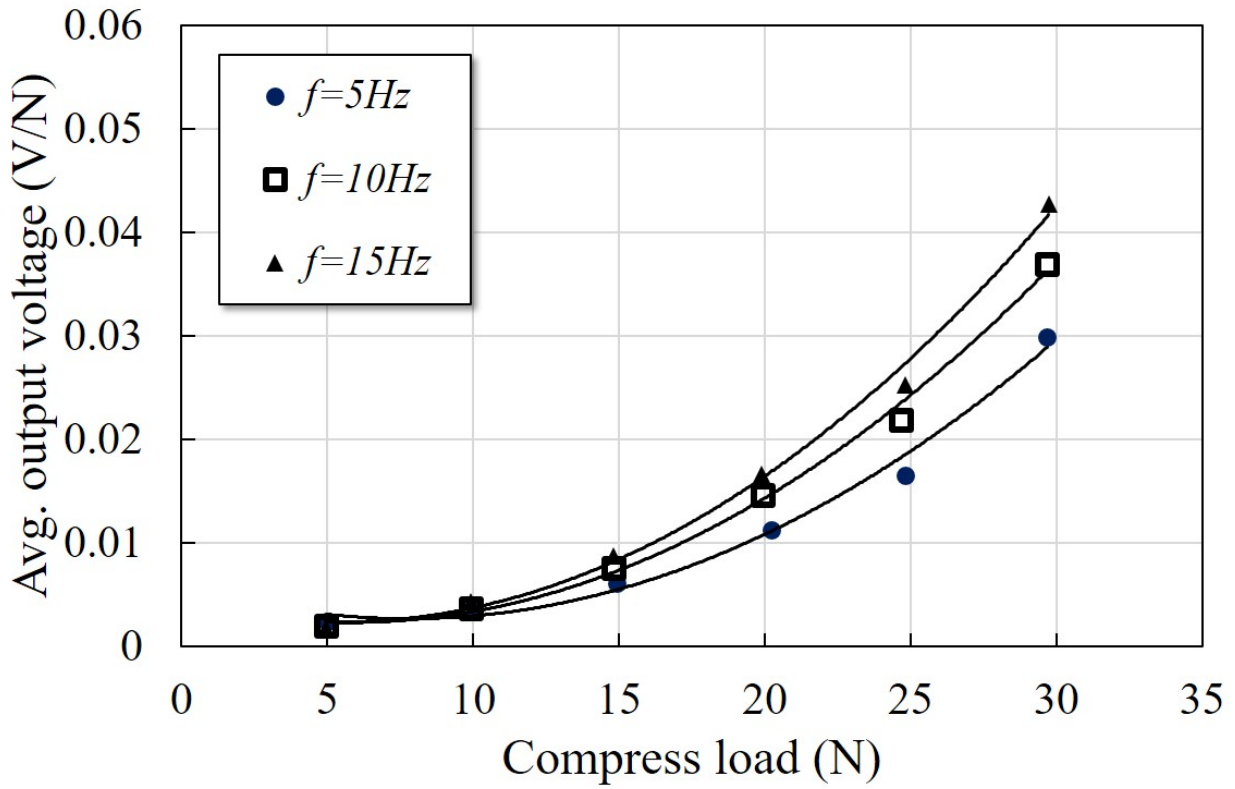
Figure 2.25: Relationship between max./min. output voltages and separation velocities

2.4.4 Effect of the compression load on the output voltage

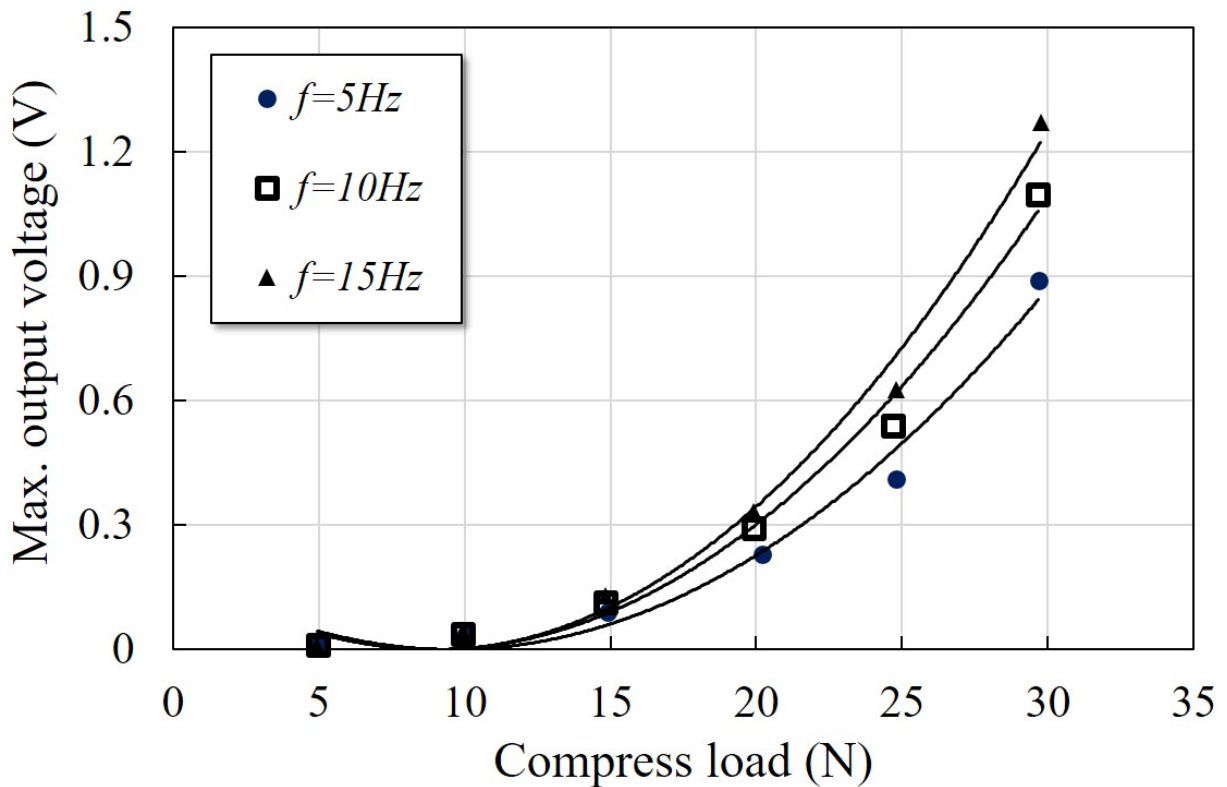
Based on our previous findings, several results indicated that compression load might be crucial in generating large electrical energy. This indication is important since the FC-TEG needs to be able to utilize various ambient energy. For this reason, the FC-TEG needs to use not only the contact-separation mode but also the compression mode for increasing its electrical efficiency as a whole energy harvester. This is especially important because direct contact based on natural energy mainly has a large force, which in turn makes the compression mode occur much more often. Thus, this section examines the effects of the compression load on the FC-TEG output voltage.

The initial load on the FC-TEG was zero since, in the beginning, no contact and compression occurred. Once the vibration generator started to move and make both elastomer and copper films contact and compress, the compression load started to emerge. The compression load value is around $0.5 \sim 3.3 \text{ N/cm}^2$, and it acts periodically on the FC-TEG.

The averaged and maximum output voltages normalized by the compression load can be seen in Fig.2.26. The figures displayed that the output voltage is also increased drastically by increasing the compression load. This is especially apparent in a case with high frequency (i.e., 15 Hz case). Another parameter, such as FC-TEG strain rate, was also observed to present its relationship with the thickness of the dielectric elastomer. Fig.2.27 presents the effect of the strain rate for the average output voltage (Fig.2.27a) and the maximum output voltage (Fig.2.27b). Based on this result, the FC-TEG can generate electrical power from both the contact-separation mode and the compression mode. Moreover, because the strain rate has a positive correlation with the voltage value, the vertical strain rate is one of the key factors for generating efficient electrical energy.

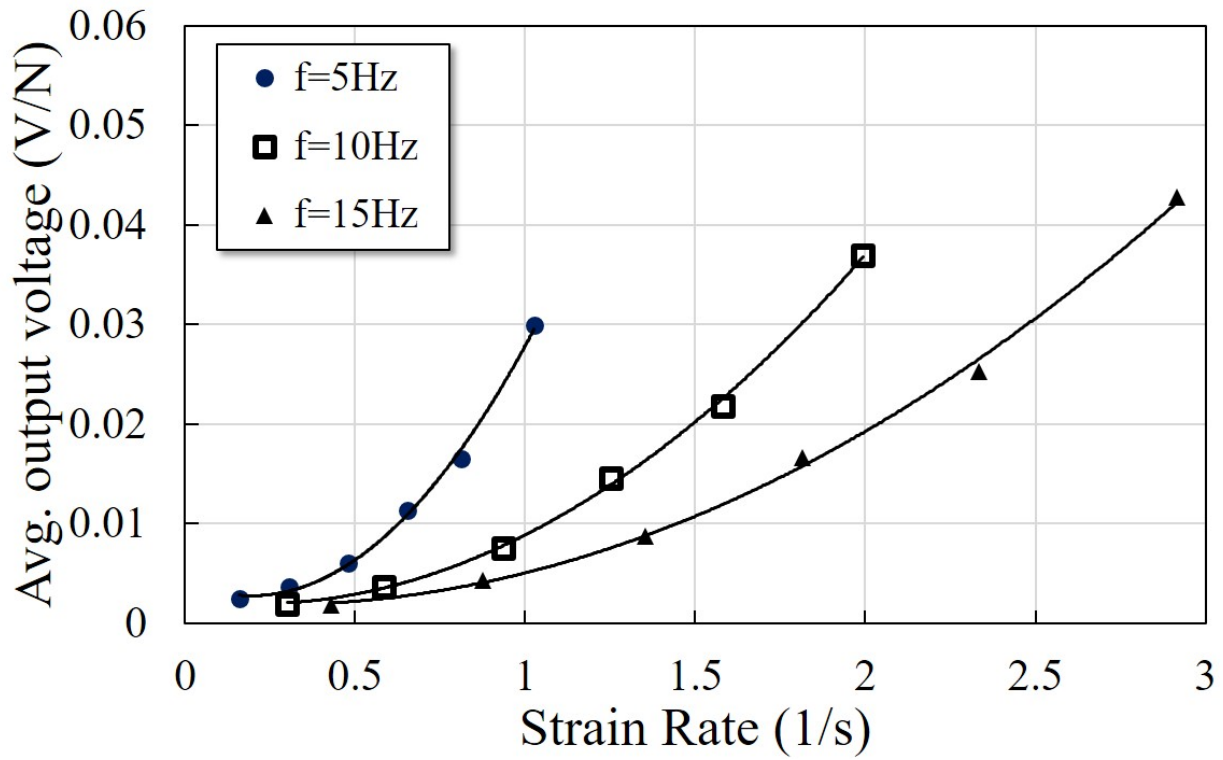


(a) Averaged output voltage

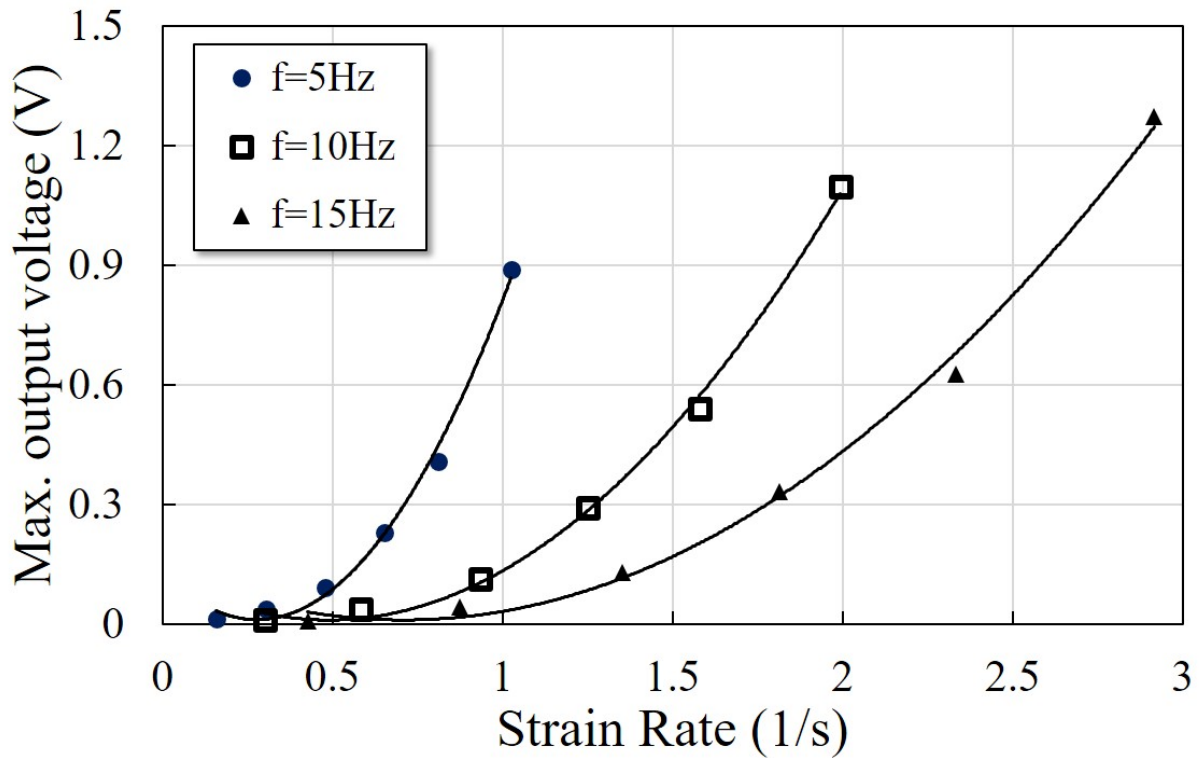


(b) Maximum output voltage

Figure 2.26: Relationships between the output voltages and the compression load of the FC-TEG



(a) Averaged output voltage



(b) Maximum output voltage

Figure 2.27: Relationships between the output voltages and the vertical strain rates of the FC-TEG

2.5 Summary

This chapter developed and examined a flexible and compressible triboelectric generator (FC-TEG) to harvest natural energies and mechanical vibration via a tribological process. The vertical contact-separation-compression test was preliminarily conducted in the experiment for four main purposes. To essentially examine the output voltage generated by the FC-TEG, to find which taping mechanism for the FC-TEG that can provide the best output voltage, to observe the working mechanism of power generation of the FC-TEG, and to make clear the effects of some key parameters. The key parameters that are mainly compared and made clear are the separation distance and the separation velocity. All tests were conducted and observed for the FC-TEG working modes in the contact/separation/compression modes.

From all works, the main summary are obtained as follows:

- In terms of the fixation method / the taping mechanism, using one large tape in the middle of the elastomer (type 2) provides the best output value. By freeing the endpoints of the dielectric elastomer, the elastomer was able to move and contact-separate with the copper films in the most efficient way compared with the other types with similar surface area. Therefore, freeing the ends of the elastomer in the TEG device is crucial to ensure their maximum results.
- In the vertical contact-separation test, the output voltage of the FC-TEG was measured periodically under its output voltage time histories. Strong responses from the device were observed without electrical noise. The output voltage increased considerably with the increasing separation velocities (positive correlation). A suitable initial separation distance δ_c must be selected to create the triboelectric potential layer and achieve high electrical performance.
- The characteristics of the working mechanism of the FC-TEG were elucidated in the separation, contact, and compression modes. It was found that the output voltage depends not on the separation distance but on the separation velocity, which is the time variation

of the thickness of the triboelectric potential layer. This variable could be a key parameter to ensure the high electrical performance of the FC-TEG.

- The FC-TEG provided electric power in both the contact-separation and compression modes. The vertical strain rate of the FC-TEG was found to be a key factor for efficient electrical power generation.

In the future, the FC-TEG should be optimized to realize high performance and efficiency in practical use. An FC-TEG prototype should also be produced and validated for sustainable energies in real application fields.

Bibliography

- [CHIBA and WAKI, 2014] CHIBA, S. and WAKI, M. (2014). Basic Characteristic of Dielectric Elastomer and Their Applications. *Journal of the Japan Society for Precision Engineering*, 80(8):713–717.
- [Chiba et al., 2011] Chiba, S., Waki, M., Kornbluh, R., and Pelrine, R. (2011). Current status and future prospects of power generators using dielectric elastomers. *Smart Materials and Structures*, 20(12):124006.
- [Han et al., 2019] Han, K., Tang, W., Chen, J., Luo, J., Xu, L., and Wang, Z. L. (2019). Effects of Environmental Atmosphere on the Performance of Contact–Separation Mode TENG. *Advanced Materials Technologies*, 4(2):1–8.
- [Jurado et al., 2017] Jurado, U. T., Pu, S. H., and White, N. M. (2017). A contact-separation mode triboelectric nanogenerator for ocean wave impact energy harvesting. *Proceedings of IEEE Sensors*, 2017-Decem:1–3.
- [Muscle et al., 2008] Muscle, A., Carpi, F., and Rossi, D. D. (2008). Dielectric Elastomers as Electromechanical Transducers. *Dielectric Elastomers as Electromechanical Transducers*.

- [Patnam et al., 2020] Patnam, H., Dudem, B., Alluri, N. R., Mule, A. R., Graham, S. A., Kim, S. J., and Yu, J. S. (2020). Piezo/triboelectric hybrid nanogenerators based on Ca-doped barium zirconate titanate embedded composite polymers for wearable electronics. *Composites Science and Technology*, 188(July 2019):107963.
- [Wang, 2013] Wang, Z. L. (2013). Triboelectric nanogenerators as new energy technology for self-powered systems and as active mechanical and chemical sensors.
- [Wang, 2014] Wang, Z. L. (2014). Triboelectric nanogenerators as new energy technology and self-powered sensors - Principles, problems and perspectives. *Faraday Discussions*, 176:447–458.

Chapter 3

Theoretical section of a single dielectric elastomer energy harvesting

3.1 Background

The numerical model was commonly used in order to help estimate the performance of the energy harvesters. Previously, our research group made a similar theoretical model based on the vertical vibration tests but for the Piezoelectric generator (PEG) devices [Nottingham, 2013, Patel et al., 2014, Patel et al., 2016, Mutsuda et al., 2019]. In order to create a theoretical model of the triboelectric generator (TEG), the basic theories of TEG electrical generation need to be studied. The theories of nanogenerators based on Maxwell's equations were first formally introduced by Prof. Zhong Lin Wang [Wang et al., 2017, Wang, 2017]. In his equation, Prof. Wang introduced the new additional term " P_s ", the polarization produced by electrostatic surface charges. The charges themselves were owed to a mechanical trigger that is quite different from the original Maxwell equations. By incorporating the P_s , the equation becomes the keystone for deriving the output characteristics.

Based on the modified Maxwell's equation and the four different modes of TEG, Simiao Niu developed theoretical studies based on the four fundamental modes. Firstly, the theoretical model of contact mode was elucidated by presenting the Voltage-Charge-separation distance (V-

Q-x) relationship for TEGs, and different load resistances were incorporated to test its validity [Niu et al., 2013b]. Then, for the sliding-mode TEGs, the finite element method (FEM) was used in order to obtain the characteristics of electric potential, electric field and charges. Using the FEM calculation and the analytical V-Q-x relationship from previous research, an analytical V-Q-x equation for the sliding TEG was created. Finally, the numerical results were validated with the experimental results to give a sliding TEG theoretical basis [Niu et al., 2013a]. By incorporating both theoretical models from the contact-separation mode TEG and the sliding TEG were then used to create a preliminary theoretical model for the single-electrode mode and the freestanding TEG [Niu et al., 2014, Niu et al., 2015]. Lastly, based on Simiao Niu's findings on the contact-separation mode, a general optimization approach for contact-separation TEG was created by He Zhang et al. [Zhang and Quan, 2019].

HOwever, the mentioned theoretical model is commonly used only as generalization for the predicted output results. This resulted in a lack of information for predicting the electrical output generated in a real time (time history of the harvester's electrical output). To answer those problem, We propose a theoretical equation that could estimate and compute the time history of the electrical output of the FC-TEG. Our proposed theoretical model can also consider both the dielectric materials (d_1) region and the air region (δ) that mostly were not yet considered by other researcher. This addition helps the numerical model to estimate the capacitance value more accurately. Then, the following numerical results is compared with our experimental results from the previous chapter as validation of our theoretical model. Afterwards, the maximum output voltage parameter studies are conducted to estimate the practical use of sustainable harvesting energy in many applications fields.

3.2 Theoretical and Numerical Section

Fig.3.1 presents the theoretical model of the vertical contact-separation modes with a dielectric elastomer. A dielectric elastomer with thickness d_1 and relative dielectric constant ϵ_r is laminated face-to-face with an air layer (separation distance: δ and dielectric constant: ϵ_0) as

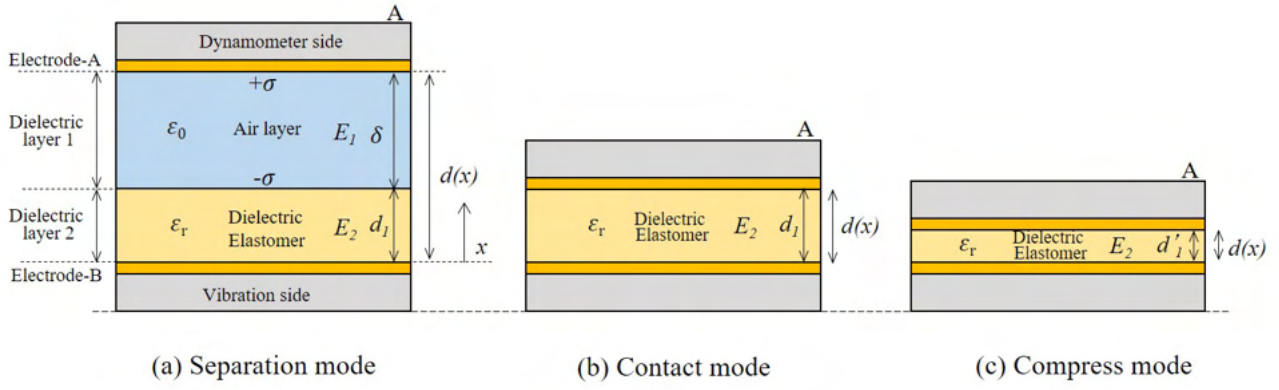


Figure 3.1: Theoretical model of power generation of the FC-TEG in three different modes

the triboelectric layer. Two electrodes are located on the top and bottom sides of the dielectric elastomer. The separation distance δ between the dielectric elastomer and the top electrode can be periodically changed with a separation amplitude A_v and a frequency f_v . A charge can be induced on the surface of the triboelectric layer with density owing to the contact-separation states. An electrical potential difference ϕ between the two electrodes is generated when external forces change the separation distance δ . The electrical potential V can drive the electrons to flow forward and backward across the two electrodes.

The following relationships can be generally expressed:

$$\Delta\phi = Ed \quad (3.1)$$

$$D = \epsilon E \quad (3.2)$$

$$D = \sigma \quad (3.3)$$

$$Q = \sigma A = DA \quad (3.4)$$

where ϕ is the electric potential difference, E is the electrical field, $d(x)$ is the distance between the two electrodes as the separation stroke, D is the dielectric flux density, ϵ is the dielectric constant, σ is the charge density, Q is the amount of charge transferred between the two electrodes, and A is the area of the dielectric elastomer. Using the above relationships, the following equation can be derived:

$$\Delta\phi = \frac{\sigma}{\epsilon} d \quad (3.5)$$

In the separation mode presented in Fig.3.1a, the air layer serves as the triboelectric layer, and the resulting electrical potential difference can be expressed as follows:

$$\Delta\phi = \Delta\phi_1 + \Delta\phi_2 \quad (3.6)$$

$$= \frac{D\delta}{\epsilon_0} + \frac{Dd_1}{\epsilon_0\epsilon_r} \quad (3.7)$$

$$= \left(\delta + \frac{d_1}{\epsilon_r} \right) \frac{D}{\epsilon_0} \quad (3.8)$$

The capacitance C of a capacitor can be defined as follows:

$$C = \frac{Q}{\Delta\phi} \quad (3.9)$$

Thus, the capacitance C in the separation mode can be rewritten as follows:

$$C = \frac{DA}{\left(\delta + \frac{d_1}{\epsilon_r} \right) \frac{D}{\epsilon_0}} \quad (3.10)$$

$$= \frac{\epsilon_0 A}{\left(\delta + \frac{d_1}{\epsilon_r} \right)} \quad (3.11)$$

In the contact mode (Fig.3.1b), when the separation distance $d(x)$ is equal to the thickness d_1 of the dielectric elastomer because the air layer cannot exist, that is, $\delta = 0$, the capacitance C can be expressed as follows:

$$C = \frac{\epsilon_0 A}{\frac{d_1}{\epsilon_r}} \quad (3.12)$$

$$= \frac{\epsilon_0 \epsilon_r A}{d_1} \quad (3.13)$$

In the compression mode (Fig.3.1c), the displacement $d(x)$ is less than the thickness d_1 , and

the capacitance C can be expressed as follows:

$$C = \frac{\epsilon_0 A}{\frac{d'_1}{\epsilon_r}} \quad (3.14)$$

$$= \frac{\epsilon_0 \epsilon_r A}{d'_1} \quad (3.15)$$

Here, Kirchhoff's law and Ohm's law are defined as follows:

$$V_R + V_{ma} = 0 \quad (3.16)$$

$$V_R = Ri \quad (3.17)$$

$$i = i_{ma} \quad (3.18)$$

$$q_{ma} = K_{ma} C_{ma} V_{ma} \quad (3.19)$$

where R is the internal resistance of the data logger, the subscript " ma " refers to a capacitor consisting of air and dielectric elastomer, and K_{ma} is the interaction coefficient between the air layer and the dielectric elastomer and depends on $d\delta/dt$ before contact as follows:

$$K_{ma} = K_f \frac{d\delta}{dt} = K_f \frac{d}{dt} \{d(x)\} = \frac{d}{dt} \{(1 - \cos 2\pi f_v t) A_v\} \quad (3.20)$$

where A_v is the separation amplitude, f_v is the vibration frequency, and K_f is the electrification coefficient considering the experimental conditions. Then, the following equations can be finally derived:

$$V_R = -V_{ma} \quad (3.21)$$

$$Ri = -\frac{q_{ma}}{K_{ma} C_{ma}} \quad (3.22)$$

$$i = \frac{dq}{dt} = \frac{dq_{ma}}{dt} \quad (3.23)$$

$$\frac{dq_{ma}}{dt} = -\frac{1}{RK_{ma} C_{ma}} q_{ma} \quad (3.24)$$

Using these equations, the output voltage generated by the FC-TEG can be obtained by time integration.

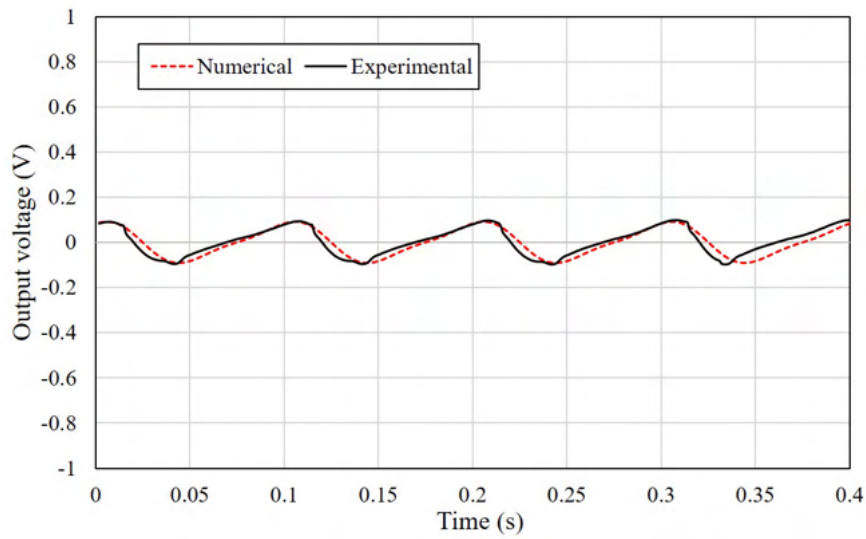
3.3 Estimation of the output voltage based on the theoretical model

This section provides the result of the theoretical model based on the numerical calculation and the experimental works. Firstly, the sample of our numerical results is presented in Fig.3.2 - Fig.3.6. All five figures present three main points: the time histories of the output voltage, separation strokes, and separation velocities, alongside their experimental results. The vibrated frequency of 10 Hz is chosen as a sample with Fig.3.2 and Fig.3.3 for the separation mode, Fig.3.4 for the contact mode, and Fig.3.5 and Fig.3.6 for the compression mode. All cases provide different tendencies. In the separation mode and the contact mode (Fig.3.2 - Fig.3.5), the theoretical results provide similar output with the experimental results with a slight difference in the maximum and minimum output voltages. This difference is especially apparent in the contact mode. However, the output voltage in the compression mode (as shown in Fig.3.6) does not coincide with the experiment results. Additionally, the model itself could not reproduce the sharp difference and drastic variations that occur in the experiments result. The resultant separation velocity also has a different peak value compared with the experiment results. The main reason for this is due to the compression process, and its theoretical model was not considered in more detail in this mode. Therefore, the existing model needs to be improved for the compression mode.

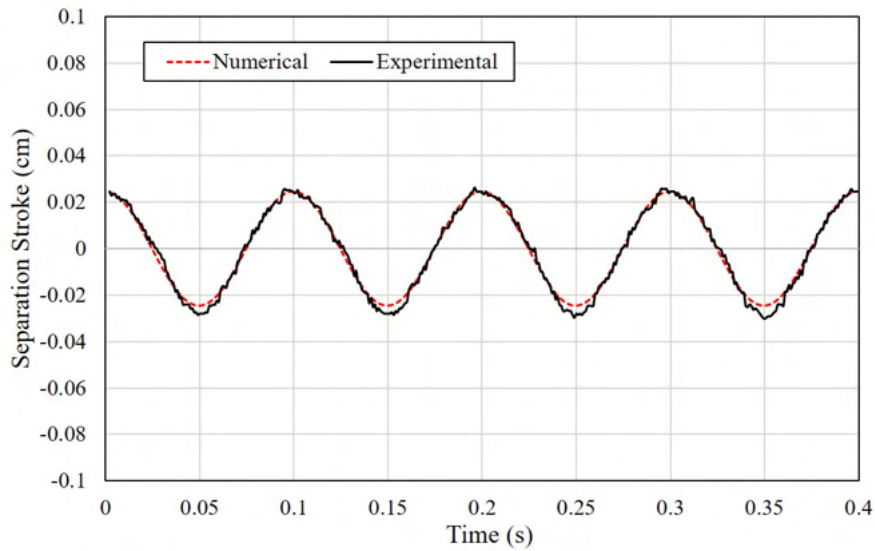
Fig.3.7 - Fig.3.9 shows the comparisons between the output voltage versus the separation stroke (Fig.3.7a, Fig.3.8a, Fig.3.9a) and the separation velocity (Fig.3.7b, Fig.3.8b, Fig.3.9b) for both numerical and experimental value. In addition, to illustrate the electrical power generated by the FC-TEG, the comparison of the electrical power density with the separation stroke are shown in Fig.3.10a, Fig.3.11a, Fig.3.12a) and the electrical power versus separation velocity in (Fig.3.10b, Fig.3.11b, Fig.3.12b). In general, the theoretical voltage in the minimum and average regions have a slight discrepancies with the value, it is a bit overestimated compared with the experimental values. On the contrary, the maximum voltages are underestimated, especially in the case of the high value of separation strokes and high separation velocities.

Though that may be the case, the tendency of the output voltage is within a reasonable result and good enough as a basic design tool to estimate the FC-TEG electrical performance and efficiencies.

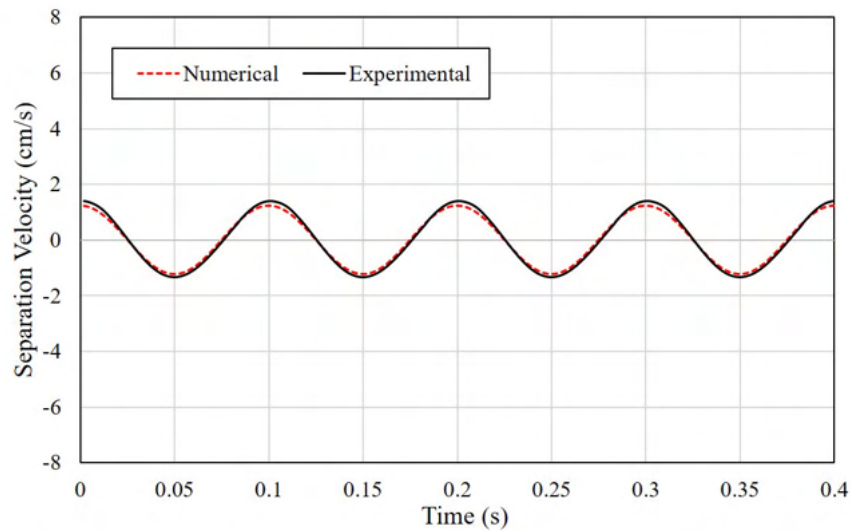
Based on this design tool and model, the parameter studies of the maximum output voltage of FC-TEG under larger separation frequency and separation velocity from the experiment were conducted. The detail of the model result can be seen in Fig.3.13 while the power density is shown in Fig.3.14. The maximum voltage is able to increase linearly with the frequency and separation velocity. The output voltage should be improved with some modifications of the FC-TEG before the harvester itself is used in more practical usage. More detailed validation, numerical tool, and model would be needed in the near future.



(a) Output voltage

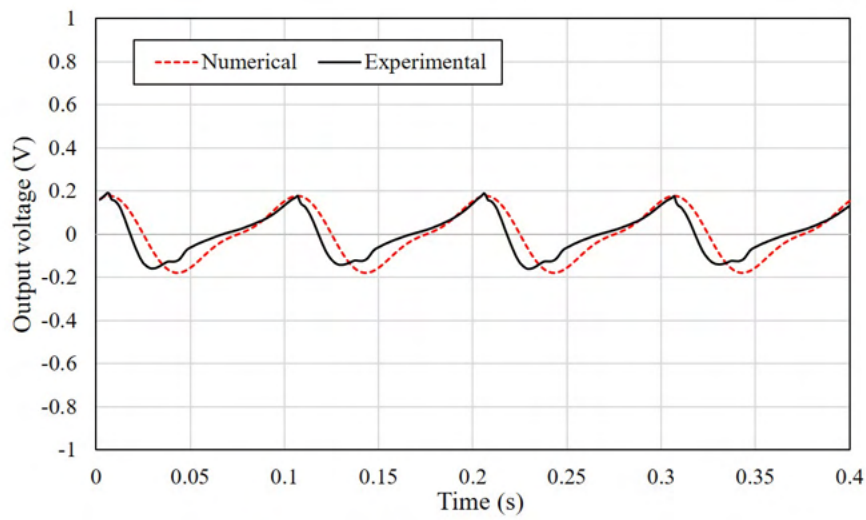


(b) Separation stroke

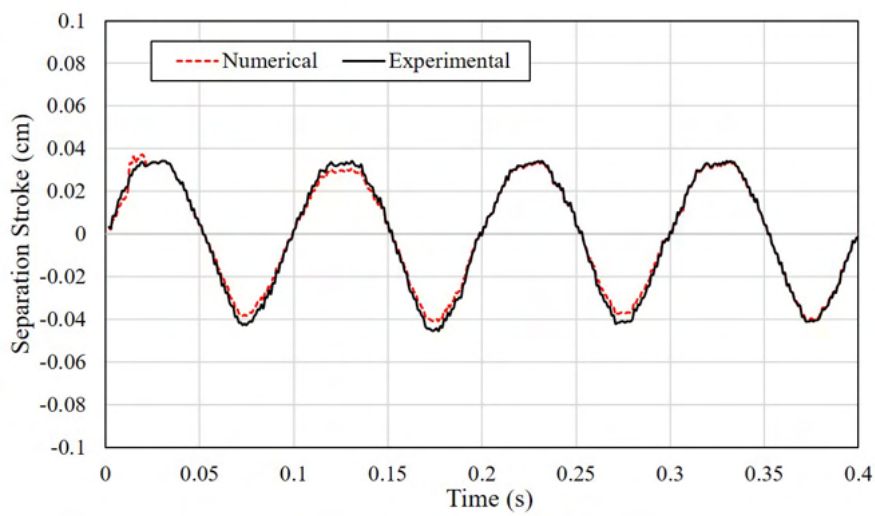


(c) Separation velocity

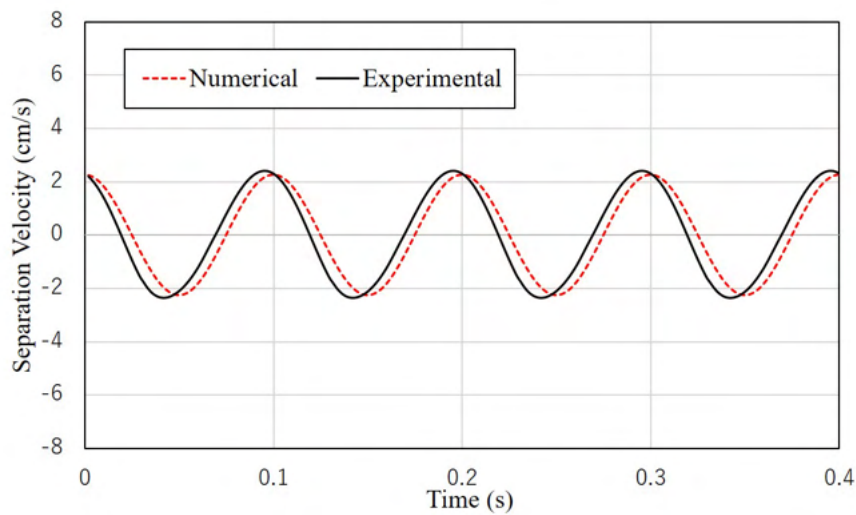
Figure 3.2: Comparisons of the time histories of output voltage, separation stroke, and separation velocity in separation mode ($A_v = 0.3\text{mm}$).



(a) Output voltage

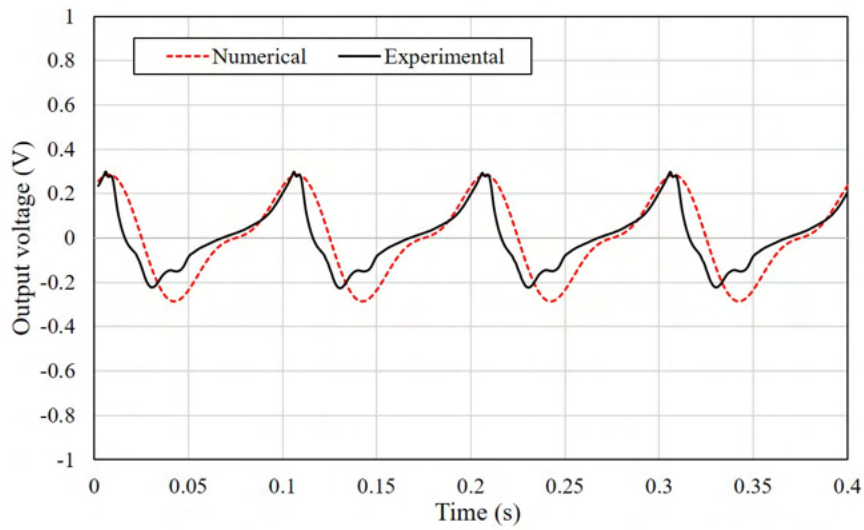


(b) Separation stroke

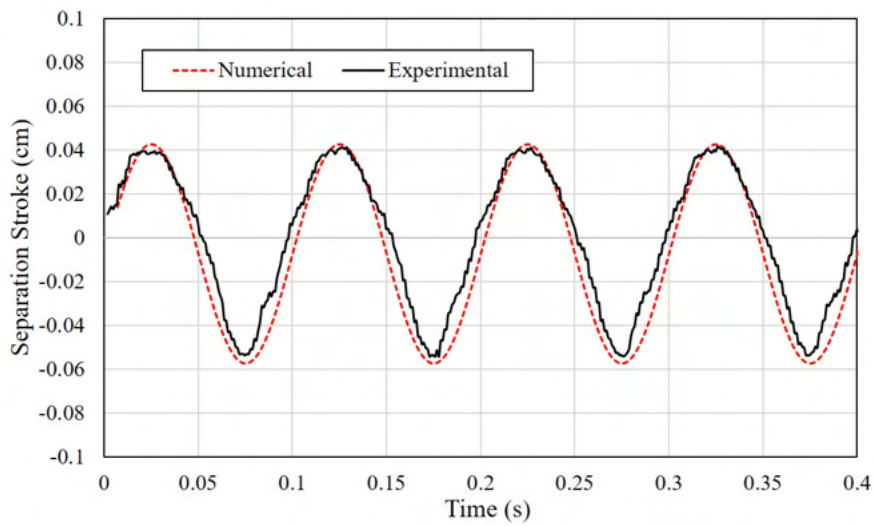


(c) Separation velocity

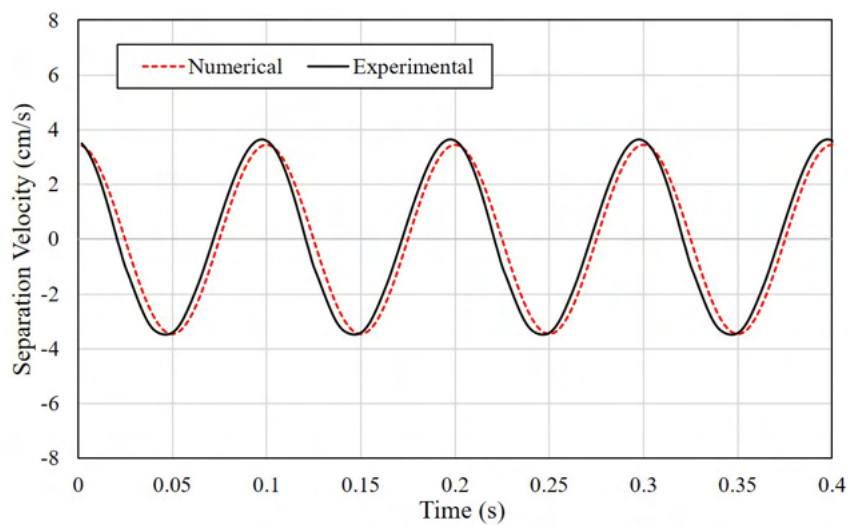
Figure 3.3: Comparisons of the time histories of output voltage, separation stroke, and separation velocity in separation mode ($A_v = 0.4\text{mm}$).



(a) Output voltage

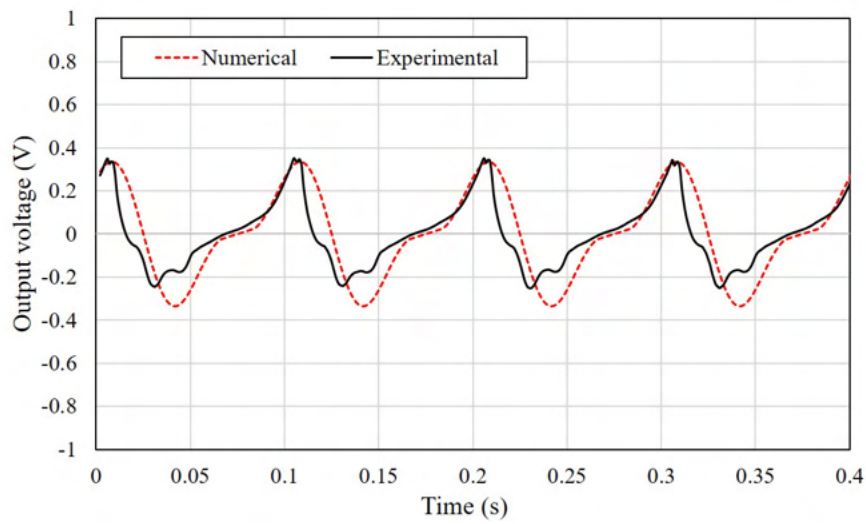


(b) Separation stroke

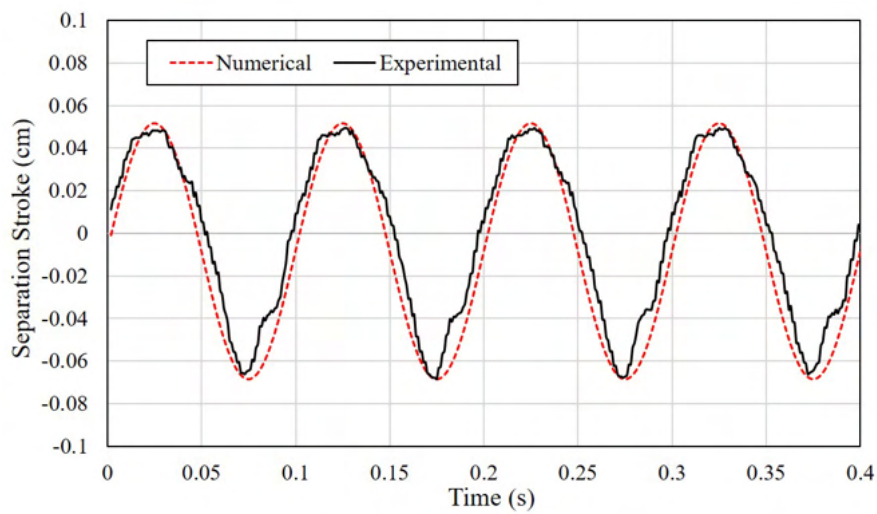


(c) Separation velocity

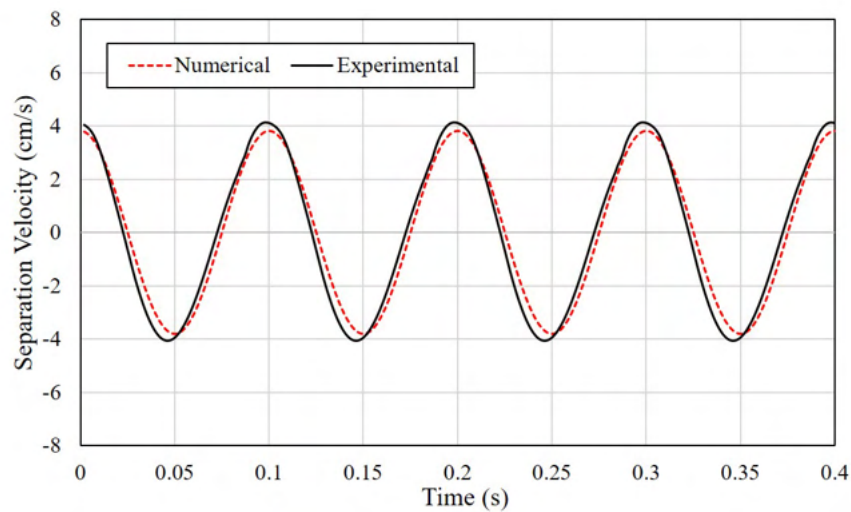
Figure 3.4: Comparisons of the time histories of output voltage, separation stroke, and separation velocity in separation mode ($A_v = 0.5\text{mm}$).



(a) Output voltage

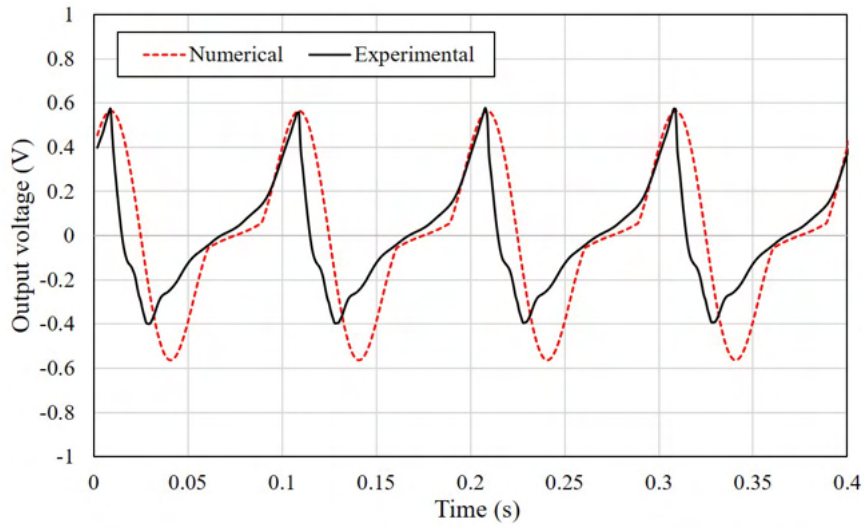


(b) Separation stroke

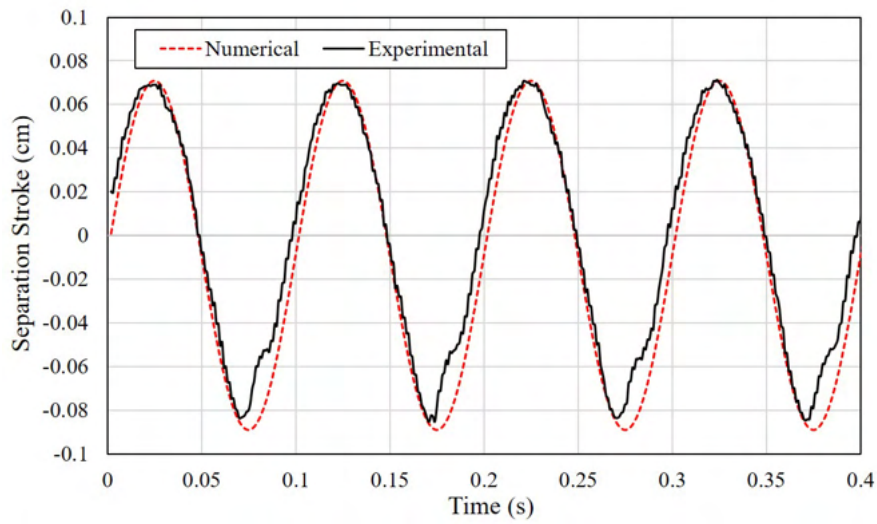


(c) Separation velocity

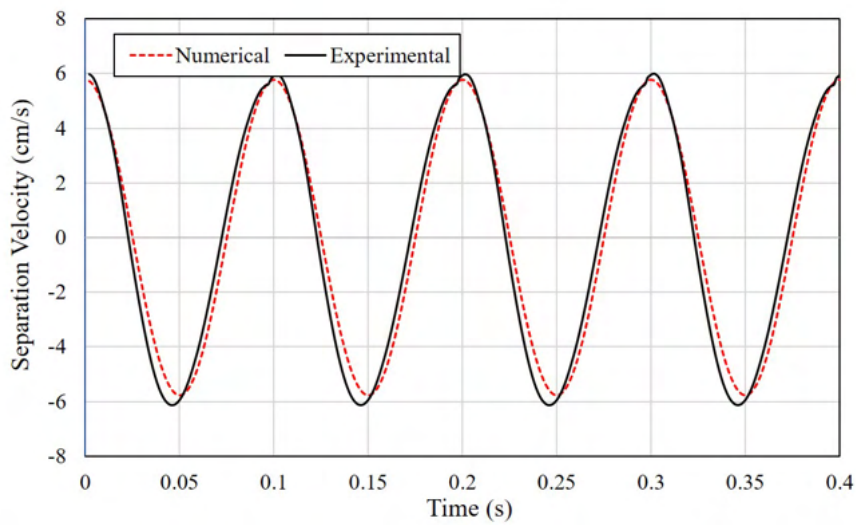
Figure 3.5: Comparisons of the time histories of output voltage, separation stroke, and separation velocity in contact mode ($A_v = 0.6\text{mm}$).



(a) Output voltage

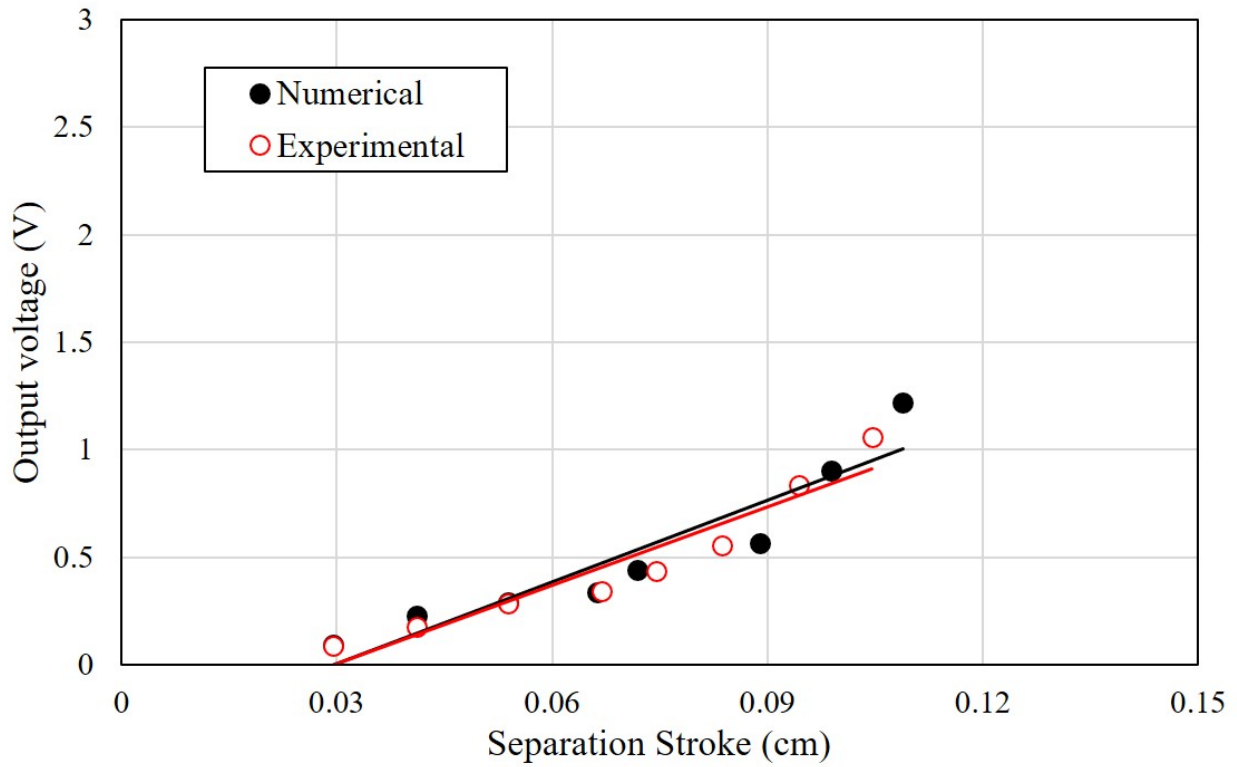


(b) Separation stroke

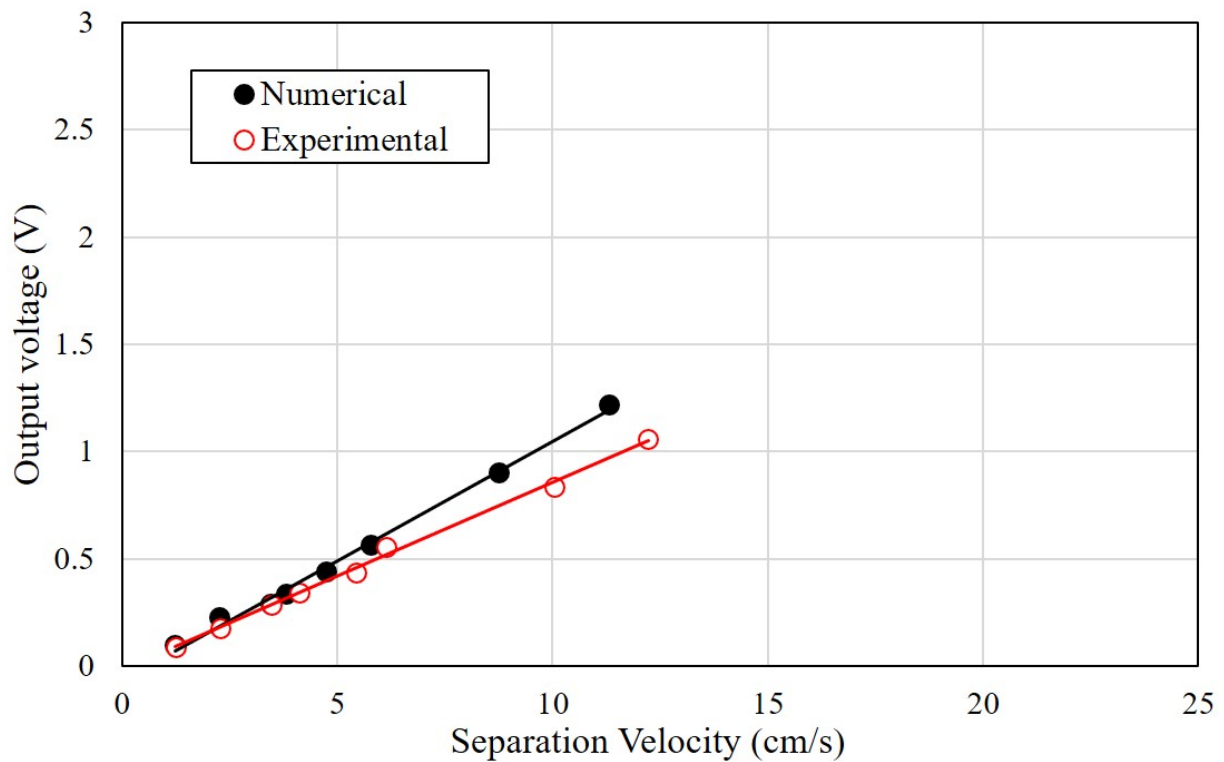


(c) Separation velocity

Figure 3.6: Comparisons of the time histories of output voltage, separation stroke, and separation velocity in compress mode ($A_v = 0.8\text{mm}$).

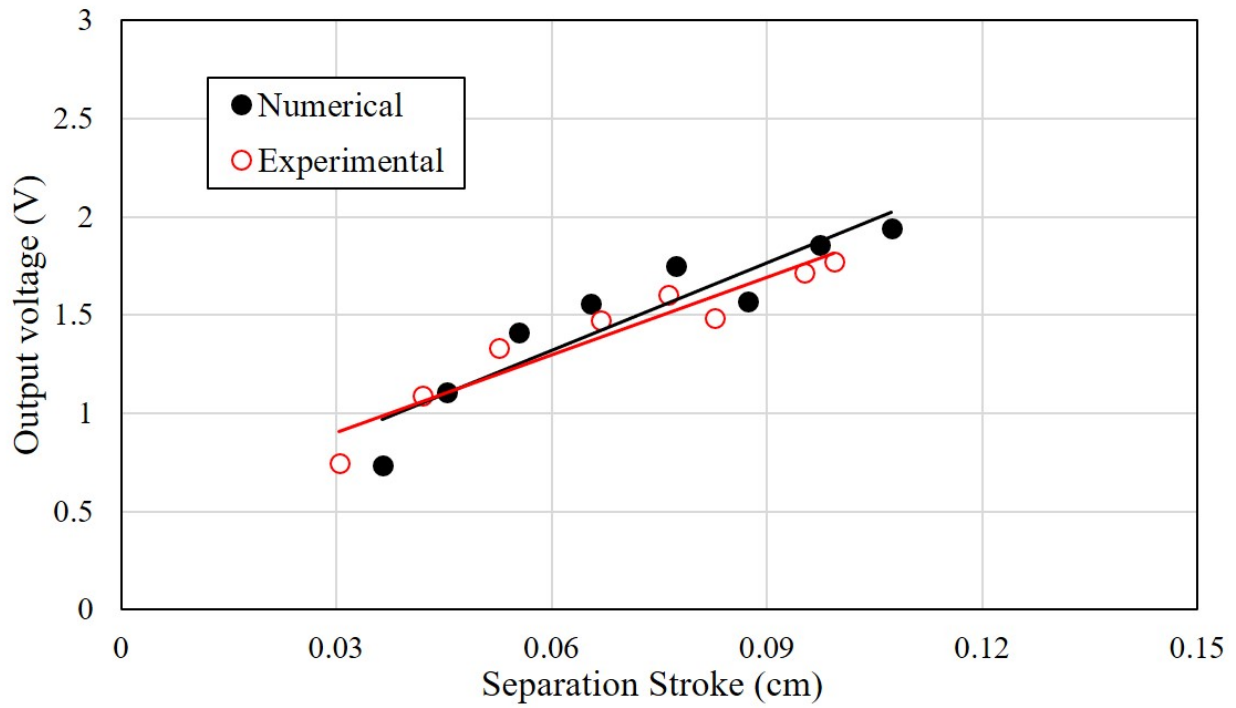


(a) Output voltage vs. separation stroke

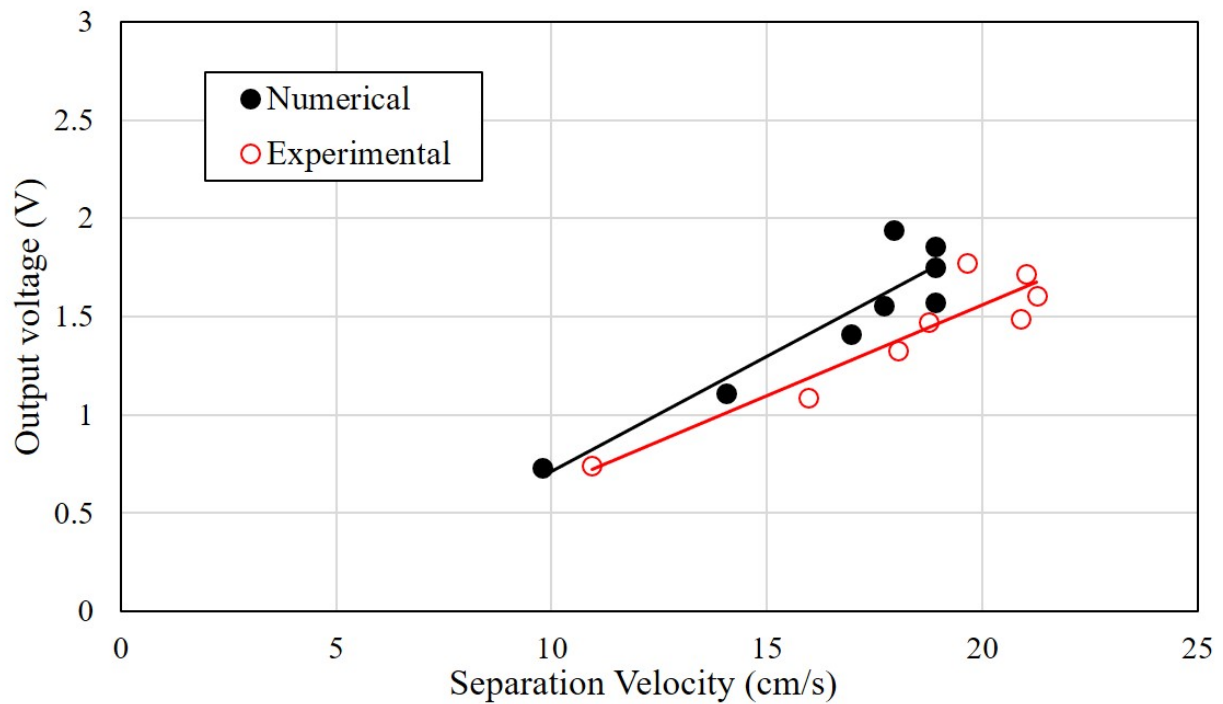


(b) Output voltage vs separation velocity

Figure 3.7: Comparisons of the experimental and theoretical averaged output voltages at a vibration frequency of 10 Hz

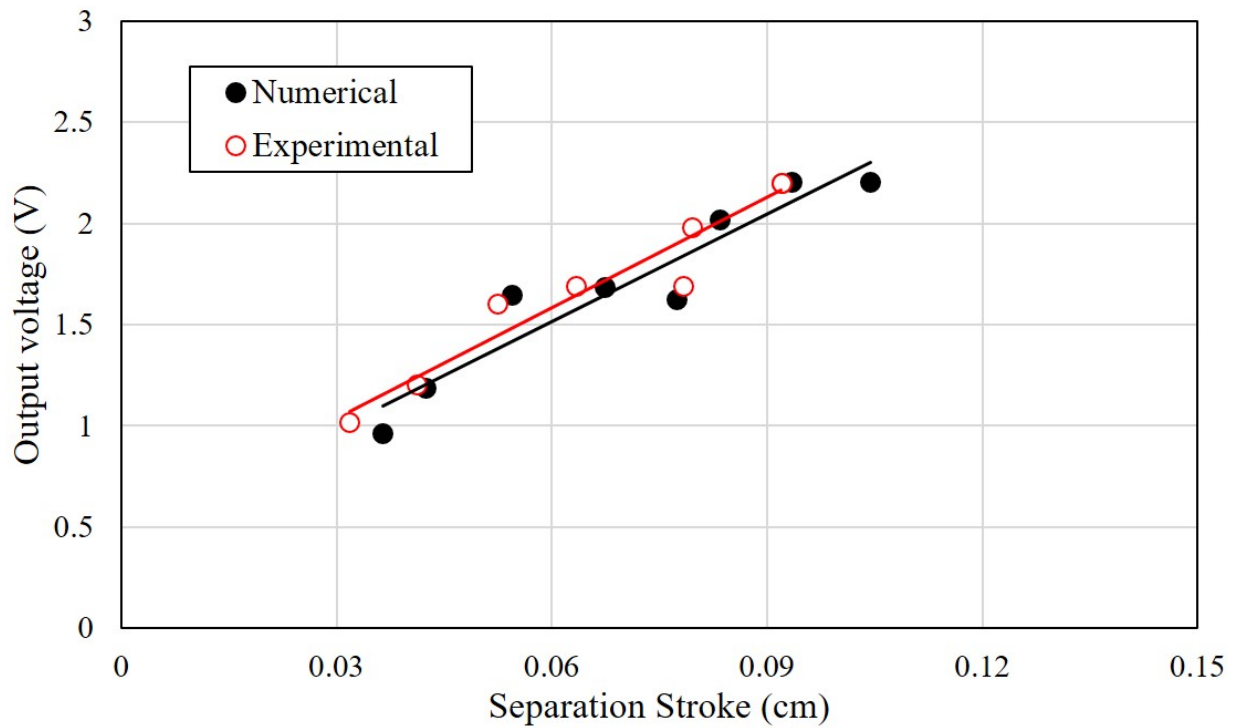


(a) Output voltage vs. separation stroke

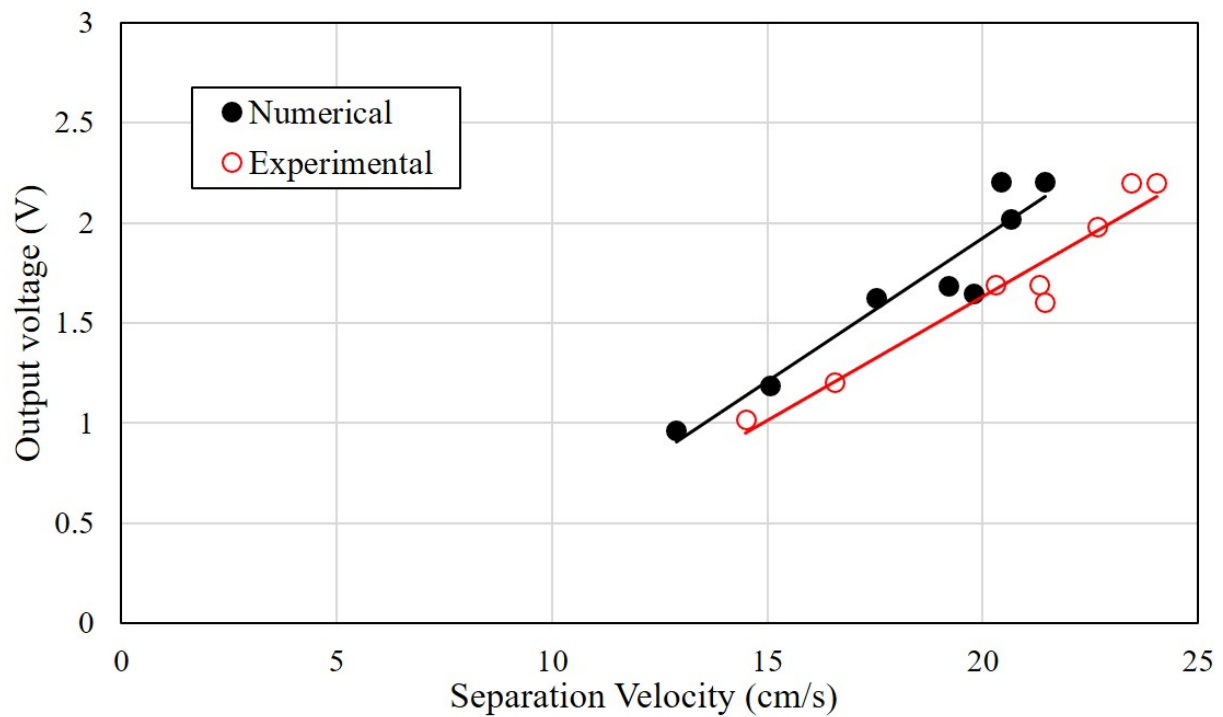


(b) Output voltage vs separation velocity

Figure 3.8: Comparisons of the experimental and theoretical averaged output voltages at a vibration frequency of 20 Hz

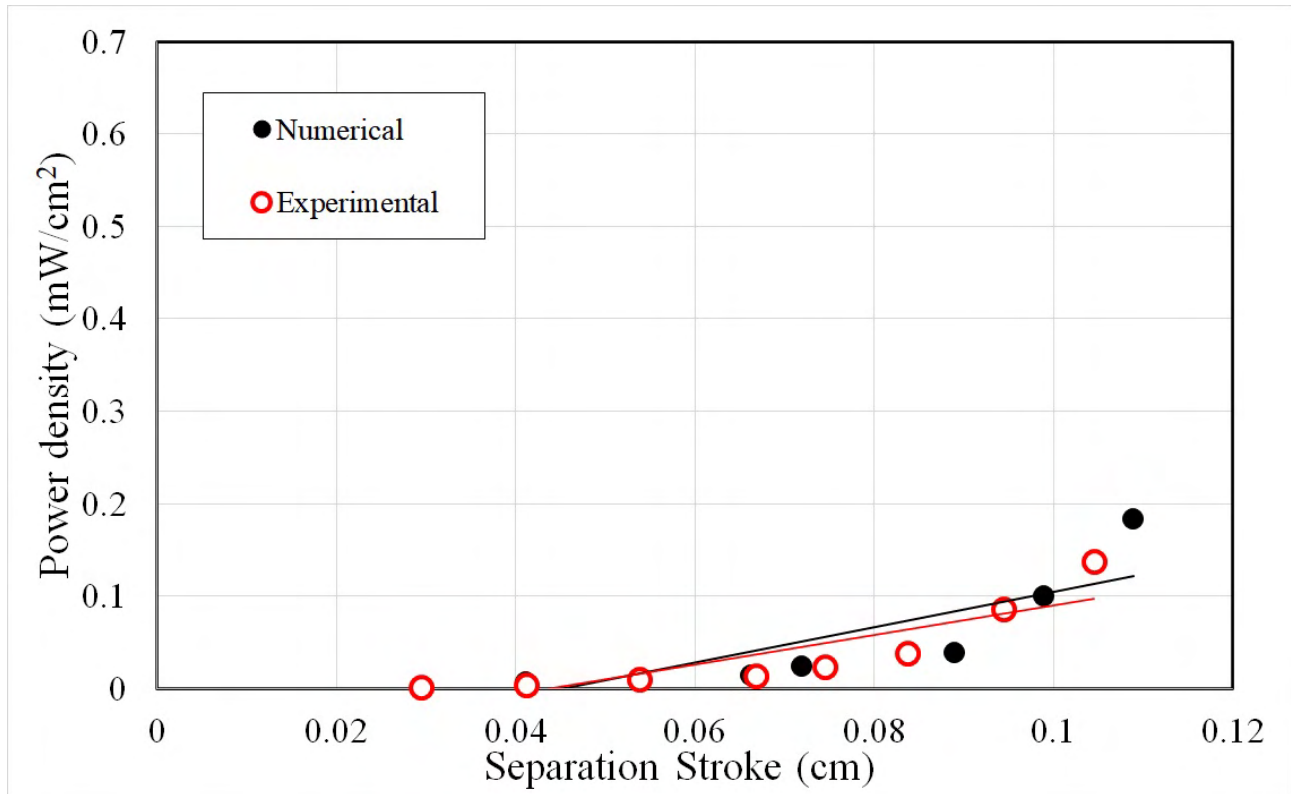


(a) Output voltage vs. separation stroke

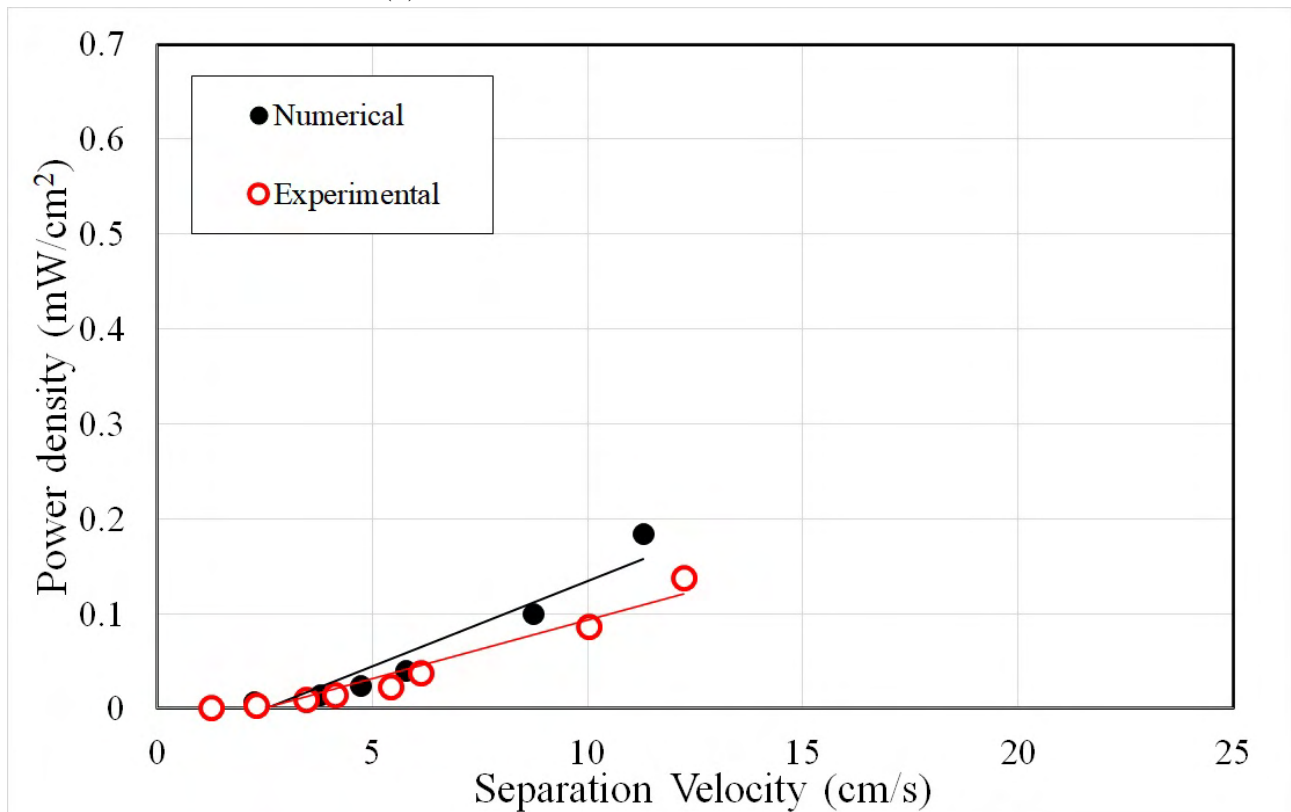


(b) Output voltage vs separation velocity

Figure 3.9: Comparisons of the experimental and theoretical averaged output voltages at a vibration frequency of 30 Hz

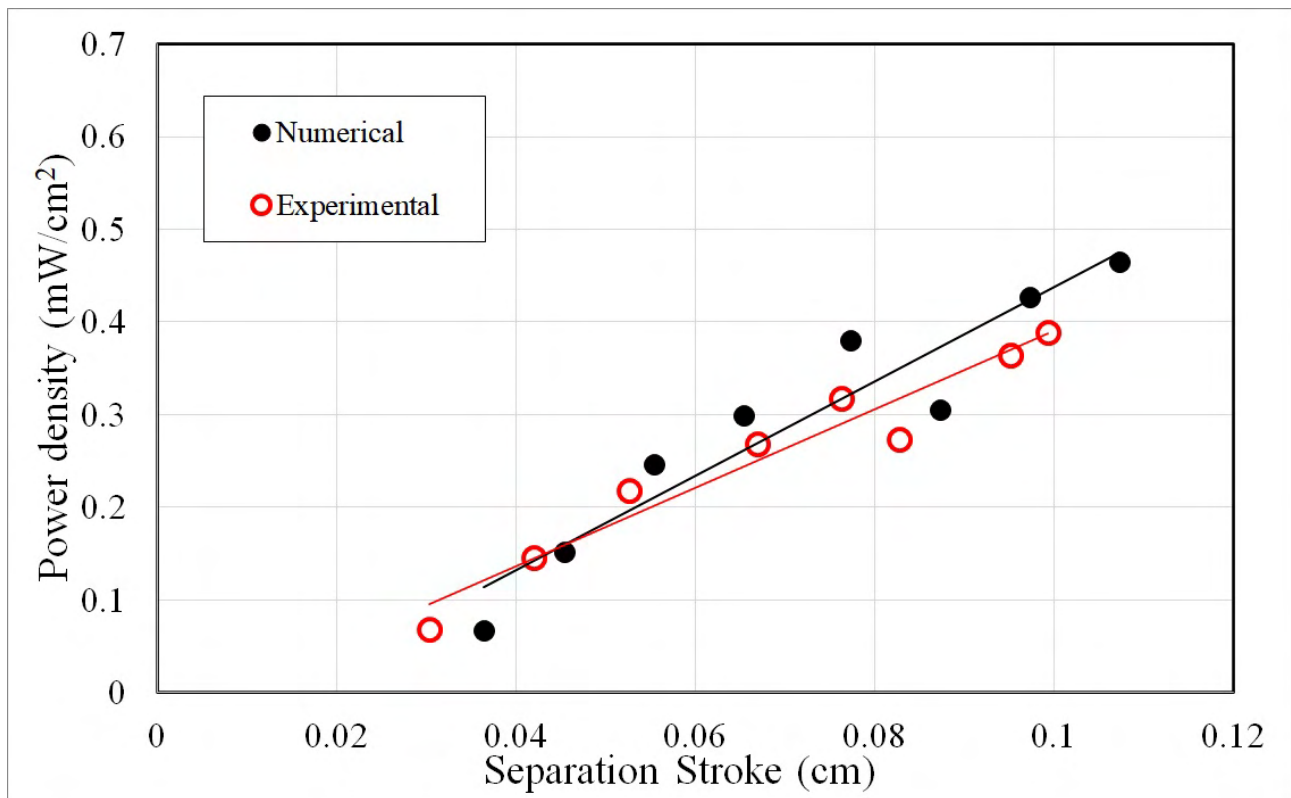


(a) Electrical output vs. separation stroke

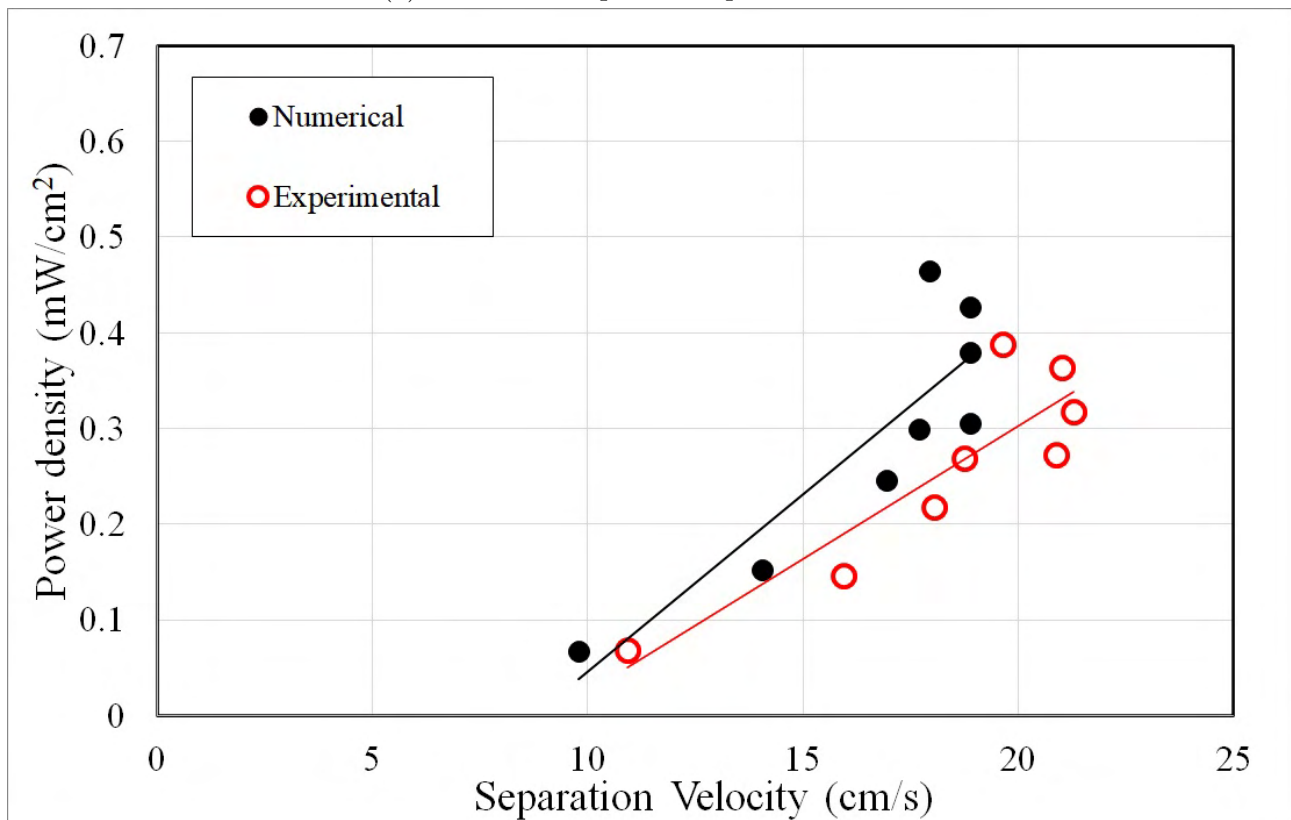


(b) Electrical output vs separation velocity

Figure 3.10: Comparisons of the experimental and theoretical averaged output power density at a vibration frequency of 10 Hz

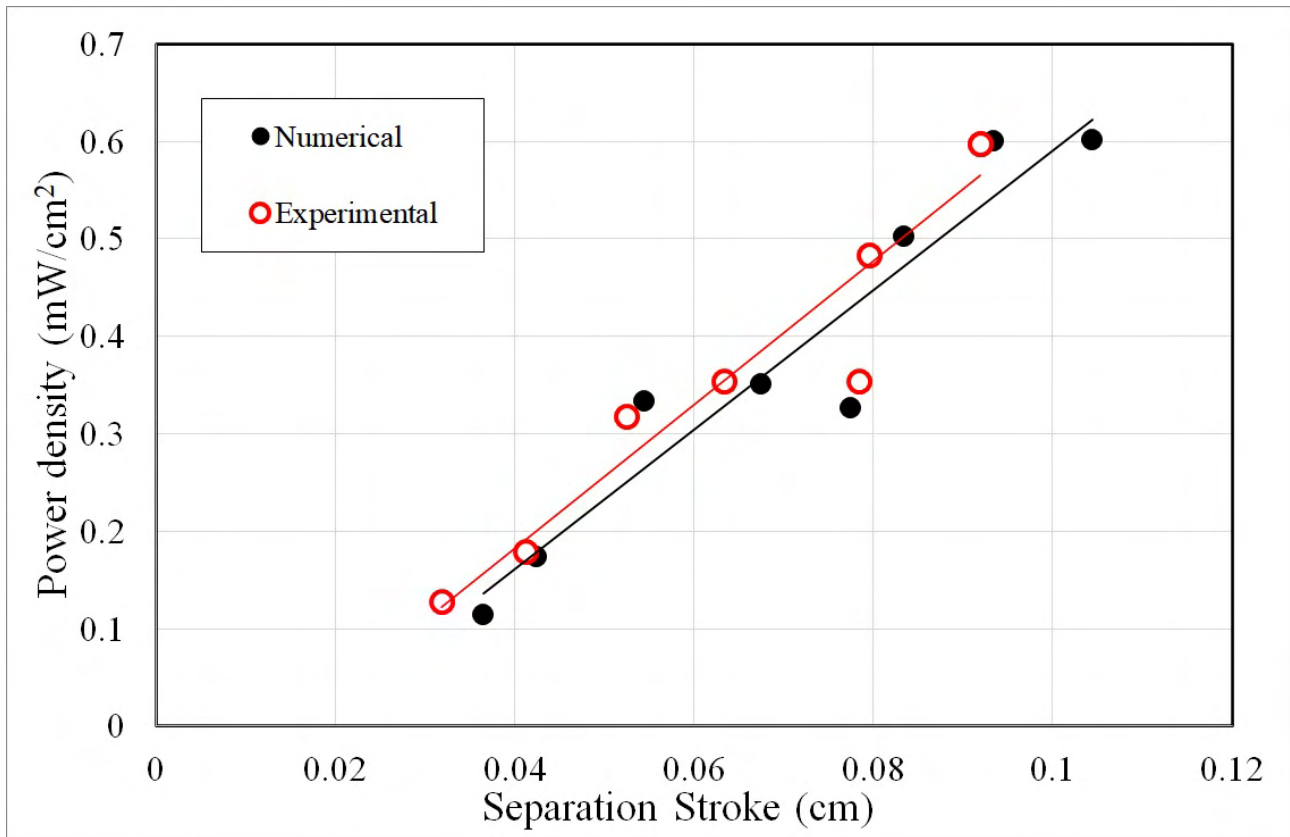


(a) Electrical output vs. separation stroke

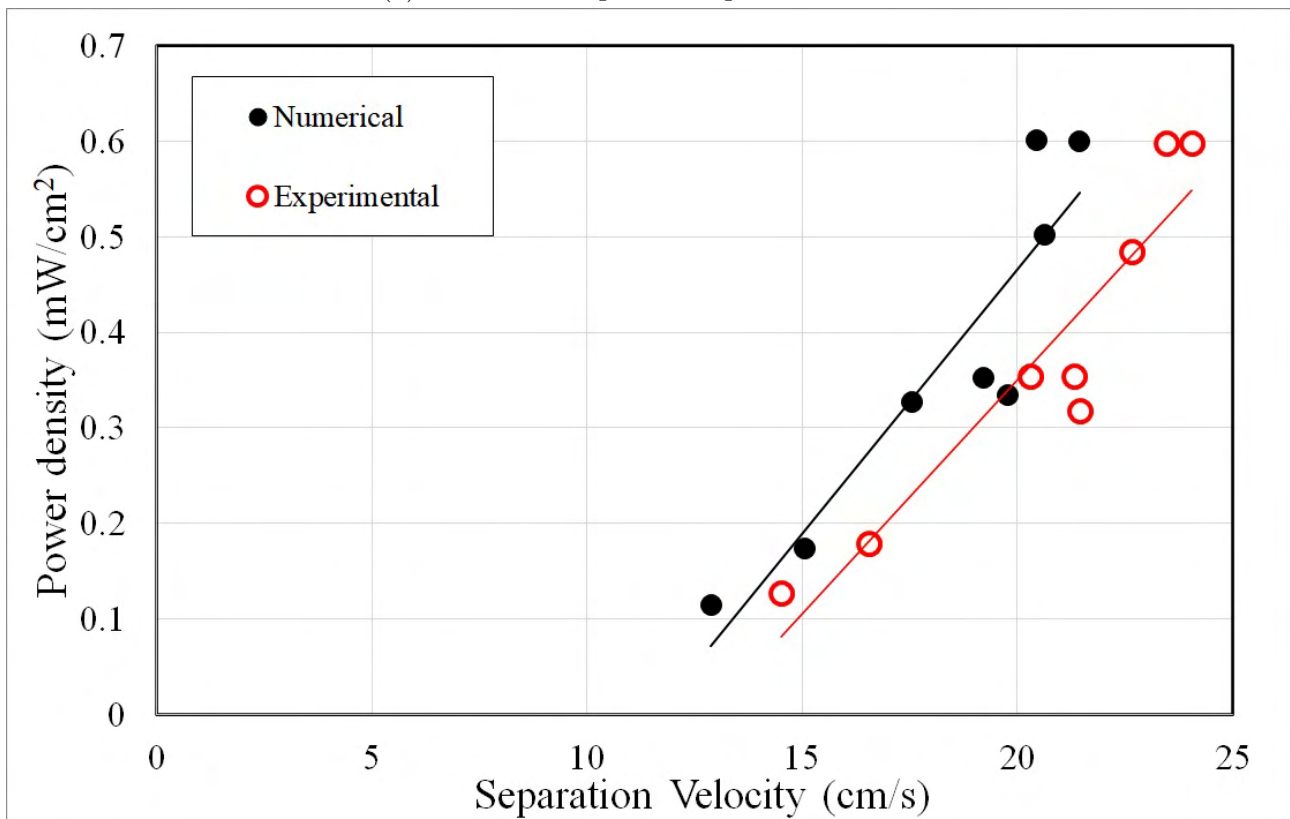


(b) Electrical output vs separation velocity

Figure 3.11: Comparisons of the experimental and theoretical averaged output power density at a vibration frequency of 20 Hz

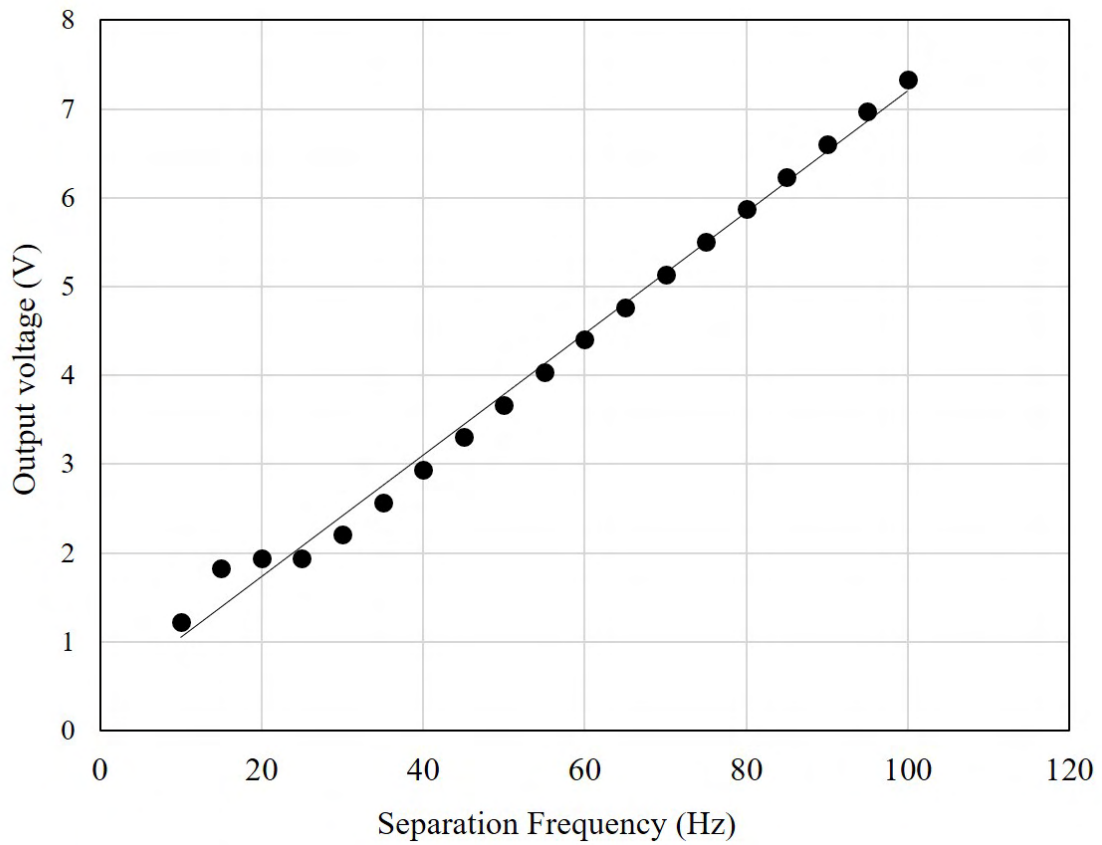


(a) Electrical output vs. separation stroke

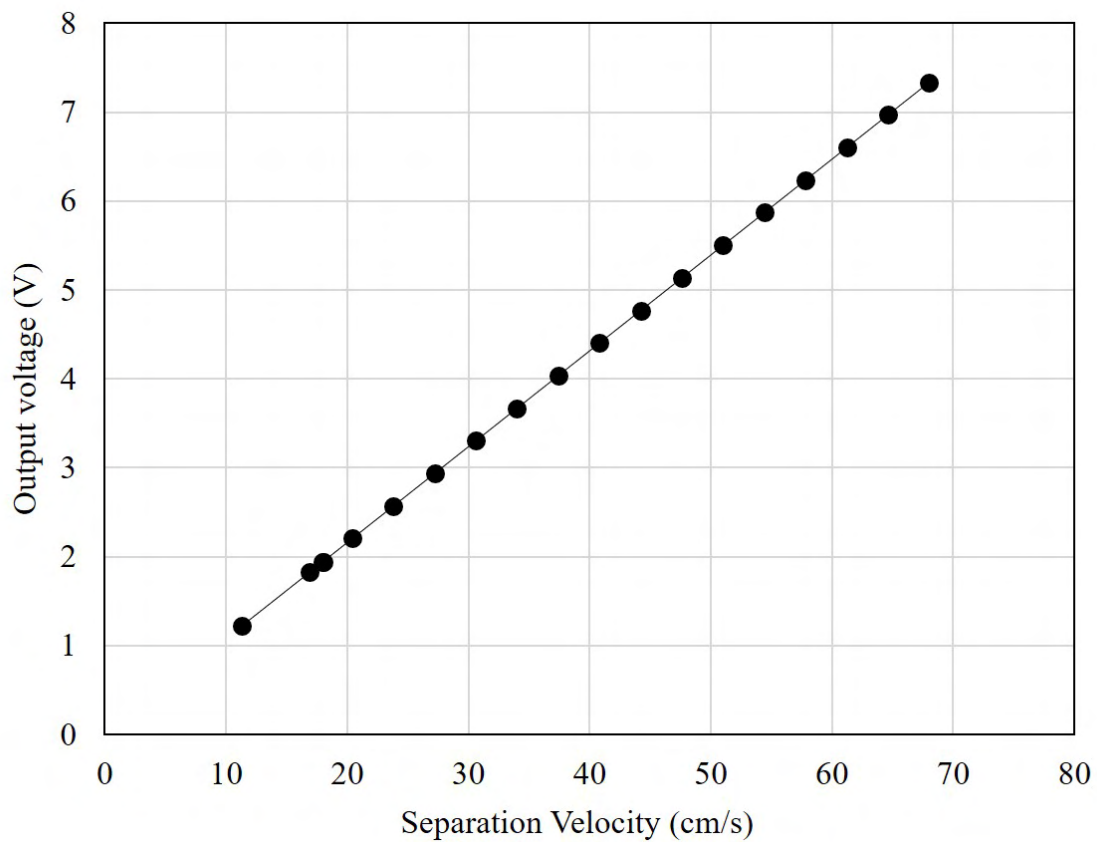


(b) Electrical output vs separation velocity

Figure 3.12: Comparisons of the experimental and theoretical averaged output power density at a vibration frequency of 30 Hz

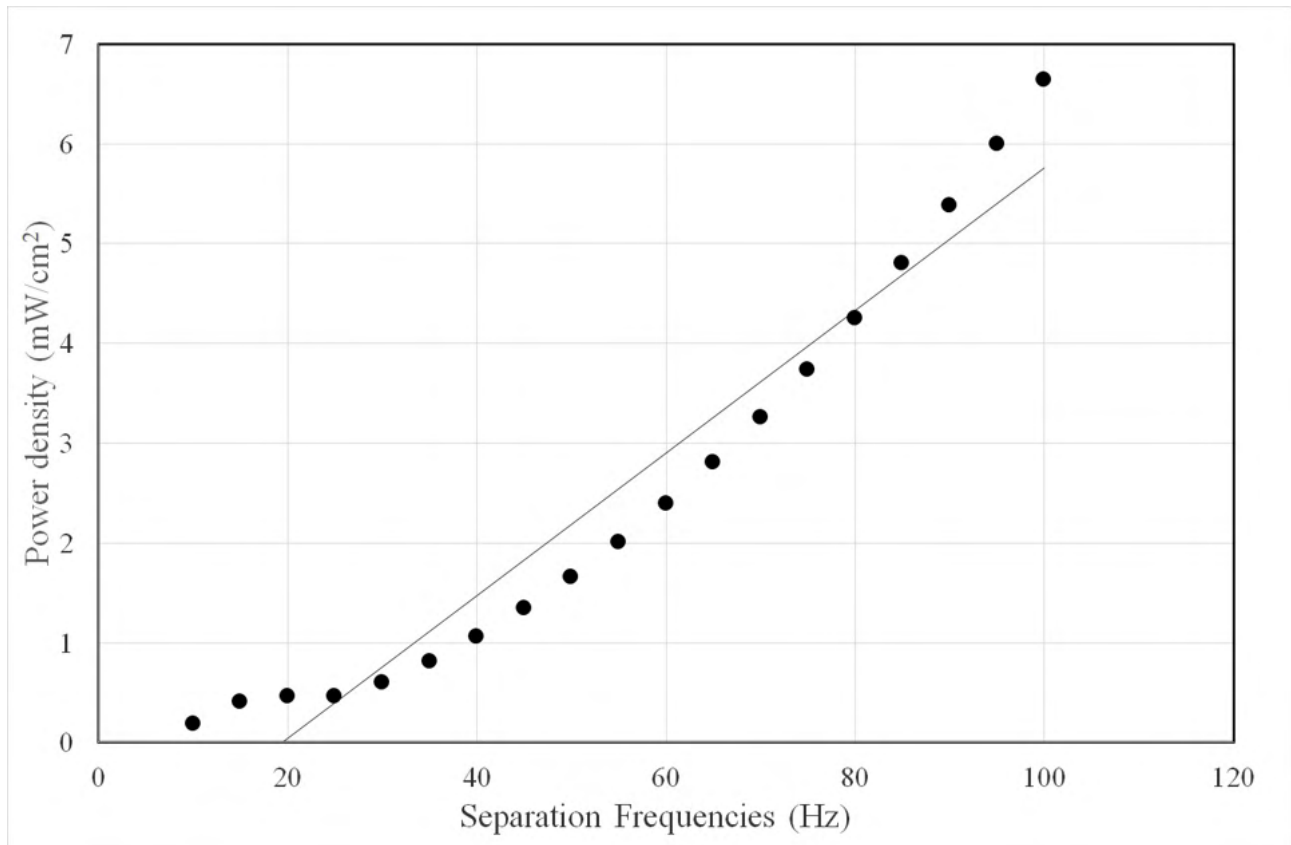


(a) Separation frequency

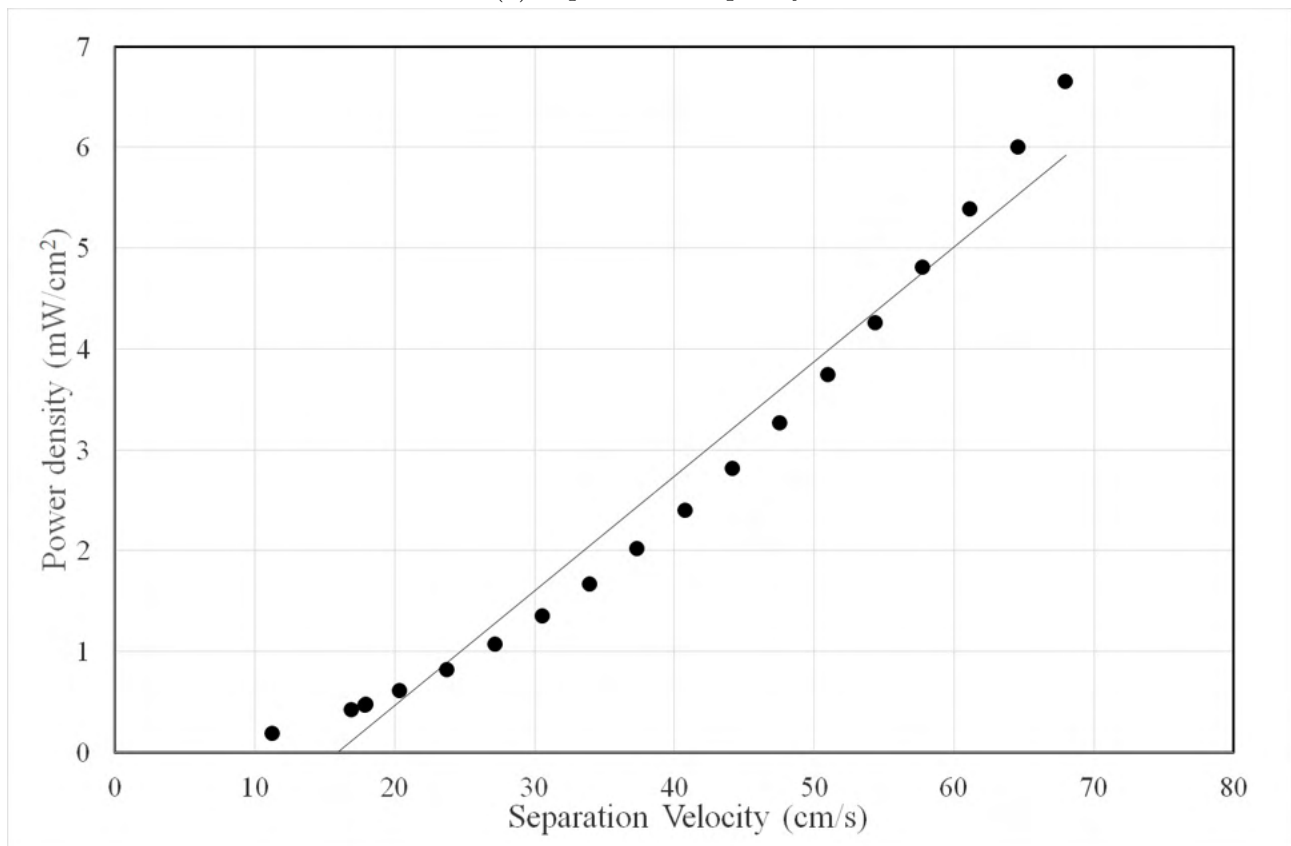


(b) Separation velocity

Figure 3.13: Estimations of the maximum output voltage versus separation frequency and separation velocity.



(a) Separation frequency



(b) Separation velocity

Figure 3.14: Estimations of the maximum output power density versus separation frequency and separation velocity.

3.4 Summary

This chapter developed and examined a flexible and compressible triboelectric generator (FC-TEG) theoretical model for the vertical contact-separation mode. A dielectric elastomer based on the vertical vibration experimental results in the previous chapter was used as a development tool for the FC-TEG theoretical model. After the theoretical model development was finished, the output voltages of the FC-TEG in the model were compared with the experimental results. Finally, the maximum output voltage parameter studies were also conducted to estimate the practical use for harvesting sustainable energy in many application fields. From all works, the main conclusions are obtained as follows:

- The theoretical model of the vertical contact-separation modes with a dielectric elastomer on the separation mode provides similar output to the experimental results.
- The theoretical model of the vertical contact-separation modes with a dielectric elastomer on the contact mode provides similar output to the experimental results with a tiny difference in the peak voltages (both minimum and maximum voltage).
- The theoretical model of the vertical contact-separation modes with a dielectric elastomer on the compression mode is unable to coincide with the experiment results. The model could not reproduce the sharp voltage value and different variations from the compression mode experiment results. The existing model for the compression mode needs to be improved and reiterated in future vibration tests.
- The comparisons of electrical output versus the separation stroke, and the output versus the separation velocity are also investigated. The theoretical value of the electrical output has a little bit of discrepancies and overestimated compared with the experimental results. The difference mainly appears in the output voltage minimum and average regions. However, the maximum voltages are underestimated in the high separation stroke and high separation velocities. Despite the minor difference, the output voltage tendency of the theoretical model is within an acceptable result and good enough to be used as a basic design tool for predicting the FC-TEG before practical usage.

In the future, the FC-TEG theoretical model needs to be optimized based on this basic model. The improvement should be focused on the condition of high frequency. Afterward, a numerical model that utilized multi TEG should also be considered based on the experiments of the next chapter section.

Bibliography

- [Mutsuda et al., 2019] Mutsuda, H., Tanaka, Y., Doi, Y., and Moriyama, Y. (2019). Application of a flexible device coating with piezoelectric paint for harvesting wave energy. *Ocean Engineering*, 172(September 2018):170–182.
- [Niu et al., 2015] Niu, S., Liu, Y., Chen, X., Wang, S., Zhou, Y. S., Lin, L., Xie, Y., and Wang, Z. L. (2015). Theory of freestanding triboelectric-layer-based nanogenerators. *Nano Energy*, 12:760–774.
- [Niu et al., 2013a] Niu, S., Liu, Y., Wang, S., Lin, L., Zhou, Y. S., Hu, Y., and Wang, Z. L. (2013a). Theory of sliding-mode triboelectric nanogenerators. *Advanced Materials*, 25(43):6184–6193.
- [Niu et al., 2014] Niu, S., Liu, Y., Wang, S., Lin, L., Zhou, Y. S., Hu, Y., and Wang, Z. L. (2014). Theoretical investigation and structural optimization of single-electrode triboelectric nanogenerators. *Advanced Functional Materials*, 24(22):3332–3340.
- [Niu et al., 2013b] Niu, S., Wang, S., Lin, L., Liu, Y., Zhou, Y. S., Hu, Y., and Wang, Z. L. (2013b). Theoretical study of contact-mode triboelectric nanogenerators as an effective power source. *Energy and Environmental Science*, 6(12):3576–3583.
- [Nottingham, 2013] Nottingham, T. (2013). Patel , Rupesh (2013) Modelling analysis and optimisation of cantilever piezoelectric energy harvesters . PhD thesis , University of Nottingham .

- [Patel et al., 2014] Patel, R., McWilliam, S., and Popov, A. A. (2014). Optimization of piezoelectric cantilever energy harvesters including non-linear effects. *Smart Materials and Structures*, 23(8).
- [Patel et al., 2016] Patel, R., Tanaka, Y., McWilliam, S., Mutsuda, H., and Popov, A. A. (2016). Model refinements and experimental testing of highly flexible piezoelectric energy harvesters. *Journal of Sound and Vibration*, 368:87–102.
- [Wang, 2017] Wang, Z. L. (2017). On Maxwell’s displacement current for energy and sensors: the origin of nanogenerators. *Materials Today*, 20(2):74–82.
- [Wang et al., 2017] Wang, Z. L., Jiang, T., and Xu, L. (2017). Toward the blue energy dream by triboelectric nanogenerator networks. *Nano Energy*, 39:9–23.
- [Zhang and Quan, 2019] Zhang, H. and Quan, L. (2019). Theoretical Prediction and Optimization Approach to Triboelectric Nanogenerator. In *Electrostatic Discharge - From Electrical breakdown in Micro-gaps to Nano-generators*.

Chapter 4

Multi-layered triboelectric generator

4.1 Background

Using the vibration vertical contact-separation test, our FC-TEG proved to generate high electrical output. In that first design of the FC-TEG, we used one dielectric elastomer to utilize the input energy from the vibration. To improve and harvest more energy, many research has used a couple of multiple devices for their triboelectric generators. Several integrations of this multi couple TEG are based on a multi-layered sliding triboelectric generator [Du et al., 2014, Xie et al., 2014], interdigitative electrodes-based TEG [Lin et al., 2015], multi dielectric layered TEG with the use of corona discharge approach [Shao et al., 2017], and the folded TEG [Tao et al., 2020, Wang et al., 2020] based on the improvement of the “paper type” TEG [Mao et al., 2017].

Based on that previous research and our study in the vibration tests of the FC-TEG, it is important to increase the number of contact-separation processes of the FC-TEG to harvest even more energy under the different spectrum. Since it is known now that the higher separation velocity could generate higher electrical power, a new idea for increasing the number of contacts and separate on each stroke of the FC-TEG movement is crucial to be observed. Therefore, the idea of using a multi-layered triboelectric generator is proposed and developed in this study.

The laminated structure of this multi-layer TEG is based on the folded type of TEG that is modified into an origami type of TEG device, which can fold up into concertinas. An origami type is based on the Japanese folding technique to create a smaller and tighter model but under a small size [Schenk and Guest, 2016, KIMACHI and MORITA, 2017]. By utilizing this technique, the multi-layer TEG device could have a similar or even better triboelectric process even though the size is relatively the same as FC-TEG. The concertina shape mimics the free-reed musical instrument's design that could expand and contract to produce an electrical output. The usage of this simple design multi-layer TEG structure is used to verify the basic output characteristics of the TEG device before a more advanced design is developed and used.

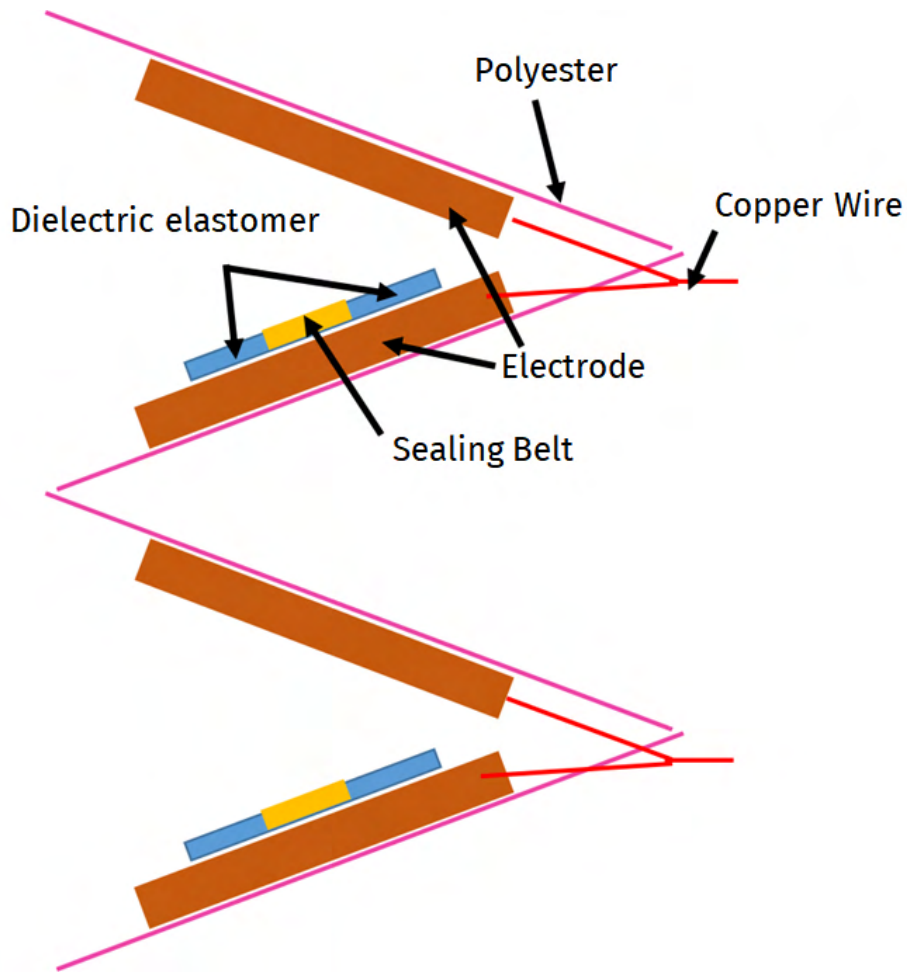
4.2 Device overview + fabrication of multi-TEG

The multi-layer TEG device's schematics can be seen in Fig.4.1a. The multi-layer TEG was made using the same materials as the FC-TEG with the addition of polyester. The electrode uses the same copper films, and the masking tape/sealing belt is based on type 2 from the previous chapter. The size of the TEG can be seen in Fig.4.1b. The vibration side is the bottom side of the whole device, while the dynamometer side is the top side of the device. The elastomer is sandwiched / placed in the middle of the top and bottom electrodes for the contact-separation process. Similar to the previous study, a 1-mm thick dielectric elastomer was used. The length and width of the elastomer were set on 30 x 30 and was placed on the top side of the bottom electrode. The electrode was created from a 40 x 40 mm copper film with a thickness of 0.07 mm. a 10 x 50 mm masking tape was also used to bond the elastomer to the electrodes. The surface roughness of the elastomer is shown in Fig.4.1c, with the roughness details shown in Table 4.1. The surface roughness data was captured using an electron microscope and measured under JIS B 0601:2001 standard. Finally, the multi-layer TEG device prototype can be seen in Fig.4.1d. The prototype is then placed on the vibration generator.

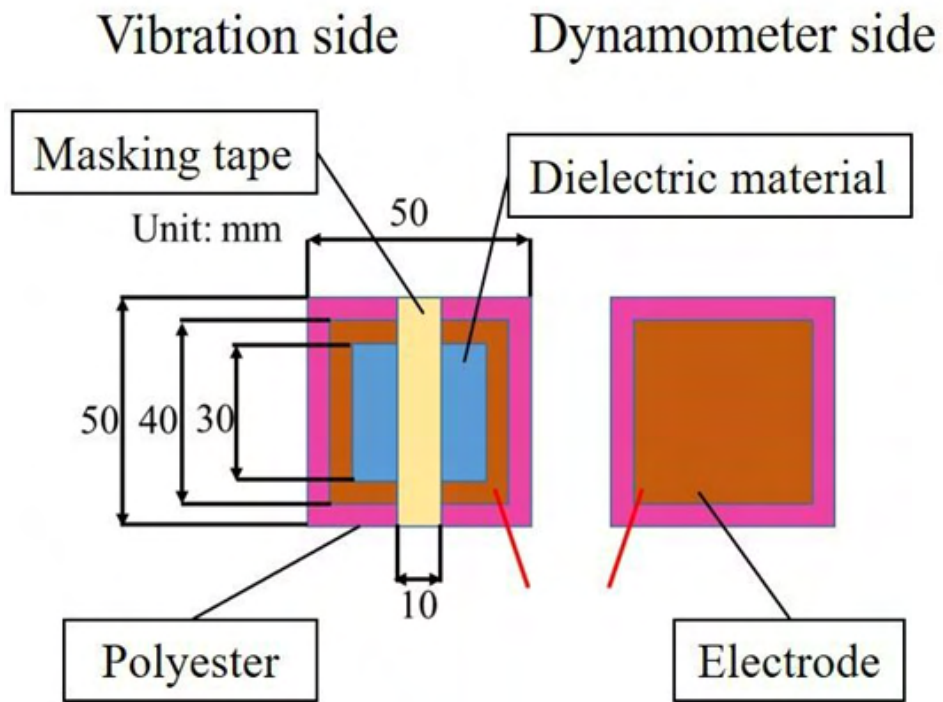
Fig.4.2a presents the experimental setup. The same vibration generator was used to simulate

the contact-separate motions of the multi-layer TEG device. To capture the data, the output voltage was measured with the A/D converter for voltage and displacement (KEYENCE, Multi-input data logger, NR-500 Series). The A/D converter's internal resistance in an open circuit was set at $1M\Omega$, and the electrical power could be calculated via Ohm's law. One laser displacement sensor (KEYENCE, CMOS Multi-Function Analog Laser Sensor, IL 300) was also used to measure the height difference on the plate where the bottom electrode is placed. This height difference will be different based on the TEG time history movement and help the observer gauge TEG modes (i.e., contact mode or compression mode). Lastly, a dynamometer to measure the amount of compression force is placed on the top plate on top of the top electrode. Details of the dynamometer can be seen in Fig.4.2b

The variables for the vertical contact-separation tests are shown in Table 4.1 under three different parameters. Firstly, the frequencies were set at 5, 10, 20, and 30 Hz. Then, the vibration amplitude, which is the magnitude of vibration caused by the vibrator generator movement, was set at 2.0, 4.0, and 6.0 mm. Lastly, the initial distance between the top plate and bottom plate of the electrodes (δ_c) was varied from 7, 10, 12, 14, 16, 18, 20, 25, and 30 mm. The data from the experiments were captured every millisecond for a whole five seconds, resulting in 5,001 data to be observed. Each case was tested three times to ensure its stability, and no electrical noise was presented on the experiment's tests. In every particular case, 10 peak values of the output voltage and 10 trough values were extracted and used as the averaged maximum voltage for further observation.



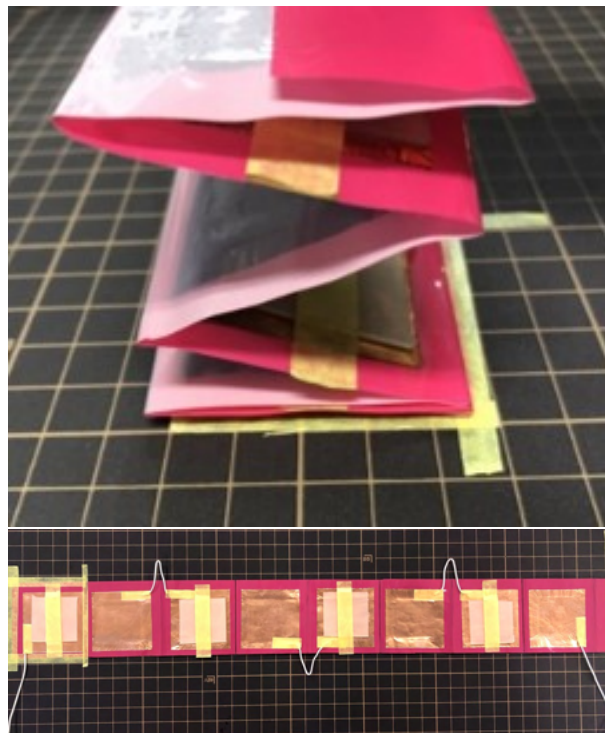
(a) Schematics of Multi-layer type TEG



(b) Size (mm)



(c) Surface roughness on the TEG dielectric elastomer



(d) Prototype

Figure 4.1: Multi-layer TEG device.

Table 4.1: Table 1: TEG roughness surface data

| Average roughness height | Route-mean-square | Skewness | Kurtosis |
|--------------------------|-------------------|----------|----------|
| 9.686 | 11.981 | 0.377 | 2.793 |

(Unit: μm)

Table 4.2: Multi-TEG vertical vibration tests.

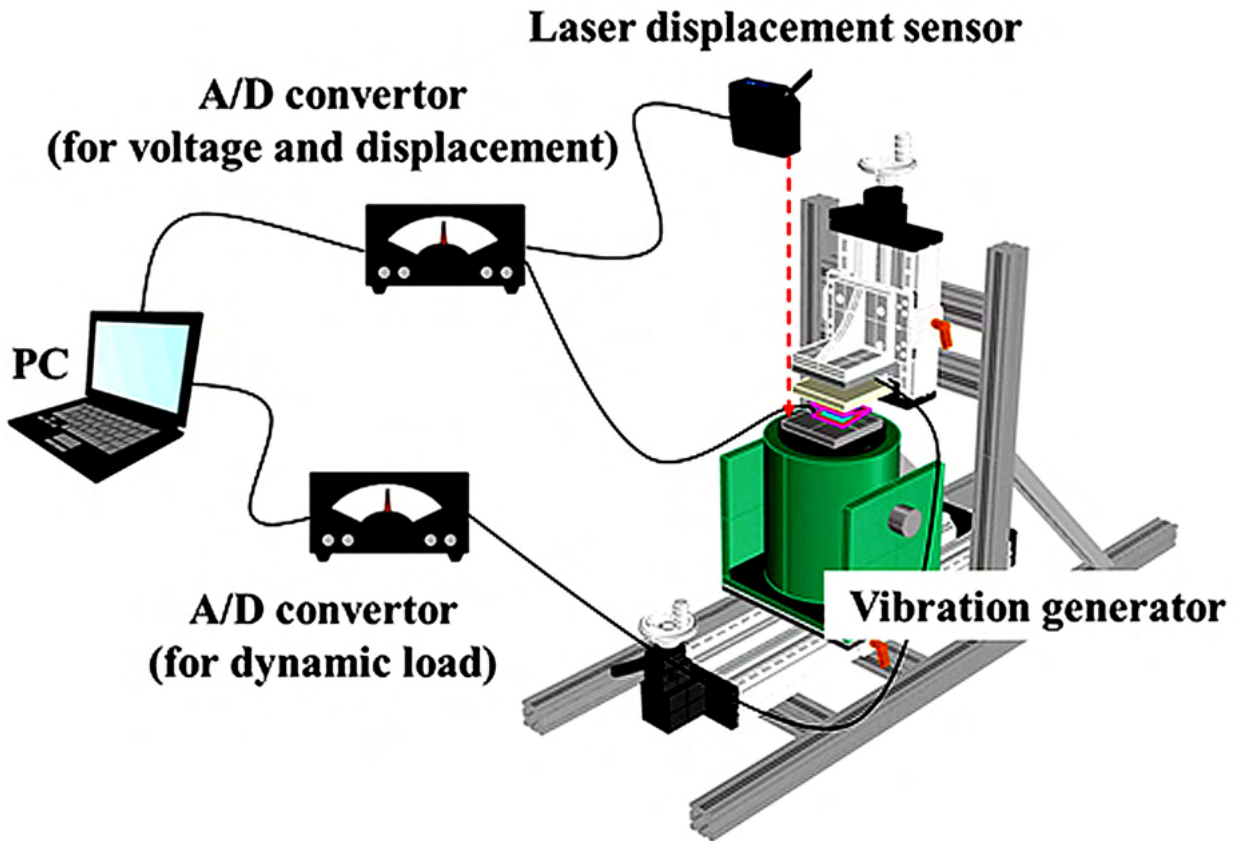
| | |
|--------------------------|-----------------------------------|
| Frequency [Hz] | 10, 20, 30 |
| Separation stroke [mm] | 2.0, 4.0, 6.0 |
| Separation distance [mm] | 7, 10, 12, 14, 16, 18, 20, 25, 30 |
| Number of tests [-] | 3 |

4.3 Multi-TEG experiments results

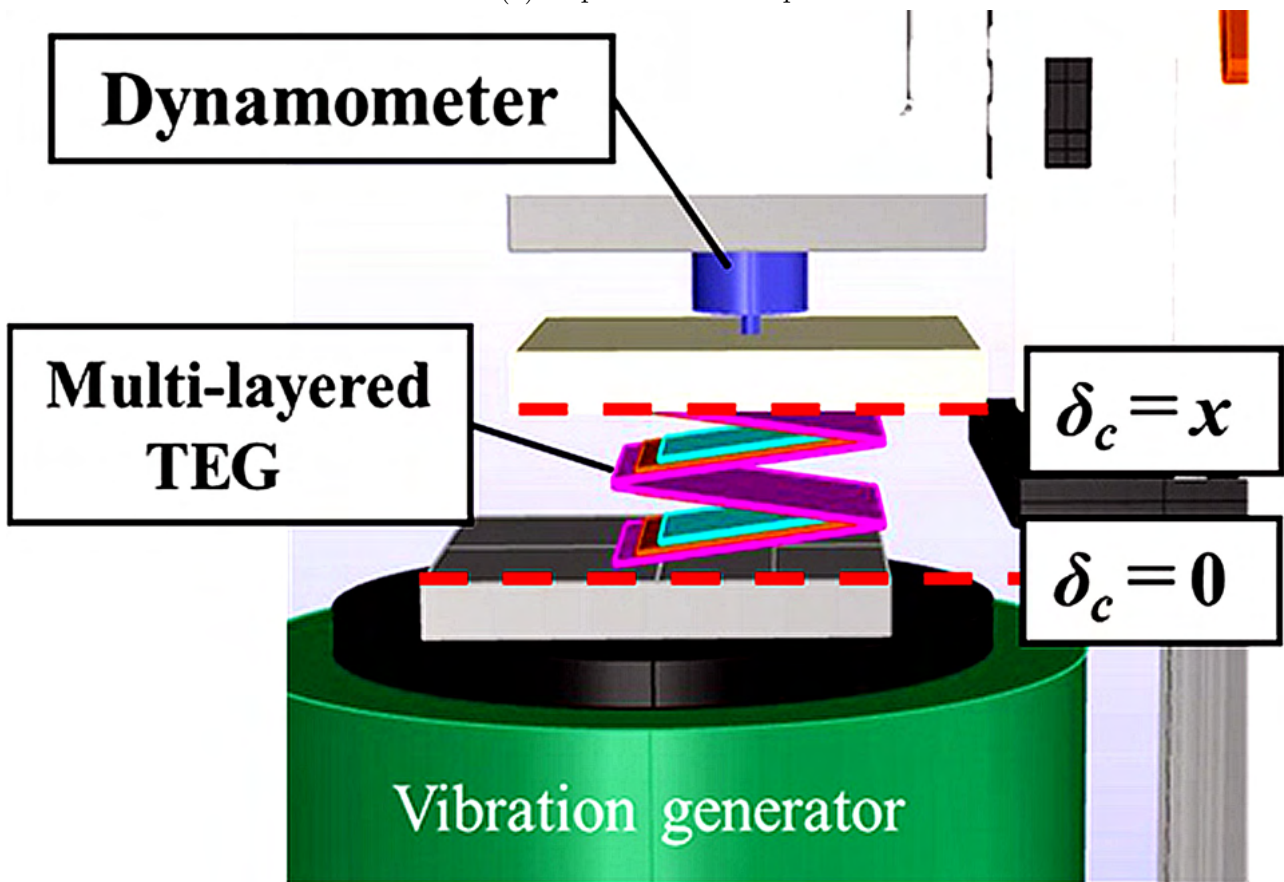
4.3.1 Effect of the multi-layered structure

The results of output voltage time histories between single layer TEG and multi-layer TEG can be seen in Fig.4.3a and Fig.4.3b. A case of frequency of 20 Hz ($f_v = \mathbf{20\ Hz}$) on the amplitude of 6.0mm ($A_v = \mathbf{6.0mm}$) was chosen as a sample for illustrating the result of the electrical output. It can be seen in the figures that the multi-layer TEG is able to generate a much higher output voltage. An approximately four times increase (compared with the single-layer TEG) was able to be generated from the multi-layer TEG.

Since multi-layer TEG has more amount of elastomer and copper films, it is crucial to ensure its effectiveness and its efficiency. The comparison of the output voltage per unit area time histories between single layer TEG and multi-layer TEG can be seen in Fig.4.3c and Fig.4.3d. Based on the figures, the multi-layer TEG can generate a slightly higher electrical output per unit area. Therefore, this confirms the device's effectiveness and shows that the multi-layer design has a minimal deficiency compared with the single-layer type.

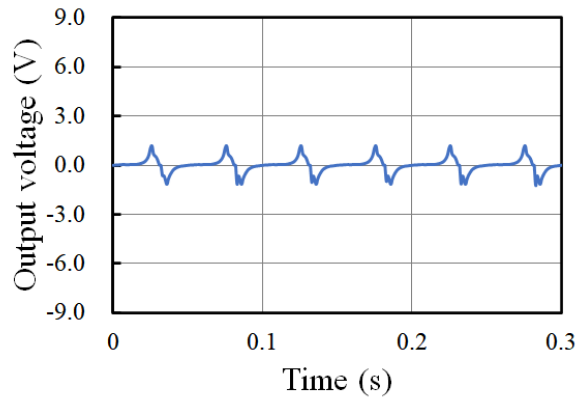


(a) Experimental Setup

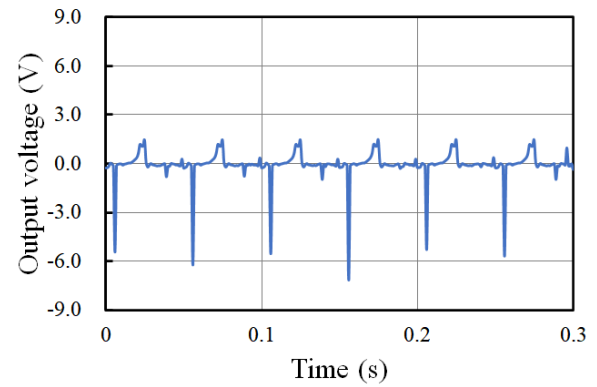


(b) More detail in the Experimental Setup

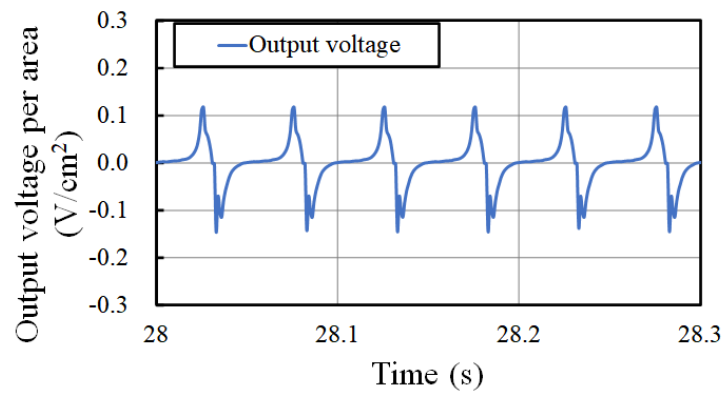
Figure 4.2: Vertical vibration setup



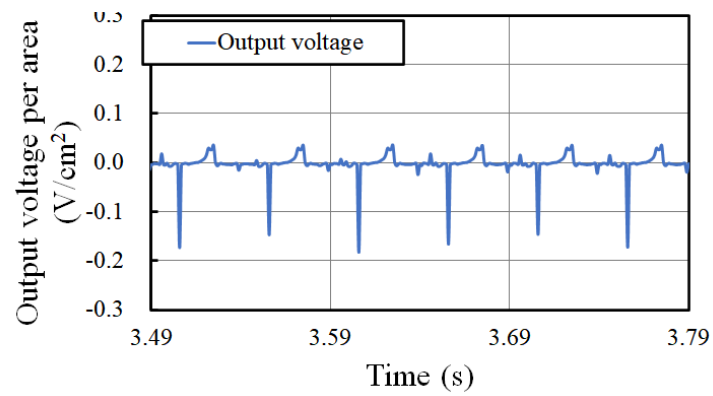
(a) Single-layer TEG



(b) Multi-layered TEG



(c) Single-layer TEG voltage per area



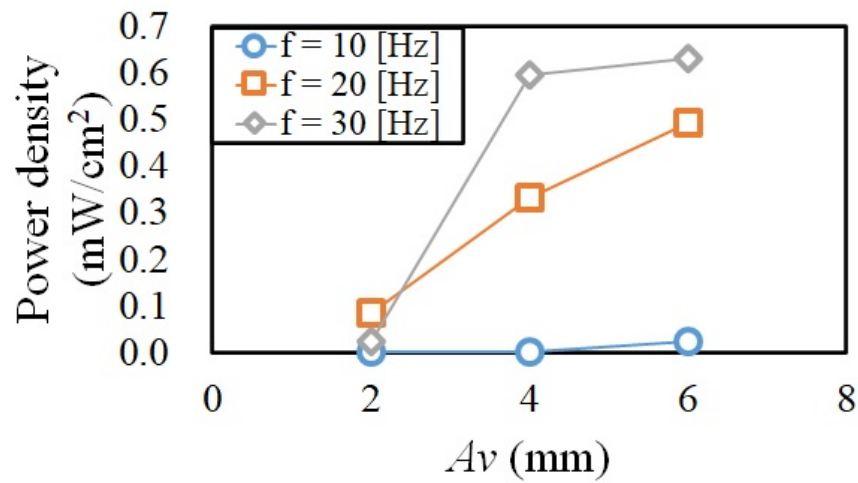
(d) Multi-layered TEG voltage per area

Figure 4.3: Comparison of the single layer and multi-layered TEG output voltage

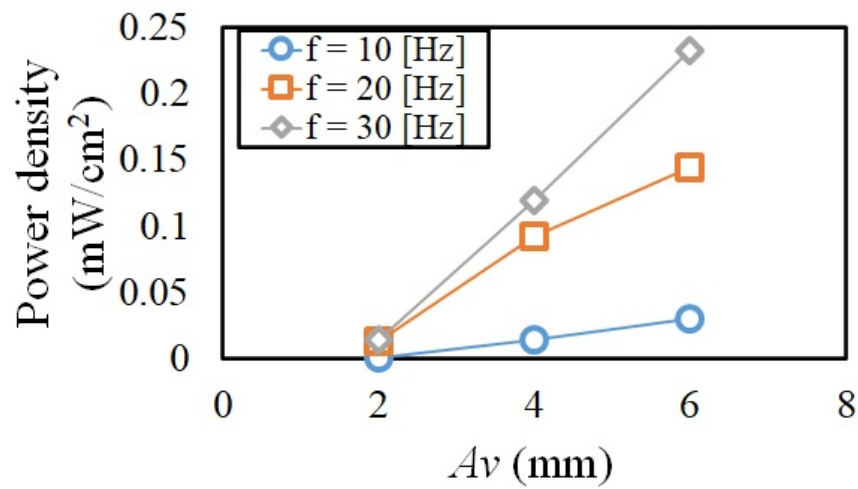
4.3.2 Effect of the Frequency and Amplitude on the Multi-layered TEG output voltage

Before comparing the single layer TEG and multi-layer TEG on the contact mode and the compressed mode, it is important to understand the effect of the vibration amplitude on TEG output voltage. Fig.4.4 shows the Relationship between vibration amplitude and electrical output on selected initial distance conditions. Three samples based on a high initial distance ($\delta_c = 12, 14, \text{ and } 20 \text{ mm}$) were chosen to illustrate the effects. Based on the figure, three main points could be observed.

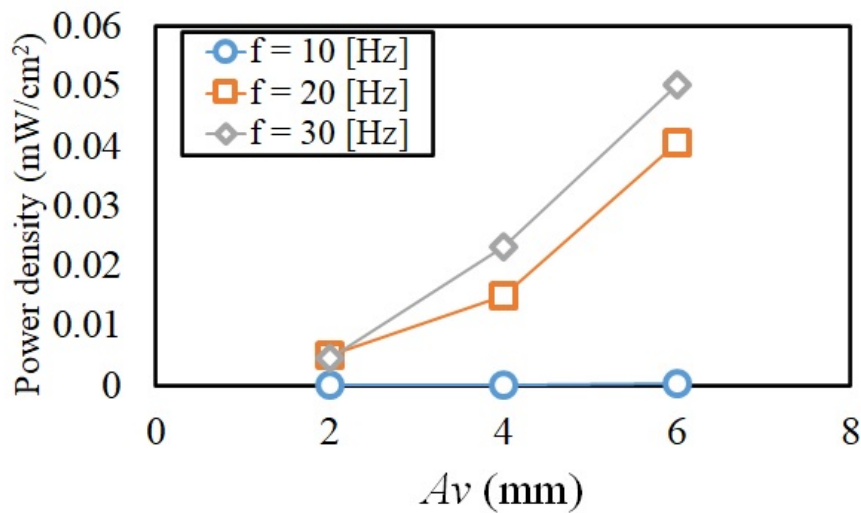
Firstly, in terms of the frequency, it is confirmed for the multi-layered TEG that the frequency provides a positive correlation with TEG electrical output. This means that a higher frequency that is tested on the same initial distance and same amplitude tends to generate higher electrical output as well. Secondly, the vibration amplitude also has a direct correlation and positive relationship toward multi-TEG output. Based on these two findings, the frequency and amplitude proved to be the main point for an effective output. Therefore, adjusting these two parameters needs to be appropriately set to ensure effective results. Lastly, the electrical output tends to be higher on the smaller initial distance, as seen in the comparison between Fig.4.4a > Fig.4.4b > Fig.4.4c. This is predicted due to the compression state of the multi-TEG. But this is not the direct relationship where lower initial distance = higher output. The following subsection will provide a clear understanding of this phenomenon.



(a) on initial distance = 12 mm



(b) on initial distance = 14 mm

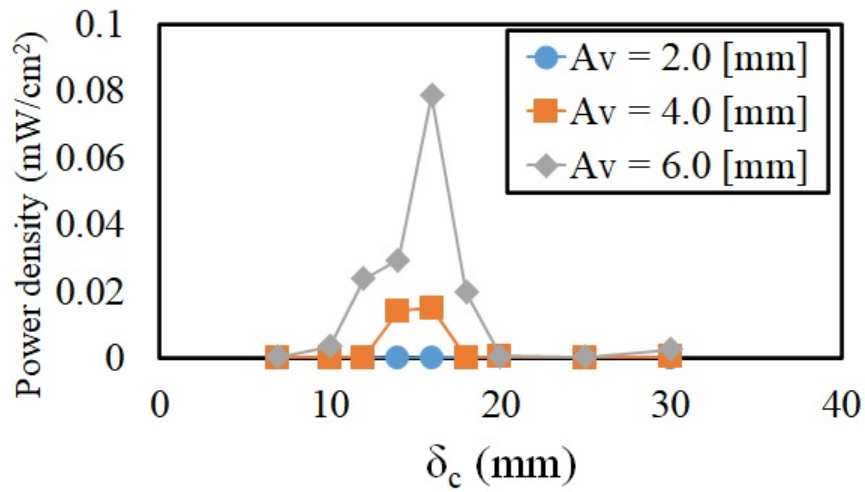


(c) on initial distance = 20 mm

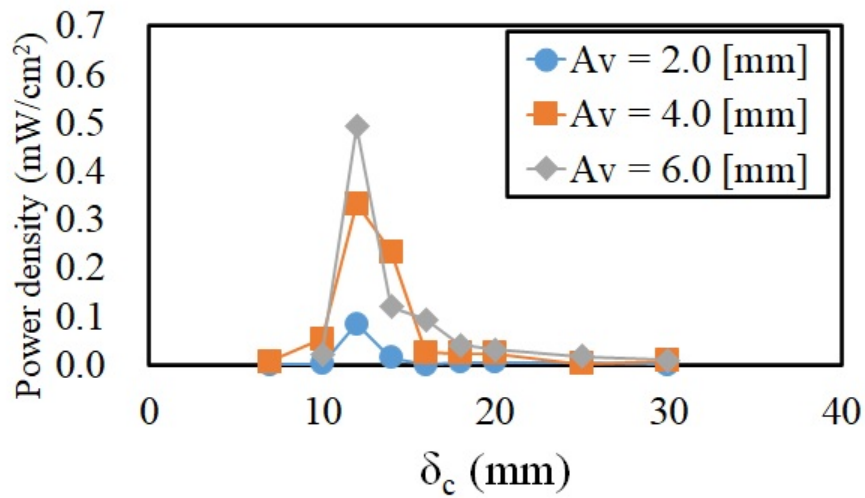
Figure 4.4: Relationship between vibration amplitude and multi-layered TEG electrical output on selected initial distance condition.

4.3.3 Relationship of initial distance with vibration amplitude and vibration frequency

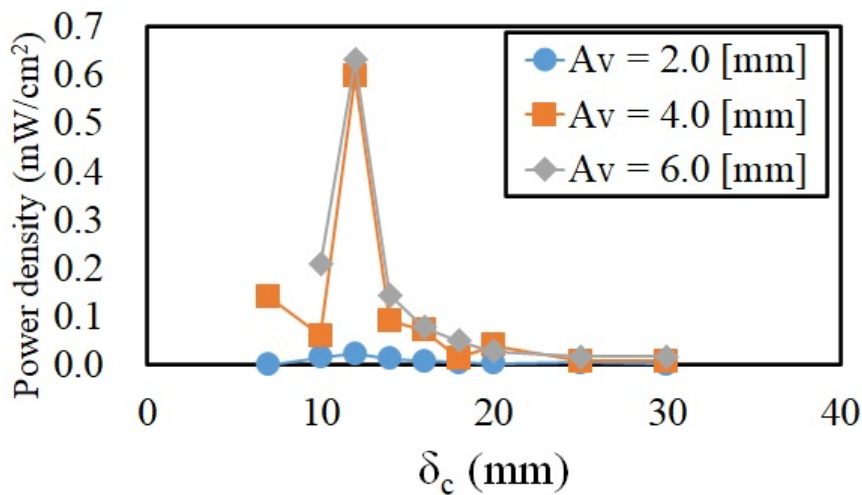
The relationship of initial distance (δ_c) with the multi-TEG electrical output is presented in Fig.4.5 with 4.5a is for the test on frequency = 10 Hz, 4.5b is for the frequency = 20 Hz, while 4.5c is for 30 Hz. The vibration amplitude (A_v) range from 2.0 – 6.0 mm is presented in the above-mentioned figures. Firstly, in terms of the vibration amplitude, it is confirmed as well in the previous subsection that higher amplitude equals larger electrical output. However, the initial distance does not have this similar tendency. From the figures, higher initial distance or lower initial distance does not equal higher output. In fact, the initial distance is constant regardless of the vibration displacement (A_v). This is especially apparent in the frequency of 20 Hz and 30 Hz (Fig.4.5b and Fig.4.5c), where the peak output occurs on the same peak distance ($\delta_c = 12$ mm) on all A_v . To provide more explanation for this phenomenon, Fig.4.6 displays the relationship between initial distance with multi-TEG electrical output under different amplitudes. Fig.4.6a is for the vibration amplitude = 2.0 mm, Fig.4.6b is for the amplitude = 4.0 mm, while Fig.4.6c is for 6.0 mm. Fig.4.6b and Fig.4.6c with the $A_v = 4.0$ and 6.0 shows that the max output occurs in different distance on each frequency. For frequency of 10 Hz, the max output is generated on $\delta_c = 16$ mm, while frequency 20 and 30 Hz is on $\delta_c = 12$ mm. Based on this finding, it can be concluded that the value of initial distance that can help multi-TEG generate the most electrical output depends on the vibration frequency (f_v).



(a) on frequency = 10 Hz

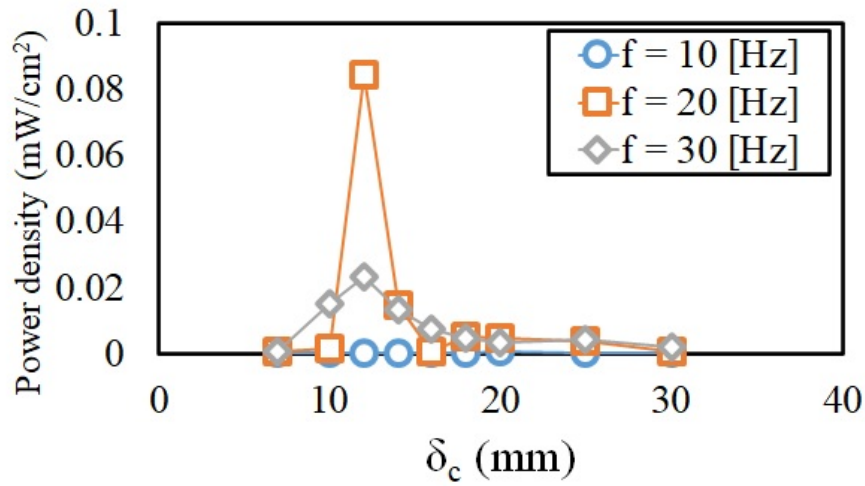


(b) on frequency = 20 Hz

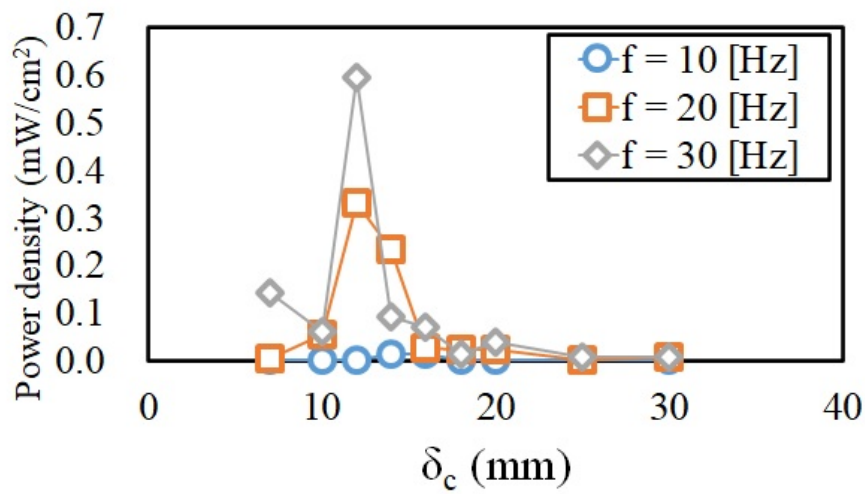


(c) on frequency = 30 Hz

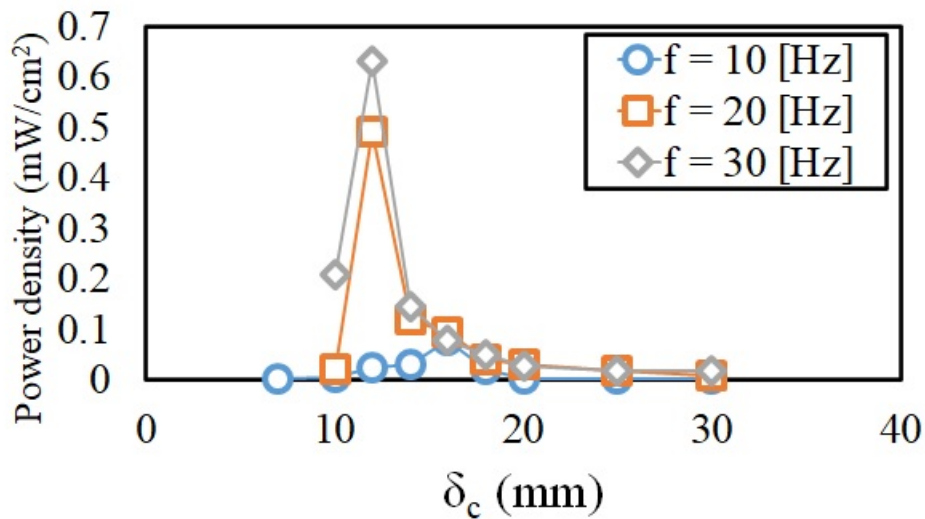
Figure 4.5: Relationship between vibration amplitude and initial distance on various frequencies.



(a) on vibration amplitude = 2.0 mm



(b) on vibration amplitude = 4.0 mm



(c) on vibration amplitude = 6.0 mm

Figure 4.6: Relationship between vibration frequency and initial distance on various amplitude.

4.3.4 Single Layer Vs. Multi-Layered TEG in Contact and Compression Modes

This section describes the multi-TEG output voltage on the contact and compress modes. Fig.4.7 shows one example of multi-TEG output voltage time history on the contact mode. This example has the vibration frequency $f_v = 20$ Hz, vibration amplitude $A_v = 6.0$ mm and initial distance $\delta_c = 3.0$ mm. Since the value $1/2 A_v = \delta_c$ (as shown on the separation stroke value = ± 3.0 mm), it is confirmed that multi-TEG is in the contact mode. The maximum output voltage is measured around 1.1 V, and a stable output result occurred during the whole experiment.

A similar case setup is presented in Fig.4.8 with multi-TEG is in the compressed mode. The vibration frequency and vibration amplitude are similar with Fig.4.7 ($f_v = 20$ Hz and $A_v = 6.0$ mm), but the initial distance is shortened into $\delta_c = 2.5$ mm. Since the value $1/2 A_v < \delta_c$ (as shown on the separation stroke value = ± 2.5 mm), it is confirmed that multi-TEG is in the compressed mode. The output voltage has a higher value than the contact mode, with the stable output voltage resulting around > 1.5 V throughout the whole experiment.

To summarize, Fig.4.9 presents the comparison between the output voltage of single-TEG and multi-TEG on the contact mode. In compress mode, Fig.4.10 shows the comparison based on each TEG's maximum voltage. Additionally, the power density of both TEG on the contact mode and compress mode could be seen in Fig.4.11 and Fig.4.12. From the figures, there are two main points found in the experiment. Firstly, the multi-TEG is able to generate a much higher output voltage (up to 4 times higher) compared with the single-TEG. This is expected since the multi-TEG mechanism can provide a better contact-separation process as mentioned in the subsection "4.3.1. effect of the multi-layered structure". However, it is also found that contact mode could provide a high output voltage. This is especially apparent in Fig.4.9b, where on the $A_v = 6.0$ mm (gray line) that the result of the electrical voltage is more than 5 V on the $f_v \geq 20$ Hz. The result of the gray line on contact mode is even higher than the result on the compressed mode that can be seen in Fig.4.10b.

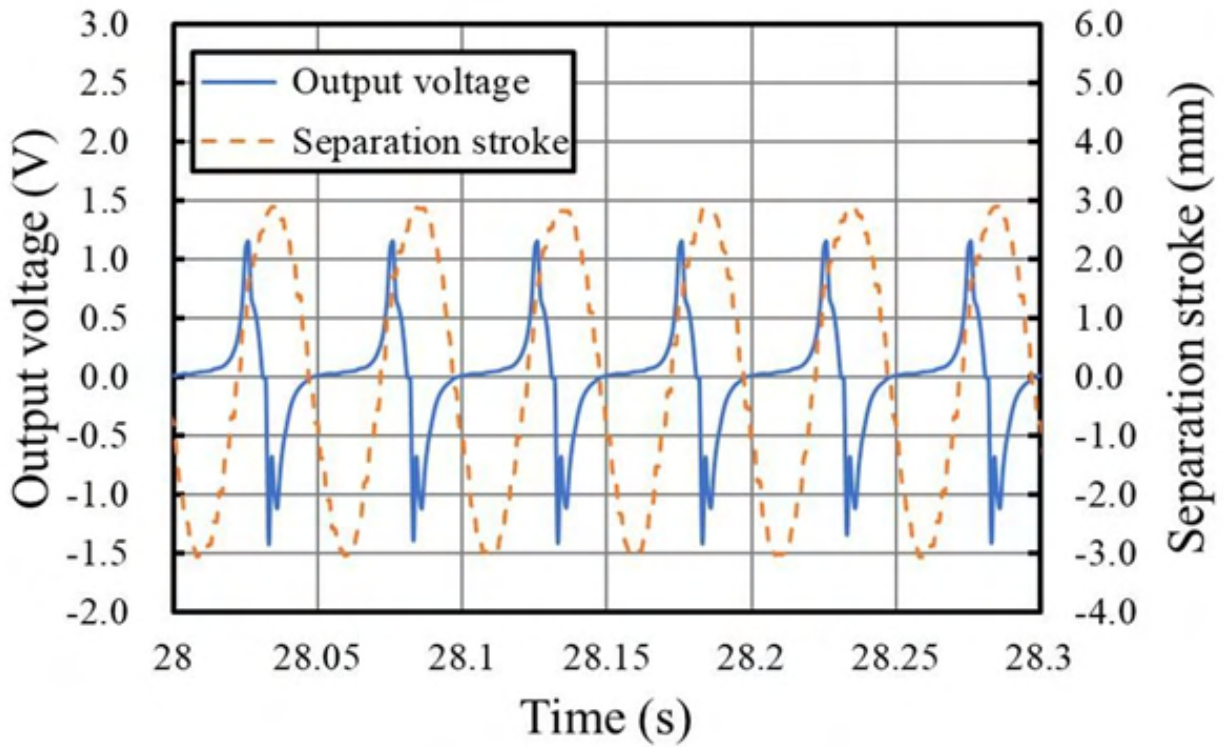


Figure 4.7: TEG output voltage and its separation stroke on frequency 20 Hz, $A_v = 6.0$ mm and $\delta_c = 3.0$ mm – contact mode

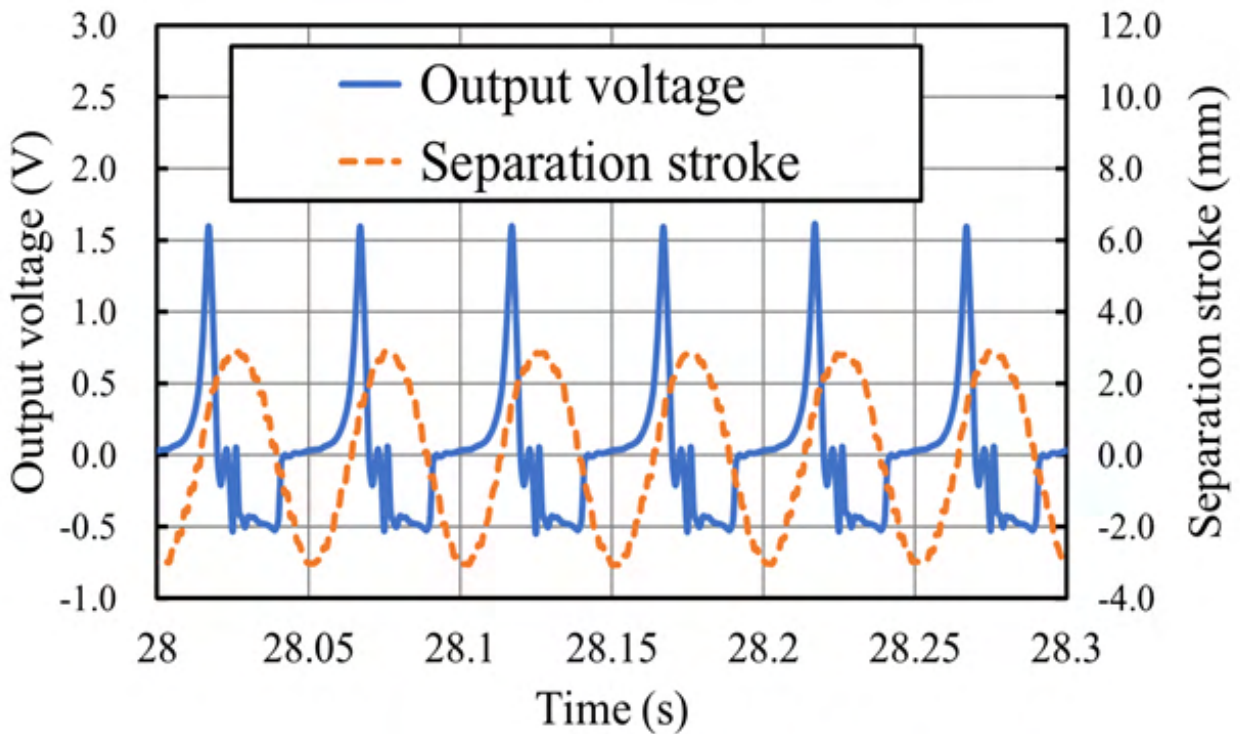
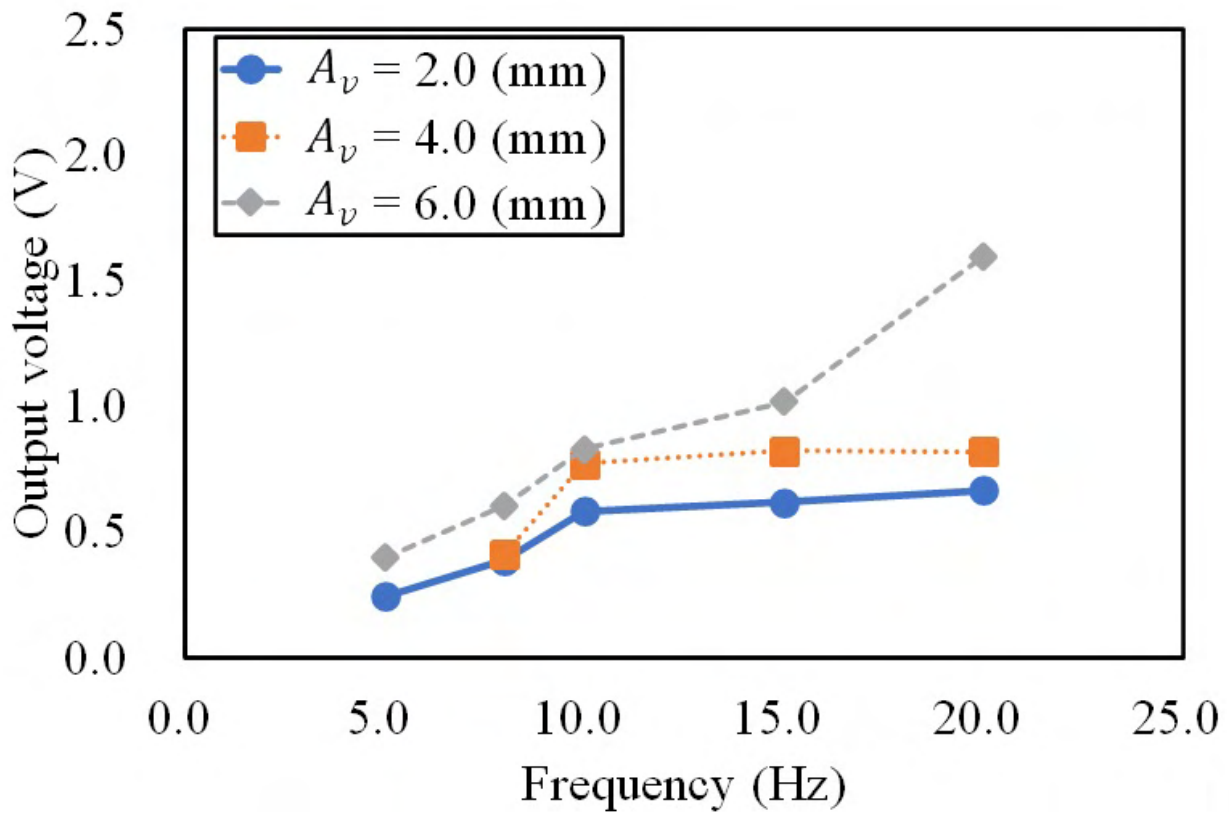
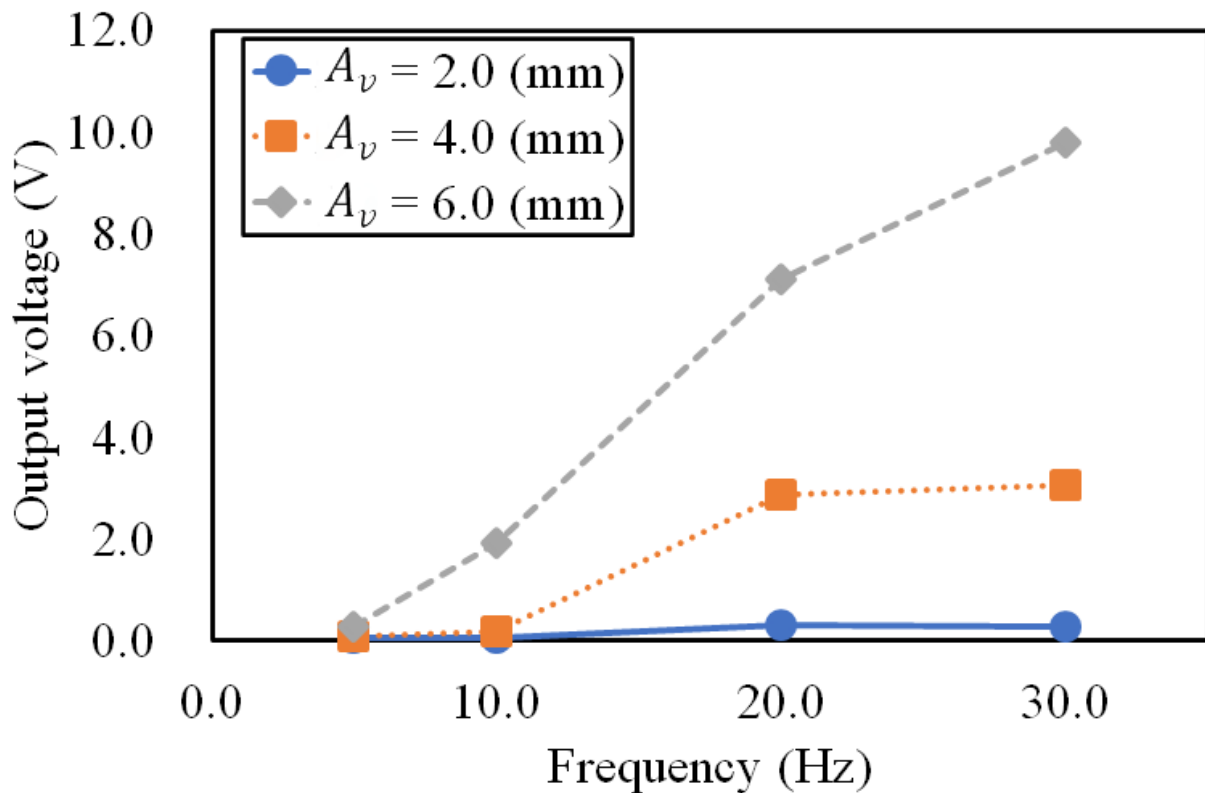


Figure 4.8: TEG output voltage and its separation stroke on frequency 20 Hz, $A_v = 6.0$ mm and $\delta_c = 2.5$ mm – compress mode

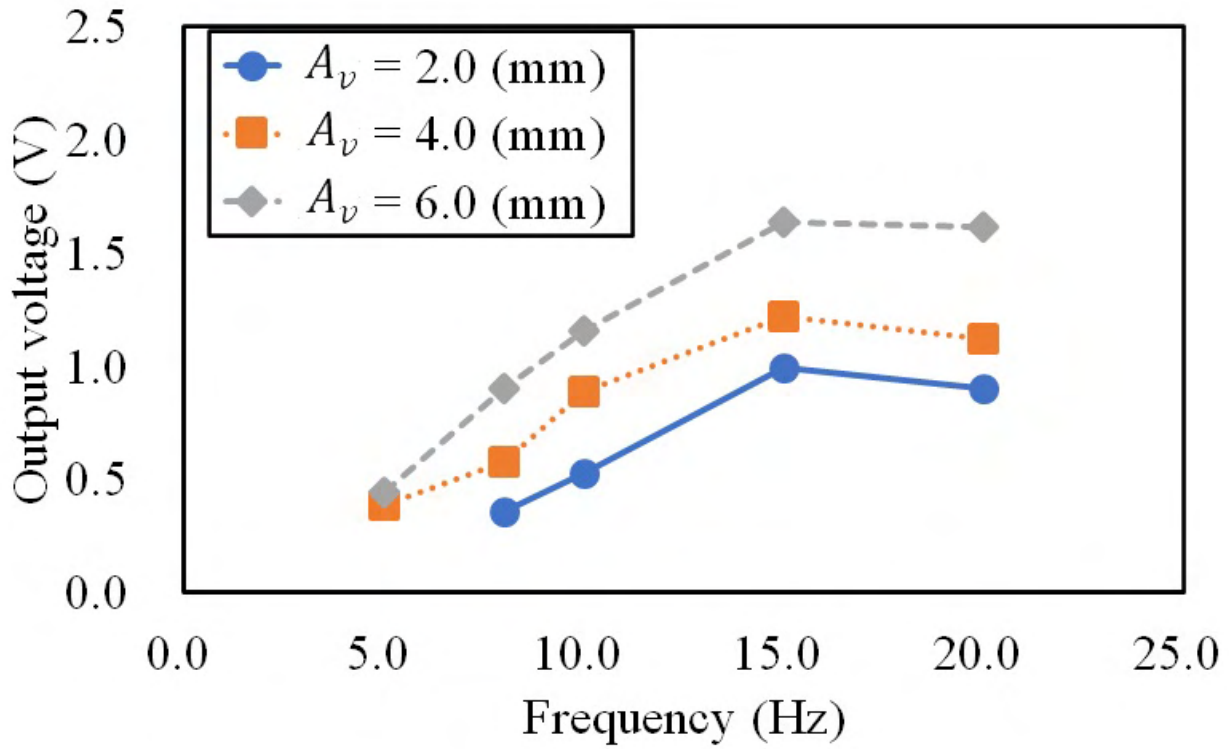


(a) Single-layer TEG

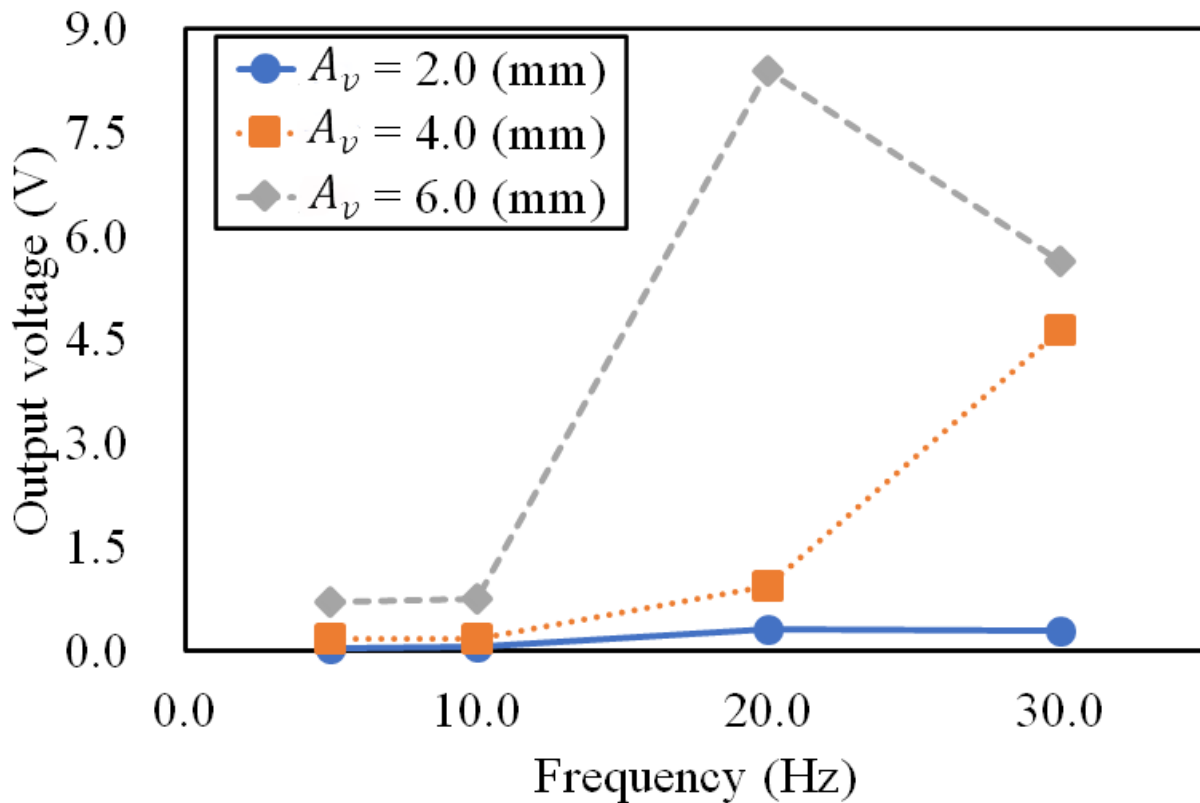


(b) Multi-layered TEG

Figure 4.9: Comparison of the single-layer TEG and multi-layered TEG output voltages (**contact mode**)

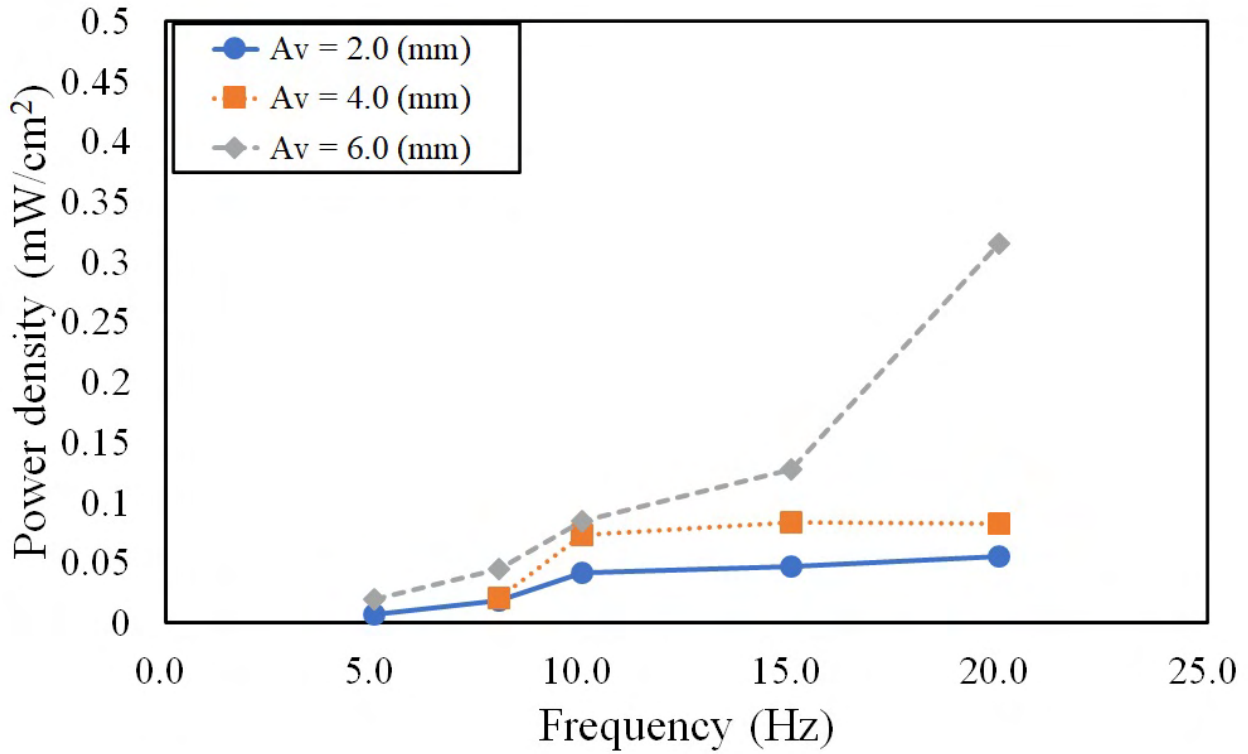


(a) Single-layer TEG

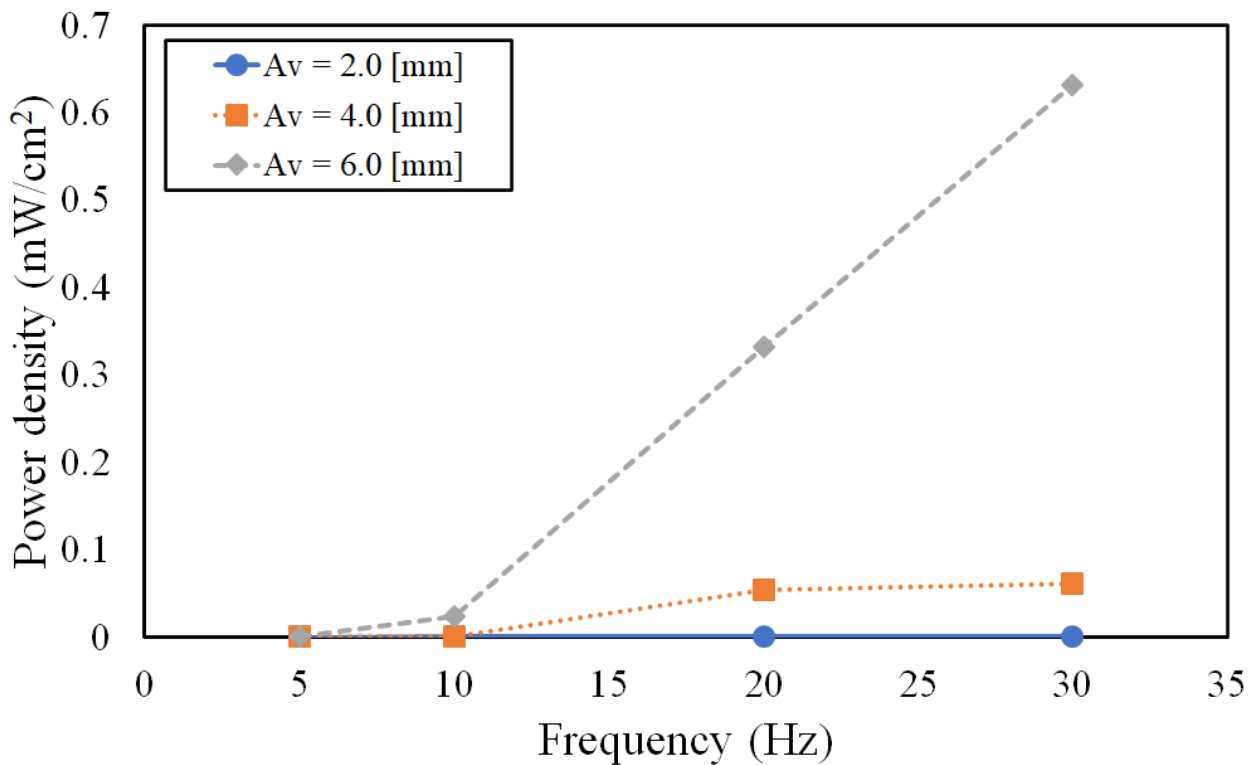


(b) Multi-layered TEG

Figure 4.10: Comparison of the single-layer TEG and multi-layered TEG output voltages (**compress mode**)

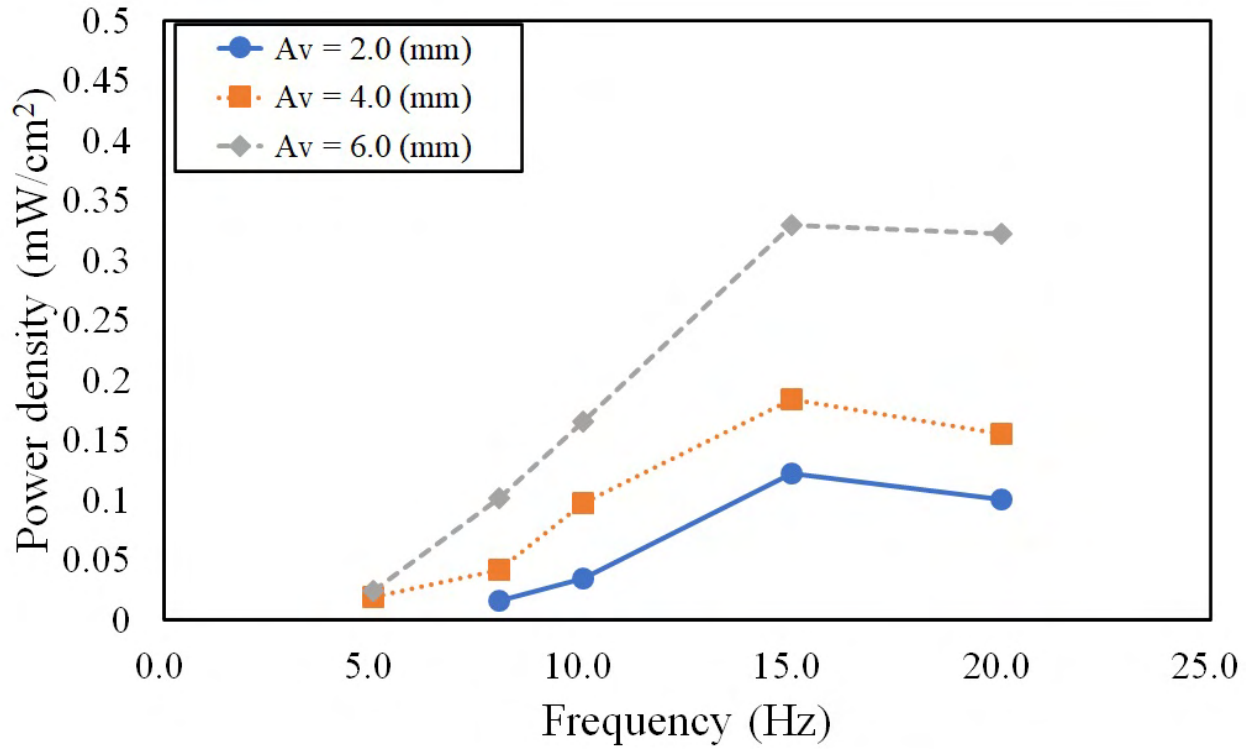


(a) Single-layer TEG

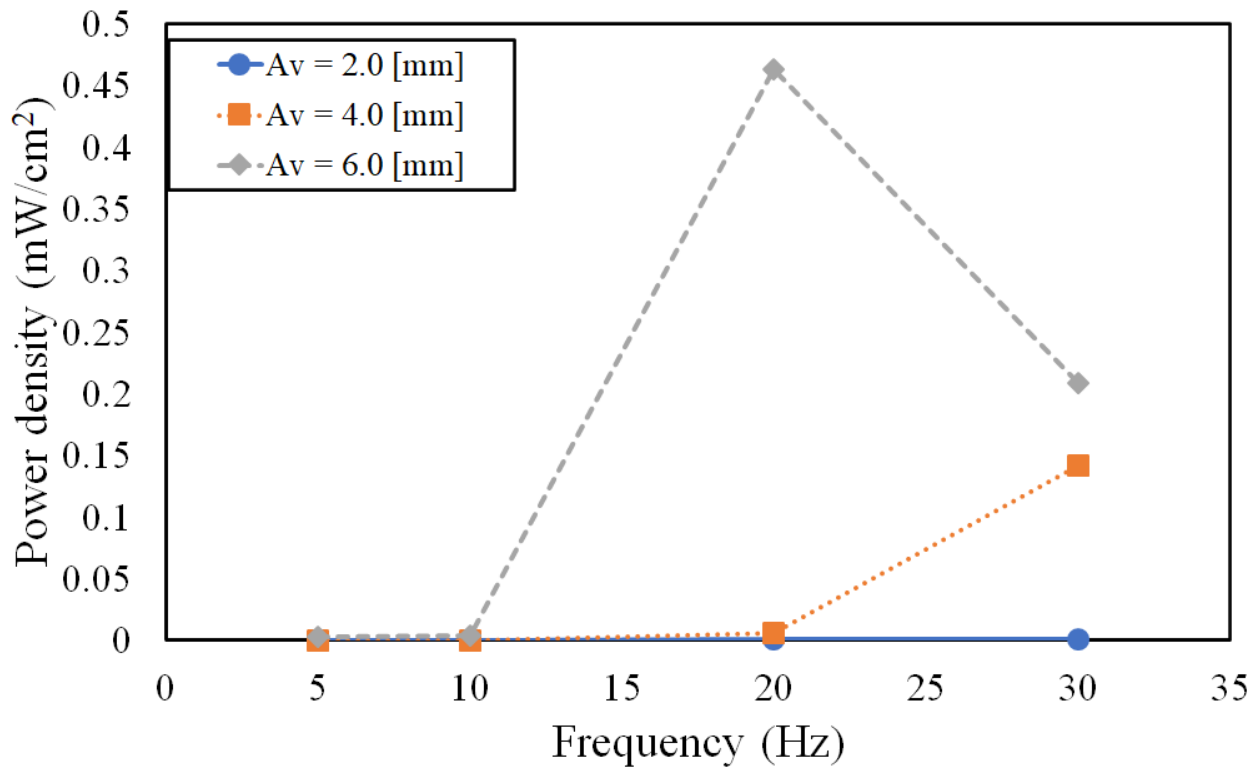


(b) Multi-layered TEG

Figure 4.11: Comparison of the single-layer TEG and multi-layered TEG power density (**contact mode**)



(a) Single-layer TEG



(b) Multi-layered TEG

Figure 4.12: Comparison of the single-layer TEG and multi-layered TEG power density (**compress mode**)

Due to this result, more investigation regarding multi-TEG needs to be investigated. Two main parameters could create this result: the compression force and acceleration amplitude. Both parameters were observed and explained in more detail in the following subsection.

4.3.5 Comparison of compression force and acceleration amplitude to Multi-layered TEG output voltage

This section elucidates the electrical output generation of the multi-layered TEG based on its compression force (stress) and the acceleration amplitude. Firstly, the influence of the compression force is elucidated. Since the multi-layered TEG has a model like a concertina, the elastomer could touch even on the slightest height movement. Therefore, we found two main modes in the compression force: the contact mode and the compressed mode. These modes can be adjusted based on the TEG's initial distance (δ_c), as previously shown in Fig.4.2. For explanatory purposes, Fig.4.13 and Fig.4.14 presents the time histories of the TEG's output voltage along with its separation stroke (Fig.4.13a and Fig.4.14a) and stress (Fig.4.13b and Fig.4.14b). The examples were based on the experiment conditions of a vibration frequency of 20 Hz + vibration amplitude of 4.0 mm and an initial distance of 20 mm and 7 mm, respectively.

The contact mode differs from the contact mode of single-layer TEG mentioned in the previous chapter 2 (FC-TEG) due to the multi-layered structure. In the multi-layer TEG, the elastomer on the lowest part of the TEG could touch with the copper films due to the gravity. However, the elastomer on the TEG's topside is not touching due to amplitude configuration. This resulted in a minimum compression force when the device was being moved. Though that may be the case, the electrical output still generates a good output.

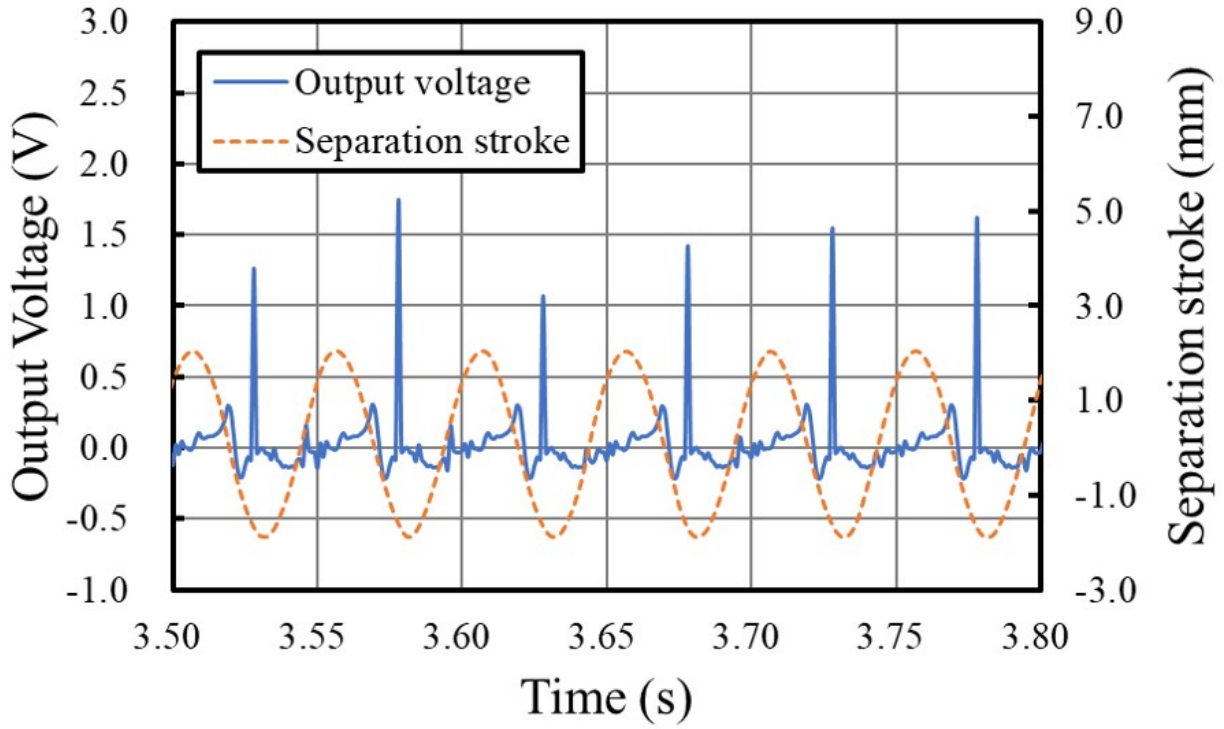
The electrical voltage value was, for the most part, above 1.2 V, albeit that it was not entirely constant. As Fig.4.13 shows, the voltage peak (highest output voltage) emerged immediately before the separation stroke trough (lowest point below the rest position) that occurred every 0.05 seconds from 3.53 to 3.78 s. From this, it can be inferred that the maximum electrical power generation can be obtained in contact mode when the space between the TEG and the

vibration machine pedestal decreases. Furthermore, as Figure Fig.4.13b shows, the high output voltage of the TEG could be generated even though the stress was minimal.

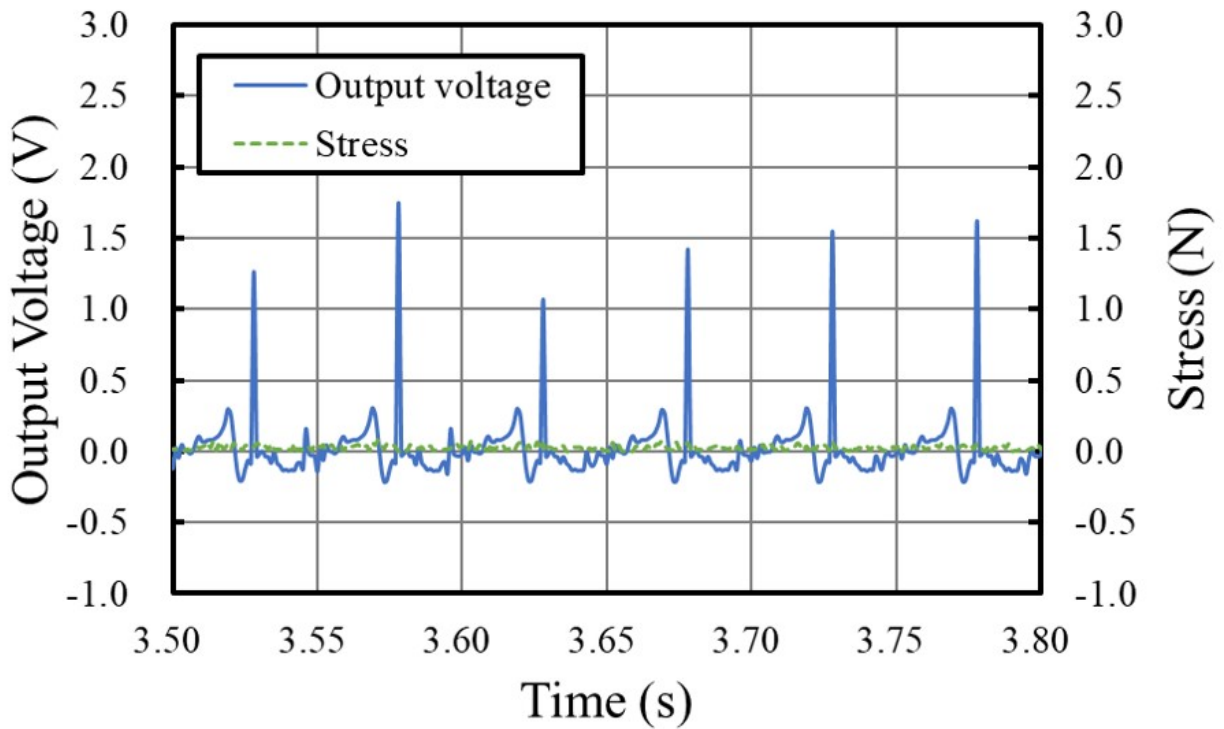
On the compression mode in Fig.4.14, the result elucidates an interesting result. To examine the influence of stress on the output voltage generation, the initial distance (δ_c) was reduced to 7 mm. Since the vibration amplitude (A_v) was set at 4 mm, the TEG device is on compression mode. In this case, the high output voltage could be achieved in a much more stable manner (around 0.8 – 0.9 V) with the stress load ranging from 0.06 to 0.92 N, periodically developing throughout the entire experiment. Based on the outcomes of the contact mode and the compression mode, the compression force received by the dielectric elastomer can be regarded as exerting a minor influence on the electrical generation. Since the compression force indirectly affects TEG output voltage, another factor (e.g., acceleration amplitude) is predicted to influence TEG voltage generation significantly.

Acceleration amplitude data were obtained via the accelerometer attached to the top plate where the multi-layered TEG was placed. The accelerometer measures how quickly the velocity of the component changes and is converted into signal data. The signal data was then transformed into a spectrum using the mathematical calculation method known as the Fast Fourier Transform (FFT) method. Finally, the acceleration amplitude value, which indicated the separation velocity of the dielectric elastomer and the electrode, was obtained. Finally, both the data of the compression force and the acceleration amplitude are observed and presented in Fig.4.15.

Fig.4.15 shows the relationship between the compression force (Fig.4.15a) and the acceleration amplitude (Fig.4.15b) with the multi-layer TEG's electrical output in the contact and compression modes. As shown in Fig.4.15a, a high output voltage could be obtained with a minimal force acting on it (contact mode), with a similar result obtained as with a larger force (compression mode). Meanwhile, as Fig.4.15b shows, the higher the acceleration amplitude, the higher the output generated by the TEG. This high electrical output was especially apparent in compression mode. Thus, we concluded that it was not necessarily the load acting on the TEG that produced such a high result; instead, it was the acceleration applied to the TEG.

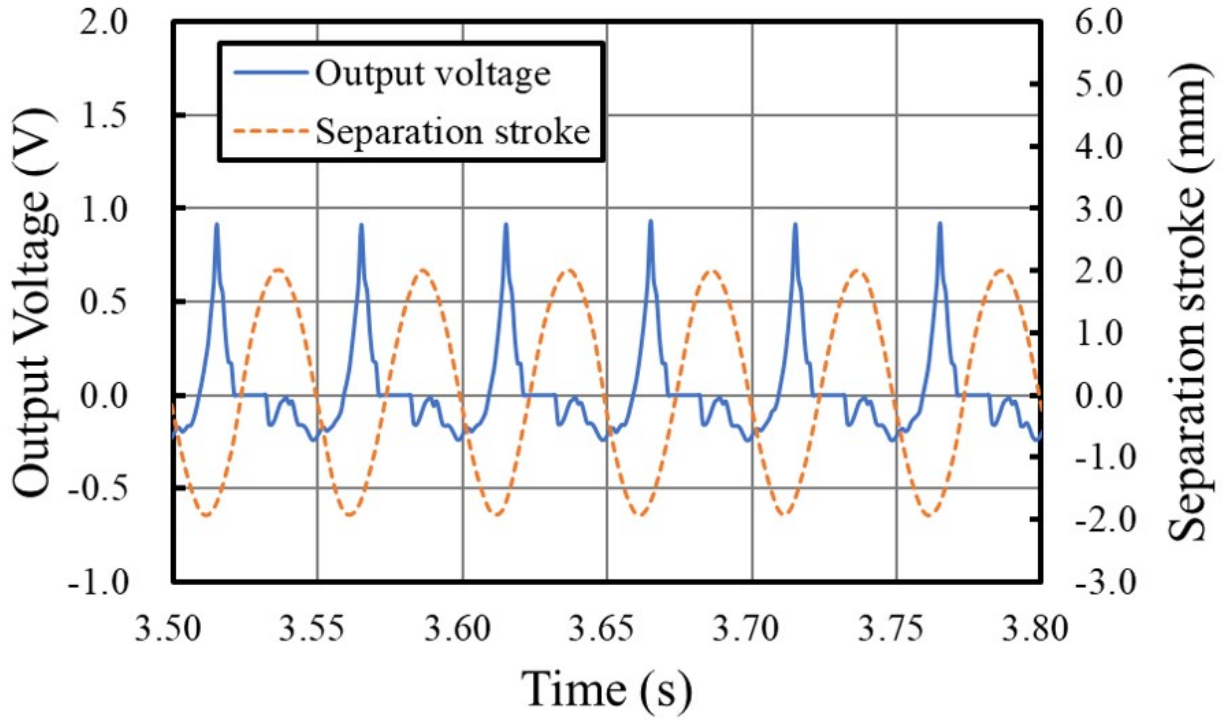


(a) Separation stroke

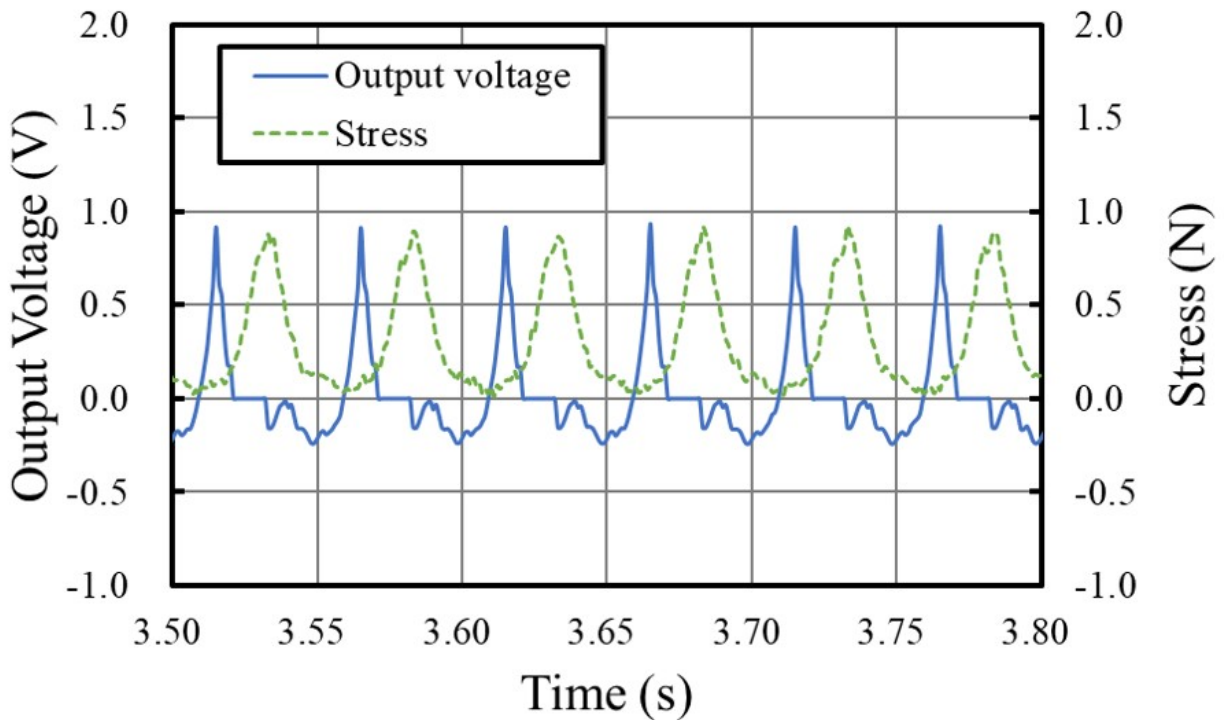


(b) Stress

Figure 4.13: Example of the TEG output voltage in contact mode ($f_v = 20$ Hz, $A_v = 4.0$ mm, $\delta_c = 20$ mm).

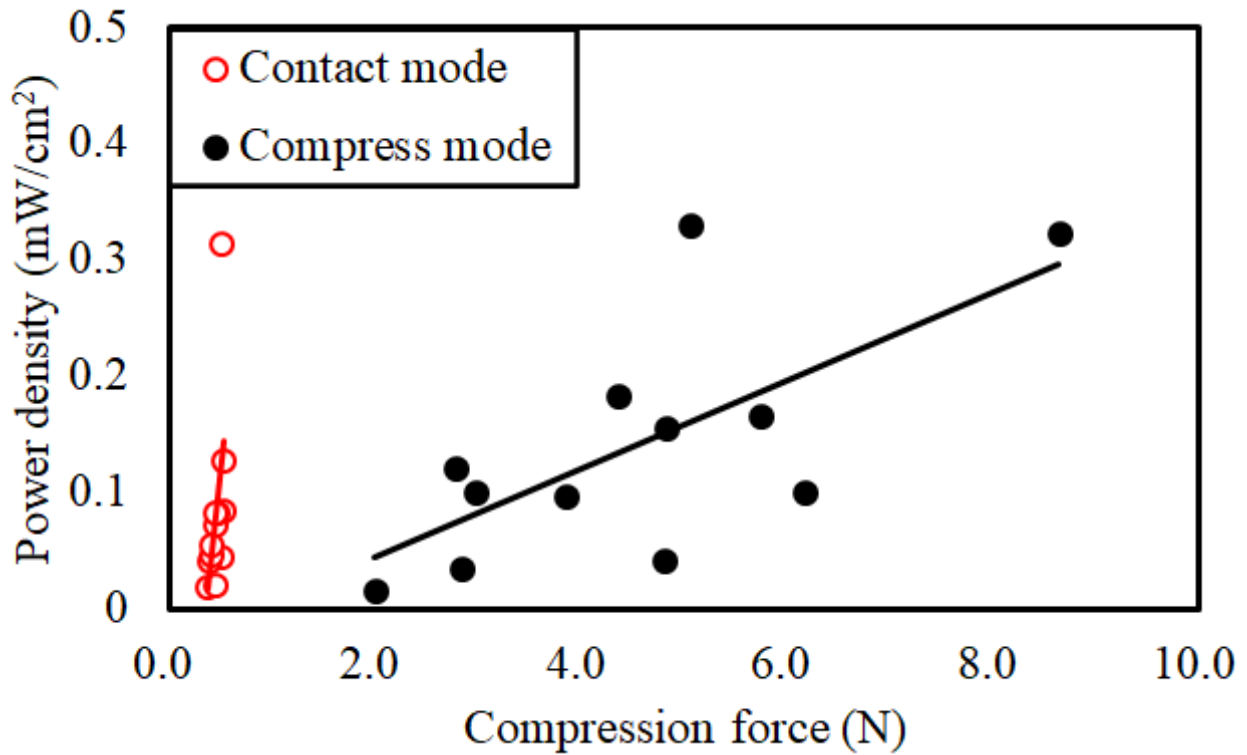


(a) Separation stroke

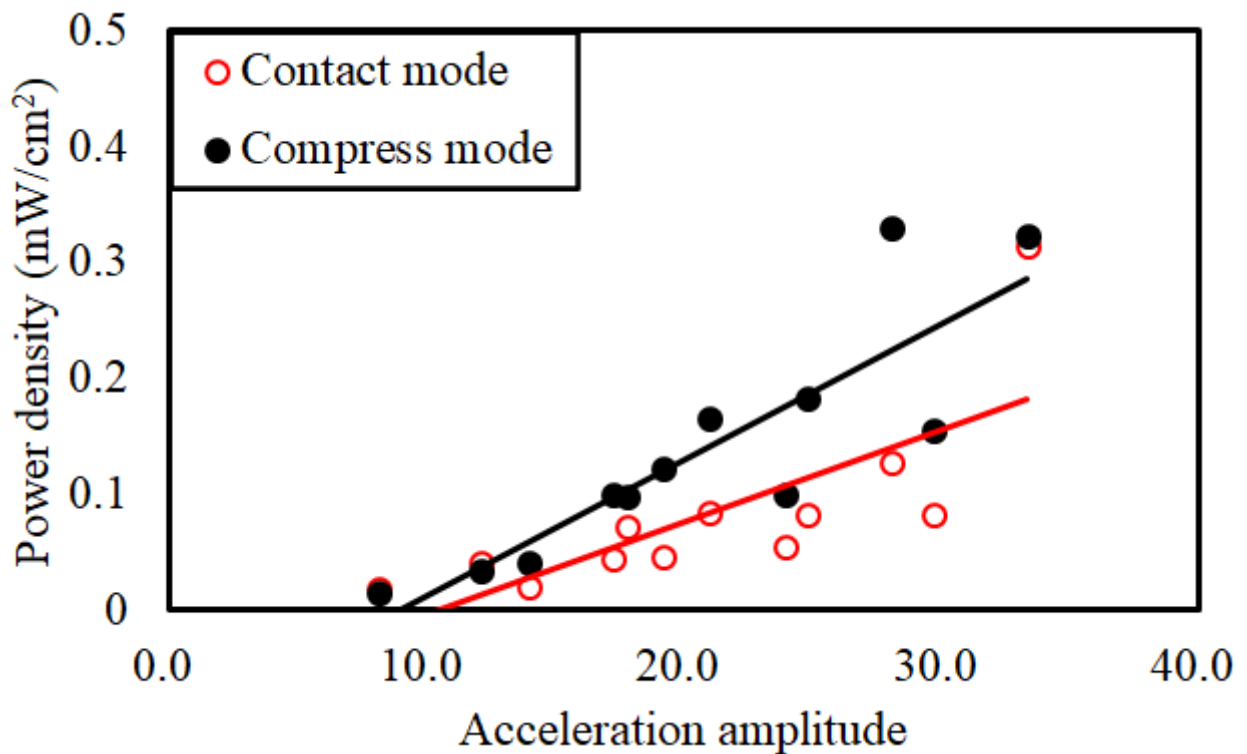


(b) Stress

Figure 4.14: Example of the TEG output voltage in compress mode ($f_v = 20$ Hz, $A_v = 4.0$ mm, $\delta_c = 7$ mm).



(a) Compression Force



(b) Acceleration Amplitude

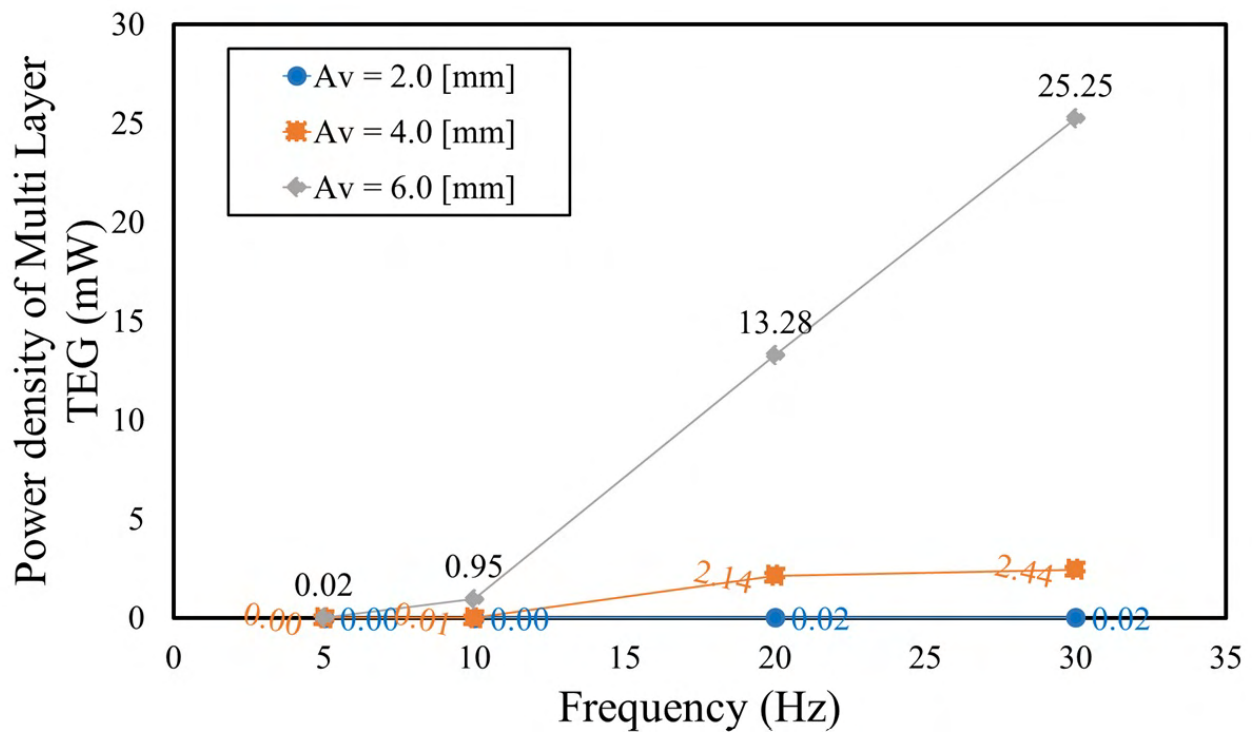
Figure 4.15: Relationship between compression force and acceleration amplitude with TEG output voltage.

The coefficient of determination value (r^2) was also calculated based on simple linear regression to support our conclusion. Here, we confirmed that the acceleration amplitude had a strong positive correlation with the TEG's output voltage, with the value found to be $r^2 = 0.81$, while that of the compression force was $r^2 = 0.48$. In short, the acceleration amplitude relation has a major influence on the multi-layer TEG electrical output.

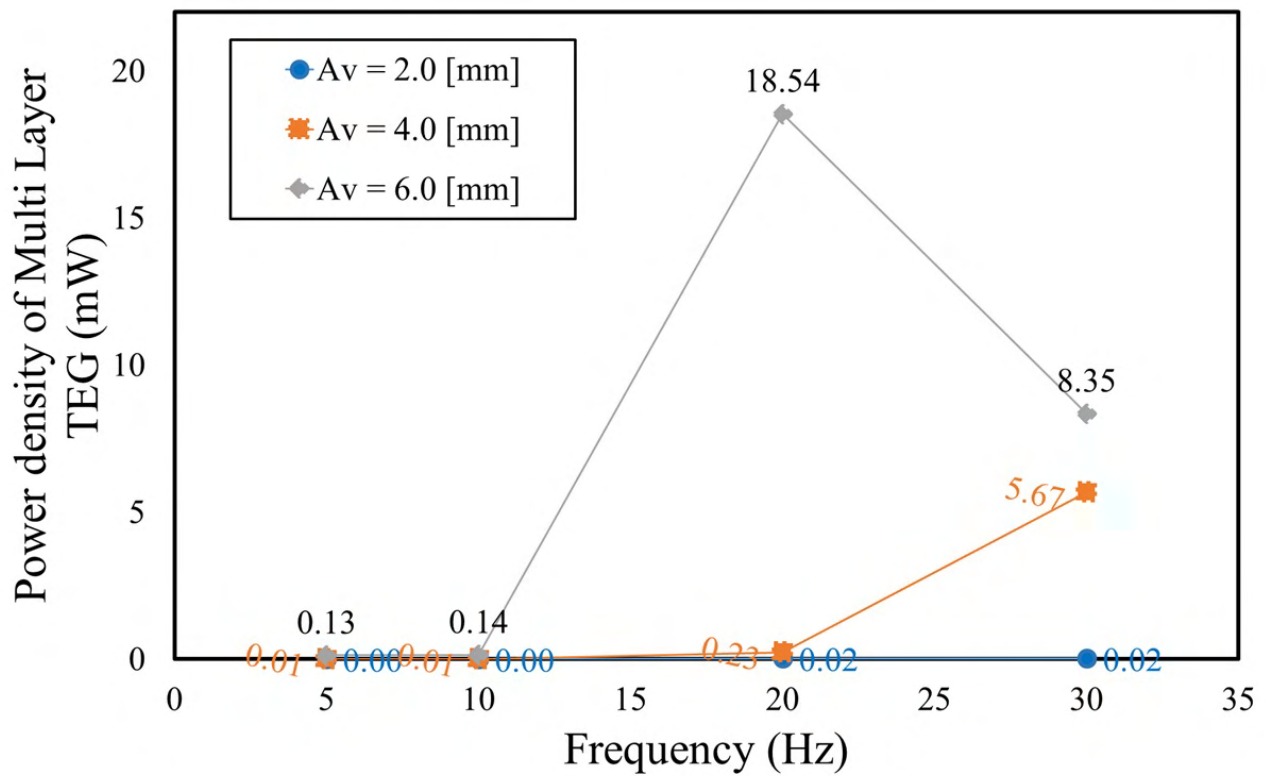
Finally, Fig.4.16a and Fig.4.16b are used to illustrate the power density of our multi-layer TEG device in this experiment with the total area of 20 cm^2 . This illustration is then used to give a rough estimation of whether the multi-layer TEG can power the mini ocean sensors or other small devices or not. However, it must be noted that this is still a rough estimation and the value of the power density still does not count the impedance matching for the two sensors. Based on the results, we can then compare those with the same state-of-art ocean sensors and ocean sensors system chart in the Chapter 1.2 Introduction. As a reminder, that chart could be seen in Fig.4.17 with the addition of the red box to show that our current Multi-TEG is able to power the top 2 Logger + sensor (roughly + not considering the impedance).

4.4 Summary

This chapter developed and examined a multi-layer triboelectric generator (multi-layer TEG) with 4 dielectric elastomers + copper films to enhance the harvesting process from the natural energies. The vertical contact-separation-compression test was preliminarily conducted, and the effect of the multi-layered structure alongside its parameters was observed. There are five primary purposes in this study. To examine the electrical output generated by the multi-layered structure and examine the effect of the vibration frequency and amplitude which lead to separation velocity on the multi-TEG. We also investigate the relationship of initial distance with vibration amplitude and vibration frequency, compare a single layer and multi-layered TEG in their working modes, and find + elucidate the compression force and acceleration amplitude as the main parameter that could influence the electrical output. From all works, the main summaries are obtained as follows:



(a) Contact Mode



(b) Compress Mode

Figure 4.16: Power density of the multi-layer TEG device in this experiment

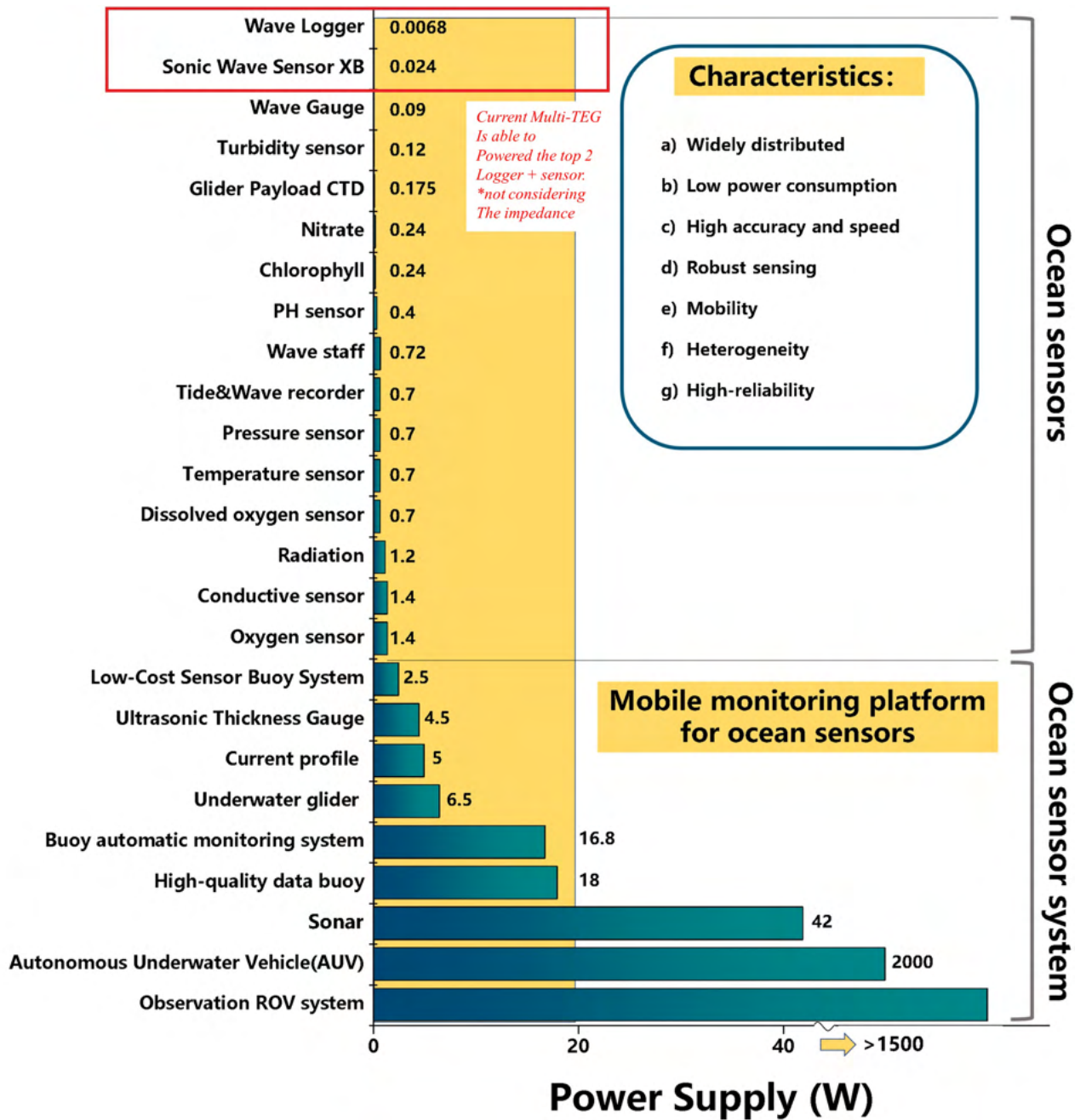


Figure 4.17: State-of-art ocean sensors and ocean sensors system that could be powered with the Multi-layer TEG [Zhao et al., 2021]

- We improved the TEG electrical energy in linear terms using a multi-layered structure. The multi-layered TEG generated output voltage four times higher than that using a single-layered TEG. Therefore, creating a more efficient energy harvester that incorporates the mechanism of a comparatively small device, such as the multi-layered TEG, is possible.
- The separation velocity, which is correlated with the settings of both the vibration frequency and amplitude has a direct correlation and positive relationship to multi-TEG output. This means that the higher the separation velocity, the higher the electrical output of the multi-layer TEG that could be generated.
- The separation distance, which is changed by the combination of both higher vibration amplitude and higher/smaller initial distance does not increase the electrical output. This means that the separation distance has a minor influence on the output value. The value of initial distance that can help multi-TEG generate the most electrical output depends on the vibration frequency. Therefore, the initial distance is not the main parameter that directly influences the multi-TEG electrical output, and careful configuration needs to be made for setting up the initial distance.
- The basic characteristics of the multi-TEG's working mechanism under the contact and compression modes were also clarified. Both contact mode and compress modes can generate a high electrical output. This is interesting since most results usually tend to generate better results when the compression is higher. Therefore, more stress load to the multi-layer TEG is not always equal to higher electrical output.
- Our investigation showed that the compression force plays a minimal role in increasing the electrical output voltage. Our experiments confirmed this, where a slight force could still produce a large output. In fact, the acceleration amplitude had a more significant influence on the electrical output of the multi-layer TEG ($r^2= 0.81$) compared with the compression force ($r^2= 0.48$). As such, the acceleration amplitude is one of the key parameters for achieving a multi-layer TEG's high electrical performance.

Future studies could design and develop a more advanced multi-layered TEG model, with

more TEG layers stacked within a model. Vertical or horizontal vibration experiments should then be conducted to verify the model's output characteristics. In addition to multi-layered TEG, a new model that uses the contact-separation mode more efficiently (e.g., the rolling freestanding triboelectric layer mode or the lateral sliding mode) could be developed to use in natural external vibration force conditions (e.g., wind power energy or ocean energy).

Bibliography

- [Du et al., 2014] Du, W., Han, X., Lin, L., Chen, M., Li, X., Pan, C., and Wang, Z. L. (2014). A three dimensional multi-layered sliding triboelectric nanogenerator. *Advanced Energy Materials*, 4(11):1–6.
- [KIMACHI and MORITA, 2017] KIMACHI, R. and MORITA, T. (2017). Development of folding method for three dimensionally foldable cylindrical structure with base. *Mechanical Engineering Journal*, 4(6):17–277.
- [Lin et al., 2015] Lin, Z.-H., Cheng, G., Li, X., Yang, P.-K., Wen, X., and Lin Wang, Z. (2015). A multi-layered interdigitative-electrodes-based triboelectric nanogenerator for harvesting hydropower. *Nano Energy*, 15:256–265.
- [Mao et al., 2017] Mao, Y., Zhang, N., Tang, Y., Wang, M., Chao, M., and Liang, E. (2017). A paper triboelectric nanogenerator for self-powered electronic systems. *Nanoscale*, 9(38):14499–14505.
- [Schenk and Guest, 2016] Schenk, M. and Guest, S. D. (2016). Origami folding: A structural engineering approach. *Origami 5: Fifth International Meeting of Origami Science, Mathematics, and Education*, pages 291–303.
- [Shao et al., 2017] Shao, J. J., Tang, W., Jiang, T., Chen, X. Y., Xu, L., Chen, B. D., Zhou, T., Deng, C. R., and Wang, Z. L. (2017). A multi-dielectric-layered triboelectric nanogenerator as energized by corona discharge. *Nanoscale*, 9(27):9668–9675.

- [Tao et al., 2020] Tao, K., Yi, H., Yang, Y., Chang, H., Wu, J., Tang, L., Yang, Z., Wang, N., Hu, L., Fu, Y., Miao, J., and Yuan, W. (2020). Origami-inspired electret-based triboelectric generator for biomechanical and ocean wave energy harvesting. *Nano Energy*, 67(October 2019):104197.
- [Wang et al., 2020] Wang, P., Zhang, S., Zhang, L., Wang, L., Xue, H., and Wang, Z. L. (2020). Non-contact and liquid–liquid interfacing triboelectric nanogenerator for self-powered water/liquid level sensing. *Nano Energy*, 72(March).
- [Xie et al., 2014] Xie, Y., Wang, S., Niu, S., Lin, L., Jing, Q., Su, Y., Wu, Z., and Wang, Z. L. (2014). Multi-layered disk triboelectric nanogenerator for harvesting hydropower. *Nano Energy*, 6:129–136.
- [Zhao et al., 2021] Zhao, T., Xu, M., Xiao, X., Ma, Y., Li, Z., and Wang, Z. L. (2021). Recent progress in blue energy harvesting for powering distributed sensors in ocean. *Nano Energy*, page 106199.

Chapter 5

TEG-PEG hybrid device

5.1 Background

After considering the TEG electrical output alongside its several parameters, model, etc., this section elucidates TEG compatibility when combined with another generator. The main purpose of this study is to examine the output voltage of piezoelectric generator (PEG) and TEG when both are used simultaneously. Additionally, the relationship of several parameters will be re-examined, and both PEG and TEG mutual compatibilities / complementary will also be investigated. The choosing of a multi-layered TEG and PEG as a basic model design used in this study is to focus on the characteristics of the key parameters that are being clarified during the experiments.

The PEG's working mechanism is based on the piezoelectric effect where the stress is applied to the PEG, the elastic strain generating an electrical charge. This electrical charge can occur due to the external force that makes the elastic body strain transmitted to piezoelectric material inside it. Due to this transmission, the piezoelectric polarization occurs, and an electrical charge can be generated.

Our previous works of the PEG, proposed by Mutsuda et al. [[Mutsuda et al., 2013](#), [Mutsuda et al., 2012](#)], were made based on the polyvinylidene fluoride (PVDF) and the silicone material (Si) layers

and was highly flexible. This device's flexibility makes the device experience geometric nonlinearity and exhibit high levels of material nonlinearity as well. Based on the fundamental results found in the study, a new type of PEG named a painted flexible piezoelectric device (FPED) was created. Since the FPED is very easy to apply, it can be used on various types (e.g., compressed type, roll-type, and panel type) to illustrate its versatility in practical applications [Mutsuda et al., 2015]. One of the common uses that are predicted to be quite effective is attaching the FPED to a fish aggregating device (FAD) as an ocean energy harvester. The FPED on a FAD was observed to determine the durability of the FPED large bending state caused by the ocean waves and currents [Mutsuda et al., 2017b]. In addition, various key parameters for designing the FPED and optimizing them in terms of its initial tension, support system, aspect ratio, and the bluff body for usage in natural environments based on the flow-induced vibration were investigated and clarified [Mutsuda et al., 2015, Mutsuda et al., 2014, Tanaka et al., 2016, Mutsuda et al., 2017a]. Based on the previous investigation under various wave conditions, we elucidated the relationship between the thickness of the piezo-material, the FPED pattern (unimorph and bimorph), and the painted FPED's output voltage [Mutsuda et al., 2019]. Elsewhere, R. Patel et al proposed a theoretical model for predicting FPEDs behaviors and validated it through extensive experimental testing [Patel et al., 2016]. Here, the theoretical model focuses on its dynamical behaviors, including the material nonlinearity, self-weight, and pre-stress of the FPED device. The optimum type of piezoelectric device for ocean energy harvesters was heavily considered for further investigation in this section based on the results of our previous research. Therefore, the flexible piezoelectric device type is chosen as the base of our PEG in this study.

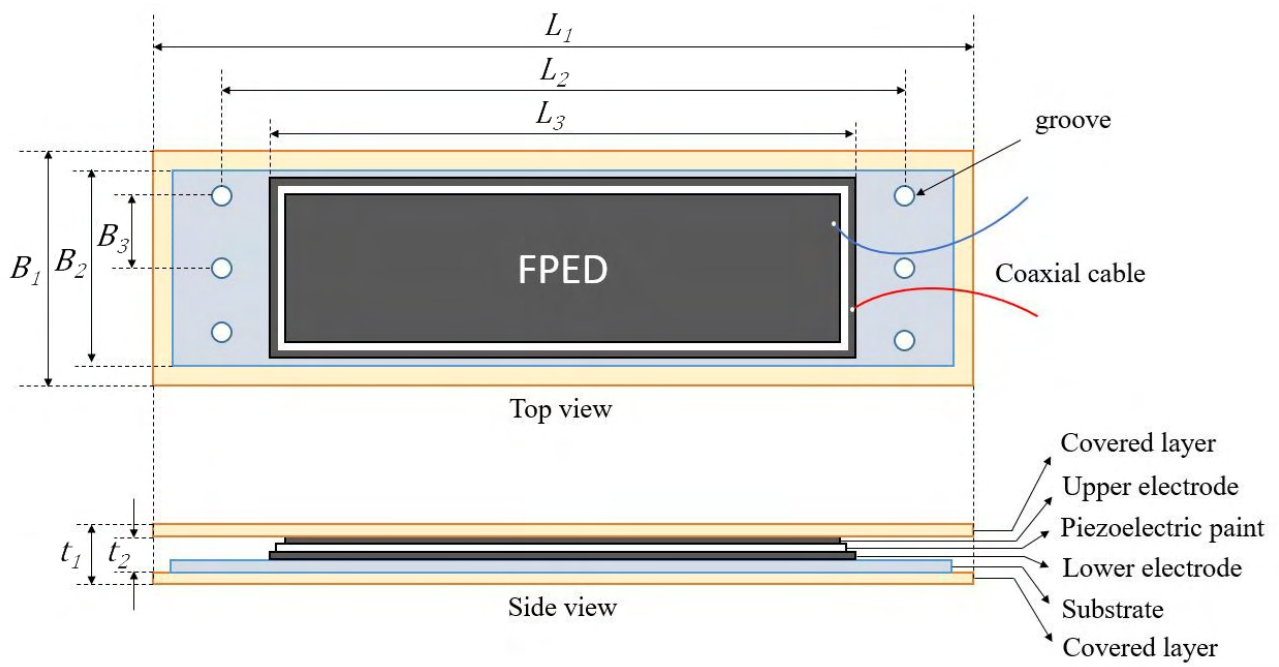
The following subsection will elucidate the overview and fabrication of the TEG-PEG device and the concept of the TEG-PEG device as the ocean energy harvesters.

5.2 Device Overview + Fabrication of TEG-PEG

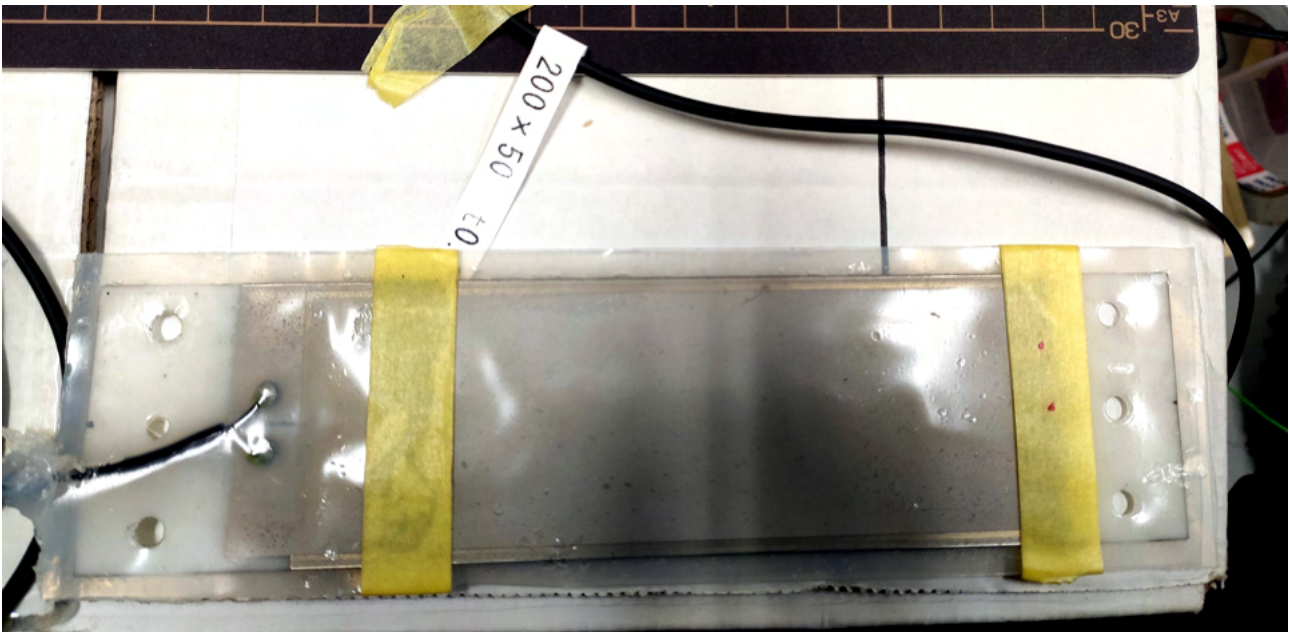
First of all, to produce the TEG-PEG device, an individual of PEG needs to be made. This type of PEG made and used in this study is known as the panel type. The panel type could produce the electrical energy by utilizing the bending motion due to the external vibration. The PEG was also optimized in this study based on several key parameters, including the thickness of the polyvinylidene fluoride (PVDF) layer as the piezoelectric material, PEG base substrate material, and also PEG aspect ratio. The schematics and prototype of the PEG used in this study can be seen in Fig.5.1.

The proportion of the PVDF layer was outlined by length (L_3) x width (B_2). The material was designed to be polarized on the upper and lower surfaces. Then, the electrodes were placed on the upper of the PVDF (positive electrons on top) and the bottom of the piezoelectric paint (positive electrons on bottom). The sizes of the electrodes were characterized by length (L_2) x width (B_2). At the same time, a substrate was also added to the bottom of the lower electrode. In order to limit the PEG movement in the vibration test, circle grooves with a width distance (B_3) were also created. Since the strain rate of the PEG could significantly affect the power generation performance, it is crucial to consider the PEG device's structural base. Therefore, an elastic silicone (as a covered layer) with a size of length (L_1) x width (B_1) was incorporated to protect and to provide a PEG structural base. The distance of the substrate to the upper electrode (t_2) and thickness of the PEG device (t_1) was also determined. The actual size used in this study is shown in the Table 5.1. Finally, to measure the PEG electrical voltage fluctuation during the vibration tests, coaxial cables were wired and installed on both the upper and lower electrodes. The cables are then connected to the A/D converter and the computer for processing the data.

After the PEG device was finished, the device was then combined with the multi-layered TEG (see chapter 4) into a TEG-PEG energy harvester device. The bonding of both devices can be seen in Fig.5.2a, while the isometric, side, and prototype view of the devices are shown in Fig.5.2b. The main purpose of combining the two devices is to take advantage of the TEG-PEG device's synergy and check their complementary role for harvesting energy.



(a) Laminated structure of the PEG device

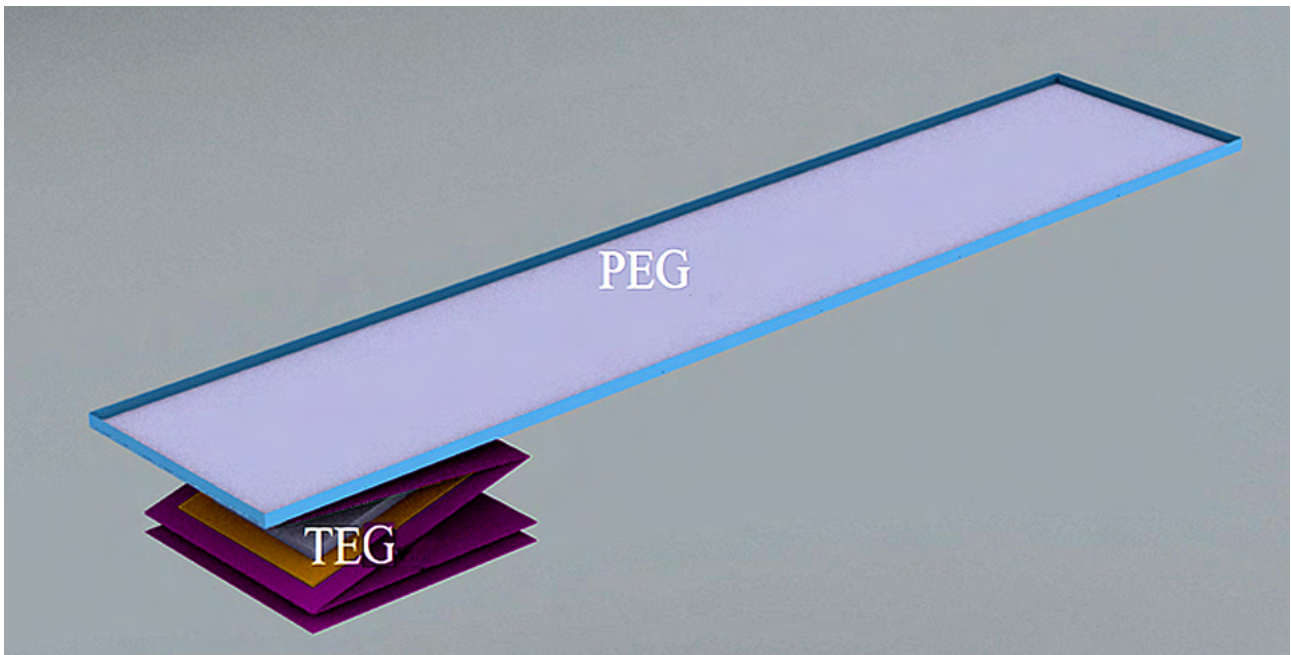


(b) Prototype

Figure 5.1: PEG device

Table 5.1: PEG Dimensions

| Name | L_1 [mm] | L_2 [mm] | L_3 [mm] | B_1 [mm] | B_2 [mm] | B_3 [mm] | AR | t_1 [mm] | t_2 [μ m] |
|------|------------|------------|------------|------------|------------|------------|------|------------|------------------|
| PEG | 200 | 180 | 150 | 60 | 50 | 30 | 1: 3 | - | 8 |



(a) Bonding of the TEG-PEG device

Isometric View



Prototype



Side View



(b) Isometric, Side and Prototype view of the TEG-PEG device

Figure 5.2: TEG-PEG device

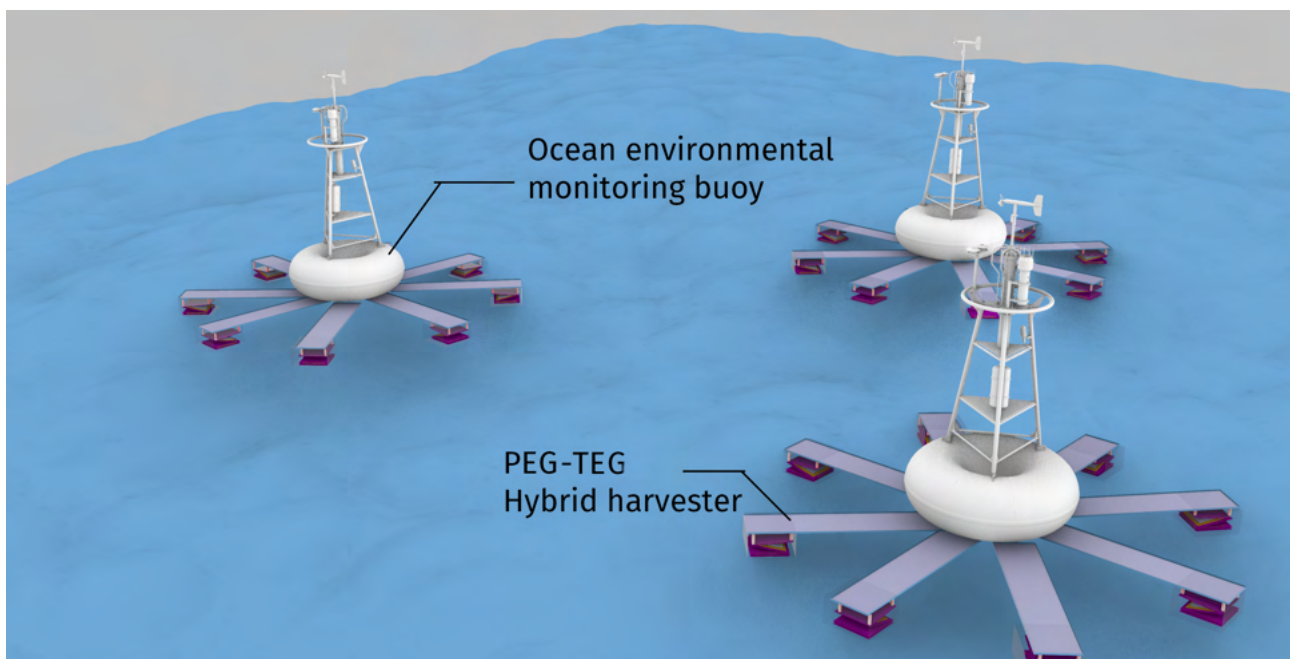


Figure 5.3: Concept of the TEG-PEG device as ocean energy harvester network

One of the applications for the TEG-PEG device is applying the energy harvesters to the ocean objects, such as environment-monitoring buoys. Since the TEG-PEG device is used as the energy harvester, the environment-monitoring buoys could act as a self-powered device to monitor the ocean environment. Fig.5.3 illustrates the concept behind the proposed idea of this TEG-PEG hybrid harvester device in the ocean space (connected to the buoys) as a network device. The multi-layer TEG is located on the ocean's surface, with a box acting as a floater. Due to the ocean wave and current motions, the box is experiencing the six degrees of freedom motion. The heaving and pitching per the ocean frequency and amplitude could mainly be converted into external vibrations to make the TEG contact and separate to generate an electrical output. A PEG is added and locked both to TEG and the ocean environment-monitoring buoys on the top of the TEG box. The upper surface of PEG is attached to the bottom of the weather buoy and the electrical cable to give the buoy electrical energy. Because of this setup, whenever TEG reaches maximum caused by the wave motion, the PEG will deform, bend, and create an electrical polarization to generate electricity. Since the harvesters are attached in a buoy and each buoy could be combined and connected through the network, the total energy that could be harvested is also potentially huge. All this could be achieved with a relatively low cost in production value, easy to make and install.

However, it needs to be noted that in a real ocean field, ocean waves have both regular and irregular periods, different wave heights, and low frequency (which lead to long periods) compared with our experimental conditions in this dissertation study with high frequency. The example of this difference (also called the frequency gap) can be seen from the data of Indonesia's regional map of annual and seasonal wave properties in Fig.5.4 [Kench and Mann, 2017]. The top figure of the Fig.5.4 is the Mean significant wave height, the middle is the significant wave period, and the bottom is the wave energy flux from Indonesia's ocean. We can see from the middle figures that the average period range: is 6 – 14, or even higher on the open ocean below (Indian ocean) which means the average frequency range: is 0.07 - 0.17 Hz. The frequency range that we did in the experiments is on a range of 5 – 30 Hz. The reason for choosing such a high frequency in this experiment is because, in this study, we want to make clear the effect/influence of the separation velocity, which in turn is influenced by the high-frequency movements. Once the

parameter is clear, the additional part could be added to the ocean harvester as future work to exchange the vibration frequency and amplitude, based on the theory of mechanism.

For this reason and to keep the device as efficient as possible, an additional part that converts the low frequency-high force from the ocean wave can be used and installed in the harvesters to convert it to high frequency-smaller amplitude for the generators in the future. As a preliminary suggestion, a mechanism that uses the gear (Fig. 5.5), flywheel (Fig. 5.5c), spring (Fig. 5.6), elastic plate, and spring-bearing-mass (Fig. 5.6d) assisted structure has been proposed as a potential tool for exchanging the vibration frequency and amplitude of the ocean to the TEG-PEG hybrid harvester requirement. However, as an alternative, we choose to use and combined with another harvester (i.e., the flexible PEG) to see whether this additional harvester can also improve the output voltage as well or not. This comparison will be explained in the later part of this chapter.

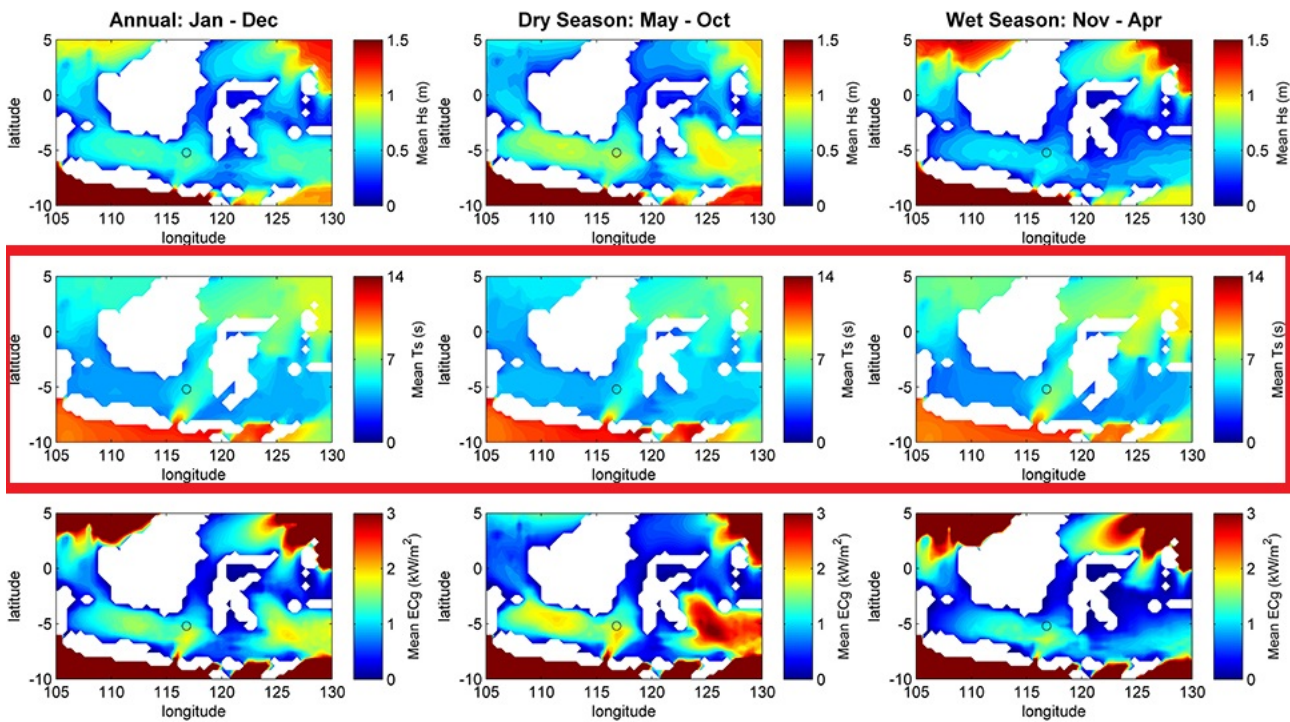
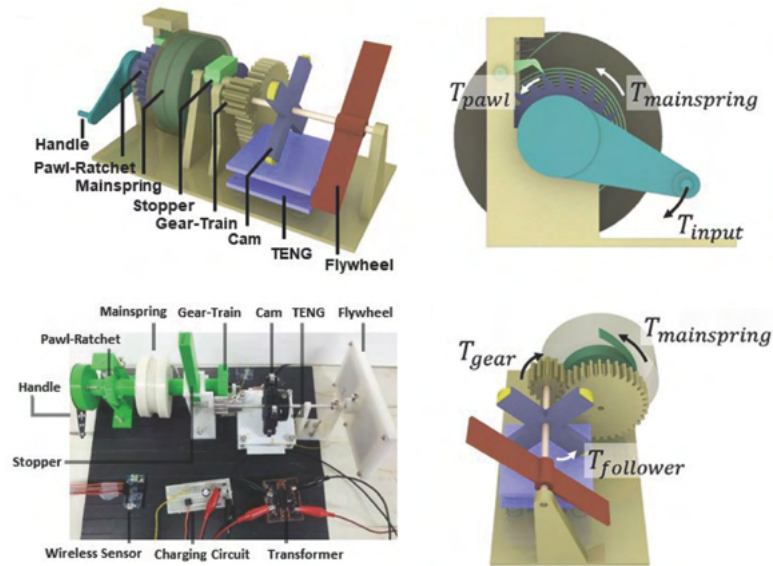
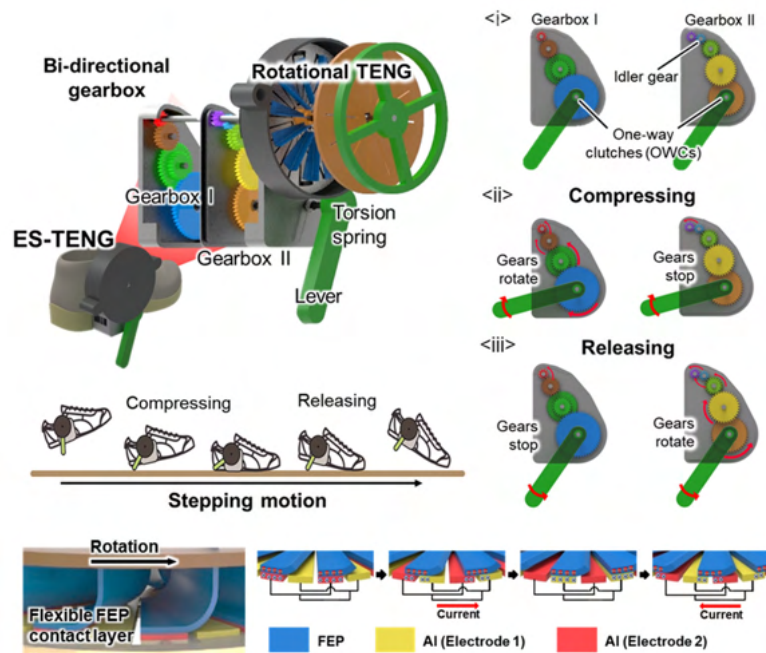


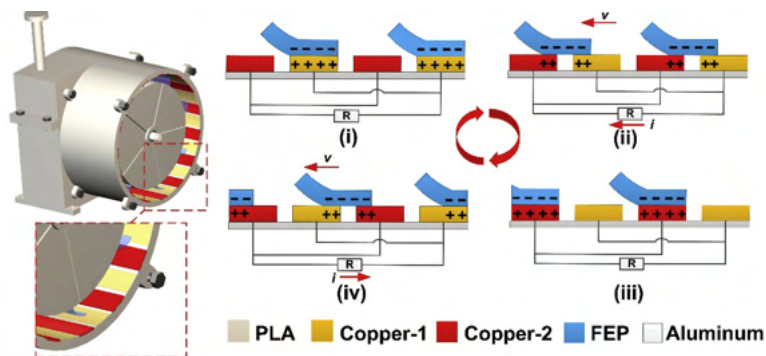
Figure 5.4: Indonesia's regional map of annual and seasonal wave properties. Middle figures is showing the mean period in Indonesia's ocean [Kench and Mann, 2017]



(a) Mechanical Frequency Regulator TENG using gear [Liang et al., 2020]

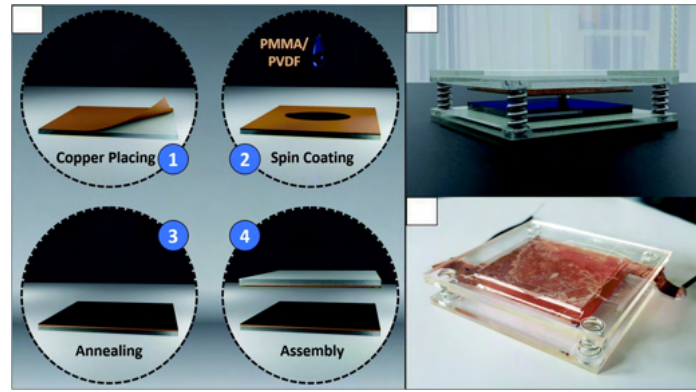


(b) Exo-shoe TENG with bi-directional gearbox [Yun et al., 2021]

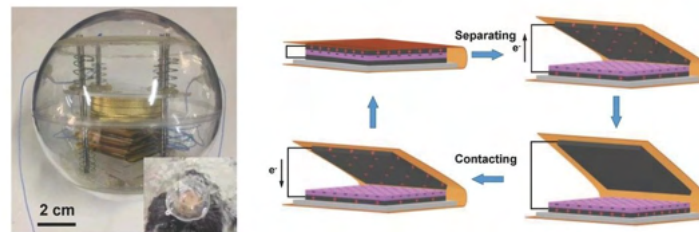
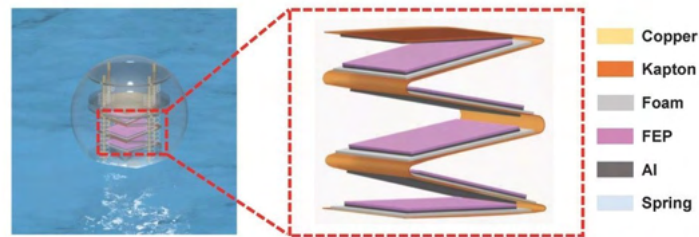


(c) Integrated flywheel and spiral spring TENG [Yang et al., 2019]

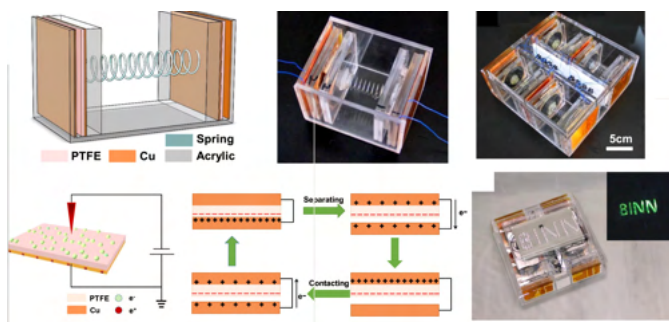
Figure 5.5: Applications of the additional part for improving TEG output - Gear and flywheel.



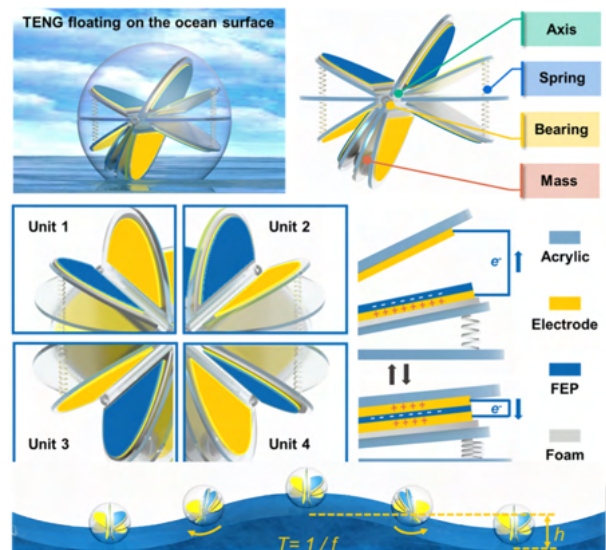
(a) Spring assisted TEG [Varghese and Chandran, 2021]



(b) Spring-Assisted Multilayered Structure TEG [Xiao et al., 2018]



(c) Horizontal spring assisted TEG [Jiang et al., 2017]



(d) spring-bearing-mass assisted TEG [Liang et al., 2021]

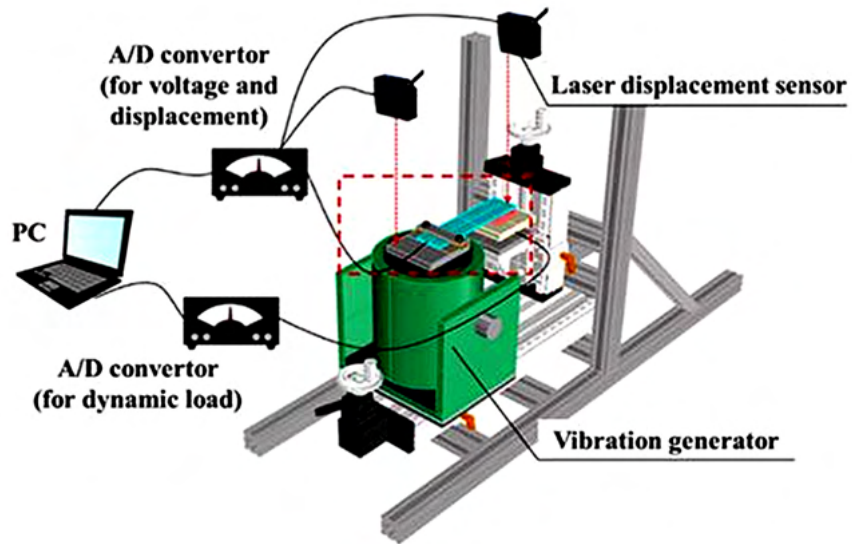
Figure 5.6: Applications of the additional part for improving TEG output - Spring

5.2.1 Device Overview of TEG-PEG case 1 and case 2

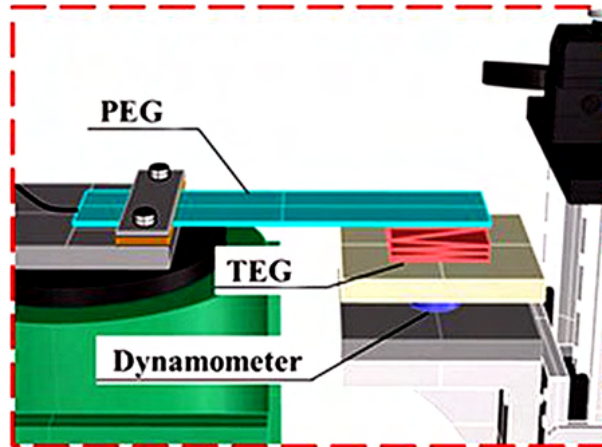
Based on the previous study of energy harvesters, the generators' vibration frequency, amplitude, and initial distance from the external vibration motions are some of the main parameters influencing the electrical output. We conducted the vertical vibration test with the external motions from the axial direction to examine the TEG-PEG characteristics. In these experiments, the PEG and TEG need to be appropriately adjusted to ensure that the generators that received direct mechanical pressure are not hindering other device movements, limiting the generation of its output voltage. Due to this reason, two cases were implemented in the preliminary experiment and observed which ones generate the best electrical output.

TEG-PEG case 1 (only used in the preliminary experiment)

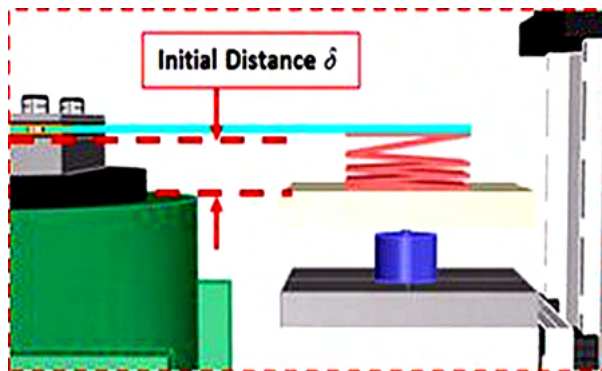
In TEG-PEG case 1, as shown in Fig.5.7a, the PEG is the device that directly receives the external vibration from the vibration machine. The PEG was locked on top of a vibration generator plate while the PEG right end side was in a free state condition. Also, on the right side of the PEG, the TEG's top part is attached below the PEG, while TEG's bottom part is attached on top of a dynamometer used to measure the compression force. This configuration's schematics can be seen in Fig.5.7b. There are three variables tested in this preliminary experiment. Firstly, the initial distance (δ) of TEG-PEG, as shown in Fig.5.7c, was set in the range from 2 to 8 mm with a 1 mm increment. Secondly, the vibration frequency was set at 4.0, 6.0, 8.3, 10.0, 12.0 Hz. Lastly, the vibration amplitudes (A_v) ranged from 2.0, 4.0, and 6.0 mm, while the vibrated amplitude at the free side of PEG (a^0) will move accordingly. The illustration of both A_v and a^0 can be seen in Fig.5.7d; both parameters will be observed and measured via the laser displacement sensors. The vibration tests results were obtained and observed in a 30 second period of time histories for every test.



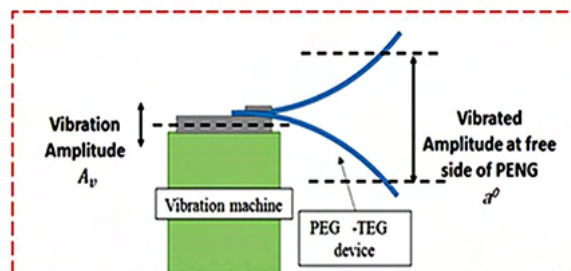
(a) Experimental setup of TEG-PEG vibration test case 1



(b) dynamometer



(c) initial distance measurement



(d) vibration amplitude

Figure 5.7: Vibration experiment setup case 1

TEG-PEG case 2

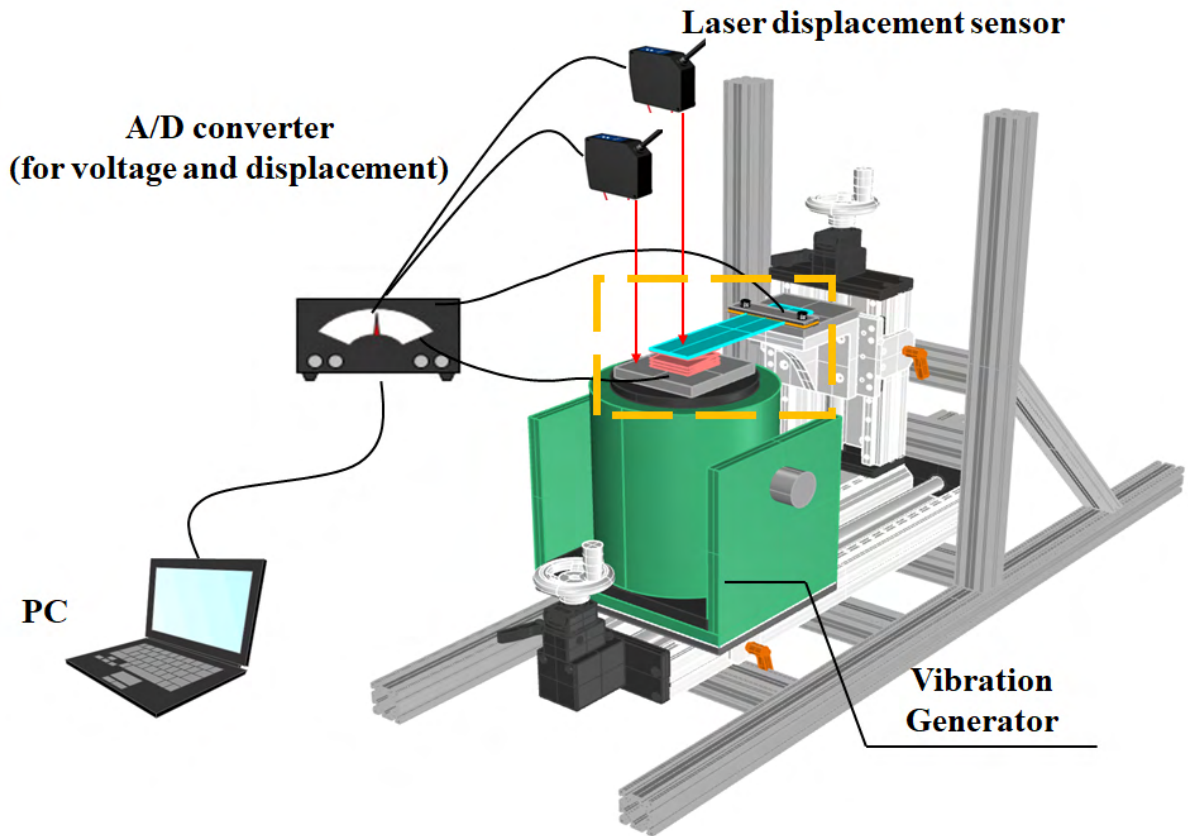
In the TEG-PEG case 2, as shown in Fig.5.8, the position of the PEG and TEG is switched. TEG is now the device that directly receives the external mechanical force from the vibration machine. The outside polyester films from the bottom part of the multi-layered TEG were locked on top of a vibration generator plate, while the PEG left end side is now a free state condition that moved alongside TEG contact-separation mode. On the right side of the PEG, a rubber sponge and small aluminum frame are placed to make the PEG fixed. Due to this fixedness, the PEG right side has a movement limitation that could cause PEG's deformation rate to be increased. In addition, a shear strain also emerged on the surface of the PVDF film in the PEG. The external force will cause the multi-layer TEG contact-separate and the PEG bending to generate an electrical voltage potential across both TEG and piezoelectric layers.

Similar to the TEG-PEG case 1, the vibration generator performed the vertical motions for the TEG-PEG hybrid harvester in these experiments. To observe the data, the output voltage from both PEG and TEG were individually measured with an A /D converter for voltage and displacement (KEYENCE, Multi-input data logger, NR-500 Series). The data were captured at every millisecond for a whole five seconds, resulting in 5,001 data. The A/D converter's internal resistance in an open circuit was set at $1M\Omega$. The electrical power calculation could be conducted using Ohm's law based on this resistance value. Two laser displacement sensors, the first of which (KEYENCE, CMOS Multi-Function Analog Laser Sensor, IL 300) was used to measure the TEG plate displacement. At the same time, the other laser sensor was used to measure the PEG displacement on its free-end side. These detailed schematics can be seen in Fig.5.8a for the experimental setup, while the more detailed setup for PEG-TEN on top of the vibration generator can be seen in Fig.5.8b.

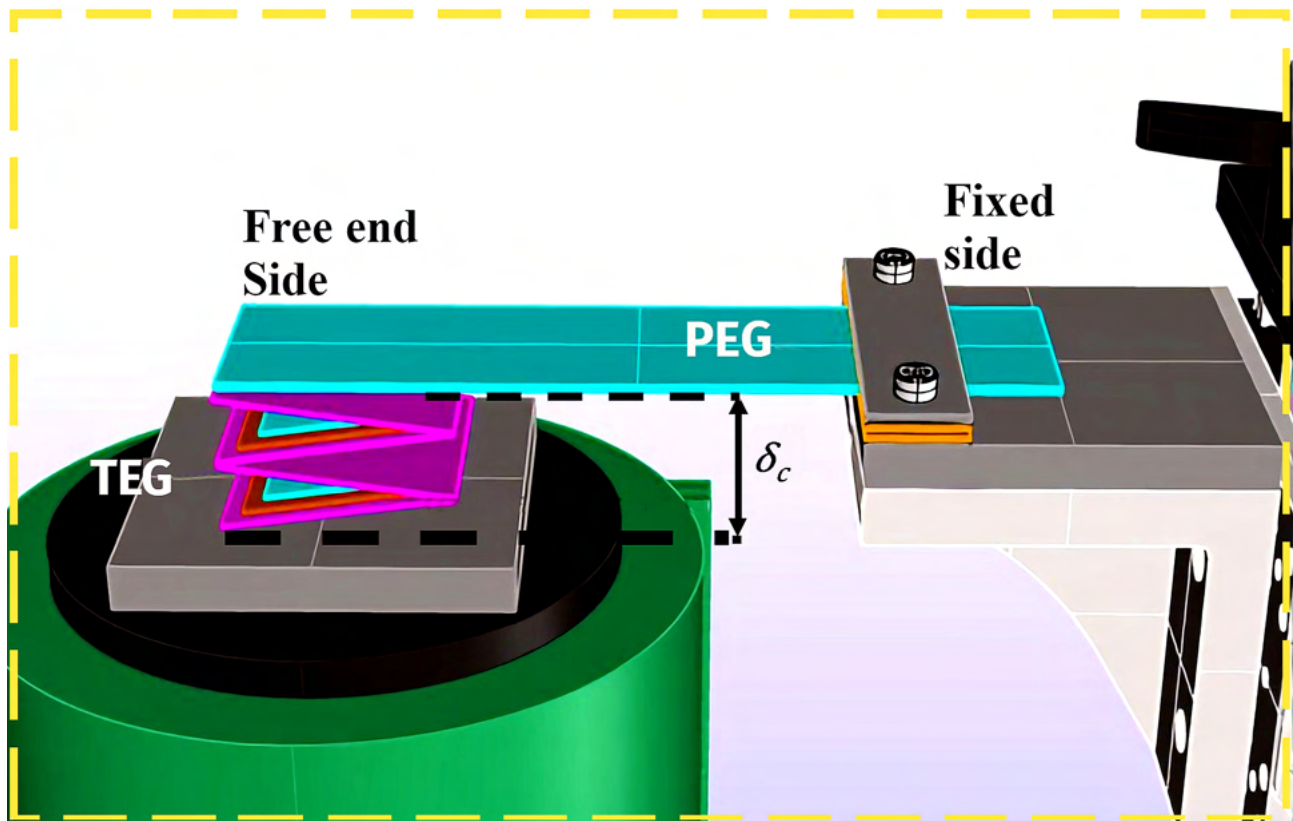
The TEG-PEG in case 2 has two different conditions for the experimental conditions. The first conditions are the preliminary vibration tests. This test has a similar condition with the TEG-PEG case 1. The initial distance was set on in the range from 2 to 8 mm with 1 mm increment; the vibration frequency was set on 4.0, 6.0, 8.3, 10.0, 12.0 Hz., and the vibration amplitudes (A_v) were ranged from 2.0, 4.0, and 6.0 mm.

But, after it was found that TEG-PEG case 2 is better in terms of the electrical output, further tests were conducted again to examine the relationship of the key parameters. In this 2nd vibration test, there are also three varying parameters. First, the initial separation distance (δ_c) ranged from 0 to 30 mm with 2 mm increments were set. Next, the vibration frequency was set at 5, 10, 20, and 30 Hz to clarify the effect of the frequency towards both TEG-PEG output voltage. Lastly, the vibration amplitude (A_v) was also ranged from 2.0, 4.0, and 6.0 mm as TEG-PEG case 1.

The design/model of the TEG-PEG configuration both on case 1 and case 2 could be considered a simple TEG-PEG model. This is intentional since by creating a simple and basic model and then testing it in the vibration test, the maximum electrical output could be obtained, and the key parameters could be clarified. Afterward, the result of this clarification will then be used as a base to design and create a more innovative design and mechanism for further application of the TEG-PEG device in the near future.



(a) Experimental setup of TEG-PEG vibration test case 2



(b) Setup of the TEG-PEG device in the yellow dashed line area of Fig. 5.8a

Figure 5.8: Vibration experiment setup case 2

5.3 TEG-PEG hybrid device experimental results

5.3.1 Characteristics of output voltage generated from TEG-PEG in the preliminary vibration test

In this section, the output voltage from both PEG and TEG in the preliminary vibration test is observed and analyzed. The main purpose of the preliminary tests is to observe the result of the electrical voltage on TEG-PEG and select which case (case 1 or case 2) produces the most efficient result to be observed on the further vibration tests. Unless specified, the output voltage that is shown is based on the maximum absolute value of the output voltage. Maximum absolute value is obtained based on 10 peak data points and 10 trough data points of the output voltage on each case. Then both peak and trough data points are turned into the absolute value (the magnitude of a real number without regard to its sign). Afterward, the average of all 20 absolute values is calculated, and the result is called the maximum absolute value of the output voltage.

Even though Both PEG and TEG are combined, both harvesters are measured individually for their respective output voltage. The reason for this is to be observed how the electrical output is generated on each device. By understanding the electrical generation on each PEG and TEG, a modification could be used in a future study to improve their harvesting capabilities. The results of study case 1 are explained in subsection 5.3.1 while study case 2 is shown on the subsection of 5.3.1

Study case 1

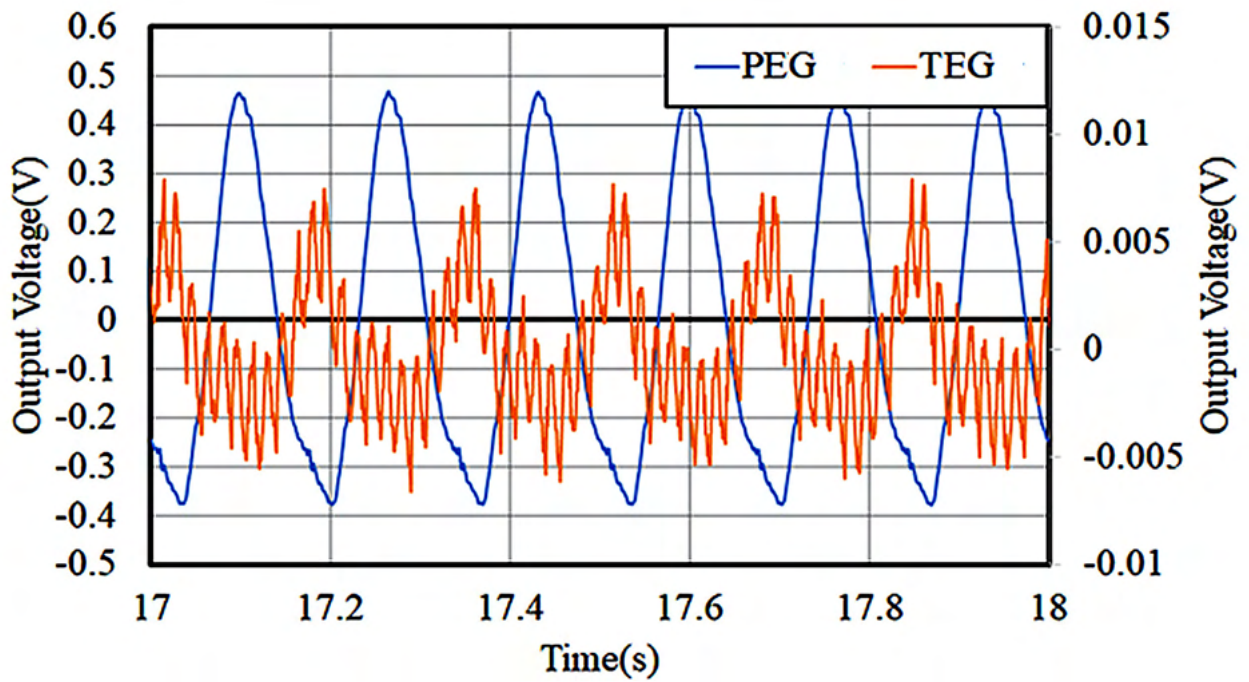
The TEG-PEG output voltage time history can be seen in Fig.5.9. Two examples were given to illustrate, the output voltage time histories for both PEG and TEG on the vibration frequency = 6.0 Hz and initial distance $\delta = 2.0$ cm (Fig.5.9a), and on the vibration frequency = 6.0 Hz and initial distance $\delta = 5.0$ cm (Fig.5.9b). The left y-axis shows the output voltage for PEG, while the right y-axis shows the output voltage for TEG. Additionally, since the PEG has a

free end side, the role of the bending motion of PEG and compression force on TEG-PEG caused by vibration could be observed to confirm its significance for the harvester's output. Fig.5.10 and Fig.5.11 displayed the relationship between compression force and the PEG free end amplitude to PEG output voltage. Fig.5.12 shows the compression force to TEG output voltage, and Fig.5.13 shows the PEG free end amplitude to TEG output voltage. It can be seen on all four figures that the compression force received by the harvesters is minimal. However, a good output voltage could still be generated by both PEG and TEG. Moreover, the graph also showed that a larger force does not equal higher output. Additionally, for PEG, the effect of the PEG free end amplitude under a larger initial distance seems to generate a much higher output. This higher output could occur due to the bending motion of the PEG being higher under a larger initial distance, and higher electrical can be achieved as well.

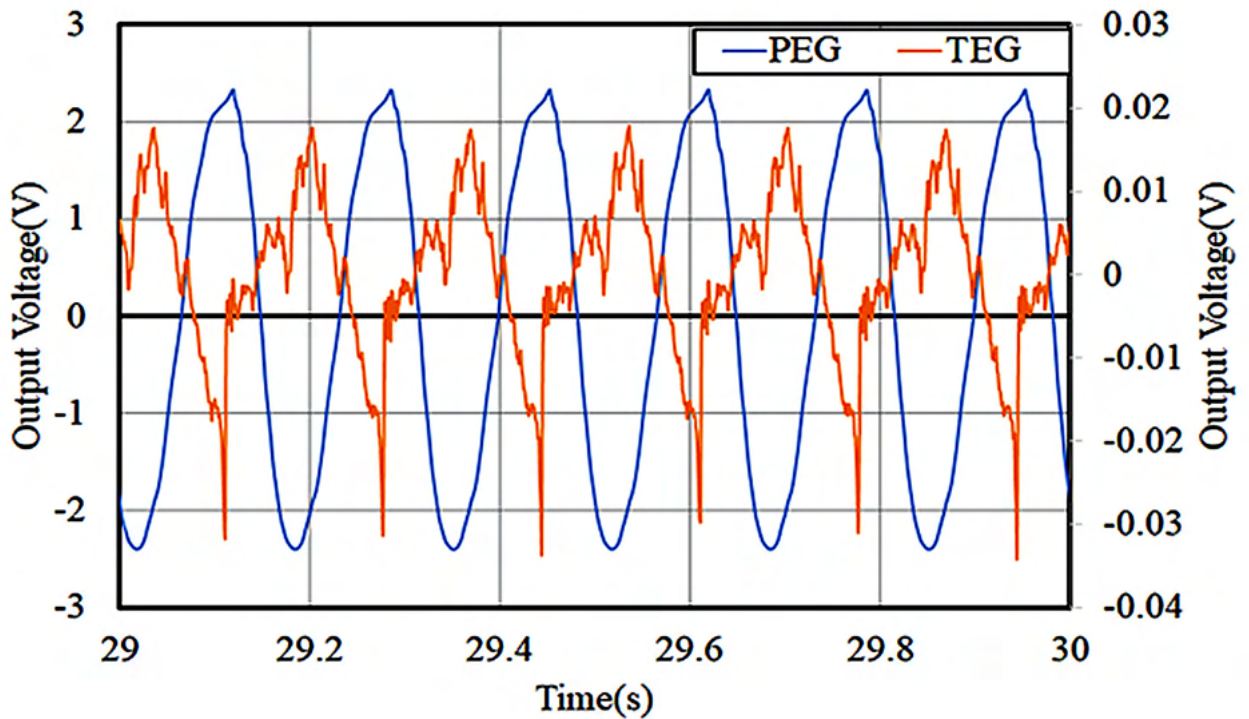
Study case 2

The example of both TEG-PEG output voltage time history can be seen in Fig.5.14, with (Fig.5.14a) is for the vibration frequency = 10.0 Hz and initial distance $\delta = 1.0$ cm, and (Fig.5.14b) is for the vibration frequency = 10.0 Hz and initial distance $\delta = 5.0$ cm. From these two examples, the TEG-PEG in study case 2 tends to reach a higher output voltage than the study case 1. All results from the preliminary experiments were then collected and shown in Fig.5.15 and Fig.5.16.

Based on Fig.5.15 and Fig.5.16, the TEG-PEG output voltage in study case 2 is able to reach the highest output voltage for both PEG and TEG. Due to this reason, study case, 2 is chosen as the default setup for the TEG-PEG vibration test. Further vibration tests were conducted, and the results are explained in the next sections.



(a) Time histories of output voltage generated by **TEG-PEG** on study case 1, the vibration frequency = 6.0 Hz and initial distance $\delta = 2.0$ cm



(b) Time histories of output voltage generated by **TEG-PEG** on study case 1, the vibration frequency = 6.0 Hz and initial distance $\delta = 5.0$ cm

Figure 5.9: Example of the TEG-PEG output voltage on study case 1

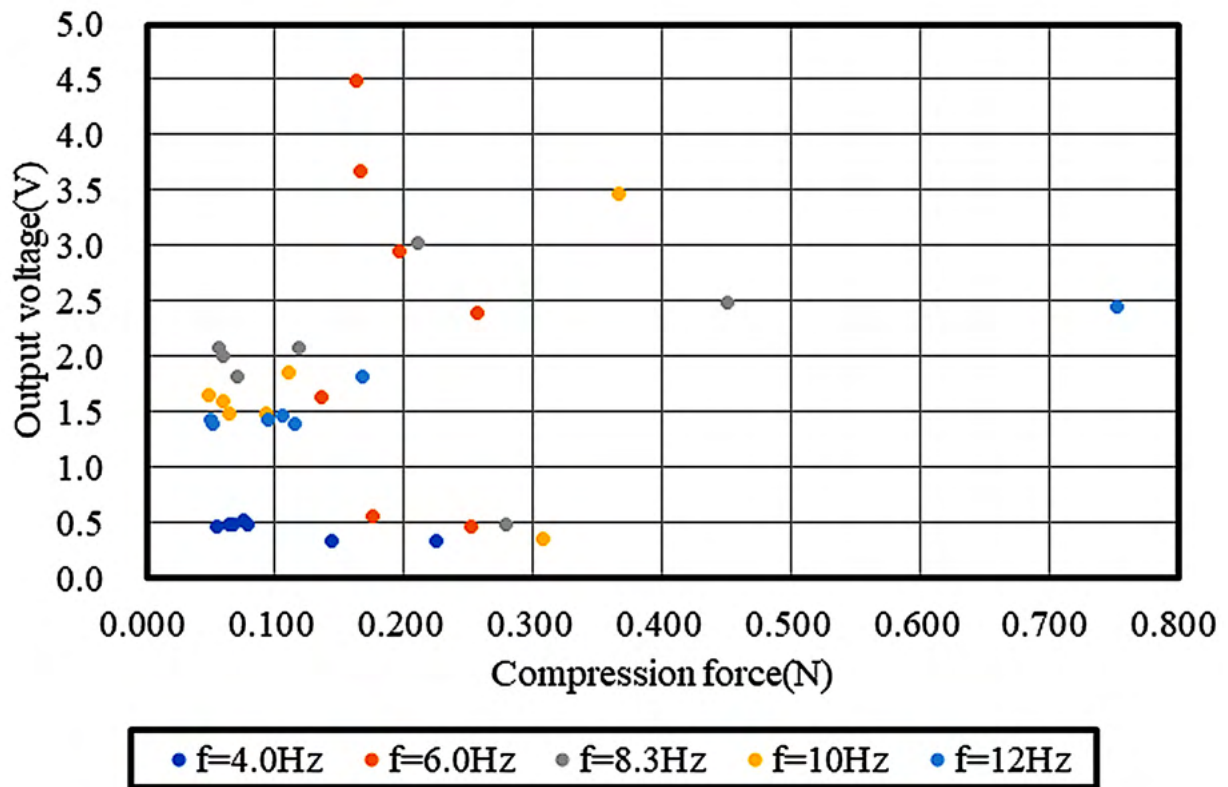
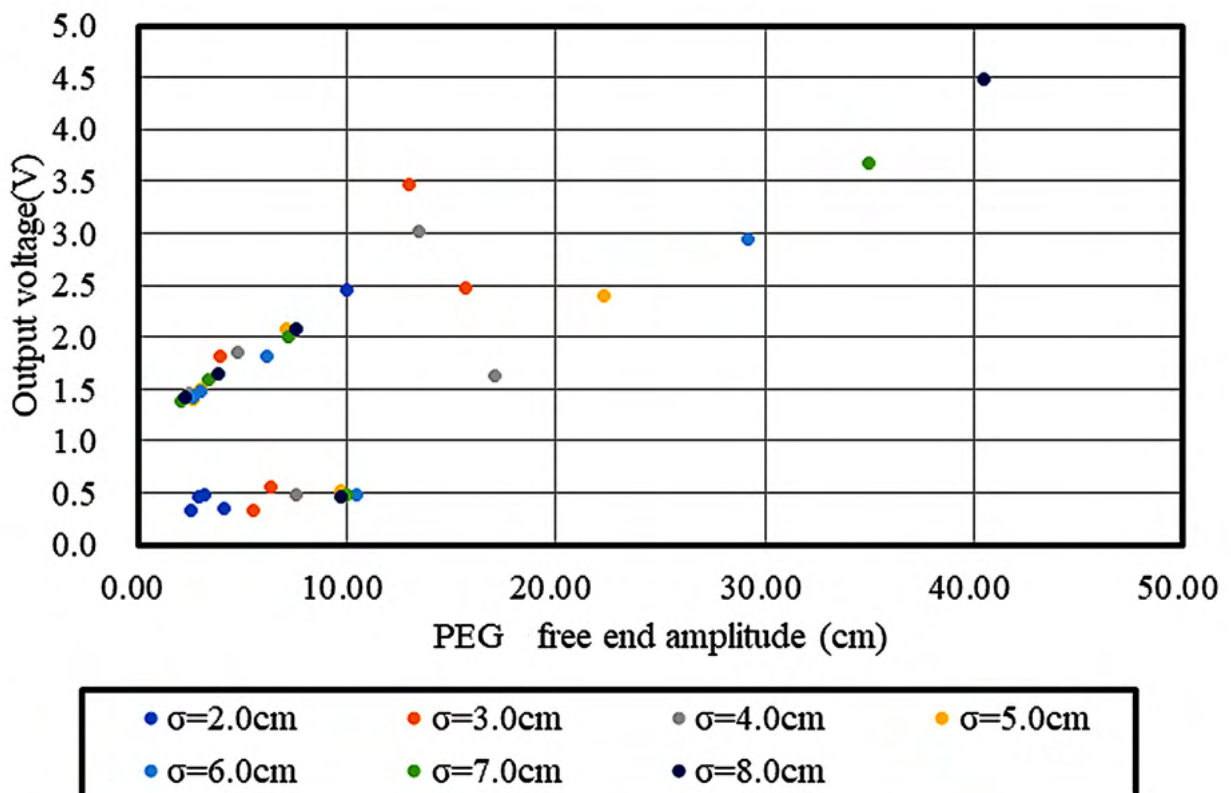


Figure 5.10: Relationship of compression force with PEG max voltage



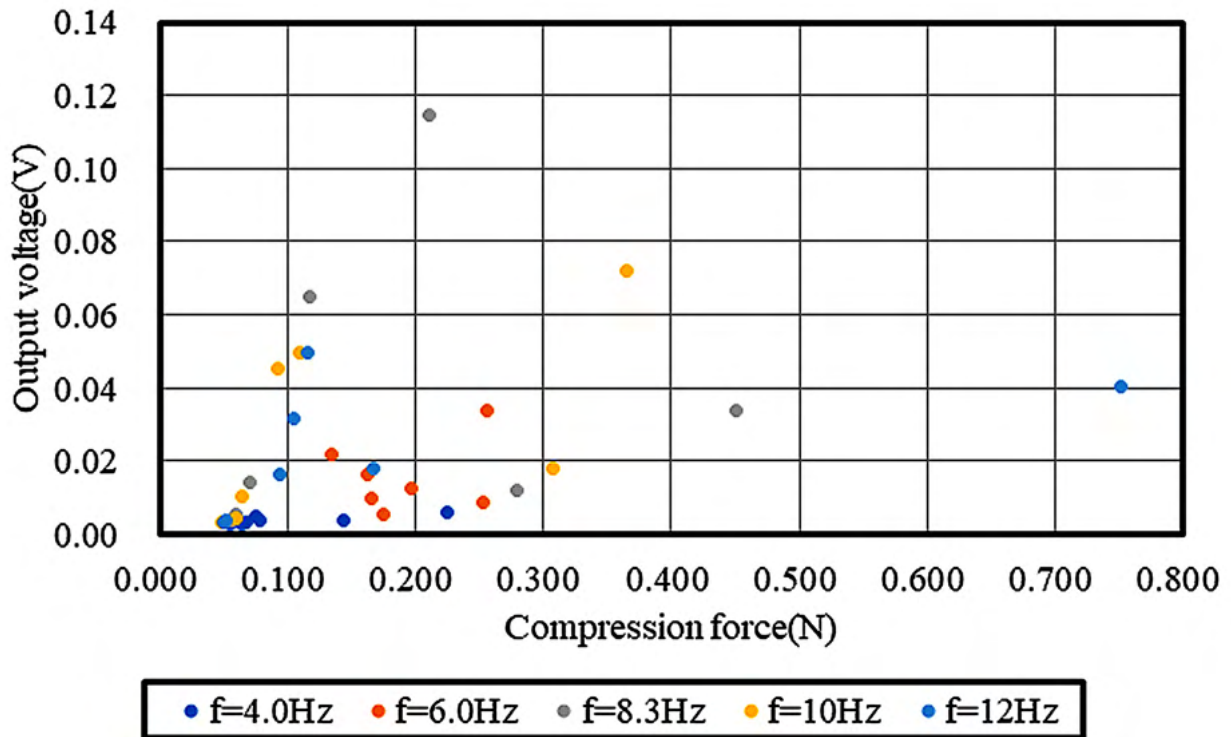


Figure 5.12: Relationship of compression force with TEG max voltage

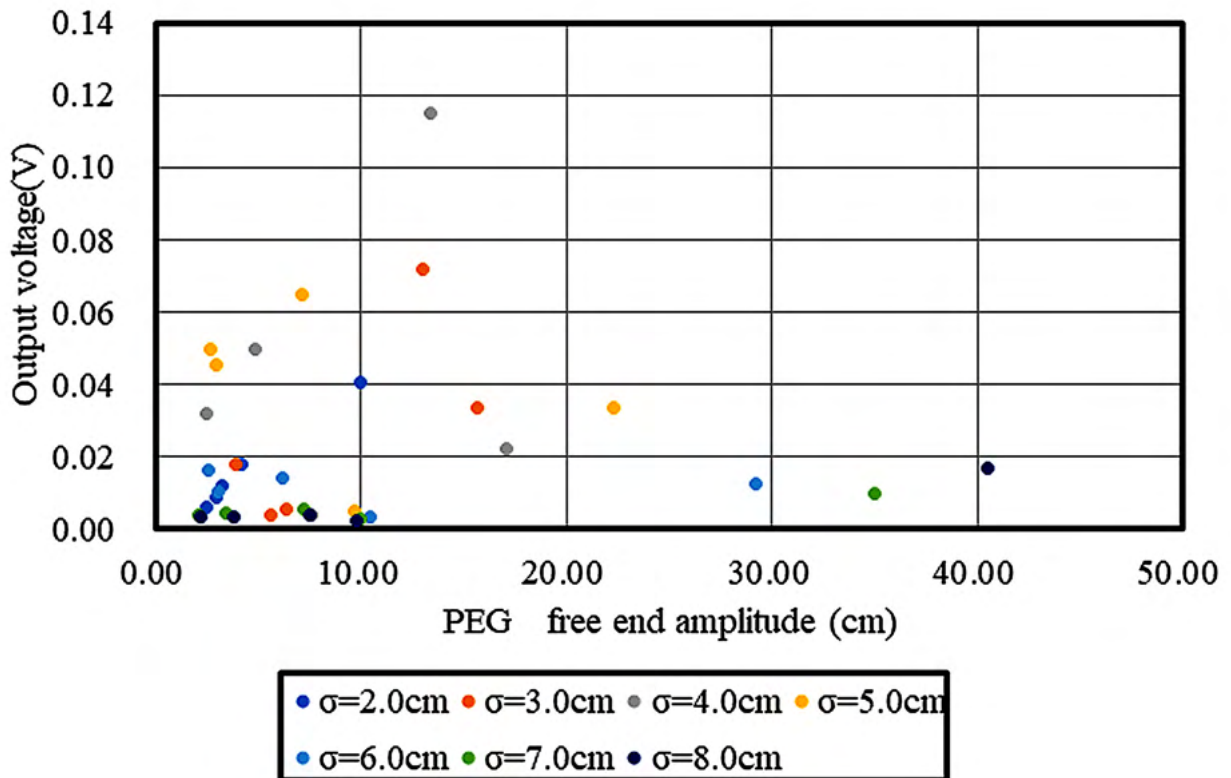
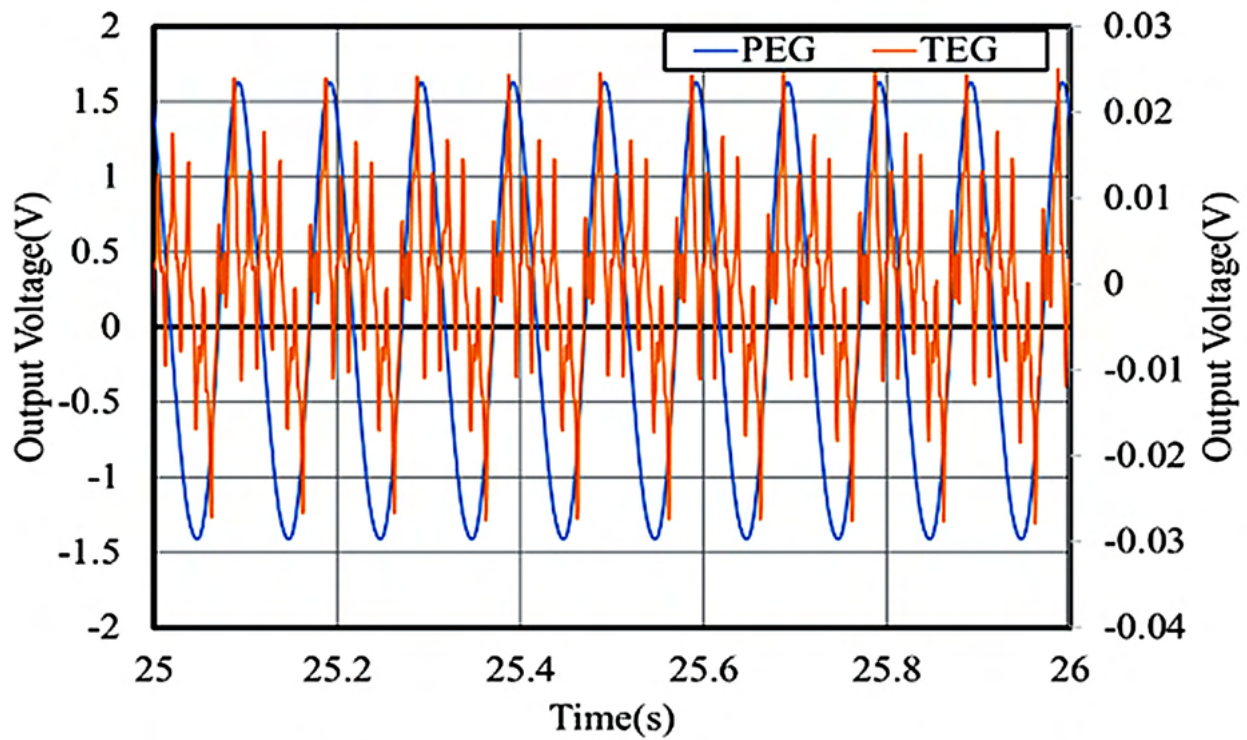
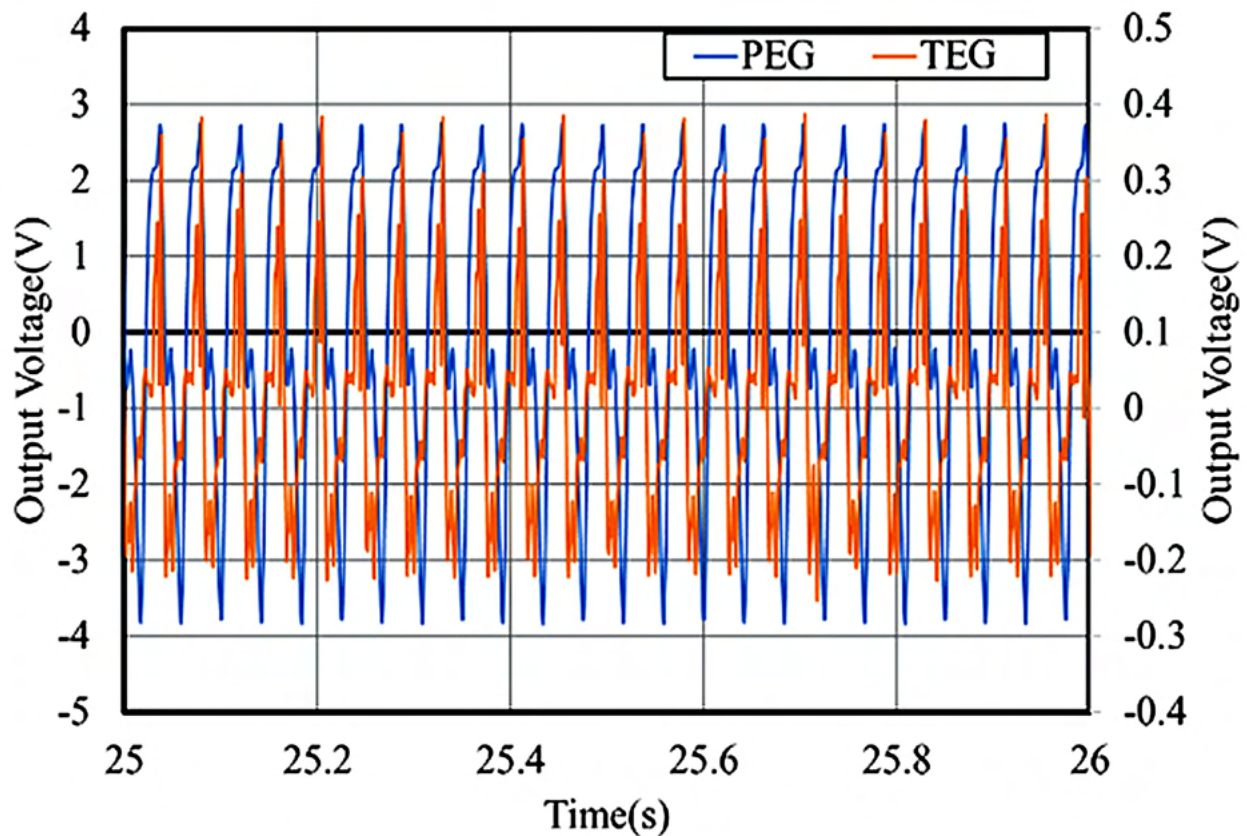


Figure 5.13: Relationship of PEG free end amplitude with the TEG output voltage

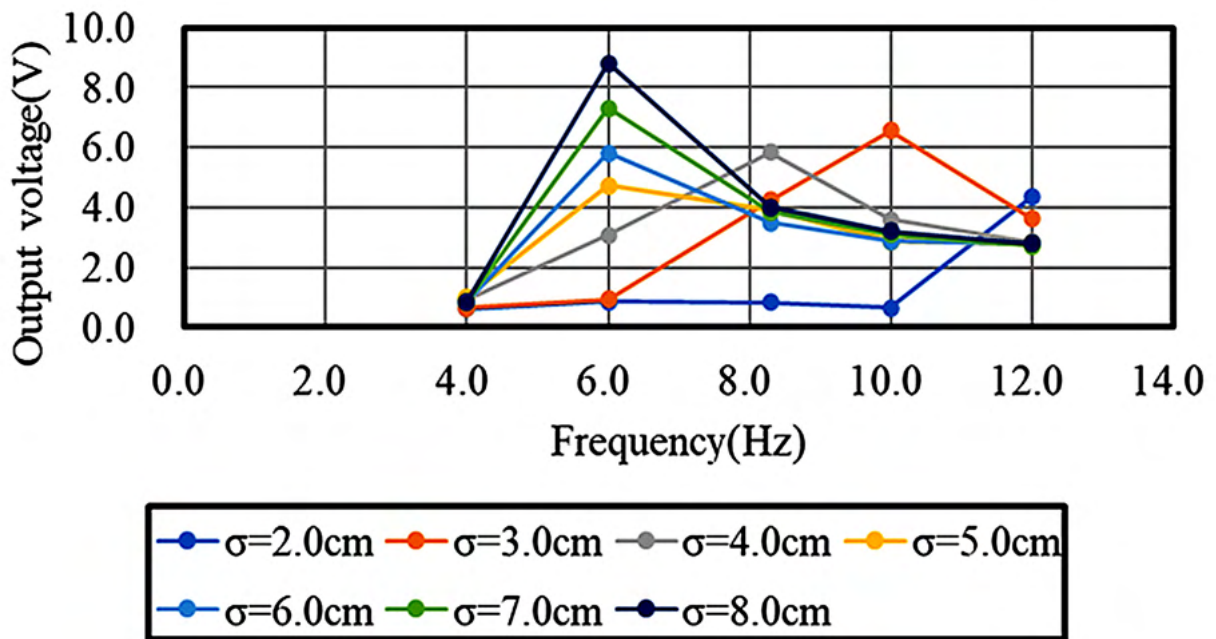


(a) Time histories of output voltage generated by **TEG-PEG** on study case 2, the vibration frequency = 10.0 Hz and initial distance $\delta = 1.0$ cm

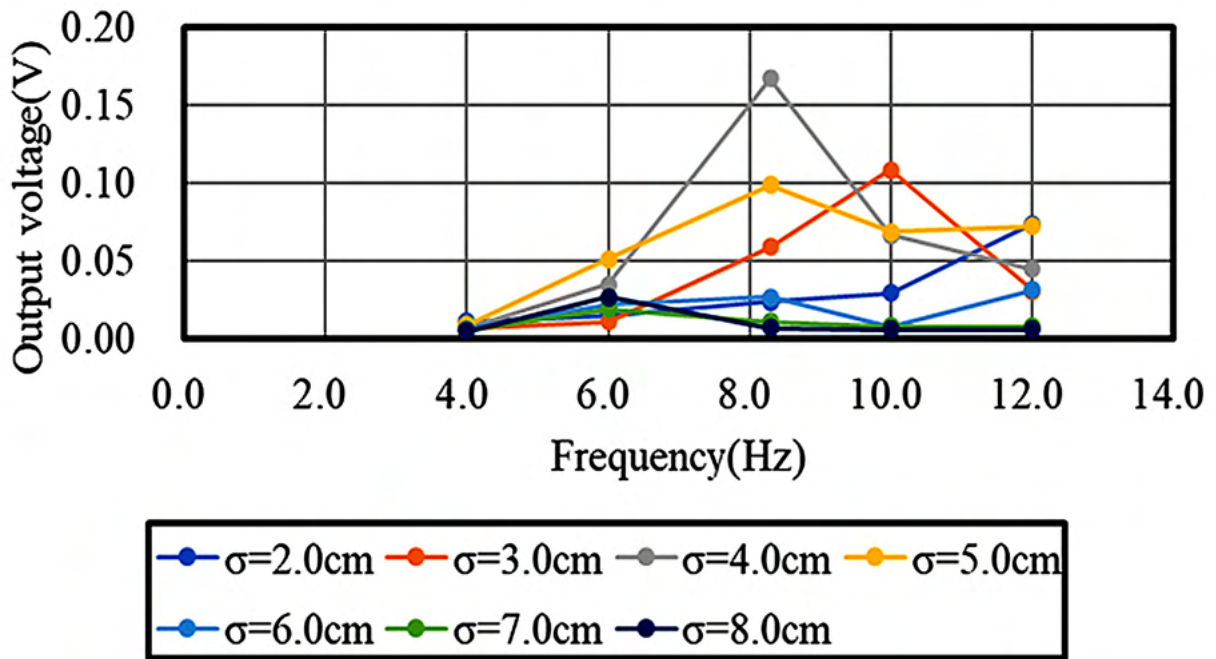


(b) Time histories of output voltage generated by **TEG-PEG** on study case 2, the vibration frequency = 10.0 Hz and initial distance $\delta = 5.0$ cm

Figure 5.14: Example of the TEG-PEG output voltage on study case 2

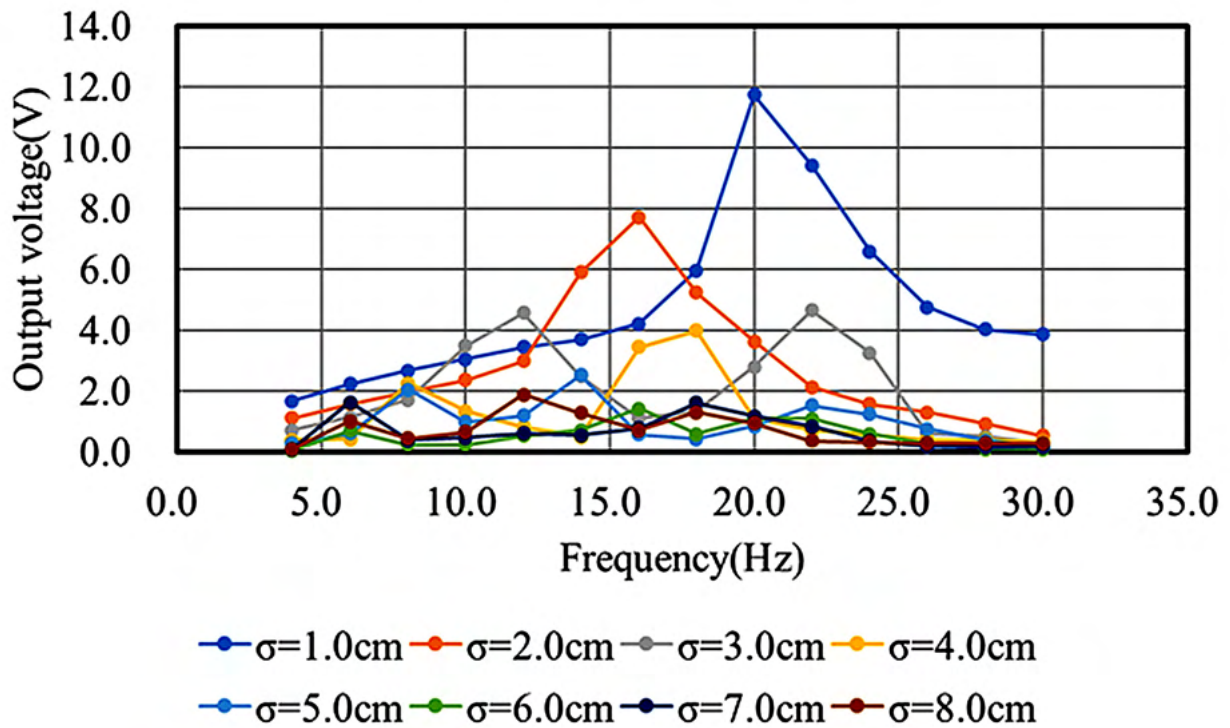


(a) Relationship of the frequency with PEG max voltage under various initial distances

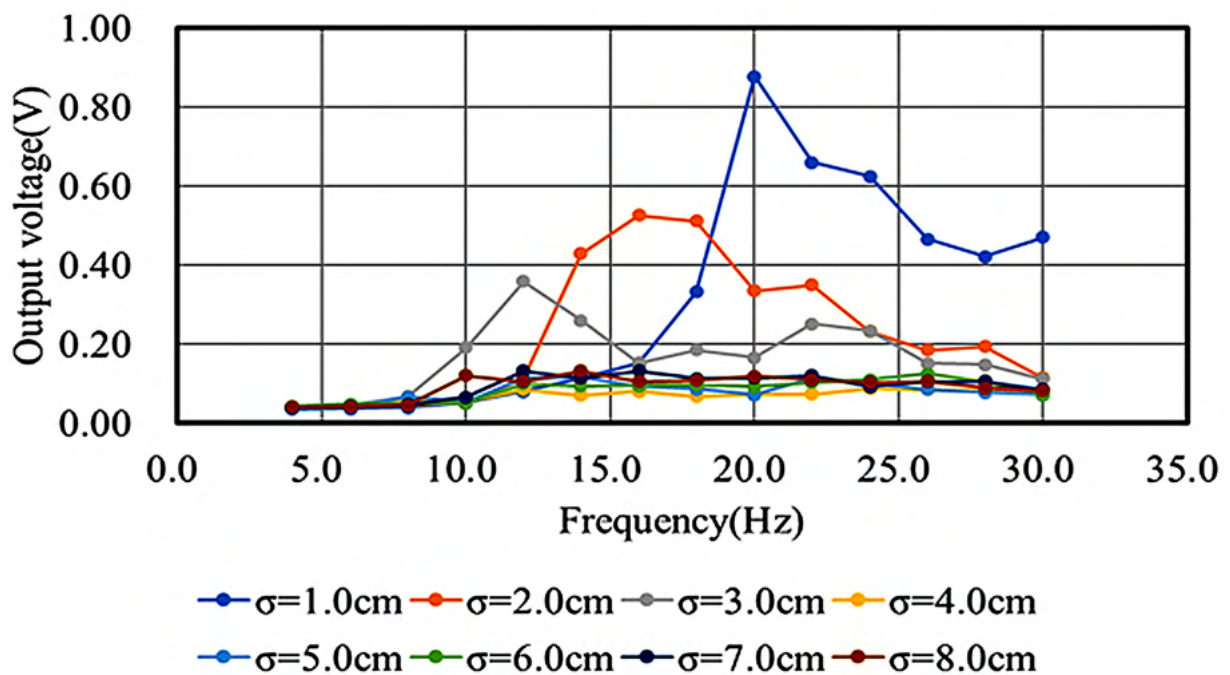


(b) Relationship of the frequency with TEG max voltage under various initial distances

Figure 5.15: TEG-PEG output voltage on study case 1



(a) Relationship of the frequency with PEG max voltage under various initial distances



(b) Relationship of the frequency with TEG max voltage under various initial distances

Figure 5.16: TEG-PEG output voltage on study case 2

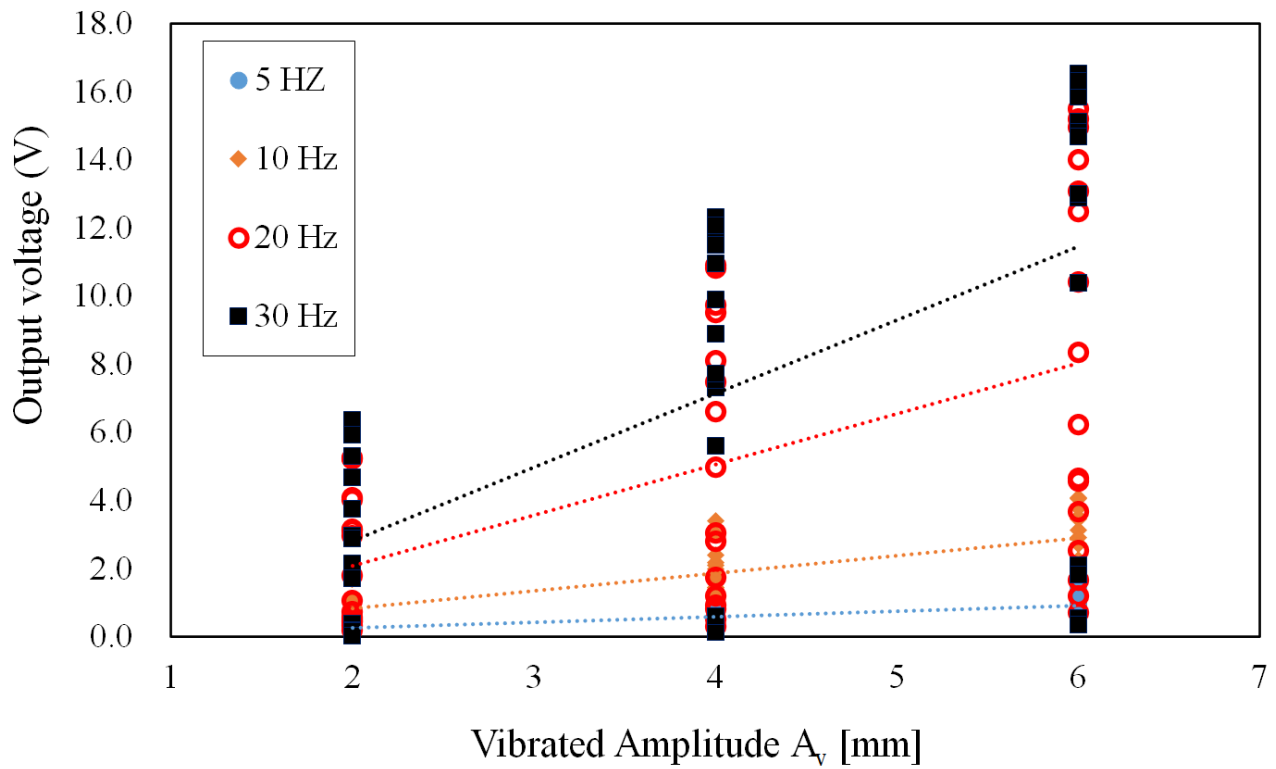
5.3.2 Relationship between vibrated amplitude to the PEG and TEG output voltage

This subsection covers the results of both PEG and TEG output voltage from the further vibration tests (case 2 only). Moreover, the results were shown alongside the vibration amplitude to clarify the relationship between the vibration amplitude and the PEG and TEG output voltage. Three vibration amplitude cases were adopted in the experiments: namely, the amplitudes of 2.0, 4.0, and 6.0 mm. The PEG and TEG devices were investigated independently, with each device having a cable attached to it to record their respective output voltages. Similar to the preliminary experiments, the output voltage illustrated in the figures is the maximum absolute value of the output voltage. Ten peak data points and ten trough data points from the PEG and TEG's electromotive force were chosen and converted into absolute values before being averaged into the output voltage in the figures.

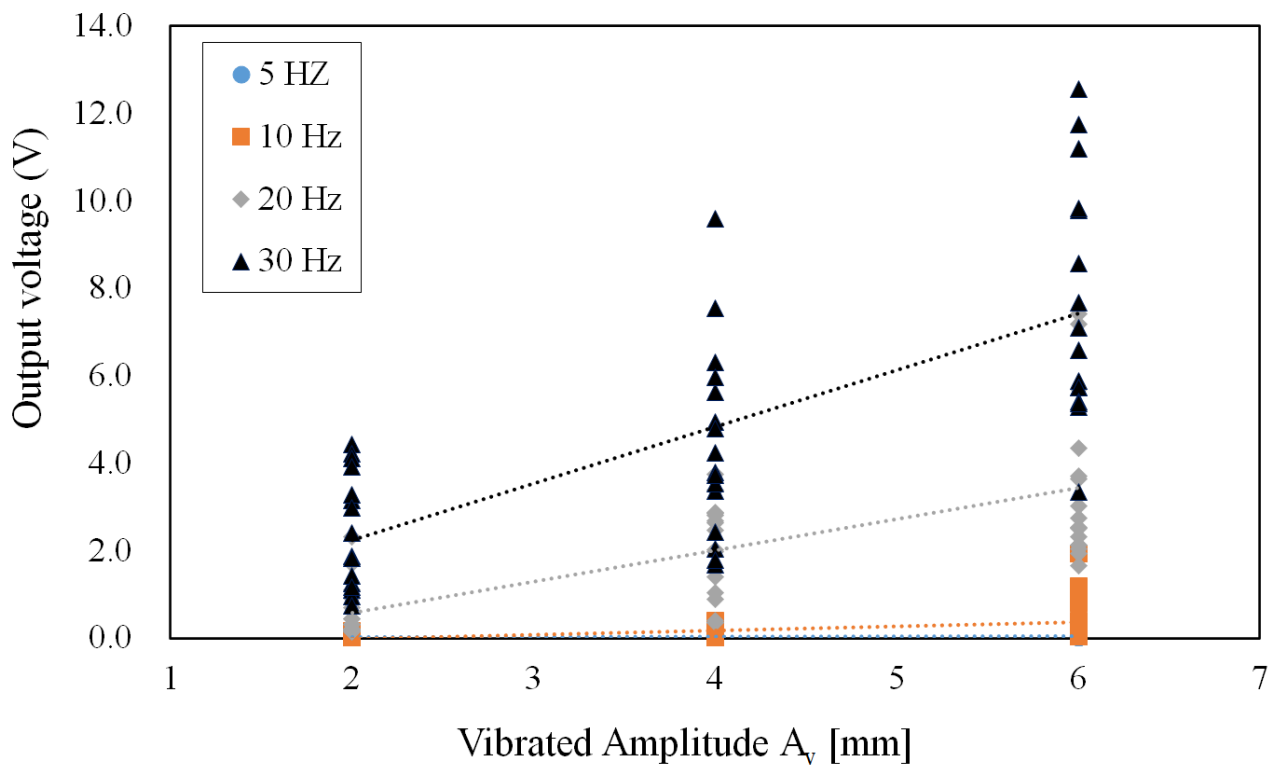
The results of the TEG-PEG output voltage on study case 2 and their relationship with the vibration amplitude could be seen in Fig.5.17 with (Fig.5.17a) is for the PEG output voltage and (Fig.5.17b) is for the TEG output voltage. The results show a higher output voltage value obtained with a higher vibration amplitude. In other words, the vibration amplitude positively correlates with the output voltage. This was especially seen on PEG, which exhibited a more substantial linear increase once the vibration amplitude was also higher. The vibration amplitude of 6.0 mm has an almost four times larger output voltage compared with the amplitude of 2.0 mm. In general, a 40% increase of the output voltage could be obtained every 2.0 mm increments of the vibration amplitude. The reason for this increase is likely due to the increase in the shear and the tensile strain from the vibration generator's stroke once it was set on a much higher amplitude. Since both PEG and TEG show the direct relationship with the vibration amplitude and vibration frequency to its electrical output, both parameters are considered to be one of the main factors in the contact electrification of the TEG device and the material deformation for PEG. Since the separation velocity is obtained by setting up the vibration amplitude and vibration frequency, this also means that the separation velocity have a positive correlation with the electrical output of both harvesters

Initially, it seems that the PEG is able to generate electrical output than TEG. However, the PEG have different size than PEG. Therefore, Fig.5.18 is shown to elucidate into more details of both TEG and PEG electrical power per area. Based on the figure, it can be seen that TEG is able to generate almost twice the electrical power compared with PEG. This indicates that not only that the TEG is able to generate electricity efficiently, it also shows that the multi-layer setup is very suitable to increase the output (No need to use the bigger/larger size of the generator) and can be use simultaneously with PEG.

Next, we will compare the vibration amplitude + initial distance to illustrate the influence of the separation distance.

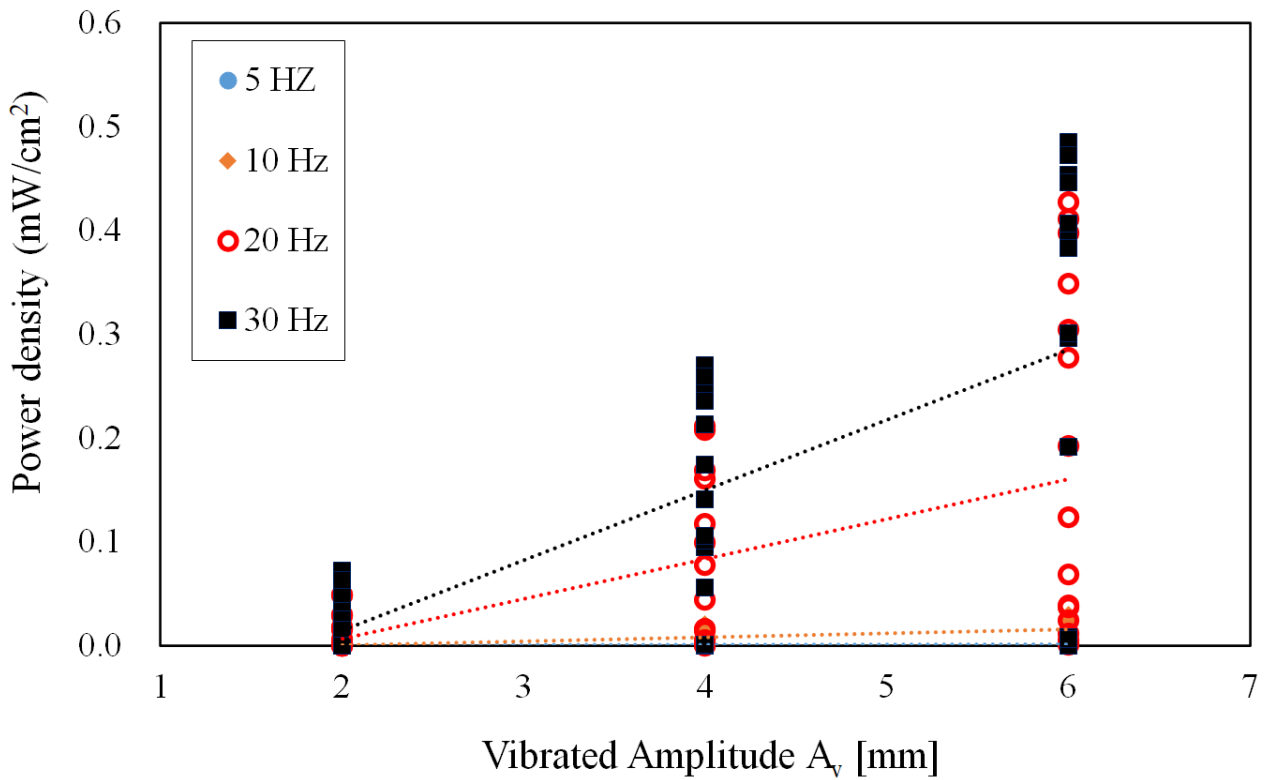


(a) PEG

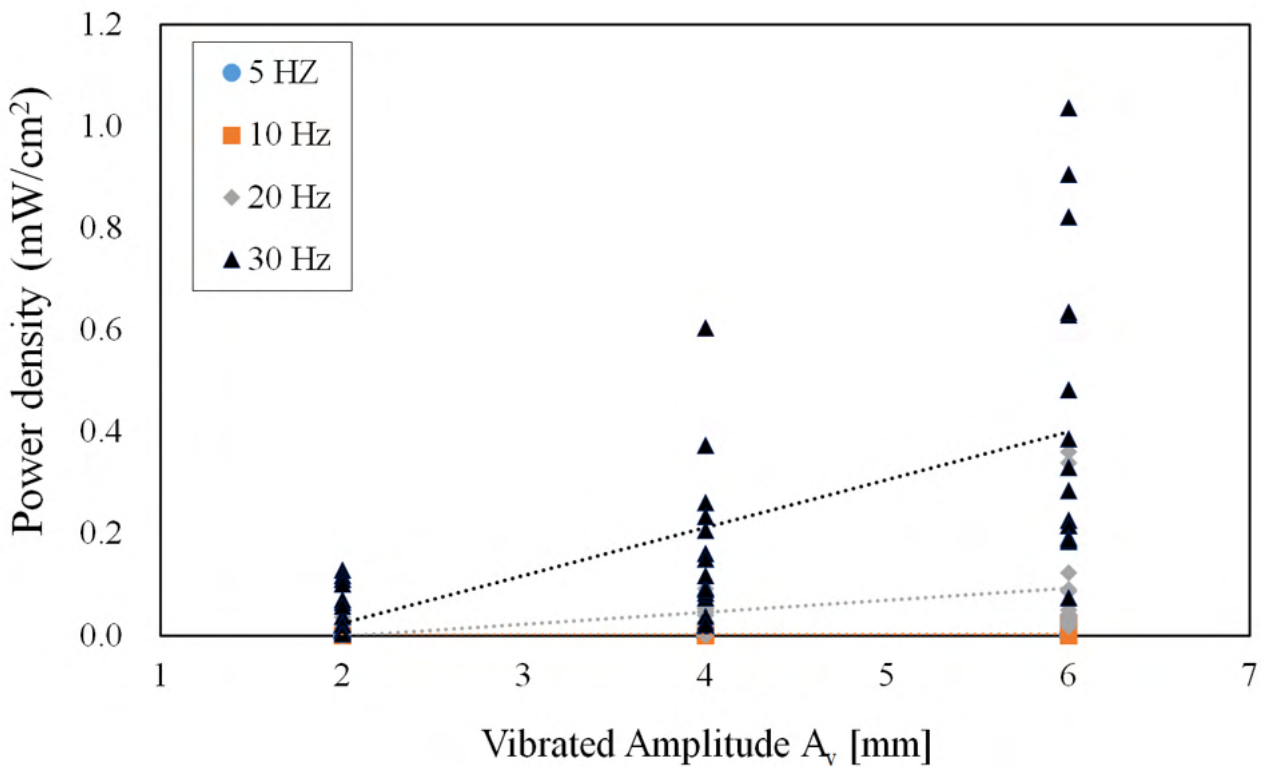


(b) TEG

Figure 5.17: Relationship between the output voltage and vibration amplitude



(a) PEG



(b) TEG

Figure 5.18: Relationship between the electrical output per area and vibration amplitude

5.3.3 Relationship between initial distance to the PEG and TEG electrical output under various frequencies

The initial distance, vibration amplitude, and vibration frequency are observed in both this and the following subsection. We found that the initial distance is not directly affecting the electrical output (non-linear correlation). The relationships between the initial distance and TEG-PEG electrical output are presented in Fig.5.19 for the frequency of 5 Hz, Fig.5.20 for 10 Hz, Fig.5.21 for the 20 Hz, and Fig.5.22 Hz for the 30 Hz results. All figures display different tendencies in each case.

Firstly, on the frequency of 5 Hz, the PEG seems to be decreased once the initial distance is increased, while on TEG, it doesn't seem to have any effect. Due to the small frequency test (5 Hz), it is predicted that the contact electrification on TEG can't generate much electrical output, and thus the effect of the initial distance on TEG, in this case, is not substantial. Next, on the frequency of 10 Hz, the effect of initial distance starts to appear. On PEG, the initial distance of 0 – 10 mm could cause an effective output on a three amplitude. The output gets stagnates at a distance of 12 – 18 mm. But, the voltage increases once the initial distance gets higher on δ_c of 20 – 30 mm. Interestingly, on TEG, the electrical output seems to be increased alongside the increase of the distance. With the highest result achieved on the highest initial distance (30 mm). Finally, we observed that the voltage for both PEG and TEG achieved its highest results on the high-frequency case of 20 Hz and 30 Hz. However, the effect of the initial distance seems to be inconsistent since both PEG and TEG have various tendencies on each test. More observation of the initial distance effect with the frequency is elucidated in the following sub-section to clarify this situation.

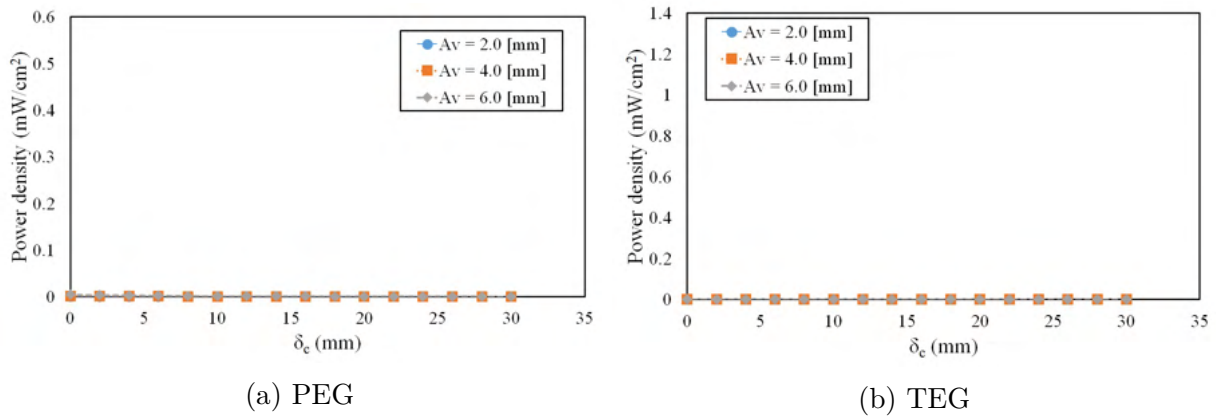


Figure 5.19: Relationship between the initial distance and electrical output on frequency 5 Hz

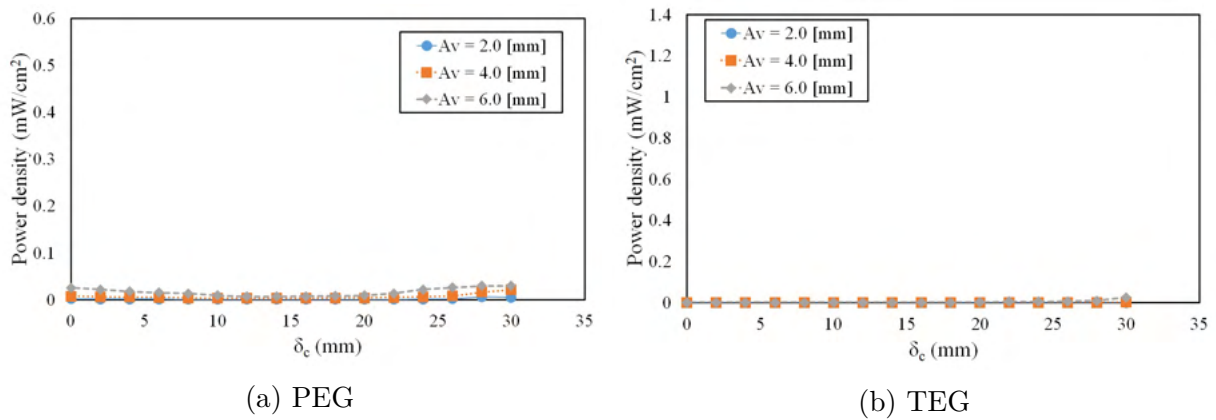


Figure 5.20: Relationship between the initial distance and electrical output on frequency 10 Hz

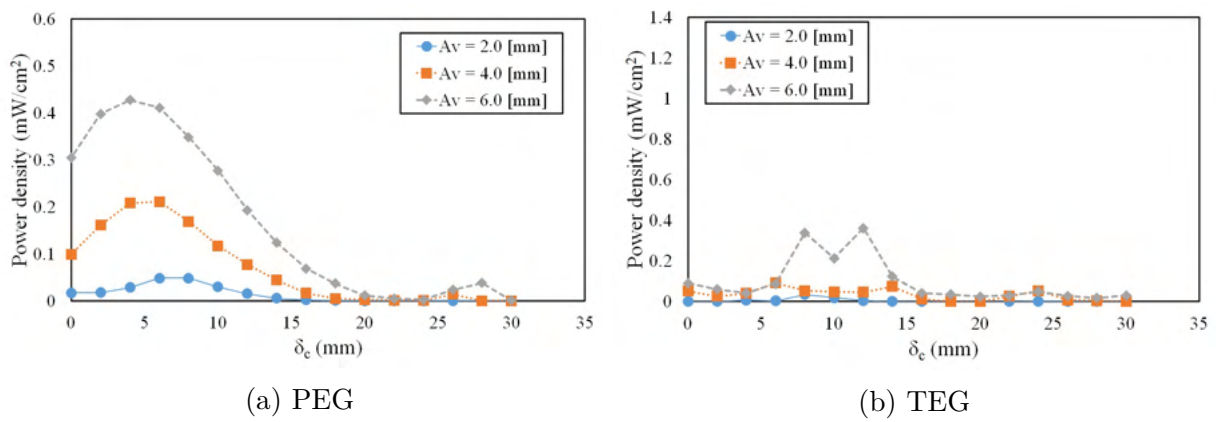


Figure 5.21: Relationship between the initial distance and electrical output on frequency 20 Hz

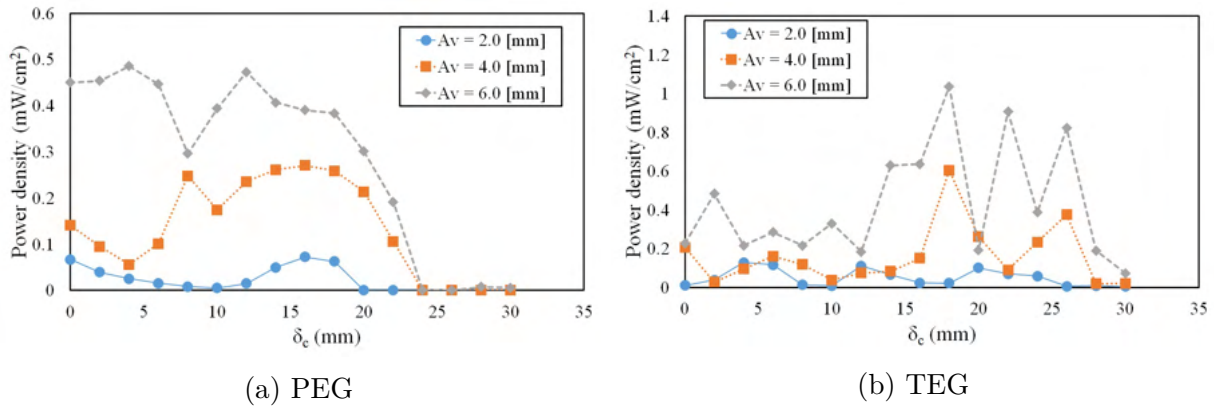
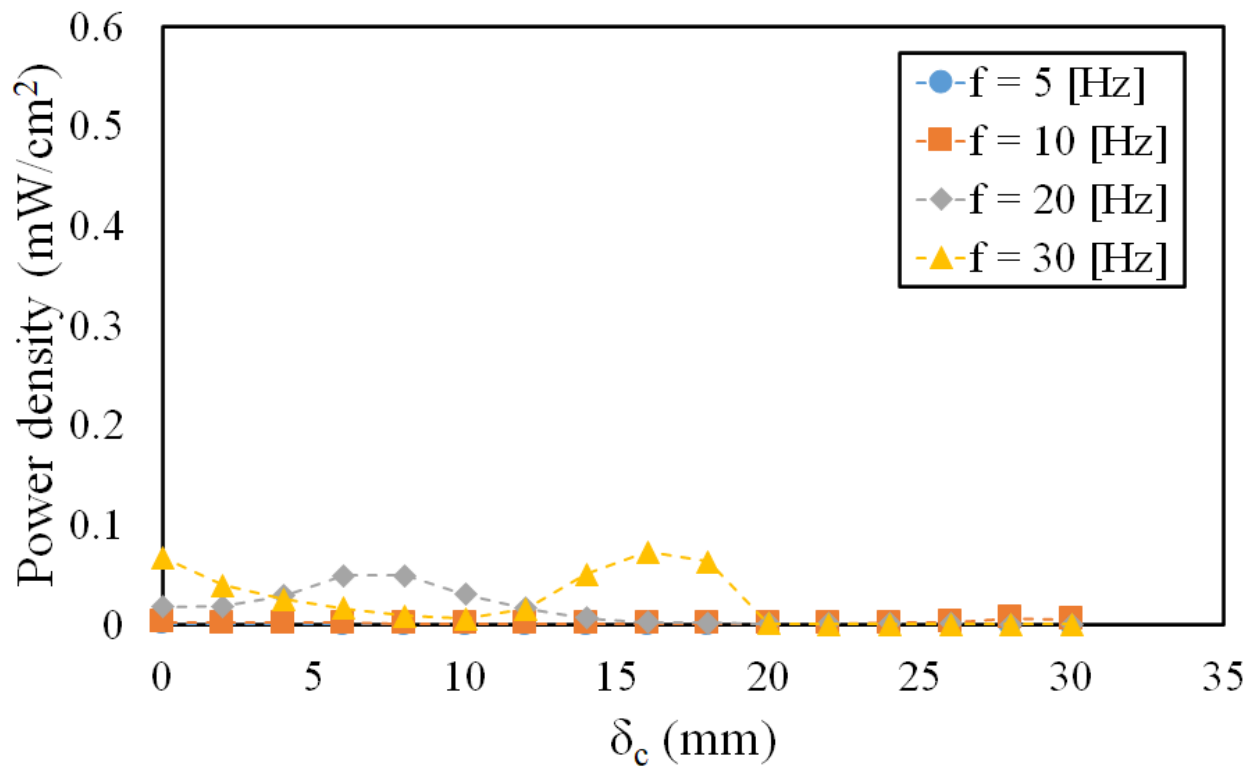
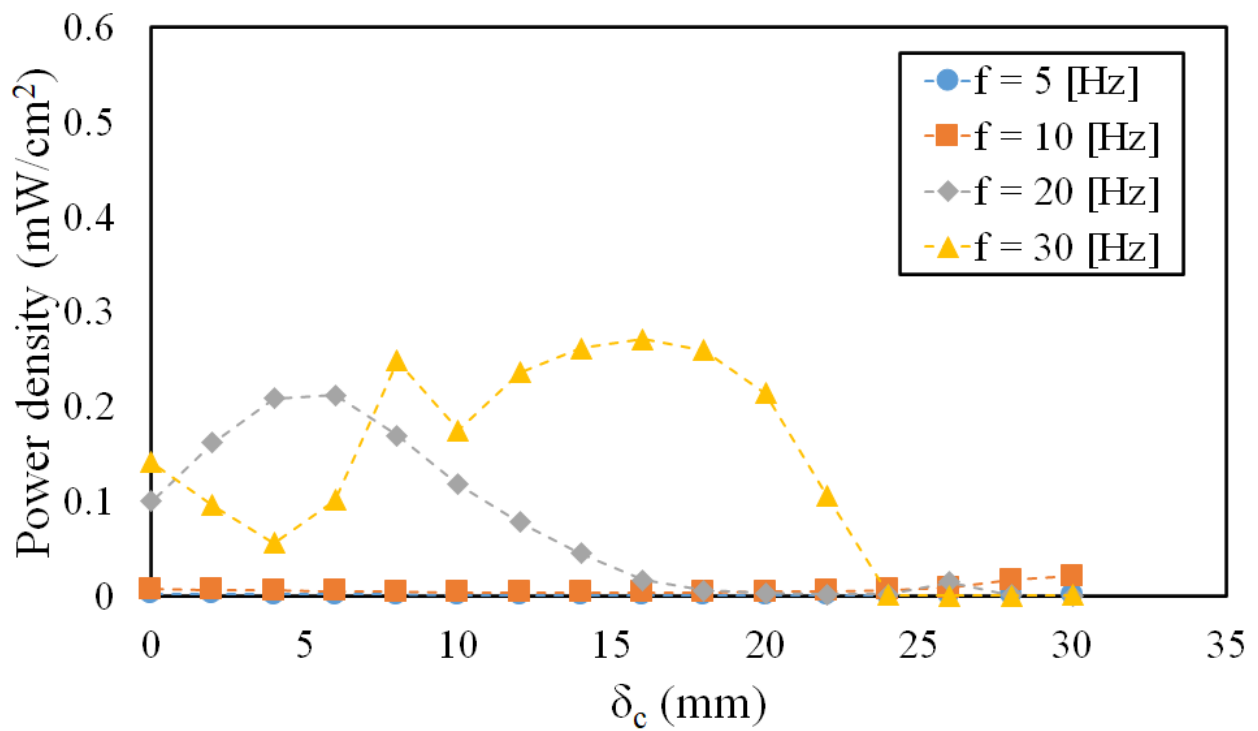


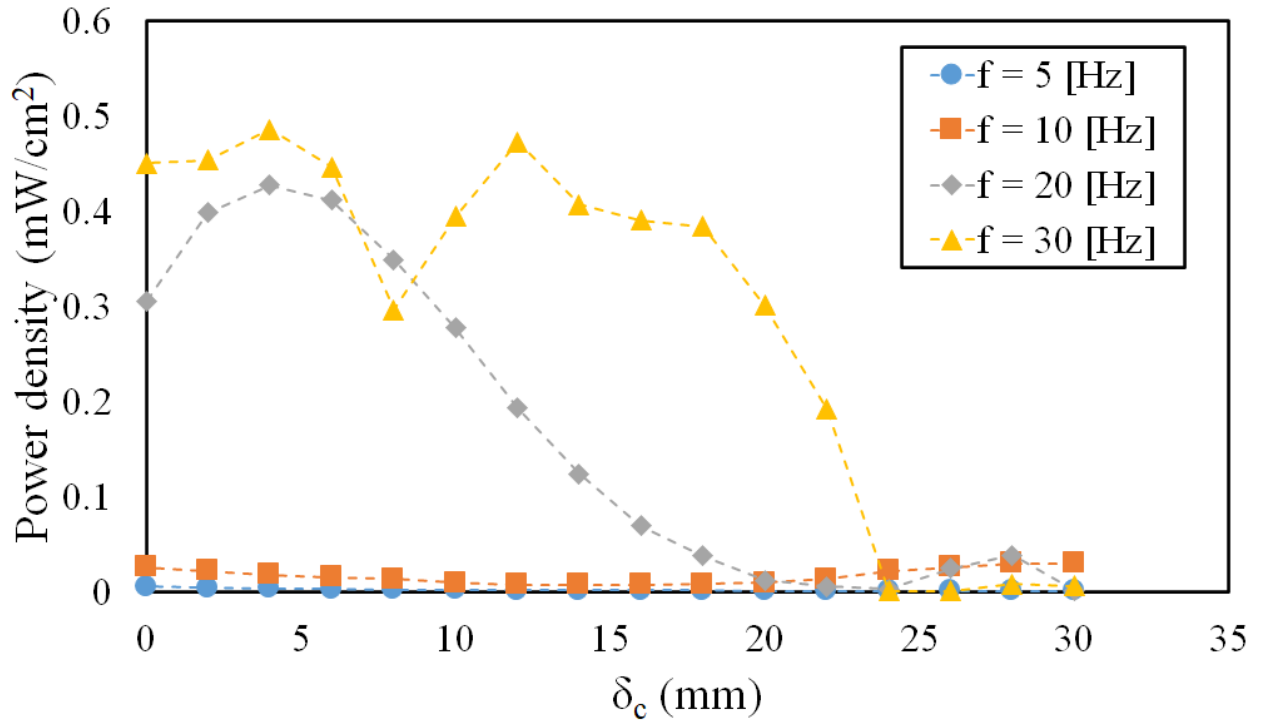
Figure 5.22: Relationship between the initial distance and electrical output on frequency 30 Hz

5.3.4 Relationship between initial distance to the PEG and TEG output voltage under various amplitudes

Fig.5.23 and Fig.5.24 illustrate the initial distance's role to both PEG and TEG output voltage under three different amplitude values. As briefly mentioned in the previous subsections, the vibration frequency influences both harvesters' maximum output voltage value, especially on the high-frequency test. Both PEG and TEG output under the 20 and 30 Hz vibration test was significantly higher than that under 5 and 10 Hz frequencies.

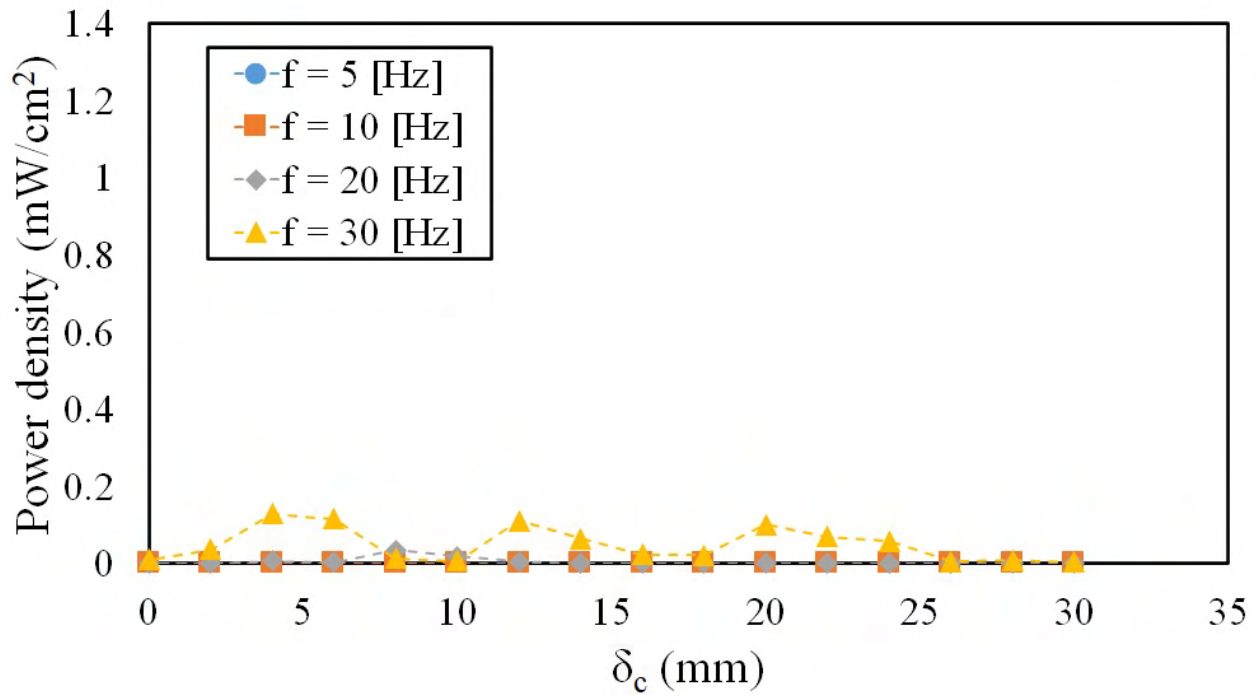
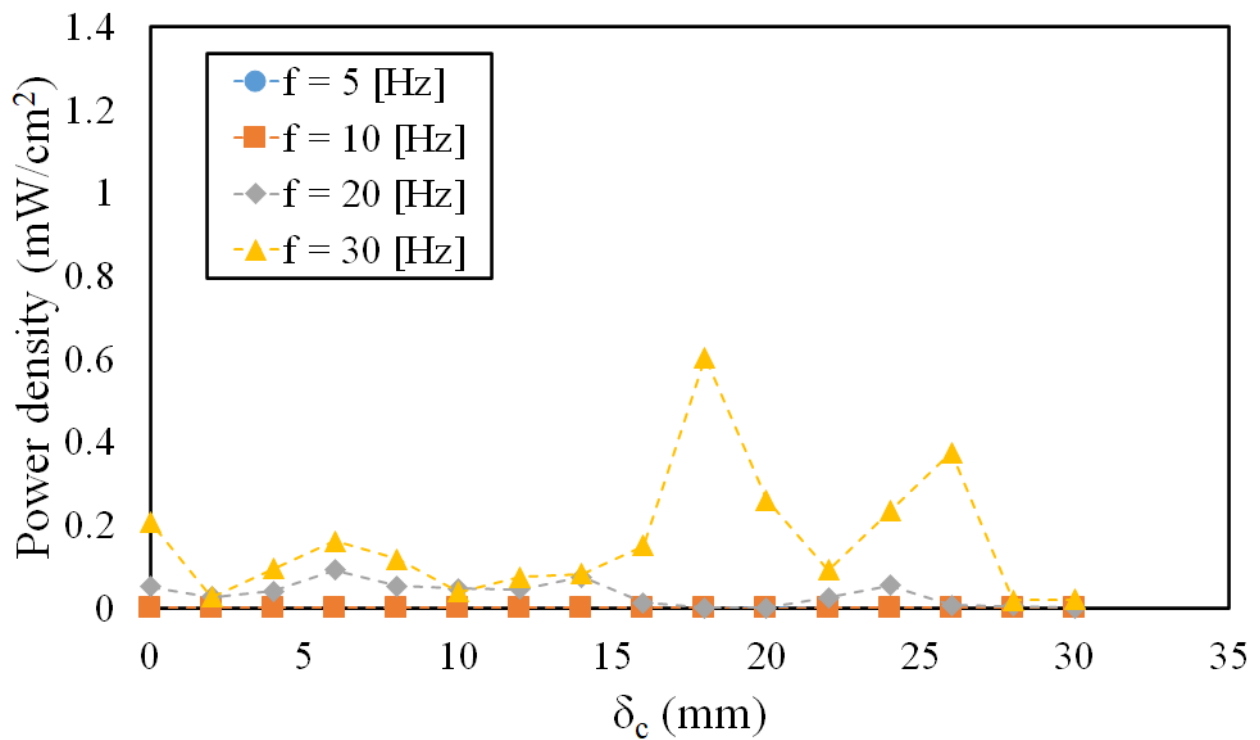
As for the initial distance effect to the electrical output, it is confirmed that the relationship between the initial distance and the electrical output of both PEG and TEG was nonlinear. The ratio of electrical output generation was not constant and did not necessarily increase or decrease under different δ_c . It can be seen in all figures that the power density has a different tendency for every vibration frequency and initial distance. For the PEG on $A_v = 2$ mm, the Max output at $\delta_c = 16$. On $A_v = 4$ mm, the max output at $\delta_c = 16$. While $A_v = 6$ mm have max output at $\delta_c = 4$. In contrast, for the TEG on $A_v = 2$ mm, the max output at $\delta_c = 4$. On $A_v = 4$ mm, the max output at $\delta_c = 18$. While $A_v = 6$ mm have the max output at $\delta_c = 18$. This finding means that the PEG and TEG distances must be adjusted to a specific distance to ensure the device resonates appropriately. Both devices needs the resonance movement to create a consistent material deformation for PEG and contact electrification for TEG, which generates a stable and effective output. Therefore, this phenomenon also means that the separation distance have minimum influence for the TEG PEG output.

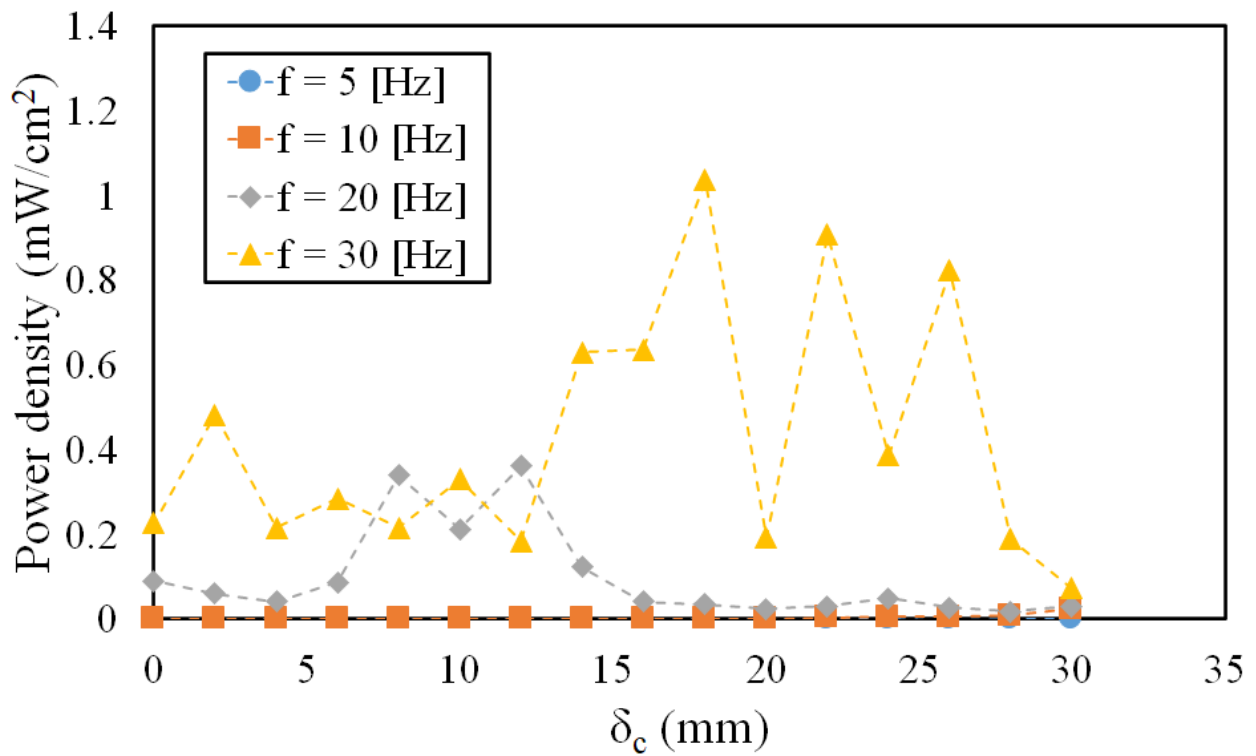
(a) $A_v = 2.0$ mm(b) $A_v = 4.0$ mm



(c) $A_v = 6.0$ mm

Figure 5.23: Relationship between the electrical output and the initial distance (δ_c) on PEG.

(a) $A_v = 2.0$ mm(b) $A_v = 4.0$ mm



(c) $A_v = 6.0$ mm

Figure 5.24: Relationship between the electrical output and the initial distance (δ_c) on TEG.

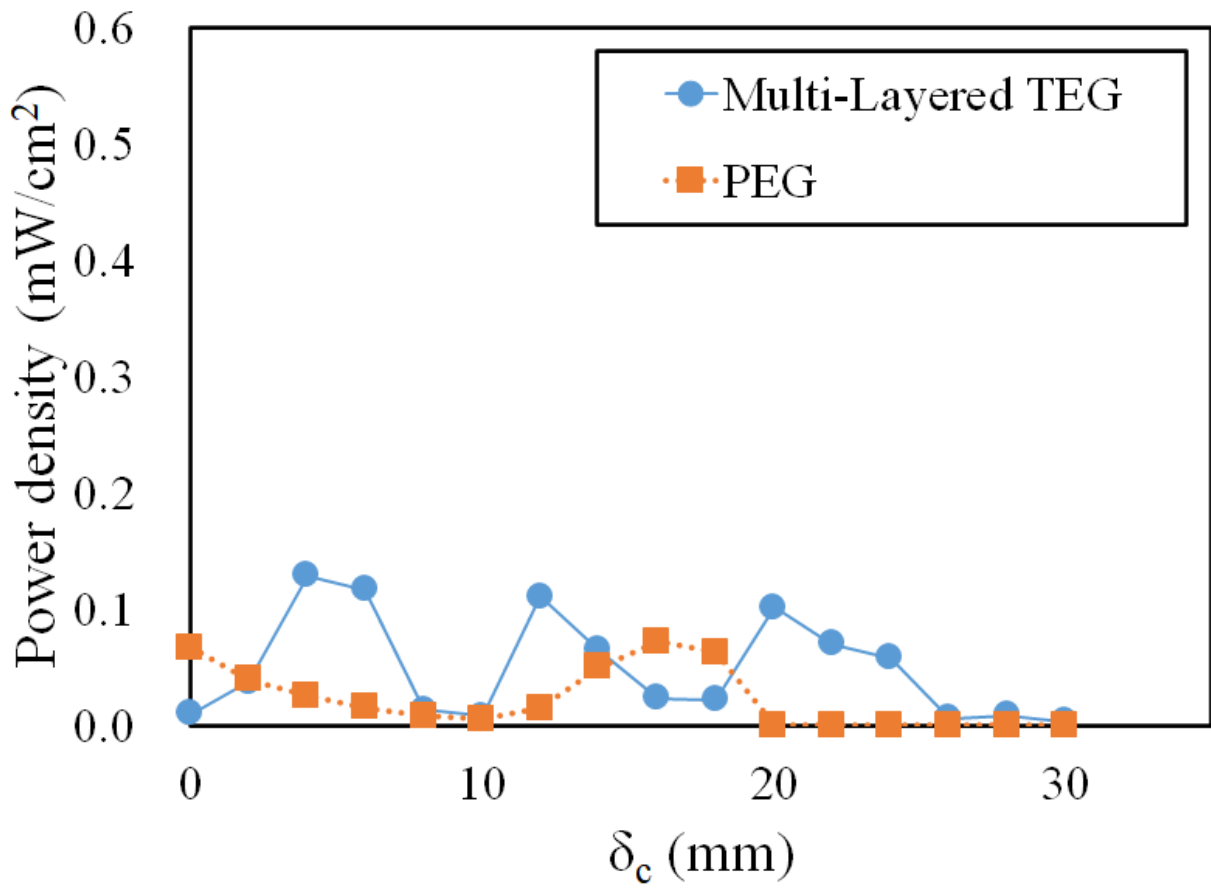
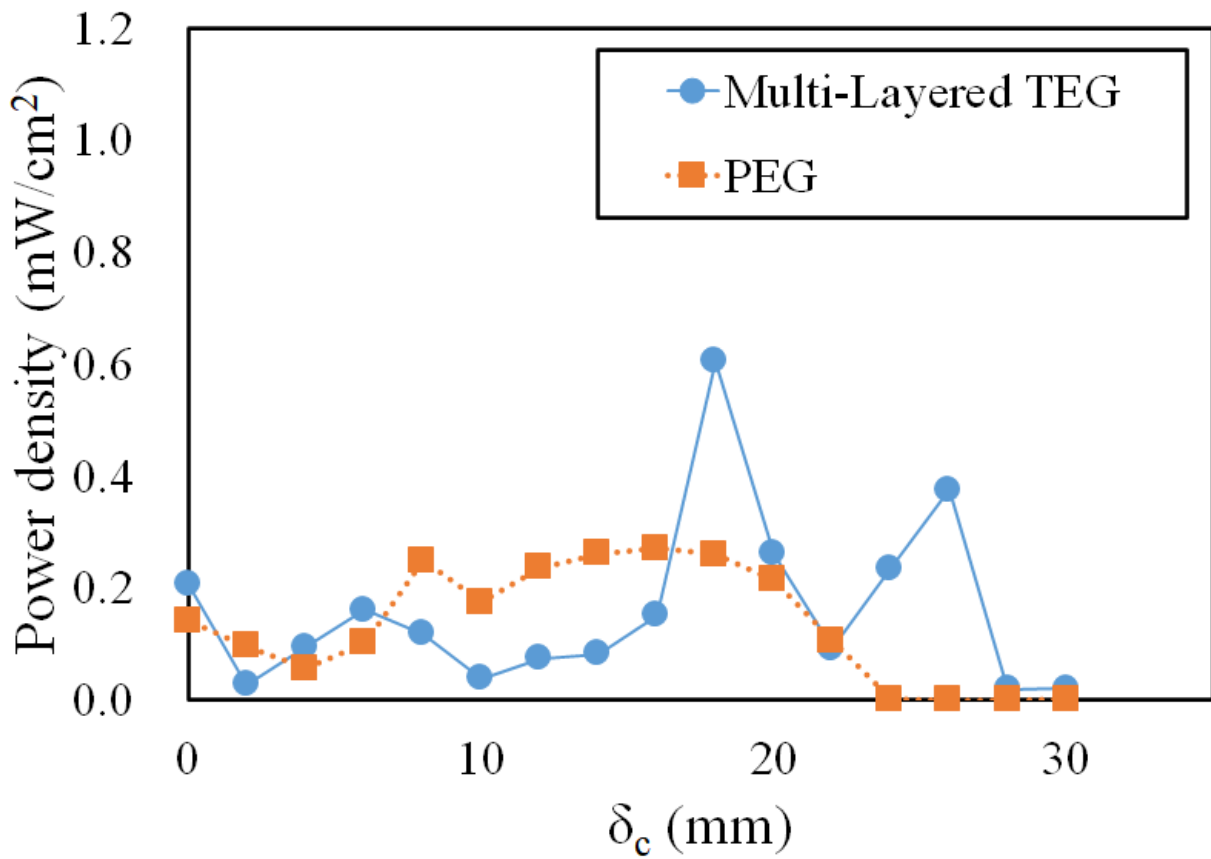
5.3.5 TEG-PEG Hybrid Mutual Complementary

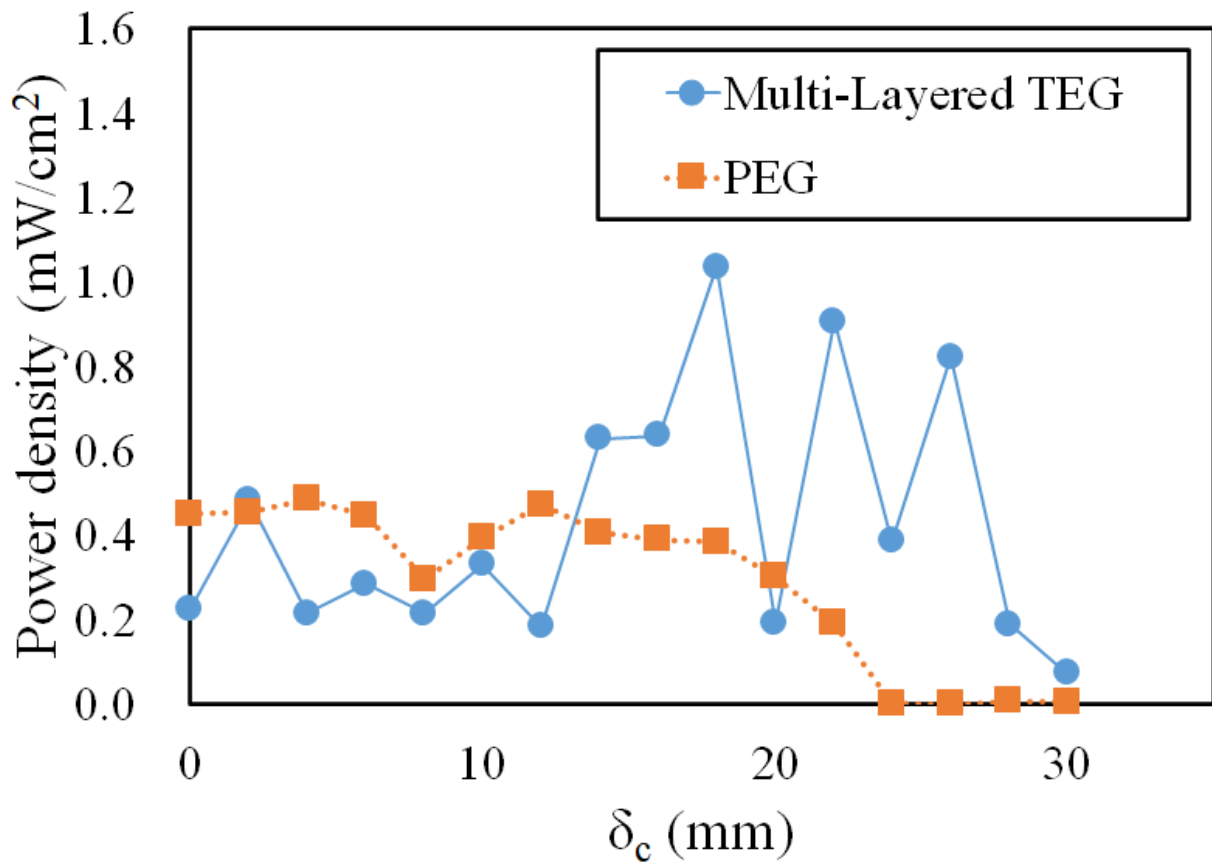
To clarify the complementary relationship between the PEG and the TEG energy harvester, the further assessment was also investigated both devices under a frequency of 30 Hz and three vibration amplitudes. The representative can be seen in Fig.5.25.

Fig.5.25a displays the relationship between the multi-layered TEG and the PEG electrical output under an amplitude of 2.0 mm. At this lower amplitude state, the output from both PEG and TEG devices exhibited an opposite behavior. Here, the PEG output tends to increase under the initial state of $0 \text{ mm} < \delta_c < 6 \text{ mm}$. Additionally, the PEG power density also tends to sharply increase δ_c at $= 12$ and 20 mm . Apart from the aforementioned initial distance conditions, the PEG output decreases. For TEG, it has exhibited a more uniform response. At the start of the experiment (initial distance = 0 mm), the TEG generated a high electrical output, while following this, the maximum voltage of TEG decreased up to the initial distance of 10 mm case. The increasing trend then emerged again and peaked at an initial distance of 18 mm. After the 18 mm case, the next setup tended to make the output voltage drop until the final initial distance case.

In order to understand the complementary of both harvesters on a much larger amplitude, Fig.5.25b and Fig.5.25c are shown. In the case of 4.0 and 6.0 mm amplitudes, an equally uniform response was observed alongside the $\delta_c = 0 - 20 \text{ mm}$. Interestingly, the PEG and the TEG demonstrated an identical response (except on the initial distance of 18 mm), where the TEG exhibited a considerable. This result indicated that both PEG and TEG moved in unison to shift to their deformation and contact-release states.

Regarding the relationship with the δ_c , PEG and TEG slightly differ. The PEG tended to provide a higher electrical output in the case of $\delta_c \leq 20 \text{ mm}$ (similar as well on the case where $A_v = 2.0 \text{ mm}$), while all the PEG results suddenly showed a significant decrease once the $\delta_c > 21 \text{ mm}$ (with the exception of $\delta_c = 28 \text{ mm}$ at $A_v = 6.0 \text{ mm}$). This decrease was likely due to the inability of the external vibration force to move the PEG at a large separation distance.

(a) $A_v = 2.0$ mm(b) $A_v = 4.0$ mm



(c) $A_v = 6.0$ mm

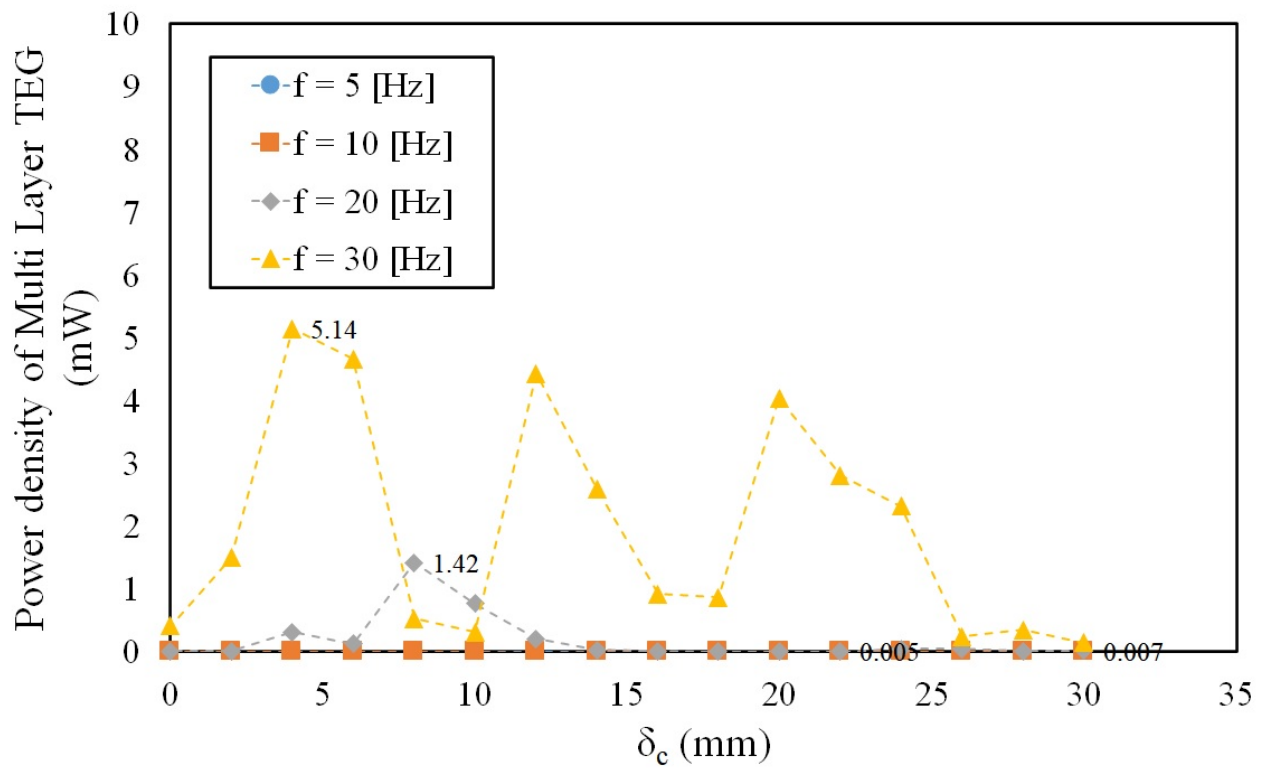
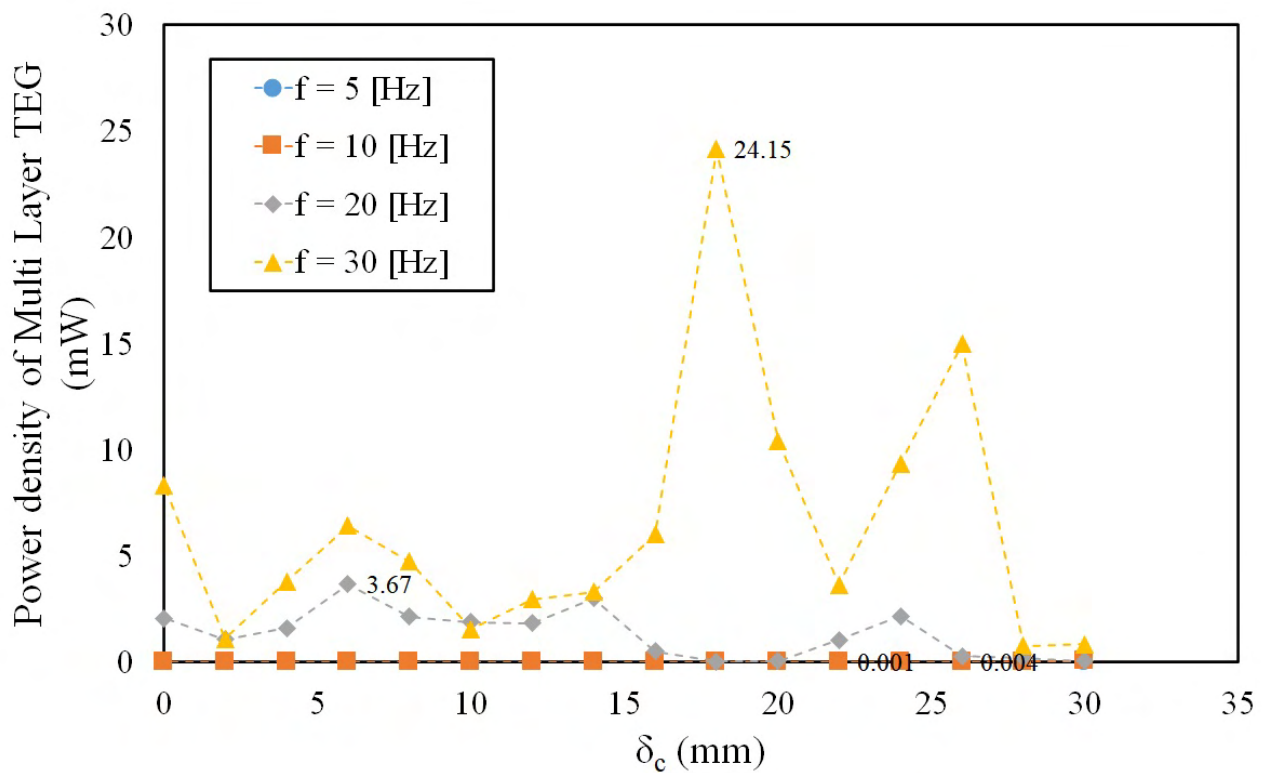
Figure 5.25: Relationship between the electrical output and the initial distance (δ_c) on the vibration frequency ($f_v = 30$ Hz).

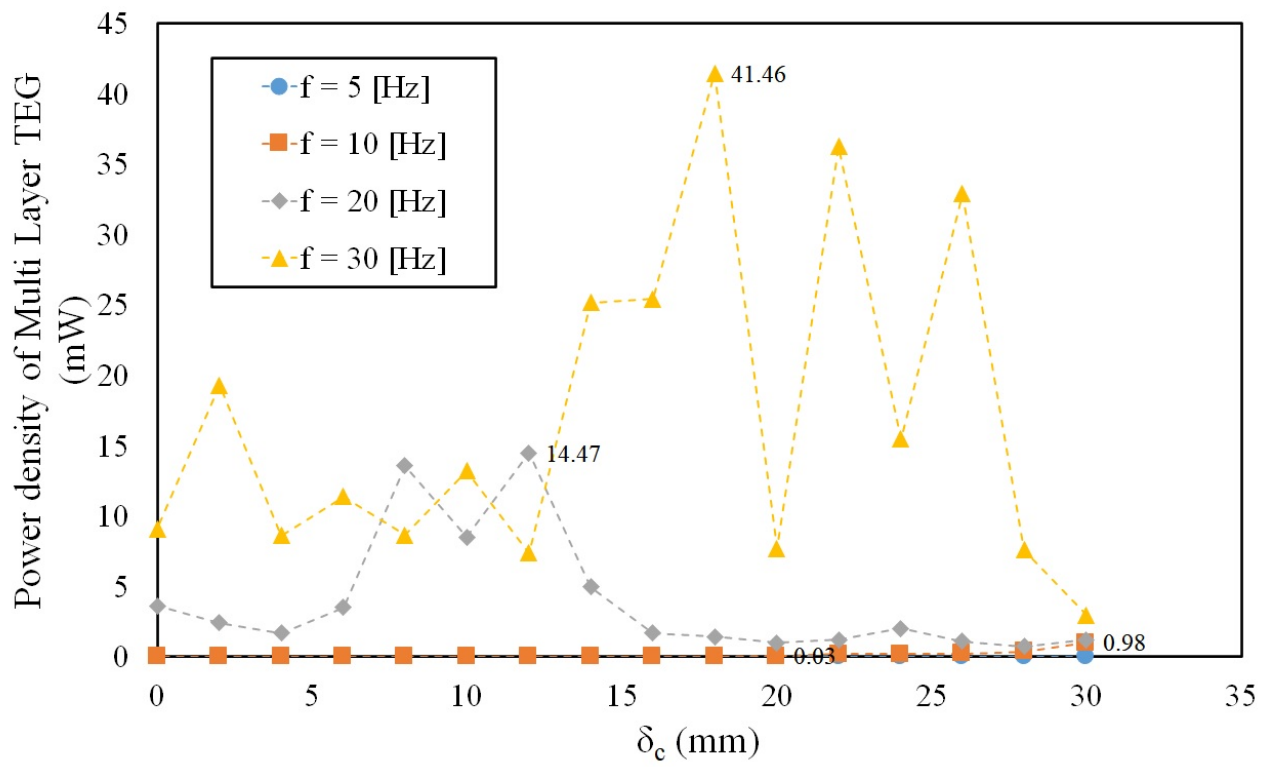
However, the multi-layered TEG generated a good result at the initial distance of $18 \leq \delta_c \leq 26$ mm or on the $\delta_c \geq 20$ mm that could accommodate the PEG results under a large initial distance. Therefore, TEG could support and align the relative strength and weakness of both devices for generating electricity output. Consequently, the TEG-PEG hybrid harvester has the capacity to generate energy in a broader spectrum of initial distance due to the highly complementary relationship.

5.3.6 TEG-PEG Power Density Comparison

Firstly, to show whether the addition of the flexible PEG could influence the multi-layer TEG output or not, Fig.5.26 is shown. Three figures showed only the Multi-layer TEG on the hybrid harvester electrical output and compared with previous Multi-layer TEG only experiments in the previous chapter 4.3 and specifically on the Fig.4.16. As a reminder, the previous Multi-layer TEG in the previous chapter has an output power range from 0.01 - 25.2 mW, while the multi-TEG on the hybrid harvester in this chapter has an output power range from 0.001 – 41.46 mW. The multi-layer TEG on the hybrid harvester has the same size and same experimental setup but has different configurations due to the addition of the PEG. We can see that those additions act as efficient tools that make the multi-layer TEG able to generate higher output compared with only multi-layer TEG in the previous study.

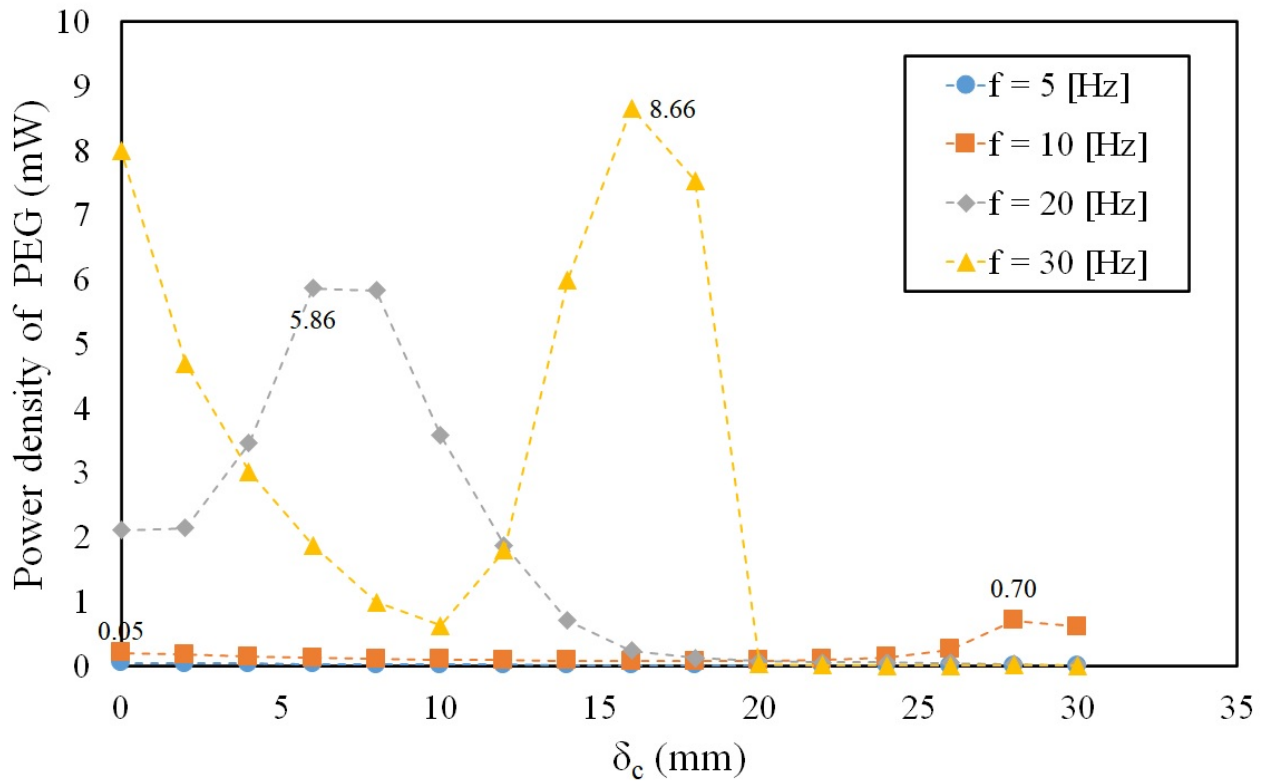
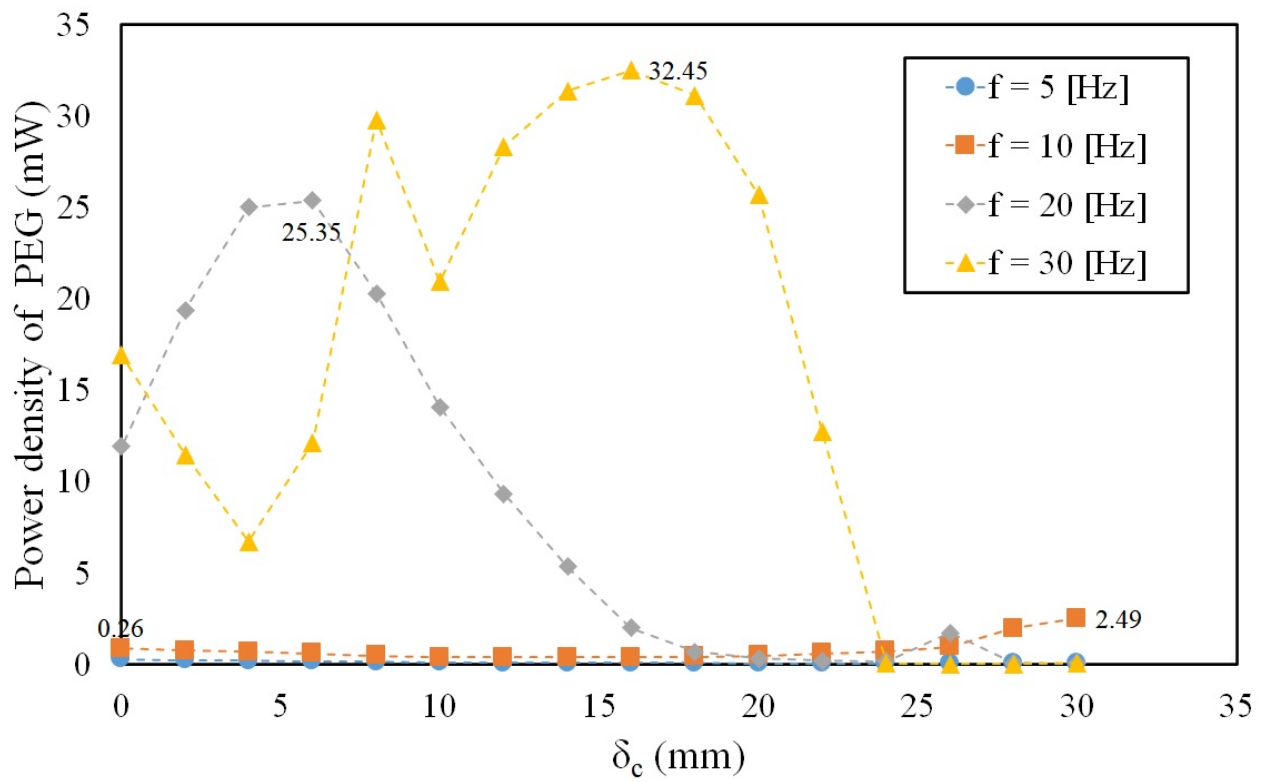
In addition, the Flexible PEG output power density is also shown on the Fig.5.27 with the output power range from 0.05 – 58.3 mW and the Total Area of 120 cm^2 . In this rough estimation and not yet considered the impedance matching, the current Multi-TEG or PEG can power the top 2 Logger + sensor from the Fig.5.28. Larger size is needed to power other devices and sensors, For example: by increasing the size of the PEG twice from this experiments or increase the size of the multi-layered TEG three times larger to power the “wave gauge” “turbidity sensor”.

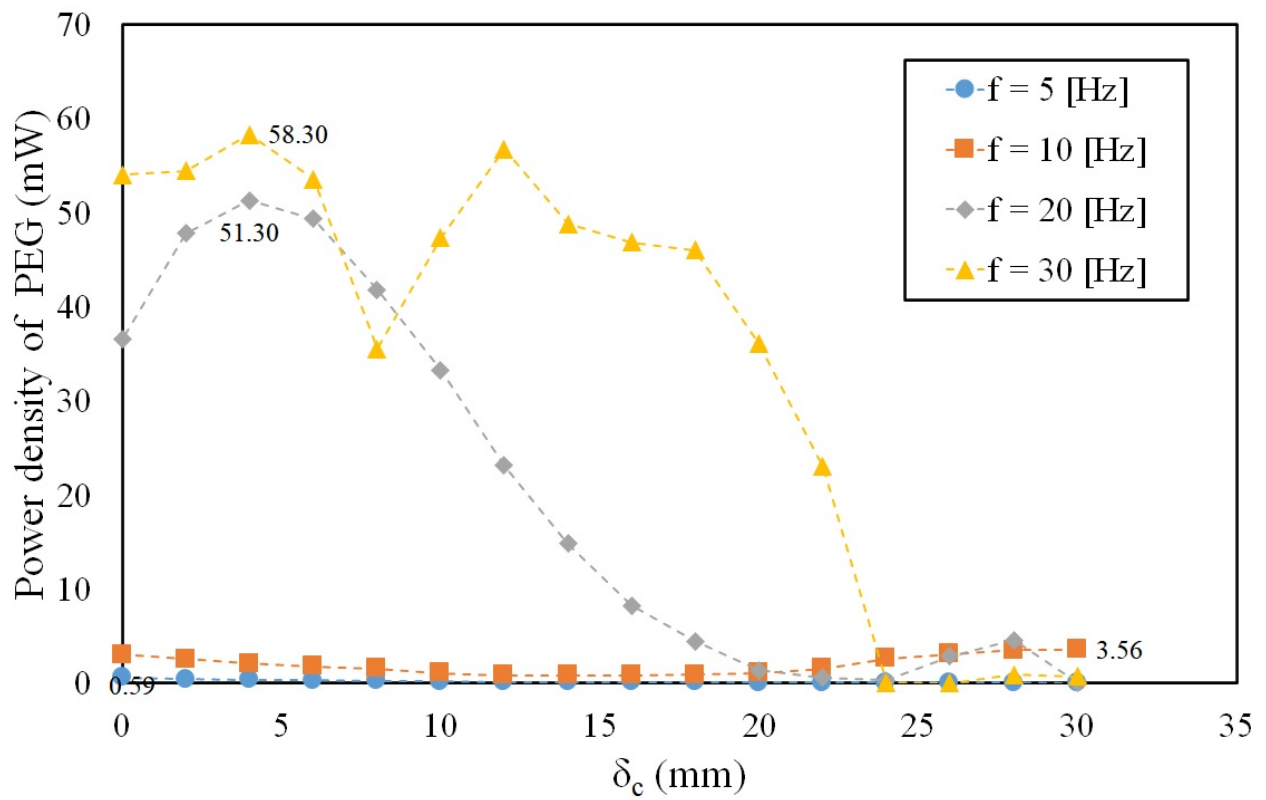
(a) $A_v = 2.0$ mm(b) $A_v = 4.0$ mm



(c) $A_v = 6.0$ mm

Figure 5.26: Multi-layer TEG power density on the Hybrid Harvester.

(a) $A_v = 2.0$ mm(b) $A_v = 4.0$ mm



(c) $A_v = 6.0$ mm

Figure 5.27: Flexible PEG power density on the Hybrid Harvester.

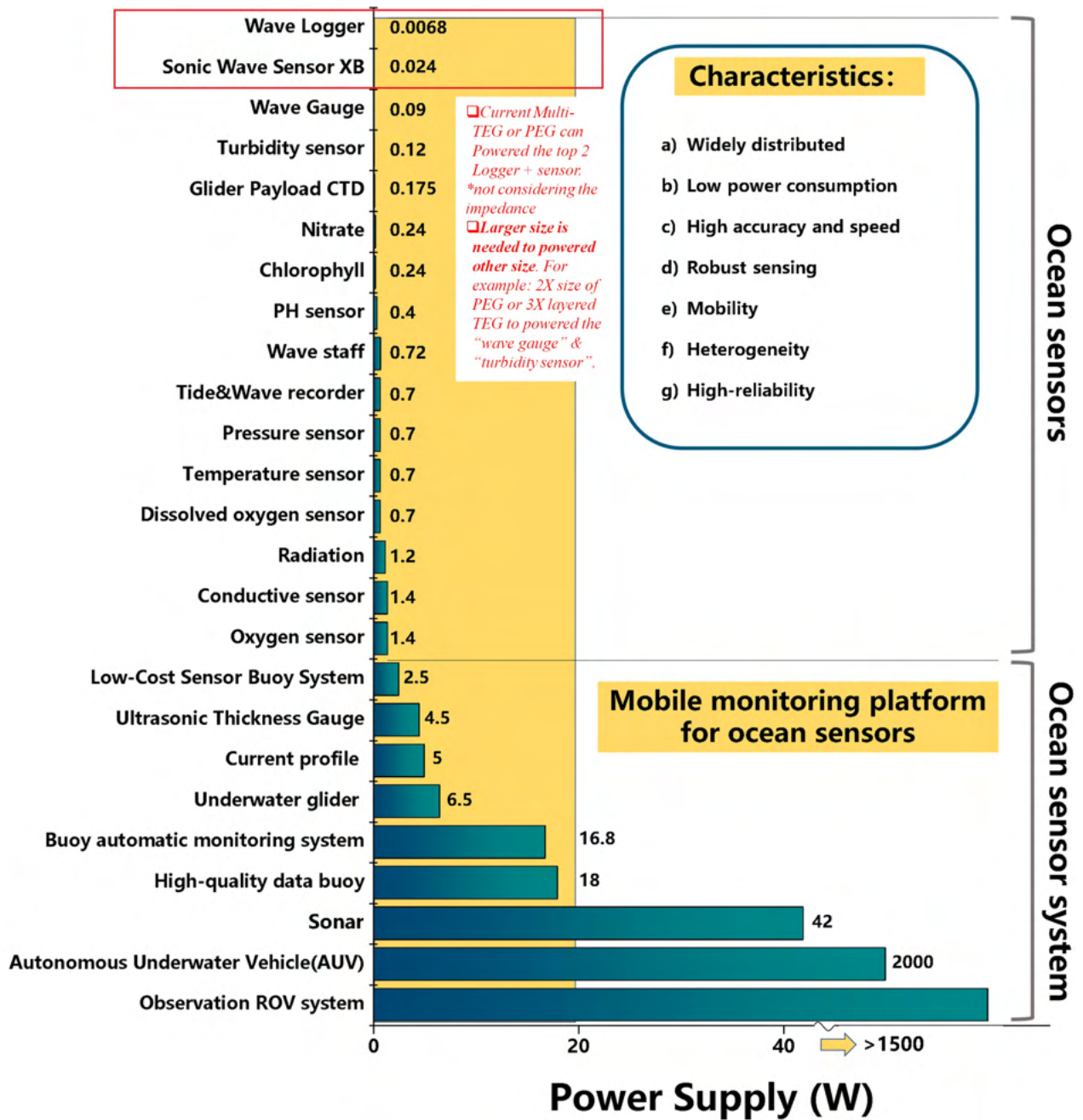


Figure 5.28: State-of-art ocean sensors and ocean sensors system that could be powered with the Hybrid Harvester [Zhao et al., 2021]

5.4 Summary

In this chapter, We proposed and developed the hybrid triboelectric-based generator and piezoelectric generator labeled a TEG–PEG hybrid harvester was developed. The electric performances of both generators were investigated individually under various vibration frequencies, vibration amplitude, and initial distance. The main findings are summarized as follows:

- The configuration of TEG-PEG study case 2 has a higher electrical output value compared with study case 1. Case 2 is able to reach higher than 10 V compared with study case 1.
- The vibration frequency and amplitude have a direct correlation and positive relationship to multi-TEG output. Similar to previous chapters, this led to the higher separation velocity, which caused the higher electrical output of the multi-layer TEG that could be generated.
- The initial distance of the TEG–PEG hybrid harvester indirectly influenced the output voltage generation. Both high and low electrical output occurs in the observation, but no tendency could be obtained. Therefore, we conclude that the setup of initial distance needs to be combined with either vibration frequency or vibration amplitude to ensure the maximum electrical output. This means that the separation velocity influence the high output more than separation distance.
- It was also found that the TEG–PEG hybrid harvester could compensate for the shortcomings of each device under different distance spectra. The TEG and PEG have different tendency on different distances. During the initial distance of $\delta_c < 20$ mm, the PEG generate higher electrical output (or have similar output on low amplitude). However, at $\delta_c \geq 20$ mm, the TEG can produce higher electrical output and compensate for the deficiency of the PEG to provide good electrical output results. It confirmed the PEG and TEG as devices that could help other devices generate better output.

In the future, a mechanism can be installed on the TEG-PEG energy harvester to scavenge low mechanical energy. This mechanism can either be a gear system, a spring system, or another

system that could absorb low frequency-high amplitude energy density (such as the ocean wave) and convert it into a high frequency-low amplitude suitable for the generators.

Bibliography

- [Jiang et al., 2017] Jiang, T., Yao, Y., Xu, L., Zhang, L., Xiao, T., and Wang, Z. L. (2017). Spring-assisted triboelectric nanogenerator for efficiently harvesting water wave energy. *Nano Energy*, 31(November 2016):560–567.
- [Kench and Mann, 2017] Kench, P. S. and Mann, T. (2017). Reef Island Evolution and Dynamics: Insights from the Indian and Pacific Oceans and Perspectives for the Spermonde Archipelago. *Frontiers in Marine Science*, 4.
- [Liang et al., 2020] Liang, X., Jiang, T., Liu, G., Feng, Y., Zhang, C., and Wang, Z. L. (2020). Spherical triboelectric nanogenerator integrated with power management module for harvesting multidirectional water wave energy. *Energy and Environmental Science*, 13(1):277–285.
- [Liang et al., 2021] Liang, X., Liu, Z., Feng, Y., Han, J., Li, L., An, J., Chen, P., Jiang, T., and Wang, Z. L. (2021). Spherical triboelectric nanogenerator based on spring-assisted swing structure for effective water wave energy harvesting. *Nano Energy*, 83(January):105836.
- [Mutsuda et al., 2014] Mutsuda, H., Miyagi, J., Doi, Y., Tanaka, Y., Takao, H., and Sone, Y. (2014). Flexible Piezoelectric Sheet for Wind Energy Harvesting. *International Journal of Energy Engineering (IJEE)*, 4(2):67–75.
- [Mutsuda et al., 2015] Mutsuda, H., Otake, M., Morisaki, K., Tanaka, Y., and Doi, Y. (2015). Wave energy converter using a compressed type of flexible piezoelectric device. *Proceedings of the International Offshore and Polar Engineering Conference*, 2015-Janua(2):1059–1065.
- [Mutsuda et al., 2019] Mutsuda, H., Tanaka, Y., Doi, Y., and Moriyama, Y. (2019). Application of a flexible device coating with piezoelectric paint for harvesting wave energy. *Ocean Engineering*, 172(September 2018):170–182.

- [Mutsuda et al., 2017a] Mutsuda, H., Tanaka, Y., Patel, R., and Doi, Y. (2017a). Harvesting flow-induced vibration using a highly flexible piezoelectric energy device. *Applied Ocean Research*, 68:39–52.
- [Mutsuda et al., 2017b] Mutsuda, H., Tanaka, Y., Patel, R., Doi, Y., Moriyama, Y., and Umino, Y. (2017b). A painting type of flexible piezoelectric device for ocean energy harvesting. *Applied Ocean Research*, 68:182–193.
- [Mutsuda et al., 2013] Mutsuda, H., Watanabe, R., Azuma, S., Tanaka, Y., and Doi, Y. (2013). Ocean power generator using flexible piezoelectric device. In *Proceedings of the International Conference on Offshore Mechanics and Arctic Engineering - OMAE*, volume 8. American Society of Mechanical Engineers Digital Collection.
- [Mutsuda et al., 2012] Mutsuda, H., Watanabe, R., Hirata, M., Doi, Y., and Tanaka, Y. (2012). Elastic floating unit with piezoelectric device for harvesting ocean wave energy. In *Proceedings of the International Conference on Offshore Mechanics and Arctic Engineering - OMAE*, volume 7, pages 233–240. American Society of Mechanical Engineers Digital Collection.
- [Patel et al., 2016] Patel, R., Tanaka, Y., McWilliam, S., Mutsuda, H., and Popov, A. A. (2016). Model refinements and experimental testing of highly flexible piezoelectric energy harvesters. *Journal of Sound and Vibration*, 368:87–102.
- [Tanaka et al., 2016] Tanaka, Y., Oko, T., Mutsuda, H., Ichikawa, K., Yamamoto, T., and Okihama, K. (2016). Study of power generation using FPED assuming engine vibration. *International Journal of Applied Electromagnetics and Mechanics*, 52(3-4):1377–1383.
- [Varghese and Chandran, 2021] Varghese, H. and Chandran, A. (2021). A facile mechanical energy harvester based on spring assisted triboelectric nanogenerators. *Sustainable Energy and Fuels*, 5(20):5287–5294.
- [Xiao et al., 2018] Xiao, T. X., Liang, X., Jiang, T., Xu, L., Shao, J. J., Nie, J. H., Bai, Y., Zhong, W., and Wang, Z. L. (2018). Spherical Triboelectric Nanogenerators Based on Spring-Assisted Multilayered Structure for Efficient Water Wave Energy Harvesting. *Advanced Functional Materials*, 28(35):1802634.

- [Yang et al., 2019] Yang, W., Wang, Y., Li, Y., Wang, J., Cheng, T., and Wang, Z. L. (2019). Integrated flywheel and spiral spring triboelectric nanogenerator for improving energy harvesting of intermittent excitations/triggering. *Nano Energy*, 66(August):1–8.
- [Yun et al., 2021] Yun, Y., Jang, S., Cho, S., Lee, S. H., Hwang, H. J., and Choi, D. (2021). Exo-shoe triboelectric nanogenerator: Toward high-performance wearable biomechanical energy harvester. *Nano Energy*, 80(September 2020):105525.
- [Zhao et al., 2021] Zhao, T., Xu, M., Xiao, X., Ma, Y., Li, Z., and Wang, Z. L. (2021). Recent progress in blue energy harvesting for powering distributed sensors in ocean. *Nano Energy*, page 106199.

Chapter 6

Conclusions and Future Works

6.1 Conclusions

In this final chapter, the results of this research, which is based on objectives in Chapter 1 are briefly described. As a reminder, There are four objectives of the research of this dissertation. Those are:

- To explain characteristics of the TEG based on the vertical contact-separation-compression vibrations.
- To clarify the effect of the vibration amplitude, acceleration amplitude, frequency, and the initial distance to the TEG electrical output.
- To design and develop a multi-layered TEG for maximum electrical output.
- To investigate whether the TEG device could be combined with the PEG device to create a hybrid TEG-PEG device and check their complementary abilities.

There is four main development in this research. This research started with investigating a single FC-TEG electrical voltage based on the vertical contact-separation-compression vibrations. The second development elucidates the key parameters and develops the theoretical model.

The third progress aims to improve the energy harvester by incorporating multiple dielectric elastomers (Multi TEG). Finally, we combine the TEG with the PEG device to create a hybrid TEG-PEG device.

After conducting this study, the main conclusions are mentioned as follows:

1. Our developed FC-TEG created with a single dielectric elastomer + electrode is able to generate an effective electrical output in all modes (separation, contact and compression mode). We found that the output is higher from these modes (compression > contact > separation mode).
2. We developed the theoretical model of the FC-TEG which produced the time history of the TEG and the separation mode as our originality. We found that in separation and contact modes, the results of the time histories is similar with the experimental results except the compression mode.
3. To improve the TEG electrical energy, a multi-layered structure is proposed. We found that this structure is able to generate the electrical voltage in linear terms (Around 4 times higher output compared with the single-layer).
4. Then, the multi-layered TEG is combined with the flexible PEG to harvest more energy especially in a different distance spectra. We found that both devices are able to accommodate each other with the PEG is able to generate high output on the Initial distance $\delta_c < 20\text{mm}$, while the TEG produced higher output on the Initial distance $\delta_c \geq 20\text{mm}$.
5. In this study, we found that the separation velocity which is characterized by the combination of the vibration amplitude and vibration frequency is influencing the electrical generation more than separation distance or compression load. Our results showed that the distance needs to be adjusted properly (non-linear correlation) in order to generate highest output, while the compression load have less influence compared with the acceleration amplitude.

6.2 Future Works

From this study, an enhanced understanding of the TEG output voltage, its key parameters for improving electrical results, and its compatibilities when the TEG is combined with PEG to create a hybrid generator device. Understanding these fundamental characteristics is the first step / first stage in developing the ocean energy harvester with the TEG and PEG. Details of the future works and future studies in this research can be seen in Fig.6.1. There are five stages to investigate, starting from Stage 1 (this dissertation), which focuses on elucidating the fundamental characteristics. Stage 2 is developing a small-scale model and testing in the laboratory stage. Created a bigger model and tested them in water tanks such as Towing tank in Stage 3. Then, we created and deployed the prototype in the small port as Stage 4. And finally, deployment of the ocean energy harvester itself in stage 5.

For the immediate future work; although we successfully elucidated the mechanical properties and the harvester's electrical performance, there is still an unknown correlation between the dielectric elastomer surface configurations with the TEG electrical output. During the single dielectric elastomer and multi-layered TEG testing, we examine that the elastomer's surface could potentially change the electrical outcomes. The surface of the elastomer itself is varied based on its setup. The inner layer could be different since the amount of air pocket inside the elastomer could be made differently. On the outer side, the surface roughness of the elastomer could be made either completely smooth to a certain degree of roughness. Lastly, we must confirm whether the materials' thinness significantly correlates with the electrical voltage. To confirm these hypotheses, we will conduct vibration tests that focus on three variables:

- Porosity.
- Thickness of the materials.
- Surface roughness.

Future work in this stage also will investigate impedance matching. Since the FC-TEG device is fabricated using dielectric material, it is considered a high impedance device. a Future

study needs to be done by measuring the TEG electrical output using varying resistive loads to find the optimum load for maximum electrical power transfer. After the effect of the inner impedance of the FC-TEG is found, we can then start modify the structure and dimensions in the multi-layer TEG to reduced the impedance without losing output power and to match low impedance practical applications.

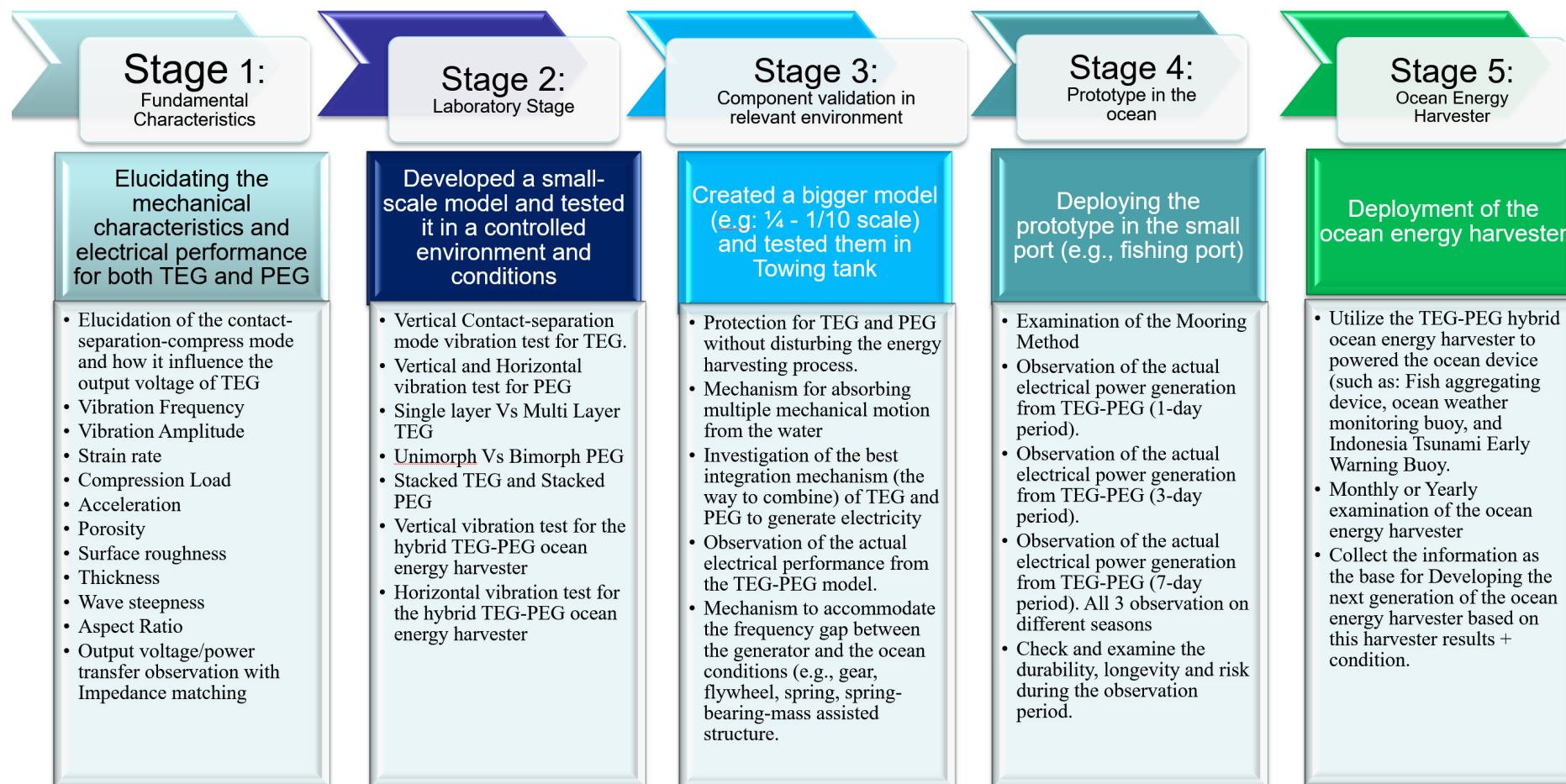


Figure 6.1: Details of the Future work of the TEG-PEG ocean energy harvester